TO STUDY THE PERFORMANCE ANALYSIS OF SOLAR THERMAL BASED COMBINED CYCLE FOR POWER GENERATION AND WASTE HEAT RECOVERY

A Thesis submitted to the Delhi Technological University, Delhi in fulfillment of the requirements for the award of the degree of

DOCTOR OF PHILOSOPHY

In

Mechanical Engineering

HARWINDER SINGH

(2K15/PhD.ME/10)

Under the Supervision of

Prof. (Dr.) R. S. Mishra

(Professor)
Mechanical Engineering Department
Delhi Technological University

MECHANICAL ENGINEERING DEPARTMENT
DELHI TECHNOLOGICAL UNIVERSITY
Shahbad Daulatpur, Bawana Road
Delhi- 110042, INDIA

DECLARATION

I hereby declare that the thesis entitled "**To study the performance analysis of solar thermal based combined cycle for power generation and waste heat recovery**" is an original work carried out by me under the supervision of **Professor R.S. Mishra**, Department of Mechanical, Production and Industrial, Automobile Engineering, Delhi Technological University, Delhi. This thesis has been prepared in conformity with the rules and regulations of the Delhi Technological University, Delhi. The research work reported and results presented in the thesis has not been submitted either in part or full to any other university or institute for the award of any other degree or diploma.

Harwinder Singh

(2K15/Ph.D./ME/10)

Research Scholar

Mechanical Engineering Department,

Delhi Technological University

Date:

Place: Delhi

DELHI TECHNOLOGICAL UNIVERSITY

(Govt. of National Capital Territory of Delhi)

BAWANA ROAD, DELHI- 110042

CERTIFICATE

This is to certify that the work embodied in the thesis research proposal entitled **"To study the performance analysis of solar thermal based combined cycle for power generation and waste heat recovery"** by **Harwinder Singh, Roll No. 2K15/Ph.D./ME/10** as a Ph.D. scholar in Department of Mechanical, Production and Industrial, Automobile Engineering, Delhi Technological University is satisfactory and meets the Ph.D. requirement. This thesis work is useful to utilities based on innovations and research. He has completed his thesis work under my guidance and supervision. The matter embodied in this research work has not been submitted earlier for the award of any degree or diploma to the best of our knowledge and belief.

Prof. (Dr.) R. S. Mishra
Deptartment of Mechanical Engineering
Delhi Technological University

Acknowledgements

I express my sincere gratitude to my supervisor **Professor R. S. Mishra** for assisting me in identifying and formulating the research problem. Despite their busy schedules, Professor R.S. Mishra was always available for the advice and discussions. His valuable comments and advice gave me the confidence to overcome the challenges in the formulation of this research work.

Also, I would like to express my sincere gratitude to my parents for their endless inspiration, support, and guidance throughout my whole life.

Furthermore, I would like to thank my friends from the Mechanical Engineering department, who have supported me through their encouragement, support and friendship during this period of research work. Lastly, I would like to thank all those who directly and indirectly helped me in carrying out this thesis work successfully.

(Harwinder Singh)

2K15/Ph.D./ME/10

Abstract

One of the most mature concentrating technology, i.e. solar parabolic trough collector (SPTC) system is really a promising option to harness the solar energy between the low to medium-temperature range with the purpose of solar thermal electricity generation via power cycles. These days, combined cycles especially based on supercritical carbon dioxide (SCO_2) cycle are very much popular whose performance have been further investigated in this thesis work. Apart from this, organic Rankine cycle (ORC) and vapour absorption refrigeration (VAR) cycle have been employed as bottoming cycles. Then, the effect of replacing simple configuration by recompression SCO_2 (R-SCO_2) cycle on the cycle performance has been examined. Finally, a short analysis of supercritical ORC (SORC) has been studied.

Firstly, for the analysis of SPTC integrated combined SCO_2-ORC system, five organic fluids such as R134a, R245fa, R1234yf, R1234ze, and R407c have been chosen for the ORC. Results concluded that R407c based SCO_2-ORC system has the highest exergy and thermal efficiency, and minimum exergy destruction rate were 78.07% and 43.49%, and 4093 kW, respectively at direct normal irradiance (DNI) of 950 W/m^2 followed by the R1234ze, R1234yf, R245fa, and R134a. Also, the maximum exergy and thermal efficiency for the R407c fluid was 75.21% and 41.9% at maximum turbine inlet pressure (P_5) of 23 MPa; 81.79% and 45.57% at maximum turbine inlet temperature (T_5) of 850 K; and 69.75% and 38.86% at minimum compressor inlet temperature (T_9) of 300 K, respectively. Noted that SPTC field is a primary source of exergy destruction, i.e. more than 25% of solar inlet exergy and almost 54% of total exergy destruction rate has been destructed. Furthermore, the SPTC field's improvement potential, fuel depletion ratio, and irreversibility ratio were 5282 kW, 0.2583, and 0.5388, respectively. Secondly, for the analysis of SPTC integrated combined R-SCO_2-ORC system, eight fluids like R123, R1234ze, R1234yf, toluene, cyclohexane, isopentane, isobutene, and R290 have been selected. In general, exergy and thermal efficiency of system increases with the increase in DNI, 'P_5', and 'T_5' in contrast to the 'T_9' as it shows inverse effect on efficiency. As a result, R123 based R-SCO_2-ORC system shows maximum exergy and thermal efficiency of 86.75% and 48.33% at DNI of 950 W/m^2; 79.04% and 44.03% at P_5 of 23 MPa; 86.59% and 48.24% at T_5 of 920 K; 84.64% and 47.15% at T_9 of 327 K, respectively. Furthermore, it possesses highest net work output of 6231 kJ at T_5 of 920 K and 6090 kJ at T_9 of 327 K. Moreover, comparative study with and without recompression concludes that R123 based R-

SCO_2-ORC system shows exergy and thermal efficiency of 85.09% and 47.4% as compared to 83.63% and 46.59%, respectively in case of simple SCO_2-ORC system.

Thirdly, the performance results of SPTC integrated combined SCO_2-VAR system found that maximum exergy and thermal efficiency of SPTC for the April 15 on Mumbai was 32.58% and 63.46% at local apparent time (LAT(h)) = 1230, and 31.72% and 61.78%, respectively at LAT(h) = 1130 & 1230 for the December 15. Then, at maximum T_5 of 920 K, the highest exergy and thermal efficiency, and net work output of the SCO_2-VAR cycle were 80.13% and 44.64%, and 1668 kW, respectively. While, the highest coefficient of performance for cooling ($COP_{cooling}$) and heating ($COP_{heating}$) were 0.4675 and 1.435, respectively found to be at lower T_5 of 650 K. Furthermore, at maximum compressor pressure ratio of 2.67, the highest exergy and thermal efficiency, net work output, $COP_{cooling}$ and $COP_{heating}$ were 81.51%, 45.41%, 1813 kW, 0.4722, and 1.207, respectively. Moreover, at lower T_9 of 300 K, the maximum exergy and thermal efficiency, and net work output were 81.29% and 45.29%, and 1788 kW, respectively. Lastly, the performance of SPTC integrated SORC (SPTC-SORC system) has been examined by six fluids such as cyclohexane, isopentane, propane, R600a, n-Hexane, and n-Pentane. Findings reveal that at higher DNI of 950 W/m^2 and turbine inlet pressure of 86 bar, the highest exergy efficiency was 83.15% and 81.19%; and thermal efficiency was 39.9% and 38.96%, respectively in case of propane. Additionally, more than 80% of total exergy destruction rate was found to be only in SPTC.

Dedicated

to

My Parents

List of Abbreviations

Nomenclature

A_{ap}	area of aperture, m^2
A_a	area of absorber tube, m^2
A_{co}	area of absorber cover, m^2
Cp	specific heat of heat transfer fluid, [kJ/kg-K]
COP	coefficient of performance
Col_s	total no. of solar collector per single row in series
Col_p	total no. of solar collector in parallel rows
c_1	first order coefficient, [$W/m^2°C$]
c_2	second order coefficient, [$W/m^2°C^2$]
$D_{co,o}$	cover's outside diameter, m
D	diameter, m
DNI	direct normal irradiance
Ex	exergy, kW
Ex_{inl}	inlet exergy, kW
Ex_{DES}	exergy destruction rate, kW
$\dot{ex}_{cooling}$	cooling exergy rate, kW
EV1	evaporator 1
EV2	evaporator 2
EXV	expansion valve
$h_{coa,i}$	coefficient of heat loss between glass cover and absorber tube, [kW/m^2K]
$h_{c,amco}$	coefficient of convection heat loss between ambient and glass cover, [kW/m^2K]
$h_{r,amco}$	coefficient of radiation heat loss between ambient and glass cover, [kW/m^2K]
$h_{r,coa}$	coefficient of radiation heat loss between absorber tube and glass cover, [kW/m^2K]
H_2O	water
HPAV	high pressure ammonia vapours

HTF	heat transfer fluid
IMP	improvement potential
K_{air}	air's thermal conductivity, [W/m-K]
K_m	incident angle modifier
L	length of SPTC, m
LAT	Local apparent time
LPAV	low pressure ammonia vapours
$\dot{m}_a$	mass flow rate of heat transfer fluid in the absorber tube, kg/s
M	Molar mass, [kg/kmol]
Nu	Nusselt number
NH_3	ammonia
ORC	organic Rankine cycle
PR	compressor pressure ratio
PRV	pressure reducing valve
$\dot{Q}$	rate of heat transfer, kW
$\dot{Q}_{in}$	total heat transfer at inlet of combined system, kW
$\dot{Q}_u$	useful energy gain per unit time, kW
RES	renewable energy sources
R-SCO_2	recompression SCO_2
S	absorbed heat flux, W/m^2
SCO_2	supercritical CO_2
s	specific entropy, [kJ/kg-K]
SHE	solution heat exchange
SPTC	solar parabolic trough collector
SORC	supercritical ORC
T	temperature, K
T_{sun}	temperature of sun, K
TCO_2	transcritical CO_2
$\dot{V}$	volume flow rate, m^3/s
VAR	vapour absorption refrigeration

U_L	overall heat loss coefficient of SPTC between ambient and absorber tube, [kW/m^{2}K]
U_o	coefficient of overall heat loss, [kW/m^{2}K]
W	width of SPTC, m
$\dot{W}$	specific net work output, kJ/kg
X	concentration of ammonia, %
HX	heat exchanger
Y_{DEP}	fuel depletion ratio
Y*	irreversibility ratio

Greek letters

ρ_r	reflectance of glass mirror
α	absorber tube's absorbance
γ	intercept factor
τ	glass cover's transmittance
η	efficiency
ϵ_{co}	glass cover's emittance
ϵ_a	emittance of the absorber tube
ε	effectiveness
σ	Stefan–Boltzmann constant, [kW/m^{2}K^4]
φ	expansion ratio

Subscripts

a	absorber
a_o	outlet of absorber
a_i	inlet of absorber
am	ambient or environment
avg	average
c	cover
cv	control volume
ch	chemical

e	exit
en	energy
ex	exergy per unit mass flow rate, kJ/kg
elec	electrical
f	organic working fluid
i	inlet
ins	instantaneous
m	mean
o	outside
ph	physical
0	environmental conditions
Q	property value at state Q
u	useful

List of Contents

List of Tables

List of Figures

CHAPTER 1: INTRODUCTION

1.1. General introduction

Fossil fuels (coil, oil, natural gas) are depleting in a fast manner in the recent years and the era of these conventional resources is slowly coming to an end. Therefore, it becomes essential for us to determine the consumption rates of various energy sources and to provide some clues of energy assets available. It has been observed that there was a steady increase in production of coal, which was around 4.6% per year from 1860 to the commencement of first world war in 1914. The variations in annual production rate were irregular till the end of 1945 and then it was again increased with the rate of 2% to 4% per year till 1990. From the year 1991 to 2002, production was stagnated and varied between 4412 Mt to 4778 Mt but it has been enhancing again after the year 2002. However, India's production was 6.7% of total production of world up to the year 2000. Whereas, the world's production and consumption of oil was 1000 billion barrels and the rate of production of natural gas was around 4% per year till 2004 [1]. With the help of statistics, it is conceivable to gauge the timeframe up to which fossil fuels will be available. Therefore, the necessity of renewable energy resources (RES) will thus be established so that energy crisis and environmental concerns could be mitigate in near future.

In 1973, oil shock had received by the world, which induced a great need of shifting from fossil fuels to alternative resources and at the same time world has been aware of pollution due to the large-scale use of conventional resources. Then in 1979, second oil shock came in to existence which led to a hike in fuel price. In 1980, Iran and Iraq oil-rich countries went to war, which intensified the issue of oil crisis and energy security [2].

From the past decade, energy has been rapidly consumed globally and with significant differences it continues to grow in the coming years. It was actually due to low price of fossil fuels as well as industrialization in America, Europe, and Japan and the rate of energy utilization by these nations keeps on appearing expanding pattern, which will become more complex in the next five decades. Also, the energy demand of China and India rapidly increases because of population of these nations is approximately one-third of the total world population. Therefore, it becomes evident that oil reserves will be drained in not so distant future and the impact of humankind exercises on the climate change will worsen the environment situation very soon. On the positive side, renewable resources such as solar thermal, solar photovoltaic, biofuels, and wind are very helpful in the reduction of negative effect produced by conventional resources as well as its basic assurance in cost competitiveness. From 1971 to 2002, energy

demand of the world increased from 5536 to 10,345 million tons of oil equivalent (MOTE), which is equivalent to 2% annual increment. Up to 2008, this demand had increased by average 3% annually, which was equal to 12,271 MOTE and this increment was due to fast growing and populous economies such as China and India. This primary energy demand would double by year 2043 and triple by year 2063 [3], but it cannot increase with the same rate always and according to report of International Energy agency (IEA 2010), the global energy consumption will enhance with an average of 1.2% annually up to 2035 [3,4]. It has been estimated that up to 2050, approximately half (nearly 50%) of energy use globally will have to come from renewable sources majorly from solar and wind energy [3], which could be used to operate the power cycles such as supercritical carbon dioxide (SCO_2) cycle, recompression SCO_2 cycle, and organic Rankine cycle (ORC) so as to produce power and recovery of waste heat that have also been further discussed in the literature.

1.2. Energy scenario

From the past few decades, man has consumed energy at very fast rate. Initially, the requirement of energy was only due to basic need of human i.e. food. But after the discovery of fire, people's demand has increased. In the beginning, sun was the only source to fulfil the energy demand of human and it has been seen that people were using alternative energy resources from many years. People discovered a new conventional source known as coal after industrial revolution and other conventional resources, for instance fossil fuels (oil and natural gas) came into existence during the origination of internal combustion engine. Along with these resources, a fresh source of energy known as nuclear energy came into reality during the second world war period. For the electricity generation, nuclear and thermal energy are using widely in a comprehensive way with the establishment of nuclear and thermal power plants. However, the contribution of nuclear energy to fulfil the energy need is not so much high due to inadequate amount of uranium on earth. Nonetheless, its contribution is noteworthy for human life because it does not create any interruption to the ecosystem as compete with the thermal power plants. In the recent years, fossil fuels have been depleting at extremely high rate. So, there is a great necessity to replenish the conventional resources from sustainable resources of energy to prevent the degradation of fossil fuels and to decrease down the effect of harmful gases or waste. Energy sources can be classified into two categories like commercial and non-commercial. Commercial sources include hydroelectric, wind, fossil fuel, and nuclear power. However, non-commercial sources include wood, agriculture &

animal waste. Requirement and application of commercial sources is very high in contrast to non-commercial sources, which can be seen generally in developed countries like in USA and Europe. Although, in developing countries for instance, India is using both the sources almost in same amount [1].

With respect to the total primary energy supply of world, RES shared for almost 13.2% in the year 2011. However, the 75% share of RES was from biomass and this amount considered as 20% of what they could whenever changed over by current and effective existing technologies instead of traditional open combustion that is an inefficient technology and currently used by developing nations. Apart from this, the electricity production in 2011 by RES was around 20.1% and approximately 78% share of RES was only hydroelectric followed by wind power (10%), bioenergy (9%), geothermal (1.6%). However, solar power share was 1.4% of total electricity capacity of RES, which was increasing at an annual rate of 50% [3,6]. Figure 1.1 shows the fuel shares in primary energy consumption of world in the year 2018.

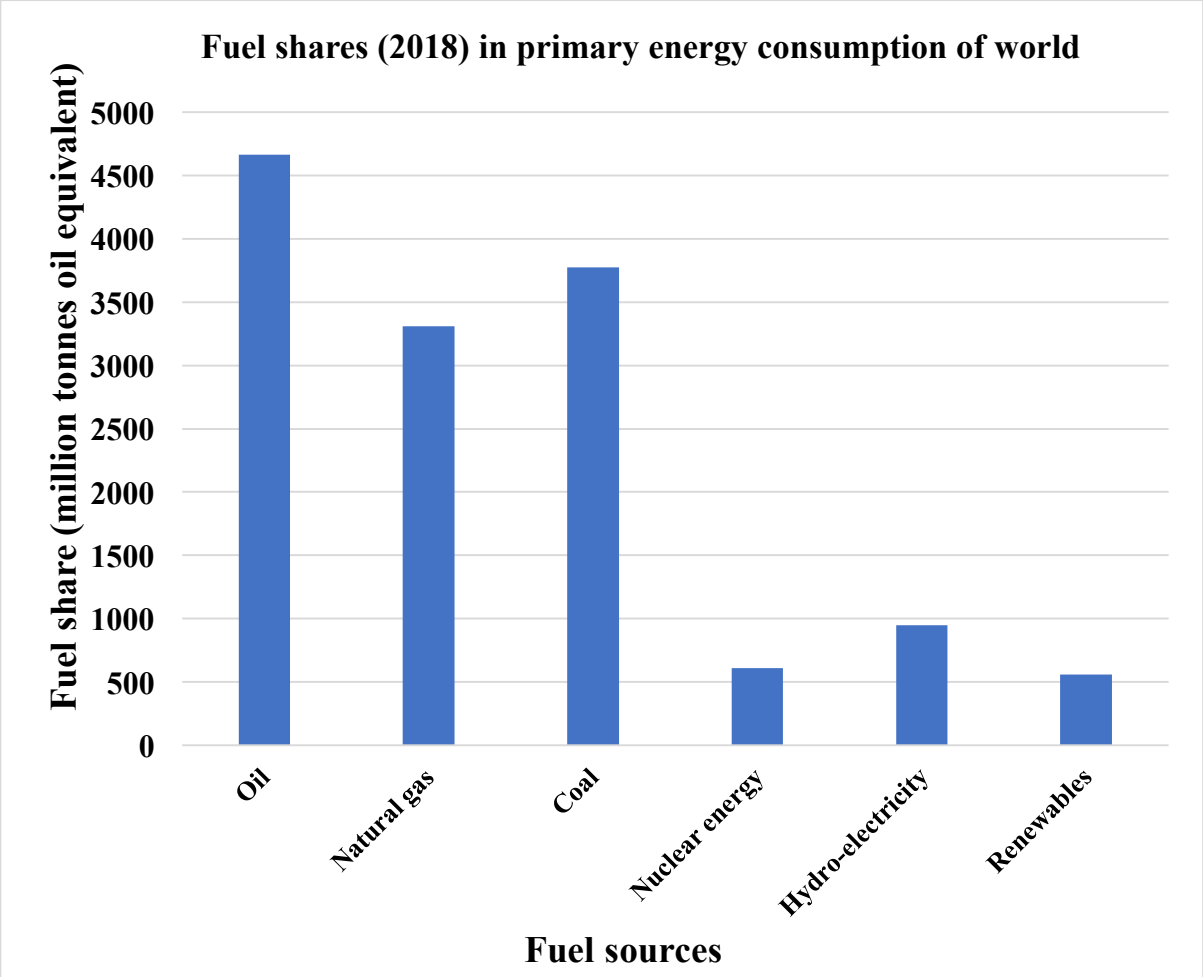

Figure 1.1. Fuel shares (2018) in primary energy consumption of world [5].

The energy development in the world has shifted from high to low-carbon energy as well as fossil to non-fossil fuels energy resources in order to reduce the ecological and environmental problems. The carbon substance of calorific value for coal is 26.37% t/TJ (tonne per terajoule) per unit, 20.1 t/TJ and 15.3 t/TJ in case of crude oil and natural gas, respectively. Apart from this, the amount of conventional oil and gas in the world is approximately 4878×10^8 t and 471×10^{12} m^3, respectively and it is recoverable and concentrated mainly in Middle East (35%), Russia (14%), North and South America (13% and 14%, respectively). However, the amount of unconventional recoverable oil and gas resources present globally is around 6200×10^8 t and 4000×10^{12} m^3, respectively and mainly located in North and South America (34% and 14%, respectively), Asia-Pacific (23%), and Russia (13%) [7]. Whereas, RES such as hydropower, solar, nuclear power, and wind are considered as carbon free. The transition of scenario from coal to hydrocarbon and then to new energy sources or alternative energy resources helps in reduction of pollutants and carbon emission [7].

Coal as a fossil energy is present in most abundant amount (i.e. more than 100 trillion tons) on the planet which is mainly distributed in the area of North America, Asia-Pacific, and Europe as shown in Figure 1.2. Up to the year 2014, the world's total coal reserves were 8915×10^8 t. The most plentiful coal reserves present in USA, Russia, China which are approximately 2373×10^8 t, 1570×10^8 t, and 1145×10^8 t, respectively [7]. Also, the data related to production and consumption of all types of energy resources in the world in year 2014 as shown in Figure 1.3.

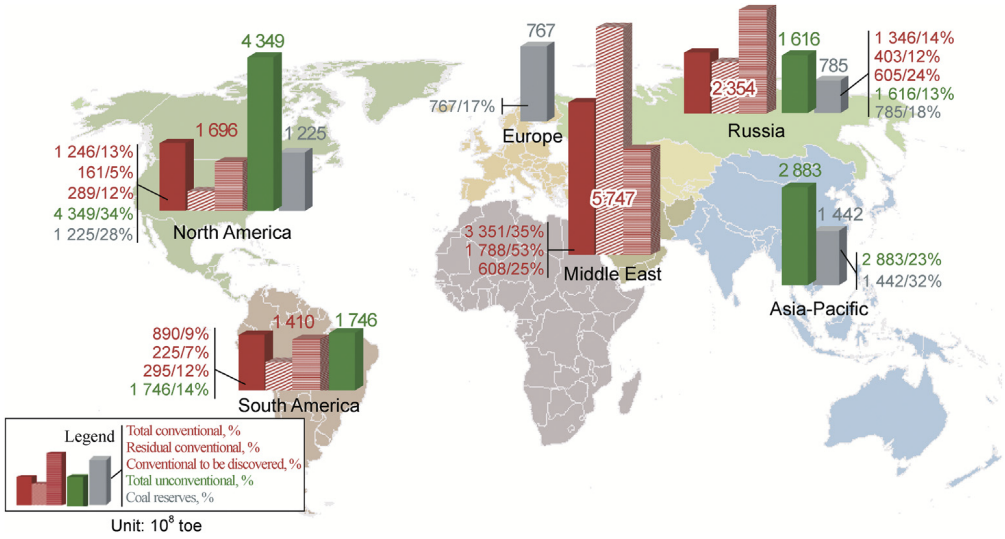

Figure 1.2. Distribution of fossil energy in the world [7].

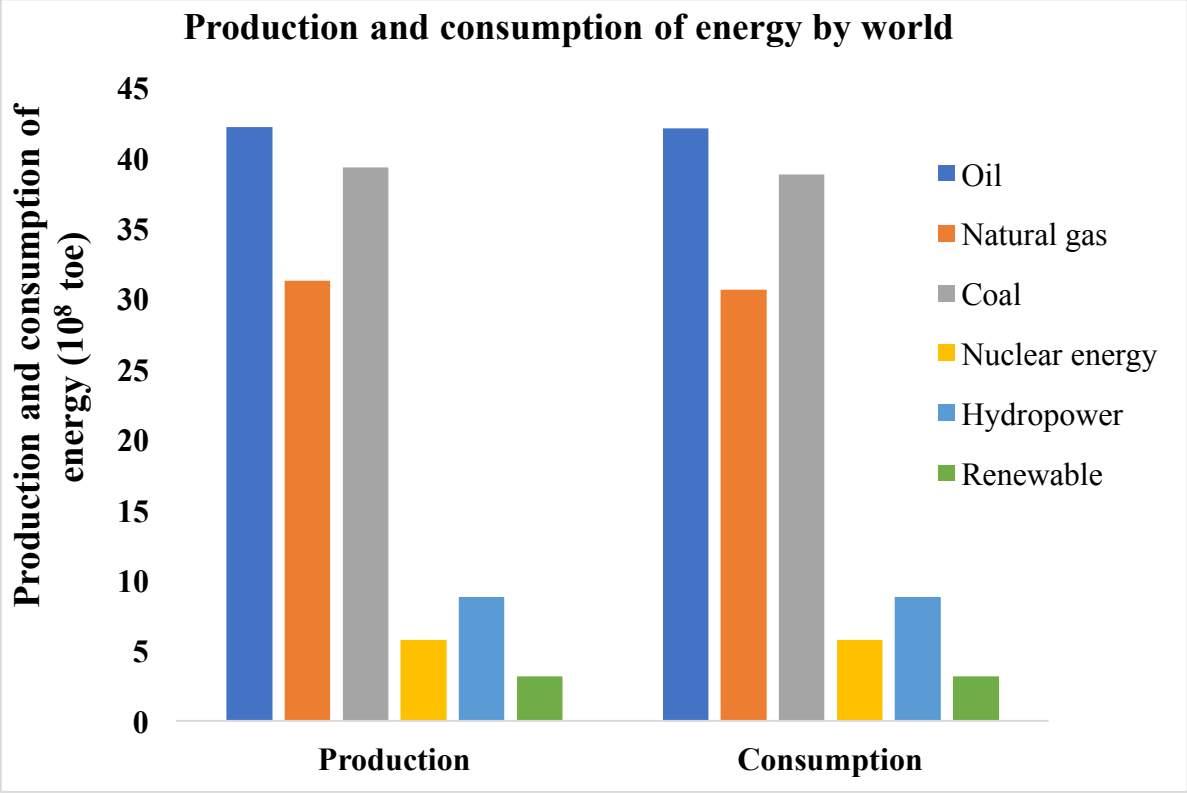

Figure 1.3. Production and consumption of energy by world [7].

In the particular developing nation, any uncertainty or interruption in the energy supply can intimidate the economy of that country and it is very important fundamentally to achieve the energy security especially for fast growing economy such as India in order to enhance its economic growth as well as to remove the poverty and unemployment. Over the last few years, India's economic growth increasing at fast rate and its economy comes on seventh place in the world by GDP after USA, China, Japan, Germany, United Kingdom, and France. However, as per International Monetary Fund World Economic Outlook (IMF-WEO), Indian economy considered as the third largest after USA and China according to purchasing power parity (PPP) [8]. Also, total GDP growth in India which was estimated at 7.3% for year 2015 and 7.5% for year 2016 and 2017 [9].

Majorly imported fossil fuels are responsible to satisfied the demand of energy in India and it is at fourth place in the world as a biggest consumer and net importer of products manufactured with the use of crude oil and petroleum. Therefore, as a big importer of energy products, it is very essential to adopt alternative energy sources to avoid any kind of unanticipated geographical situation, which can hamper the economic and industrial growth of the country. However, India's per capita energy consumption is still significantly lower in contrast to developed countries but it could be enhanced due to rapid economic growth and

scope of industrialization in the country. So, RES can be helpful to meet the energy demand for the industrial and economic growth, and also effective way to mitigate the climate change, which means that alternative technologies can be helpful in hazardous greenhouse gas emission [8].

In last decade, India has accounted total 22% annual growth rate for renewable energy. India is producing 53.22 billion units (BU) with the help of non-conventional resources in which wind and solar contribution is approximately 31.26 and 3.35 BU, respectively. In current scenario, India has total installed capacity of power generation is approximately 207.8 GW in which 25 GW producing by renewable resources. India has occupied fifth place in the world with respect to installed capacity of wind power, which is around 11087 MW and its on-shore capability is approximately 65000 MW. Apart from wind, solar energy is a free, limitless, pollution free ideal energy source. Solar radiations reaching at the surface of earth in a year provide 10000 MW more energy than the world's annual energy requirement. India has a great solar potential and its annual average temperature varies from 25℃-27. 5℃ due to its location in Tropic of Cancer and Equator. The average solar energy directed over the India per day is around 4-7 kWh/m^2 along with in a year, India has 1500-2000 sunshine hours, which is very much higher than the overall consumption of energy in country at present [8].

India is at a seventh and ninth place in the production of photovoltaic cell and solar thermal power, respectively. On the other hand, small hydro is the most reliable and oldest way to produce energy. First hydroelectric plant was installed in Appleton, USA in the year 1882, and India's first hydroelectric installation was in 1897 in Sidrapong (Darjeeling) with a capacity of 130 kW. Hydropower plant generally classified into large hydro and small hydro projects. The responsibility of large hydro comes under the India's Ministry of Power, and Ministry of New and Renewable energy (MNRE) is responsible for small hydro power with the maximum capacity of 25 MW. Small hydro can be divided into Mini hydro (101 kW to 2000 kW) and Micro hydro (up to 100 kW). MNRE want to install total 7000 MW capacity of small hydro projects up to the end of 12^{th} plan. Other potential renewable resource is tidal energy, India has total 7500 km long coastline and total island in the Bay of Bengal and Arabian sea is around 336 in which strong tides are generated that may rotate the turbines for electric power generation. The wave energy potential in India is approximately 40,000 MW but high cost and low availability of high tidal range sites or flow velocity can create difficulties in its deployment [8].

Besides, in 78 countries worldwide, geothermal energy is directly utilized for the purpose of heating. USA produced maximum amount of this energy and generating almost

3086 MW electricity. India also has great capabilities to produce the geothermal based power generation but its development in initial stages right now. Country almost has total 340 geothermal springs in which mostly have temperature range varies from 37℃ −90℃ and can be useful for direct heating. The first target set by MNRE up to year 2022 is 1000 MW with the planning of resource assessment in 2016-2017. Furthermore, due to rely of Indian economy majorly on agriculture, the country has sufficient quantity of biomass in the shells of coconut wild bushes, jute, cotton, straw and husk, which can be converted into biomass with the help of solar energy known as photosynthesis. In India, fuel based on biomass is predominately used, which accounts for one third of total fuel amount and its total utilization in rural household is 90% and in urban household is around 10%. The potential in India based on biomass is approximately 30,000 MW, which can be effectively used in saving of almost 20,000 crores every year [8].

The total installed capacity of electricity in India's each sector such as private, state, and central is shown in Figure 1.4. However, total installed capacity based on various fuel resources is shown in Figure 1.5. The share of state, central, and private sector in the total installed capacity (i.e. 3,44,002 MW) is around 24.6%, 30.2%, and 45.2%, respectively [10].

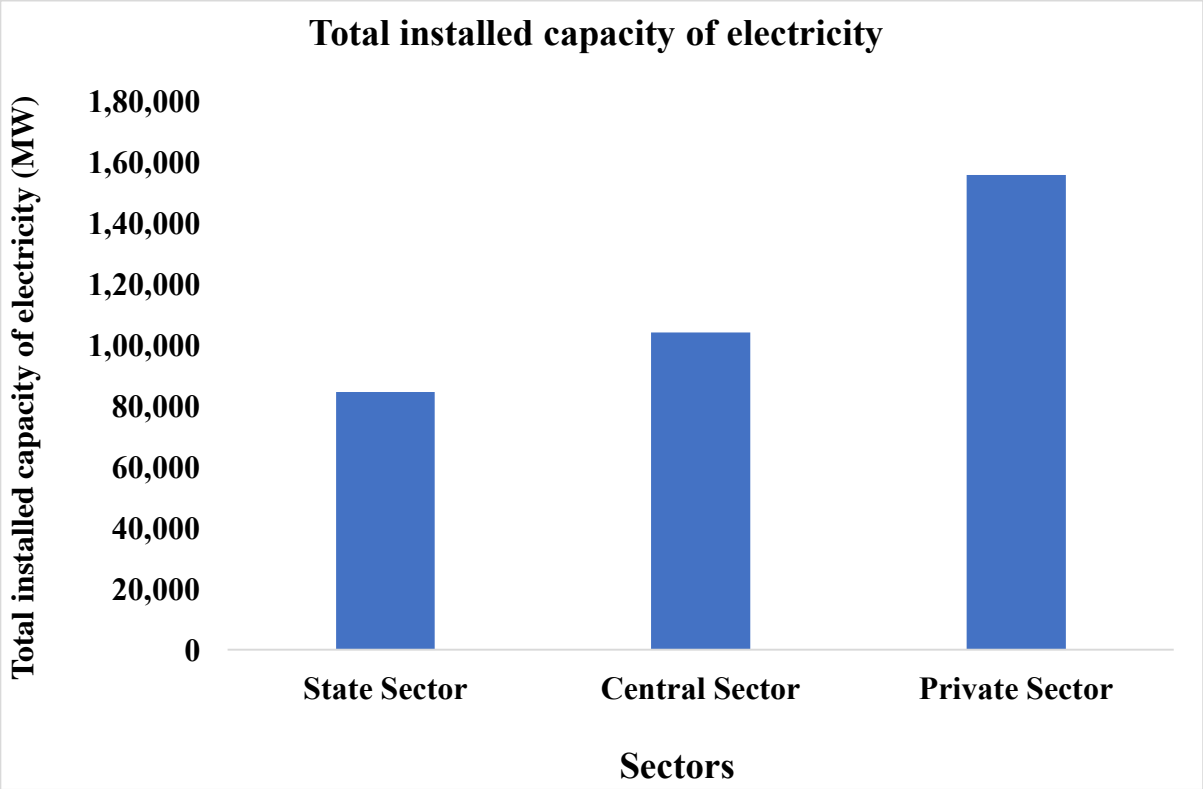

Figure 1.4. Total installed capacity of electricity in state, central, and private sector up to year 2018 [10].

Whereas, the share of fuel resources such as coal, gas, oil, hydro, nuclear, and RES (i.e. small hydro, biomass power and gasifier, urban and industrial waste, energy available from solar and wind) in the total installed capacity is around 57.3%, 7.2%, 0.2%, 13.2%, 2%, and 20.1%, respectively [10].

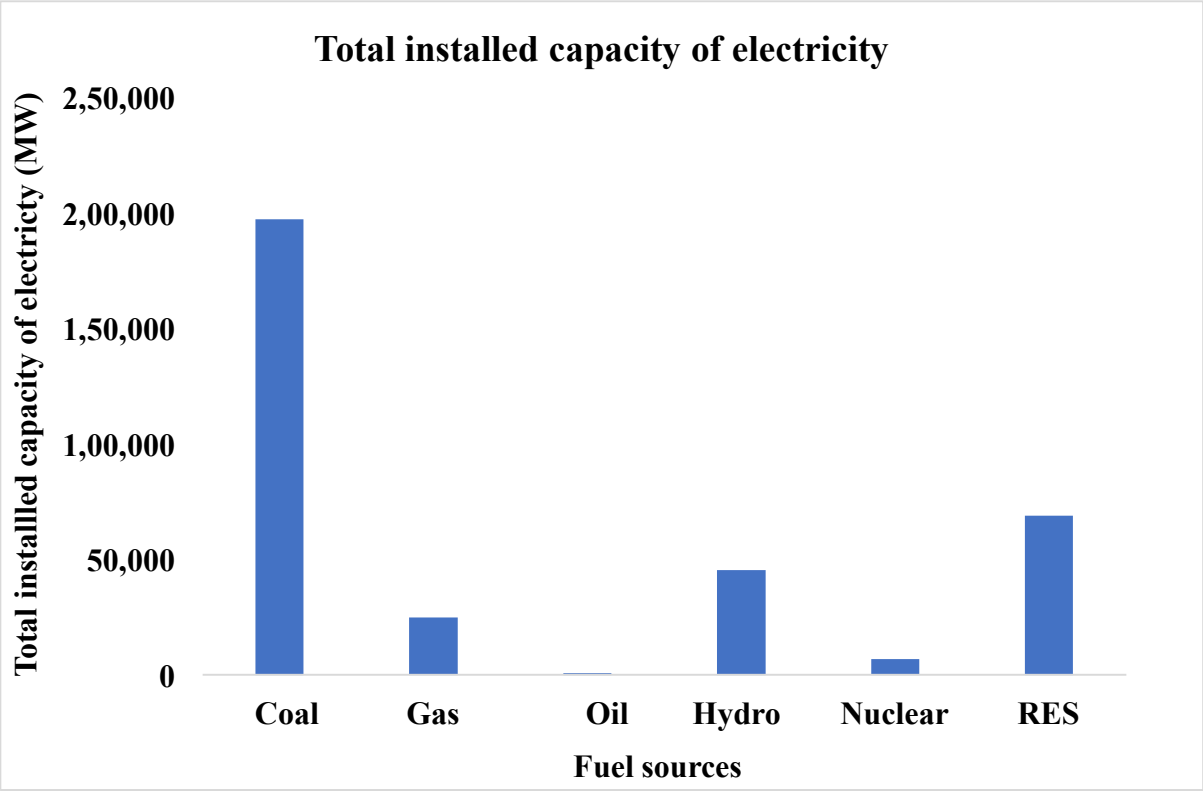

Figure 1.5. Total installed capacity of electricity based on fuel sources up to year 2018 [10].

Apart from this, target of electricity production, which was around 1229.400 BU in the year 2017-2018. This amount was equivalent to 5.97% growth over actual production of last year 2016-2017, which was around 1160.141 BU as compared to 1107.822 BU in the year of 2015-2016 showed a growth of almost 4.72% [10]. Figure 1.6 represents the energy production by conventional resources and Figure 1.7 shows the percentage energy generation growth.

Nowadays, Indian government has taken progressive steps toward the achievement of securing the energy future and launching of National Solar Mission is an effort to achieve the target of total installed capacity which is around 100,000 MWp along with the installation of decentralized roof-top solar photo-voltaic (PV) with the capacity of 40,000 MW up to 2022 [11,12].

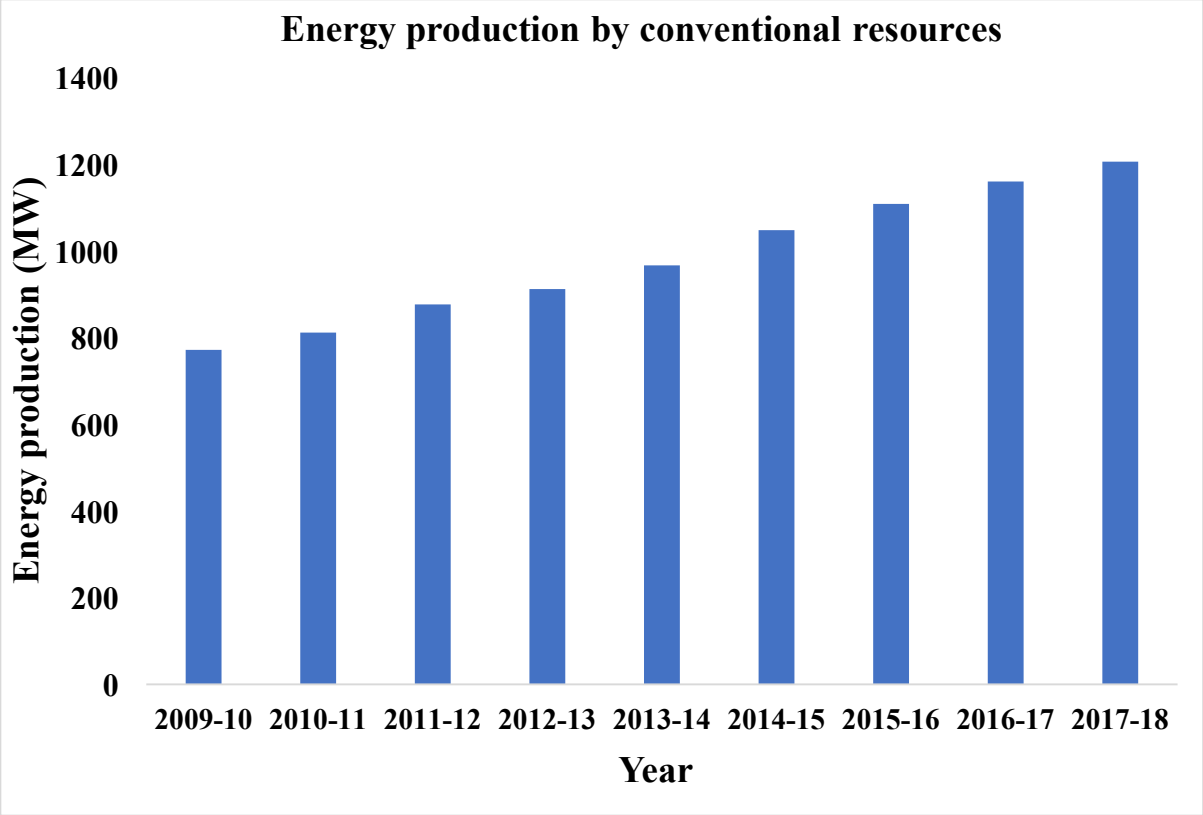

Figure 1.6. Energy production by conventional resources [10].

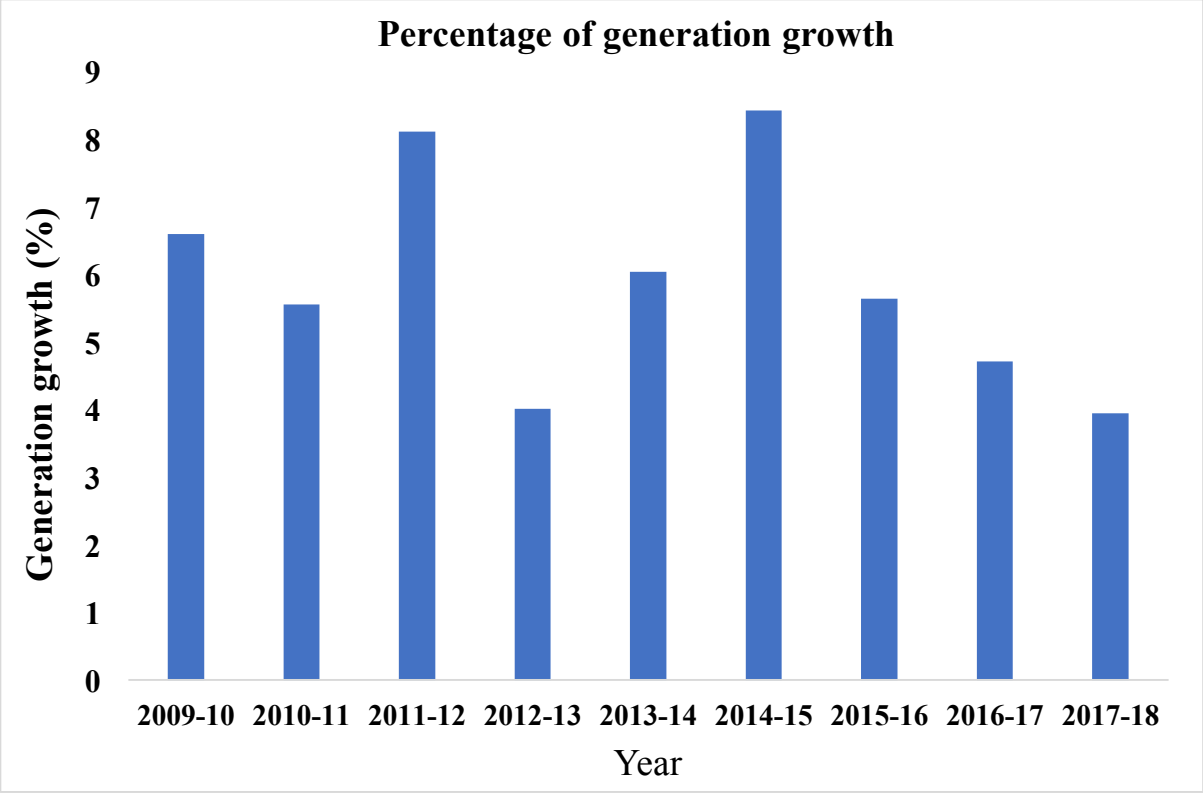

Figure 1.7. Percentage energy generation growth [10].

Figure 1.8 shows that the per capita average consumption of electricity for the world and other advanced nations [12,13] were very high as compared to India's per capita electricity utilisation, which was about 765 kWh/year [12]. Additionally, per capita energy consumption by Indian states such as Goa, Punjab, Gujarat, and Haryana almost more than twofold the Indian average. However, states like U.P., Assam, Manipur, and Bihar having the fraction of Indian average of per capita electricity utilization as illustrated in Figure 1.9 [12].

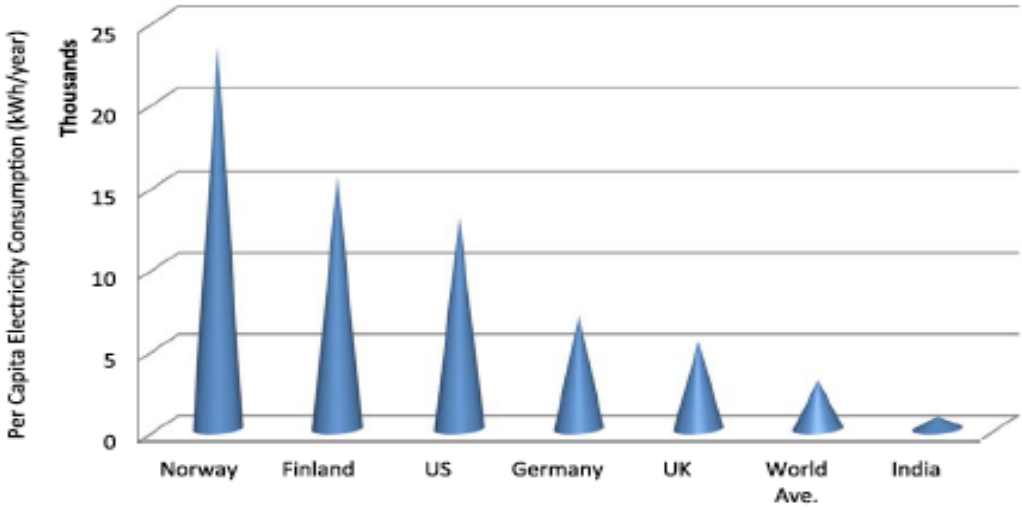

Figure 1.8. Per capita consumption of electricity (kWh/year) in world [12,13].

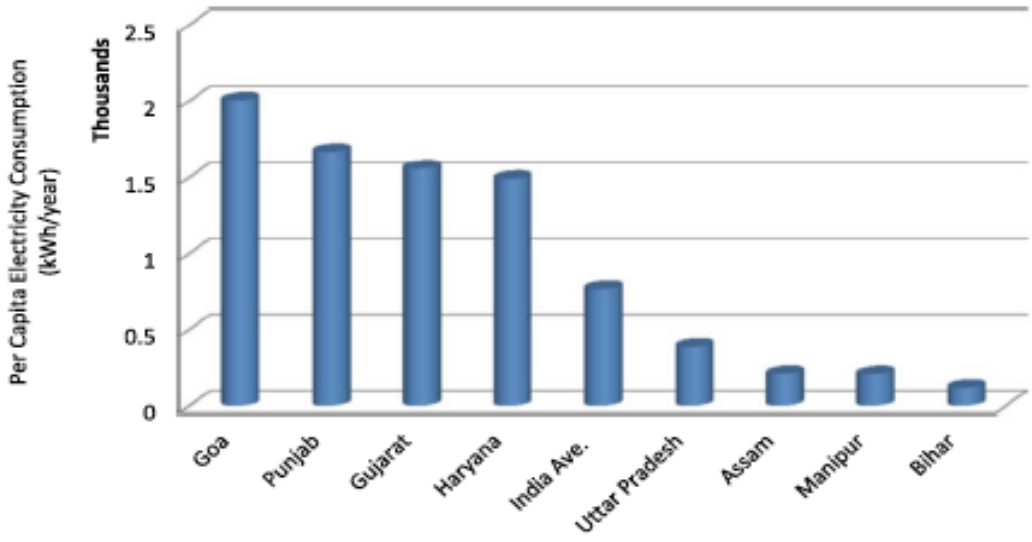

Figure 1.9. Per capita consumption of electricity (kWh/year) in Indian states [12].
(Source: Central Electricity Authority (CEA). Annual Load Generation Balance Report 2011–2012, New Delhi; 2012.)

1.3. Issues with conventional resources in India

1.3.1 Coal

Country have enough coal but its use can produce some malicious effects and problems to the entire ecosystem. In fact, the coal mining and extraction is not an environment friendly activity because of the availability of coal sites in the forest and ecologically sensitive zone that can be badly affected by such kind of human activities. On the other side, extracted coal during its use in coal-fired thermal plants for power generation can pose some serious threat to the environment. Coal plants can produce large amount of carbon dioxide (CO_2) along with SO_X, NO_X, and particulate matter that have a potential to pollute the quality of air. Other effects are waste heat can pollute the water, acid drainage, emitted ash from coal plants can pollute the soil, flue-gas desulfurization plant can produce slurry and heavy metals [12].

The main problems of coal are low calorific value and high ash content (approximately 55-60% and on an average of 35-40%) [14]. There are some adverse effect of poor coal quality and its transportation by diesel trains up to long distance can affect to the ecosystem, and health hazards, which has been discussed by Mishra [14] and these problems are challenging according to the ecological, radio-ecological, and pollution perspective in the Indian context.

1.3.2. Oil & natural gas

India do not have adequate assets of oil and natural gas in contrast to its excessive and rapidly rising energy requirement. It has been observed that the crude oil's import by India has increased up to 81% in the year 2009 as shown in Figure 1.10. From the year 1990-2009, Indian imports of energy resources has increased from 34 MTOE to 236 MTOE. In other words, dependence on imports of energy resources has increased up to 35% in the year 2009 as compared to year 1990 in which it was only 11% [12].

Asif and Muneer [15] provides an overview on energy situation of five emerging economies such as China, India, UK, USA, and Russia in which first four are the net importer of the energy. Therefore, these countries are highly dependent upon the import of conventional fuel resources to fulfil their primary energy need. They highlighted the issue of energy security especially in India that it is facing and proposed the idea of utilization of renewable technologies to avoid any kind of energy deficit.

Mathews and Tan [16] also discussed that how the energy security can be improved by enhancing the renewable capacity in developing countries like China and India. In respect of energy security, they also added an important point that renewable energy technologies can be manufactured at any place and deployed on such sites with the proper accessibility to water, wind, and sun unlike to coal, oil, and gas with the limited access as well as focus to geographical stresses. Apart from this, energy security and financial health of a country is affected by the volatility in prices of crude oil internationally because of disruptions in supply of oil which in turn a pressure is created on the country's foreign exchange reserves [17]. Also, India's crude oil import is dependent on the Middle East and any problem related to this region can create the problems in energy and national security, which can directly affect to the economical and physical situation of a country [17].

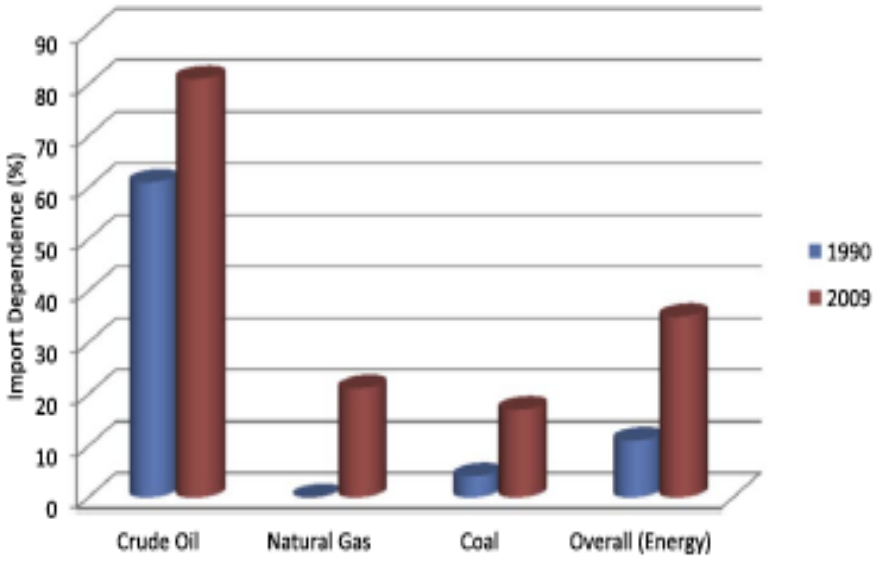

Figure 1.10. The fuel-wise growth in import dependence from the year 1990 to 2009 of Indian energy sector [12,54].

Husain Ahmad [18] discussed some positive and negative effects of oil prices on the Indian economy. On the positive side, the decrease in oil price leads to direct savings which results in capital can be invested to purchase of long term assets, whose market return is very good. As a key component of consumer price index, it can directly affect to the Inflation rate, which can decrease with the decrease in price of oil. Moreover, capital saving as a result of low oil prices can be directly invested on the roads, power, education, health, and other sector like telecommunication that are potential areas of an economy. On the negative side, Indian products have a huge market in oil producing countries. Therefore, a repulsive action can be

seen on Indian investors if a decline will come in imports and currency valuations. As a sixth major exporter of petroleum products, India would be chances to face the negative effects on its manufacturer's business due to suppressing demand of these petroleum products. Also, a negative effect of decreasing oil prices can be seen on the remittance of labour force in Gulf countries that has been employed by India.

1.3.3. Large hydro plant

India has around 18% installation of large hydro of its total installation capacity [12]. India has set up only 25% of its total potential of hydroelectric power in contrast to rich countries, who have developed around 80% of their total potential [19]. In the recent years, large hydro plants have been facing the tough times in India because of protests by local people against their impact on the environment, ecological, and social damage. Save movements related to Narmada and Anti-Tehri Dam are the perfect example of these protests, which are against the construction of large hydro projects on the Narmada and Ganges rivers, respectively [12]. Pandit and Grumbine [20] designed a model related to the species area relation (SAR) to find out the impact of recommended and under-construction dams on the Himalayan environment and their results reveal that these 292 dams could impact total 90% of the Himalayan valley. In a different study, they have proposed some policy measures and new planning and implementation procedures to mitigate the future danger to the natural ecosystem [21]. Also, one more complex and critical issue has come in these days that is sharing of water between the states through which the river is passing [12].

1.3.4. Nuclear power

The nuclear program was started in India in the year 1960 and 1969, Tarapur nuclear plant was commissioned with a capacity of 320 MW. From that time, its growth was very slow and almost steady and up to 2015, India had only twenty-two nuclear reactors in its seven plants grounded on nuclear power with the 6780 MW total capacity and almost five more nuclear reactors are under construction with the capacity of 3300 MW [12], and the share of electricity generation in the year 2017 by nuclear energy was 3.22% of the total electricity generation by all sources in country [22]. According to Jewell [23] some well-established nuclear power countries such as China, India, Korea, and Pakistan having the GDP/capita purchase power parity less than $5000. However, they also pointed out that as a well-established nuclear power country India

alongside Pakistan and Russia having low political stability. Grover and Chandra [24] present the scenario for electricity growth in India and a strategy to meet the projected demand. They projected an idea of enhancing the electricity generation from 3% to a quarter of the total amount to limit the import of cumulative energy to about 30% during the next half century. In this respect, Department of Atomic Energy has started programme to enhance the installed capacity of nuclear power of around 20 GWe by the year 2022.

Grover [25] discussed that India can accelerate its nuclear installed capacity if India will get access to the International Uranium supplies and manufacturing of nuclear equipment will results in augment the manufacturing capabilities of Industry of the country which in turn Indian nuclear equipment's export will increase.

Ramana et al. [26] found that electricity generation by coal based thermal power plant will be cheaper than the electricity produced by the Indian nuclear reactors but in case of 220 MW smaller capacity nuclear plants. However, they pointed out that electricity generation by larger nuclear power plant would be cheaper than same sized coal power plant.

Bajaj [27] has discussed that systematic evaluation, resource optimization, and available technology are the factors behind the variety in nuclear reactor programme in India. Also, to maintain the institutional capacity to satisfied the current needs, changing need of dynamic environment, and safety supervision is the responsibility of a dedicated body (AERB).

Joskow and Parsons [28] predicted the future of nuclear energy based power plants globally after the Fukushima accident. They have acknowledged that in India, total 6 units of nuclear power plants are under construction followed by the China, Russia along with former states of FSU. They have put an argument that incident of Fukushima will reduce the nuclear energy expansion in future but at the present time, its effect is quite uncertain in the world. However, the nuclear programme in India is continuously run at the same rate as planned. Thus, after accounting all the issues associated with the conventional energy resources, it has been analysed that if India want to compete with the issue of energy security, environment, and to meet its increasing energy demand in near future, renewable resources can definitely improve the situation with respect to every aspect.

1.4. Renewable energy sources (RES)

The RES is considered as a clean or green energy resources and their optimal use to minimize the environmental impacts alongside the reduction of secondary waste, and these are also considered as sustainable resources with respect to present and forthcoming economic and

social needs. Basically, the birthplace of all energy is sun, and light as well as heat are the primary forms of solar energy. The transformation and absorption of sunlight as well as heat by environment has been possible through the different ways which results in flows of renewable energy, for instance biomass and wind energy. Also, RES has a potential to mitigate the effect the greenhouse gases and global warming caused by conventional energy resources [29].

Basically, energy resources have been classified into three groups such as fossil energy, RES, and nuclear resources [29,30]. Also, RES has an ability to produce energy again and again, for instance solar photovoltaic and solar thermal, small hydro, biomass, wind, and geothermal etc. known as alternative energy resources [29]. In addition, Figure 1.11 shows the resources of renewable energy and their use in energy conversion.

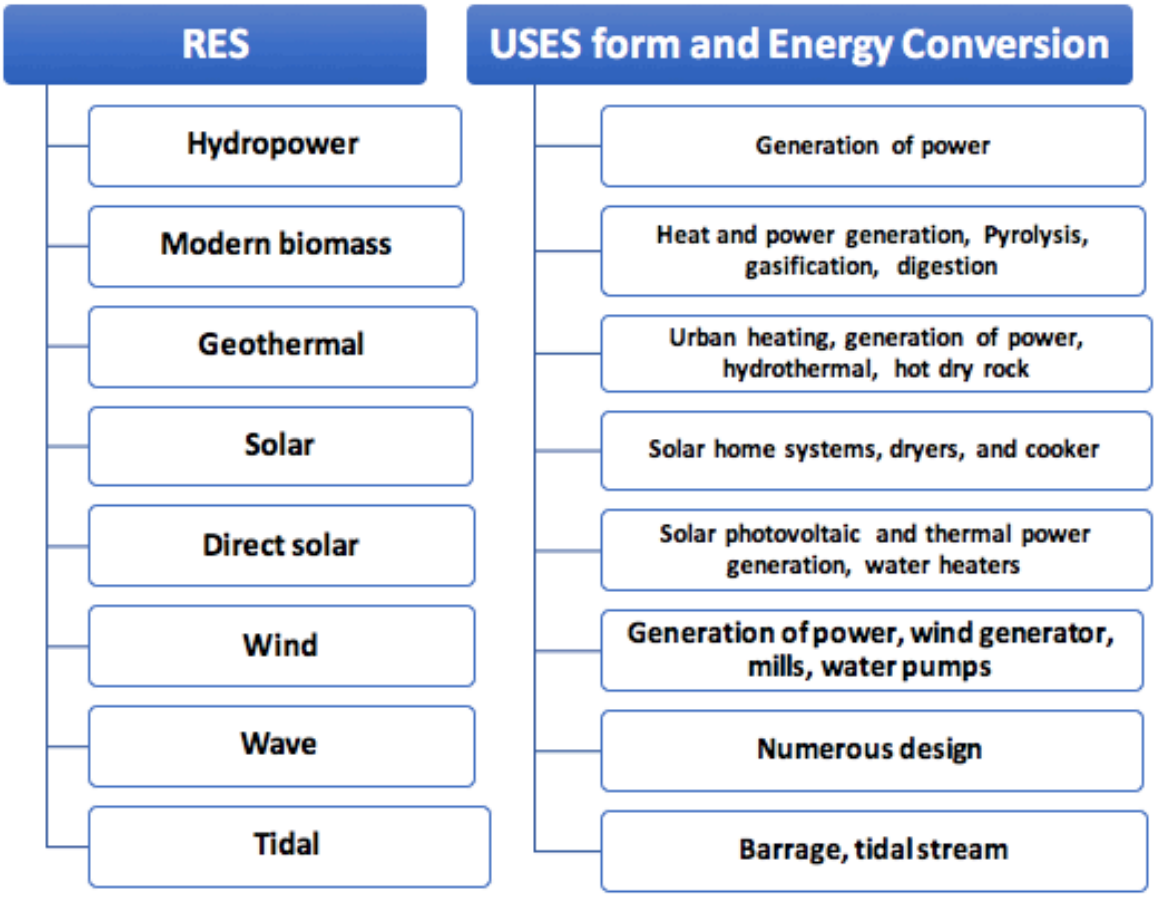

Figure 1.11. Resources of renewable energy and their use in energy conversion [29,31].

Figure 1.12. illustrates the renewable energy scenario in world from the year 2020 to 2040. It has been found that total consumption of the world will be around 11425, 12352, 13310 MOTE by the year 2020, 2030, 2040, respectively [29,32]. Moreover, world is facing more

problem related to the environment such as climate change which is popular with the name of global warming or greenhouse effect [29]. The enhancing intensity of greenhouse gases in the atmosphere is responsible to trap the heat emitted from the surface of earth which increases the temperature of surface [33]. The greenhouse gases are CO_2, CH_4, CFCs, halons, N_2O, ozone, and peroxyacetylnitrate [33].

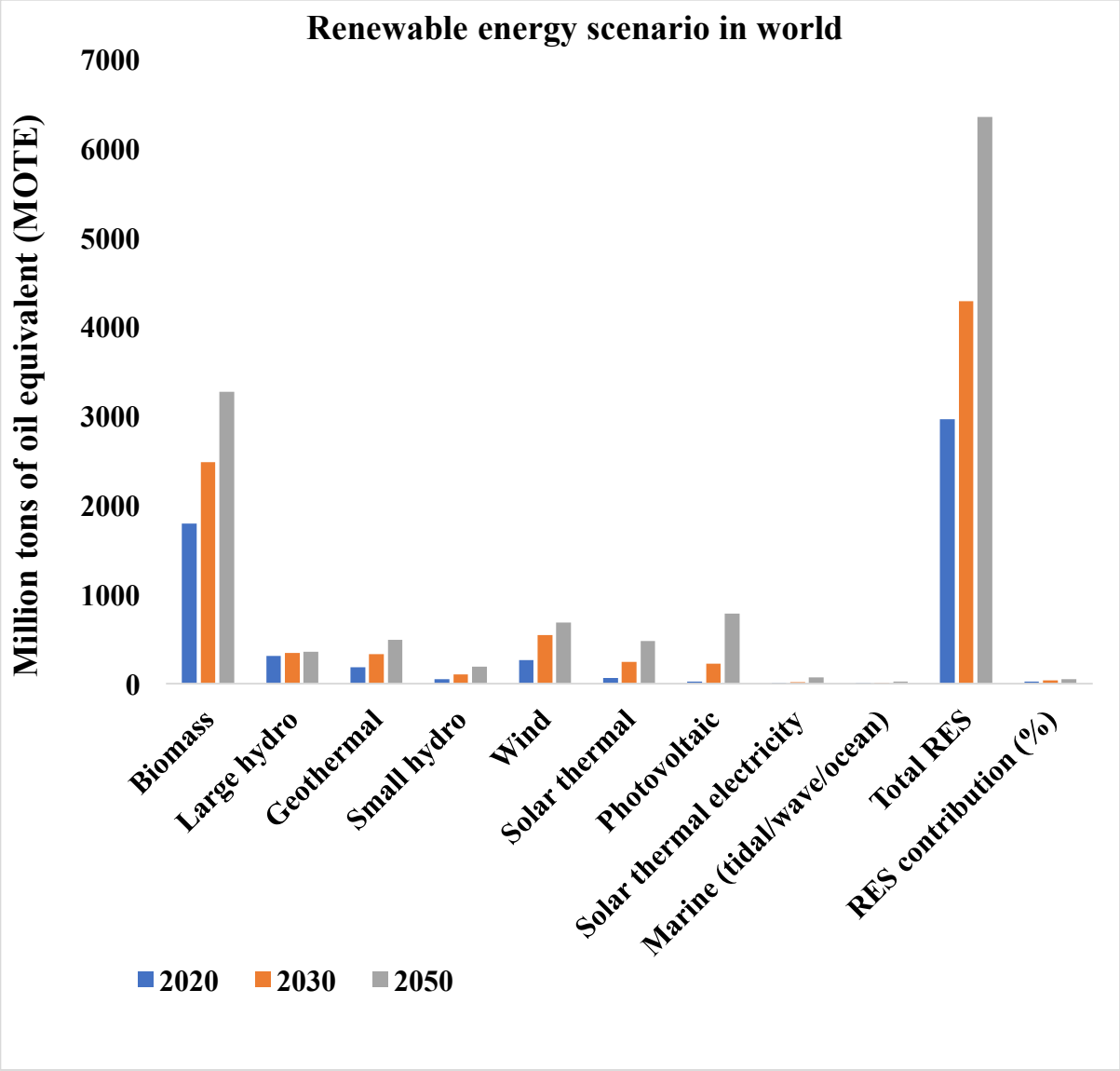

Figure 1.12. Renewable energy scenario in world from 2020 to 2040 [29,32].

Figure 1.13. shows the problem of global climate change or greenhouse effect. RES has capability to fulfil the requirement of domestic energy and to deliver the energy services with nearly negligible emission of air pollutants and gases responsible for greenhouse effect. Also, the development of systems based on renewable energy will help in the improvement of reliability in energy supply, economy of organic fuel, to resolve the issue of local energy and

supply of water, enhancing the living standard and jobs, to guarantee the sustainable growth of isolated areas, and implementation of international agreements with regard to protection of the environment [35].

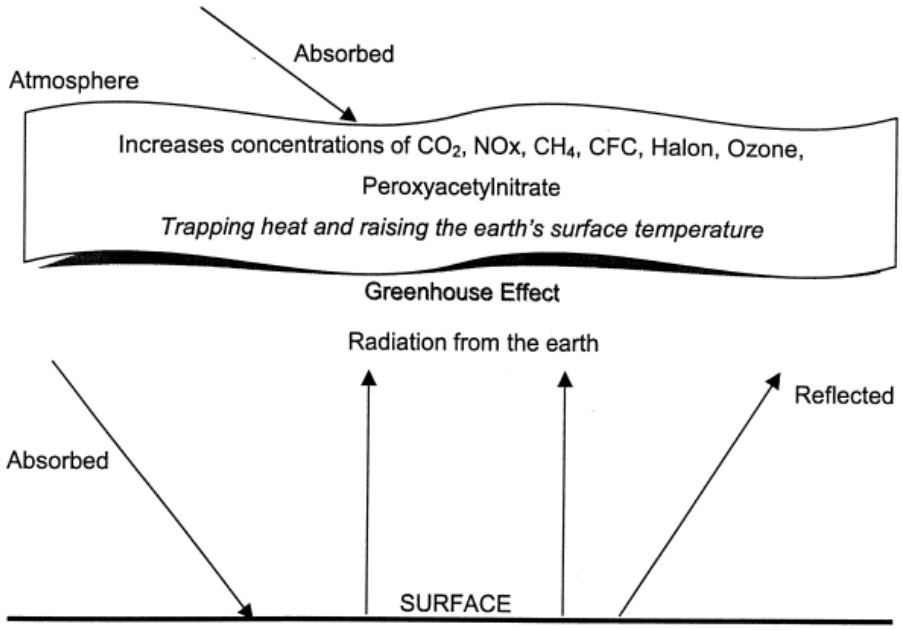

Figure 1.13. Schematic diagram of greenhouse gas effect [34].

1.5. Solar energy

Solar energy is a renewable or alternative energy source. The earth captured around 1.8×10^{14} kW of total energy emits by sun at a rate of 3.8×10^{23} kW [36]. Amount of solar irradiation received by earth surface around 1000 W/m^2 in a whole day [37].

Solar radiations are incident on the earth's atmosphere are in form of beam, diffuse and total radiation. In addition, solar radiations that directly comes to earth's surface is known by beam and direct radiations. Apart from this, scattered radiations coming to the surface of earth are known by diffuse radiations. The combination of both beam and diffuse or scattered radiations coming on the surface of earth is known as total and global radiations. Total energy received by earth from sun per unit time, on a surface of unit area kept perpendicular to coming radiation on outside the earth's atmosphere (i.e. space) is known as solar constant and its value is 1350 W/m^2 [38]. The radiation network of India is shown in Figure 1.14.

The solar energy can be utilized in cooking, water heating, and crop drying like thermal applications [29]. Solar energy for cooking can be considered as one of the promising and leading energy source [40-42].

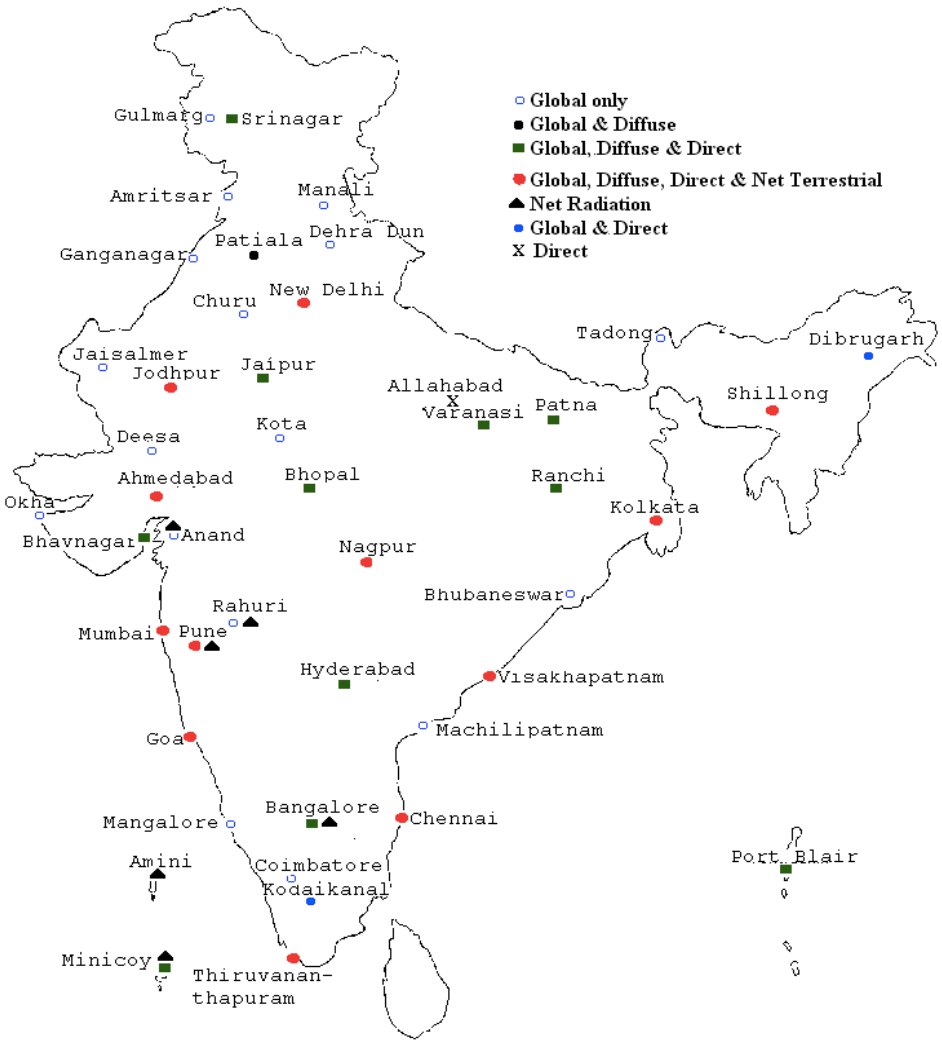

Figure 1.14. Indian radiation network [39].

Figure 1.15 illustrates the box type solar collector. Domestic size water heating system operated by solar energy has an ability to fulfil the requirement of hot water for a family of four people and to save the atmosphere due to reduction in amount of greenhouse polluting gases [43]. It has been assessed that a solar energy based water heating system of 100 liters per day capacity, which is domestically operated with the utilization of 50% capacity can mitigate emission of CO_2 of around 1237 kg in a year [44].

Figure 1.16 shows the water heating arrangement operated with solar energy. Apart from this, solar drying with zero energy cost can be used to process the vegetables and fruits in clean, hygienic, and sanitary conditions to national and international standards along with the saving of time, energy, less area required, increase the quality of product, process becomes more efficient as well as provide a protection to environment [45]. The CO_2 production for a

drying system that consumes a large amount of energy in an industrial process, electricity of 100 kWh per day required for more than 25 days/month in the operation of 11 months in a year, which came around 14.77 tons of CO_2/year [46].

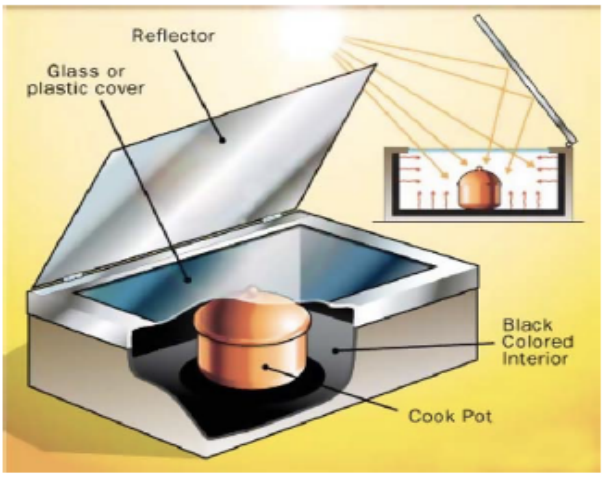

Figure 1.15. Box type solar collector [29].

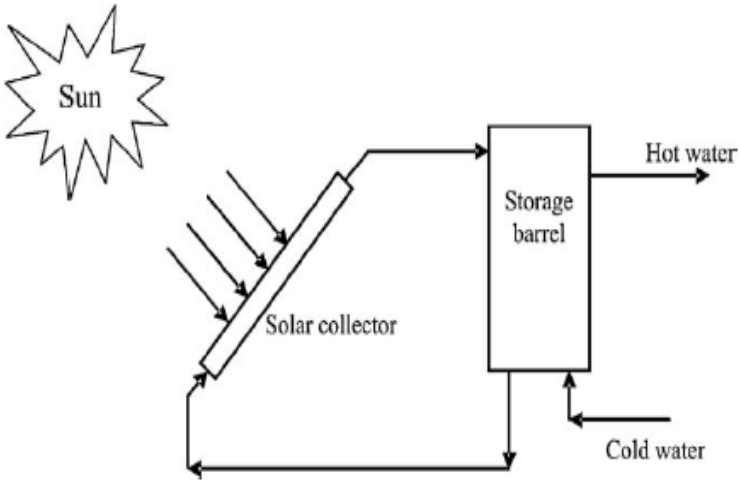

Figure 1.16. Diagram of water heating system operated with solar energy [29,47].

1.6. Solar thermal power system

Sun oriented energy is a vital asset due to its benefits and it very well may be used to give electricity to the remote regions in the world, which are in very high number but these locations have such plentiful supply of solar irradiation intensity, thus the electricity production with the help of solar energy in these areas is quite possible [48]. The process in which collected solar energy directly transformed in to electricity with the help of a device that convert heat to electricity is known as solar thermal electricity power system [49].

Solar thermal power has presumably the most noteworthy capability of any single renewable energy area, be that as it may, has been deferred in market development since the 1980s on account of market resistance to the great sizes plants, and poor support as far as political and budgetary from the incentive programmes. Nevertheless, right now there is quick growth appearing both in the basic technology and the strategy of market, and views for rapid development show up now to be very optimistic for more up to date approaches [49].

Sharma et al. [50] have discussed that emerging renewable energy technologies such as solar thermal electricity also known as a concentrated solar power (CSP) can be established as a forthcoming potential choice for generation of electricity in India and they concluded that solar energy development possesses low marginal cost of generation, native and dispersed that can enhance the energy security by spreading supply, reducing the dependence on import, and can mitigate the volatility in the price of fuel. Sharma [51] discussed that how technology can help in improvements, competition between manufacturers, supply, and installation leading to cost reduction, which is competitive to the power generation by conventional sources. Khare et al. [52] concentrates his study on major constraints that obstructing the renewable energy development in India. Ansari et al. [53] suggests the various ways for removal of barriers to implementation of solar power in India and maximum number of solar power projects can be installed in the country only if organizations and government bodies better understands that how to prioritise and manage their resources in an effective and well-organized way.

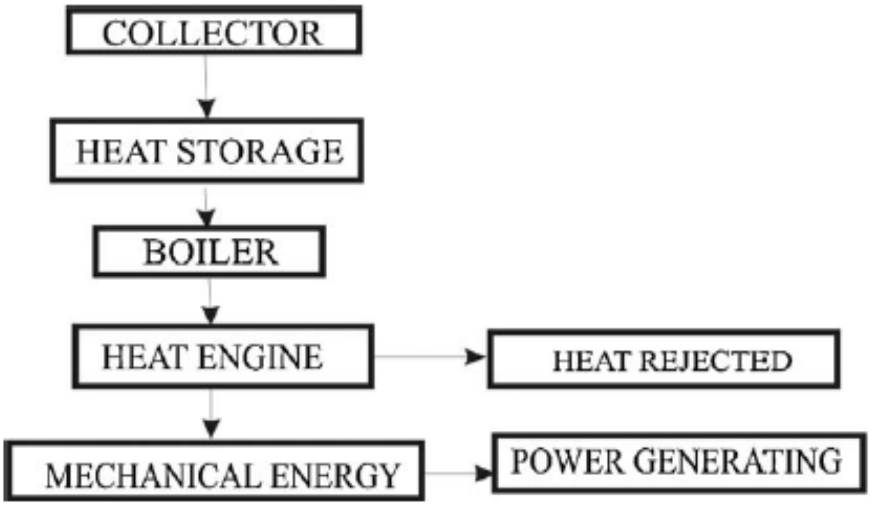

Figure 1.17. Solar thermal conversion system [29].

Commercially operated CSP plants were developed first in 1980s and in USA, the levelized energy cost (LEC) of solar electric generation system (SEGS) is around 12–14 ¢/kWh [51]. SEGS consist of nine solar power plants in Mojave Desert, California and it is a largest facility on the planet for the generation of solar energy [51]. The total installed capacity of SEGS plant is around 354 MW, which makes it the largest solar plants installation in the world [51]. The gross output on an average for all SEGS's nine plants is around 75 MWe with a capacity factor of 21%. The LUZ industries had built SEGS plants, which were commissioned between 1984 to1991 [51].

1.7. Solar collector

Solar collector is considered as a unique sort of heat exchanger that transform the energy of solar radiation to the transport medium's internal energy and it is a major element of the solar system. Basically, solar collector absorbs the solar radiations coming from the sun, convert in to heat and then transform it in to a selected fluid flowing through the collector. The fluid used can be air, water, and oil. The circulating fluid's collected solar energy can be used directly in water heating and space conditioning, and this energy can be stored in a thermal storage unit, which can be further utilized in night hours as well as in cloudy days [55]. Solar collector can be classified in to two ways: non-concentrating or stationary type collector and concentrating collector. Stationary collectors such as flat plate collector (FPC) has the same intercepting area and solar radiation absorbing area. However, in a sun-tracking solar concentrating collector, beam radiation of sun will be intercepted and then focuses on the smaller receiving area with the help of concave reflecting surfaces. Thus, radiation flux enhances [55].

FPC's position usually fixed in a permanent way and do not require a tracking system to track the movement of sun. The collector should be oriented toward the equator and in northern hemisphere, it should be facing south. whereas, it should be facing north in the south hemisphere. Also, depending on the application, the location's latitude should be with the variation in angle of 10-15° more or less, which is equal to the optimum tilt angle of collector [55].

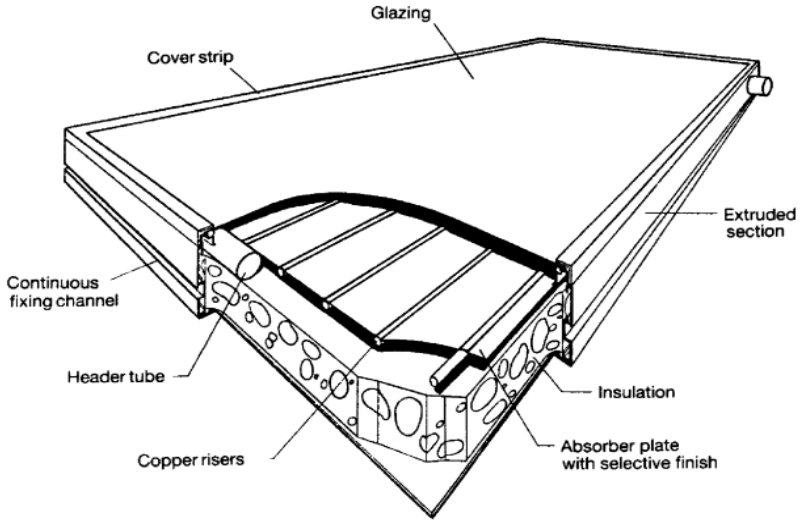

Figure 1.18. FPC in a pictorial view [55].

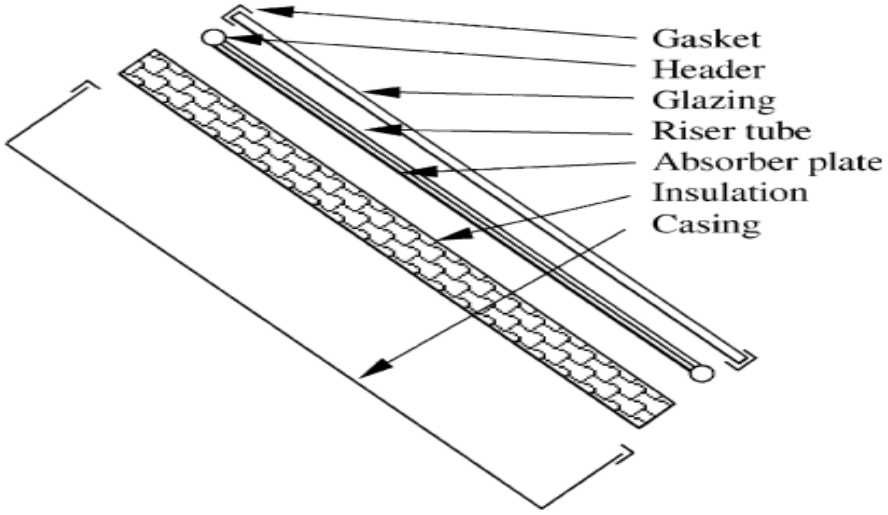

Figure 1.19. FPC in an exploded view [55].

However, sun oriented energy is optically focussed before being transferred in to heat in the concentrating collectors. The mirrors or lens are used to reflect or refract the solar radiations in order to achieve the concentration. These reflected or refracted solar radiations are concentrated on a focal axis, which increases the energy flux in a receiving target. Non-imaging and imaging are the two types of the concentrating collector depending on whether the sun image is focussed at the receiver or not. Compound parabolic collector is a type of non-imaging collector. Whereas, solar parabolic trough collector (SPTC), linear Fresnel

reflector (LFR), parabolic dish reflector (PDR), and central receiver or solar power tower (SPT) is a type of imaging collector [55].

There are various important terms of concentrating collector and these are discussed as below [56]:

1. Aperture area: solar radiations are incident on collector through this area.
2. Acceptance angle: it is denoted by '$2\theta_a$' and it is the angle upon which incident beam radiation can deviate from normal to the aperture plane and still reach to the absorber or receiver surface. If acceptance angle is very large, collector requires only occasional adjustments. Further if acceptance angle is small then collector has to be adjusted on continuous basis.
3. Absorber area: Total surface area of the absorber tube upon which solar radiations are concentrated. Noted that useful energy can be obtained from this area of collector.
4. Geometrical or area concentration ratio: it is denoted as 'C' and expressed as ratio of collector aperture's area to absorber's area, its value can vary from unity to thousands for different type of collectors.
5. Intercept factor (γ): it is expressed as the ratio of energy achieved by the solar radiations intercepted through absorber of certain width to the total energy of radiations redirected through focusing device and its value is almost unity.

Advantages of concentrating collector over conventional FPC [55]:

1. As compared with FPC, concentrating collector can achieve the higher working fluid's temperature for the same energy collecting surface which implies that thermodynamic efficiency can be higher.
2. Because of little heat loss area relative to the area of receiver, concentrating collector's thermal efficiency will be greater.
3. As compared with FPC, reflecting surfaces of concentrating collector requires less material and simple in structure. Therefore, solar collecting surface's cost per unit area will be less.
4. In concentrating collector, receiver has relatively small area per unit of collected solar energy. Thus, to diminish the heat losses and improve the collector efficiency, selective surface treatment and vacuum installation are economically viable.

Disadvantages of concentrating collector over conventional FPC [55]:

1. Depending upon the concentration ratio, concentrating collector gathers little diffuse radiations.
2. To follow the movement of sun, concentrating collector requires some form of tracking device.
3. Periodic cleaning and refurbishing may be required in the concentrating collector because of its reflecting surfaces have chances to lose their reflectance.

1.8. Solar concentrator's classification

Solar concentrators can be categorized in various ways or techniques. These can have reflecting or refracting type surface and totally relies on the concentrating device used to focus the sun's radiation on the surface of absorber. Additionally, reflecting surface are further categorized into various types, for instance flat, spherical, and parabolic. As talked about above, solar concentrators can be of imaging (i.e. line or point focussing) and non-imaging type [1].

Concentrator's characterization also relies on the measure of temperature necessity for different applications. High concentration ratio implies attainment of high temperature. Concentrating collector's effective working also relies on the adopted mechanism of tracking, which can be done on intermittent and continuous basis. Additionally, it can be achievable about one axis and two axes. FPC alongside mirror adjusted at the edges has an ability to reflect the sun oriented radiations on collector's absorber plate as appeared in Figure 1.20 (a). It's concentration ratio is low nearly unity and can attain higher temperature as contrast with FPC alone [1].

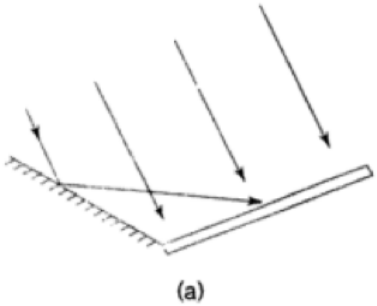

Figure 1.20 (a). FPC along with plane reflectors

Concentrating collector, for e.g. compound parabolic as discussed before is a type of non-imaging collector and also made up from curved parts of two parabolas as illustrated in Figure 1.20 (b). This kind of collector possesses concentration ratio of moderate range, for instance

3 to 10. Instead of this, it has the higher acceptance angle, which implies that collector could be adjusted on the occasional basis [1].

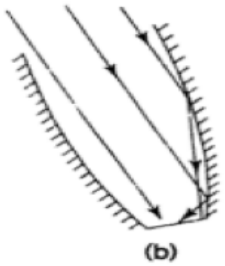

Figure 1.20 (b). Compound parabolic collector [1].

Furthermore, Figure 1.20 (c) shows the cylindrical parabolic collector, in which sun rays are focussed or image creation on the parabolic collector's focal axis and in this configuration, concentrator has to rotate to follow the movement of sun as unlike to a collector in which concentrator is fixed and receiver is moving as shown in Figure 1.20 (d) [1].

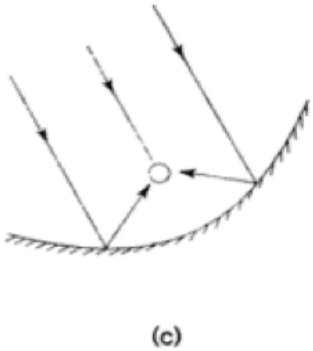

Figure 1.20 (c). Cylindrical parabolic collector [1].

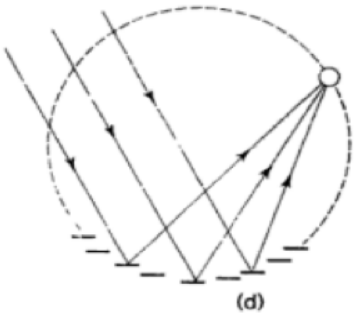

Figure 1.20 (d). Fixed circular concentrator along with moving receiver [1].

Moreover, lenses can also be utilized to focus the sun light, for instance in Fresnel lens as depicted in Figure 1.20 (e). Line concentrating collectors are presented in Figure 1.20 (c),

(d), (e) with their varying concentration ratio from 10 to 80 and achieved temperature range lies between 150°C to 400°C [1].

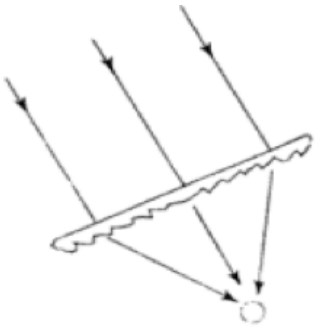

Figure 1.20 (e). Fresnel lens [1].

Besides, parabolic dish collector as a type of point focussing can attain higher concentration ratio (i.e. varying from 100 to 1000) and temperature (i.e. up to approximately 2000°C) as compete with line focussing collector. Lastly, high amount of energy can be concentrated on a point through the facility of central receiver that has been employed on a large scale in the world. In this arrangement of concentrating system, large number of mirrors also recognized as heliostats are used to concentrate sun light on the central receiver that has been positioned at the top of tower [1].

1.9. Concentrating solar power (CSP)

To focus a large area of sunlight in to a small beam, CSP use the lens or mirror and tracking device. Then, this concentrated heat may be utilized as a source of energy for a conventional power plant. There are many types of concentrating technologies available but the SPTC, LFR, PDR, and SPT are the most developed systems. Also, concentrated sunlight can be utilized to heat the working fluid, which is then utilized to generate the power and energy storage purpose [51]. CSP can be utilized for various applications depends upon the energy conversion used either electricity or heat. Figure 1.21 shows the CSP used for different applications. The SPTC is the best solution for detoxification, recycling of liquid waste, and water heating like applications in the low temperature range [51].

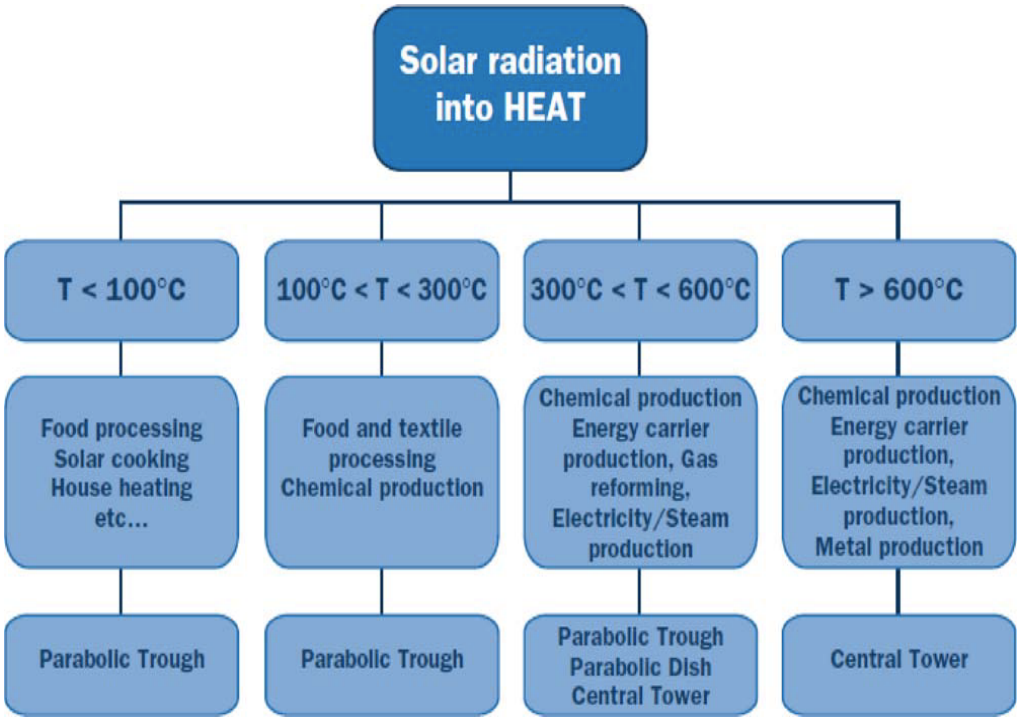

Figure 1.21. CSP system's application [51].

1.9.1. SPTC concentrating system

SPTC system use mirrored troughs to focus energy on the receiver tube in which fluid is flowing and situated at the focal line of parabola. The working fluid carrying receiver tube is located right above the middle of parabolic mirror. During the day light hours, reflector by tracking along single axis can follow the path of sun as shown in Figure 1.22 (a), To heat the fluid, troughs or the tubes are used to track the sun movement and the heated fluid is then pumped through the heat exchangers to generate the steam up to a superheated state to run the turbine generator. Also, SPTC system provides the best land-use factor [51]. SPTC can be used to produce the temperatures between 50℃-400℃. SPTC is generally manufactured by bending a sheet of reflective material into the state of parabola. The metal black tube is set along the central line of the receiver, which is covered by glass tube to reduce the losses of heat as shown in Figure 1.22 (b) [55]. In light of extensive experience and development of commercial industry with respect to produce and marketing of SPTC system makes it most advanced solar thermal technologies, and this type of system is built in modules and ground supported with the help of simple pedestals at either end [55].

As a most mature technology, SPTC is used to generate the heat with the maximum temperature of 400℃, which can be utilized to produce the solar thermal electricity and in the

process heat application. Moreover, SEGS plants are the greatest application of this sort of collector with total installed capacity of 354 MWe, which is also known by the southern California power plants [55].

Figure 1.22 (c) illustrates the parabolic trough concentrator and Figure 1.22 (d) shows the subsystems of the parabolic trough concentrator. Lastly, when collector tracking is in the north to south direction, it could be oriented in the direction of east-west, however, when collector tracking is in the east to west direction, it could be oriented in the direction north-south [55].

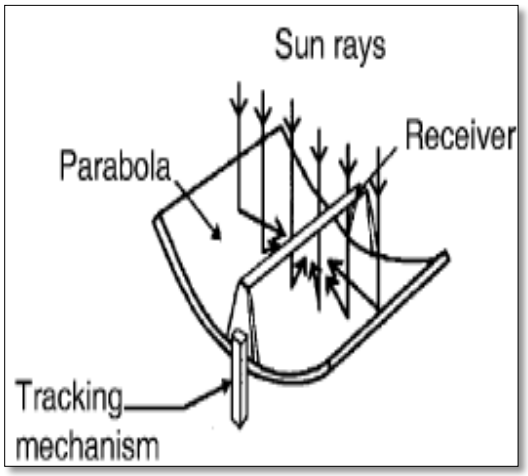

Figure 1.22 (a). SPTC system [55].

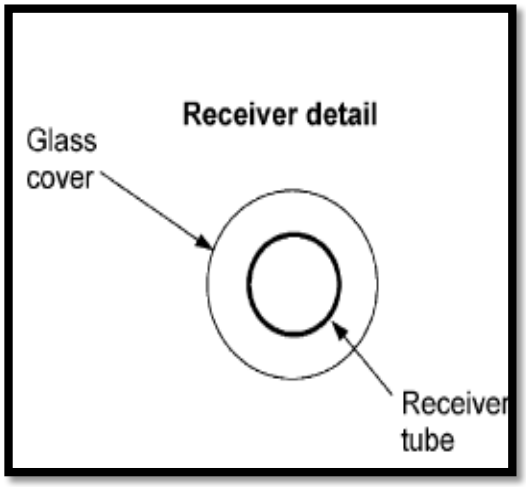

Figure 1.22 (b). Receiver of SPTC [55].

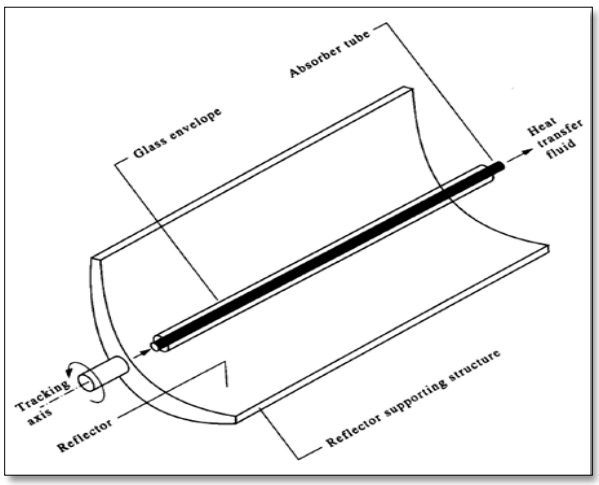

Figure 1.22 (c). Parabolic trough concentrator [57].

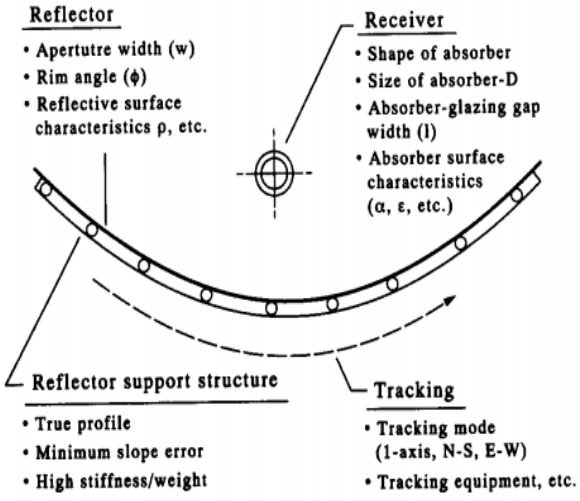

Figure 1.22 (d). Parabolic trough concentrator's subsystems [57].

1.9.2. LFR concentrating system

In this LFR system, an array mirror strips, which are arranged linearly can be used to concentrate the sunlight on a stationary receiver mounted on a linear tower. The LFR field can be considered as a split-up PTC is shown in Figure 1.23 (a) but it does not have the shape of parabola as in the case of PTC. Large absorbers can be made and their movement is restricted. Figure 1.23 (b) shows the elements of LFR collector field. The advantages of LFR over PTC system is that it utilizes reflectors of flat and elastically curved shape, which are comparatively less expensive than parabolic glass reflector. Also, to minimize the structural requirements, these can be mounted close to the ground [55].

In the 1960s, the great pioneer of solar field Giorgio Francia [58] apply the principle of LFR technology and developed linear and two-axis tracking LFR systems at Genoa, Italy. To avoid shading and blocking between neighbouring reflectors can create the necessity of additional space between reflectors. By enhancing the elevation of absorber tower, the problem of blocking can be minimized but as a result, cost increases [55].

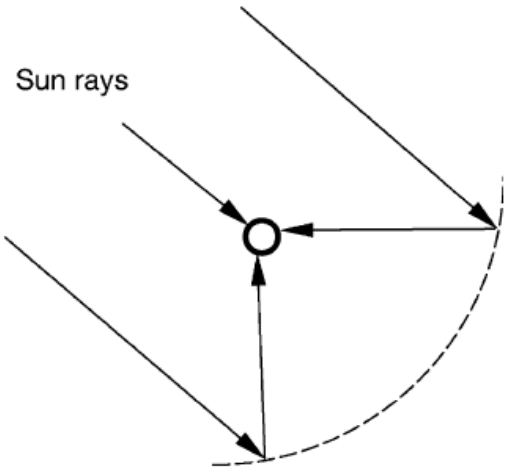

Figure 1.23 (a). Fresnel type PTC system [55].

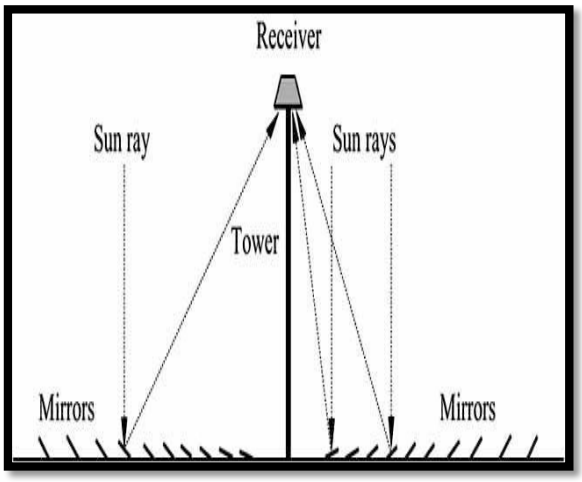

Figure 1.23 (b). Schematic diagram of LFR field along with downward facing receiver [55].

1.9.3. Parabolic dish reflector (PDR) system

PDR system use a mirror of parabolic shape that focuses incoming sun radiations to its focal point above the dish, where receiver is situated. To operate the Rankine cycle or sterling engine, PDR can be utilized. Further, it can be linked with the other dishes to provide its thermal energy to heat transfer fluid (HTF) that can be utilized to drive the turbine as illustrated in Figure 1.24 (a). The combination of a parabolic concentrating dish with the sterling engine known as sterling solar dish. The sterling solar has some advantages over the photovoltaic cells, for instance it can convert sunlight in to electricity with high efficiency and also has longer lifetime. The example of this type of technology is 500m^2 ANU "Big Dish" and it is located in Canberra, Australia [51].

Figure 1.24 (b) shows the PDR system along with receiver at the focal point and it is a point focus device that tracks the movement of sun in two axes. The radiant energy from sun is absorbed by the receiver, where it convert in to circulating fluid's thermal energy. Then, with the help of engine-generator which is coupled directly to a receiver, the thermal energy finally converted in to electricity or it could be transported by pipes to a system of power conversion. PDR system can achieve minimum temperature of 1500℃. Due to distribution of receiver throughout the collector field, PDR system is known as distributed-receiver systems. Parabolic dish has some important pros such as it is considered as most efficient device due to its focus always toward the sun, and its concentration ratio lies between 600-2000 and with respect to thermal-energy absorption and power conversion system, it can be assumed as highly efficient device. The solar dish concentrators and power conversion unit are the major components of the system. Apart from this, sterling engine is used in dish-engine systems considered as the most common sort of heat engine [55].

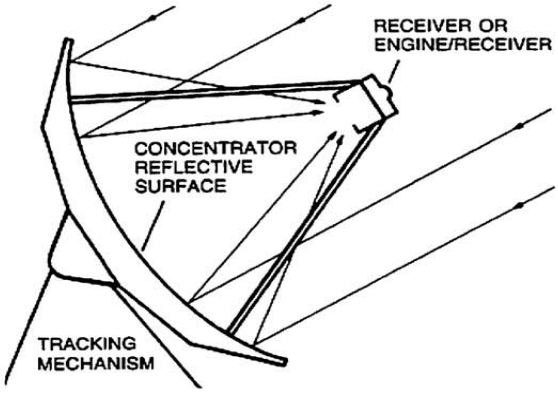

Figure 1.24 (a). PDR system [51].

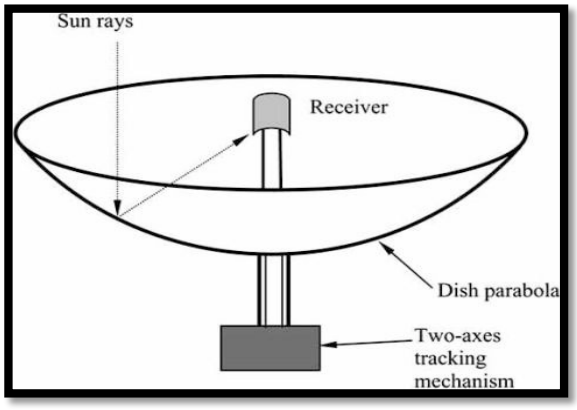

Figure 1.24 (b). Diagram of a PDR system [55].

1.9.4. Heliostats/central receiver system

In this device, a heat transfer fluid carrying receiver that is located at the top of tower that is surrounded by a field of thousands of mirrors (heliostats) used to concentrate the sunlight on central receiver and this type of configuration is known as central receiver tower or solar power tower as illustrated in Figure 1.25. A separate tracking device is connected to each heliostat that keep it focussed on the central receiver to heat the circulating or transfer fluid, which is then used to run the turbine. Among the other CSP systems, power tower is very cost effective, and its energy storage capability and efficiency is also higher. The example of this type of technology is the Solar Two in Barstow located in California and the Planta Solar 10 in San-lucar la Mayor commissioned in Spain [51].

This technology has some advantages such as their concentration lies between 300 to 1500, therefore, it is highly efficient with respect to energy collection and convert it in to electricity. Also, it can store thermal energy very conveniently. As compared to parabolic trough collector, central receiver has an ability to reduce the mid-term cost of electricity because it allows many intermediate steps between the high energy cycles using gas turbine that operates at temperature above 1000℃ and conventional Rankine cycle [55].

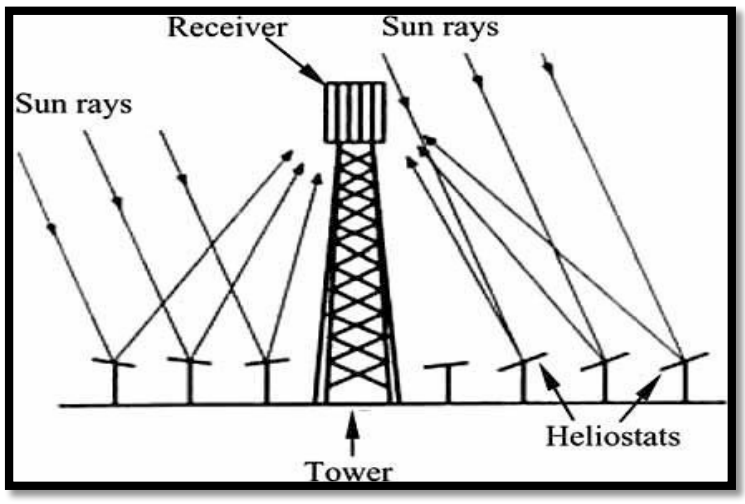

Figure 1.25. Diagram of central receiver tower [55]

1.10. Supercritical carbon dioxide (SCO_2) cycle technology

Carbon dioxide is highly stable, nontoxic, abundant in nature, inexpensive, non-flammable, and also possess low critical properties [3]. In 1960s, Feher [59] and Angelino [60,61] started their distinct studies on the utilization of SCO_2 instead of conventional working fluids and the low critical temperature of CO_2, which is around 30.98℃ needs low temperature cooling water but this facility is not present everywhere. Therefore, this limitation restricted the use of CO_2 only in gas state.

Angelino [62] reported that if CO_2 will be compressed around its critical point, specific volume will be also reduced at the critical conditions that results in decreases the compression work. Thus, efficiency of cycle will be higher. In recent years, researchers have been more attracted toward the application of SCO_2 cycle for nuclear power production in gas reactors [63,64]. Dostal et al. [63] found that recompression SCO_2 (R-SCO_2) cycle has a potential to integrate any kind of nuclear reactor with a more than ∼500℃ core outlet temperature as well as it can reduce the capital cost as competed with Rankine steam or helium Brayton cycles. Moisseytsev and Sienicki [64] has investigated the SCO_2 Brayton cycle's alternative layouts for a sodium-cooled fast reactor and in the context of power converter for the 250 MWt advanced burner test reactor, they have also calculated the efficiency of SCO_2 Brayton cycle. Turchi et al. [65] found that under dry cooling conditions (compressor inlet temperature varies from 42°–60°C), SCO_2 cycle has an ability to achieve efficiency more than 50%. Also, it has advantages such as efficiency and power density is high, large power scalability, compactness, and low cost. Moreover, SCO_2 cycle can be assumed as alternative to steam Rankine cycle (SRC) and it could be integrated to various heat sources such as nuclear energy ranging from pressurized water reactors to the nuclear reactors of next generation as well as fusion reactor uses. Apart from this, for the fossil fuel powered plants, SCO_2 cycle can be employed as a topping as well as bottoming cycle in gas combined cycle. In addition, RES such fuel cells at high temperature, CSP systems, and geothermal power plants will be developed as a promising source soon [66].

Figure 1.26 represents the comparison of power conversion systems based on air, steam, and SCO_2. Figure 1.27 shows the potential applications of SCO_2 cycle. SCO_2 cycle can be designed for the coal-fired power plant and it can also be employed for the application such as exhaust/waste heat recovery [66]. As compared to SRC system, the process for recovery of waste heat by SCO_2 cycle from small gas turbine is practically feasible [66]. The important characteristic of SCO_2 cycle is that cold side flow's specific heat is two to three times upper than the specific heat of hot side flow in recuperator [66]. Some other benefits of SCO_2 cycle technology are:

1. As compared to SRC system, the thermal efficiency of SCO_2 cycle can be increased up to 5% [66].
2. As compared with conventional SRC system, turbomachinery in case of SCO_2 cycle can be much smaller as well as size of system could be reduced overall up to four times [66].
3. As competed with SRC system, requirements of purification system in SCO_2 cycle are lower to prevent air ingress, which is due to its minimum pressure higher than critical pressure of CO_2 (i.e. 7.38 MPa). Therefore, the system of power conversion could be much simpler as contrast to steam cycle in which gas ingression will be present due to lower condenser pressure. As a result, requirement of complex purification system [66].
4. With respect to ventilation system installed to tackle with sudden release of large amount of CO_2 in power conversion system, CO_2 is relatively cheaper and less harmful among the various fluids [66].

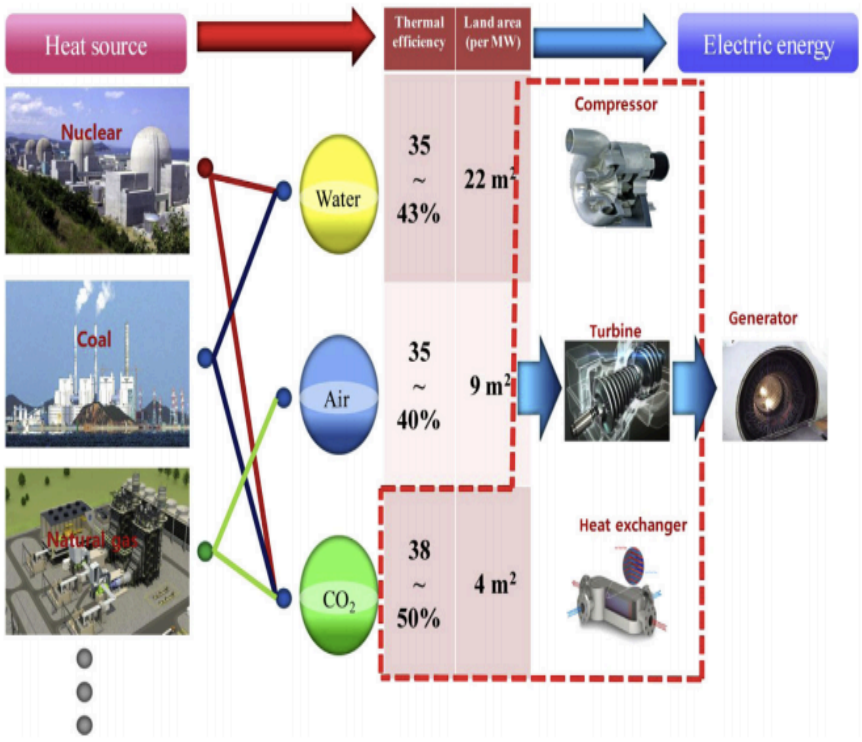

Figure 1.26. Comparison of power conversion systems based on air, steam, and SCO_2 [66].

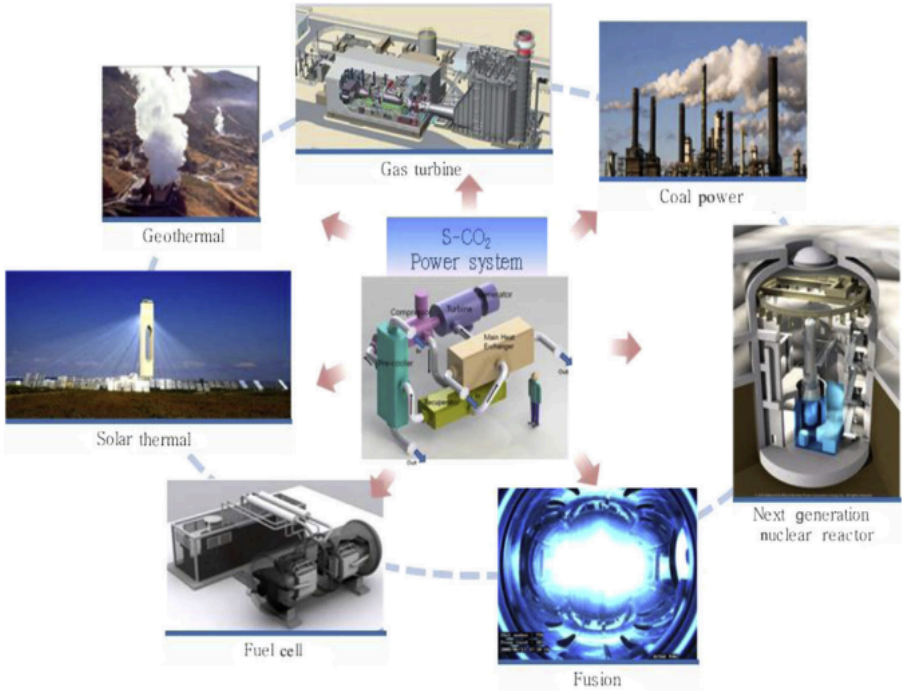

Figure 1.27. Applications of SCO_2 cycle [66].

Apart from this, CO_2 at critical conditions becomes more incompressible. The compressibility factor can be defined as fluid's molecular volumetric ratio as compared with ideal gas, which describes that up to which extent fluid behave like ideal gas. Once this factor is unity, fluids acts very near to the ideal gas and at what time this element is zero, the fluid behaves like as incompressible fluid [66].

In addition, Figure 1.28 shows that the compressibility factor drops to 0.2-0.5, when CO_2 closes to the critical point. Therefore, compression work can be decreased substantially. More benefits of SCO_2 cycle: minimum pressure of SCO_2 Brayton cycle is higher (i.e. around 7400 kPa) than any existing SRC system and or gas Brayton cycle, which is due to the operation of system beyond the critical point. Therefore, in the entire power system, fluid remains dense and due to higher density of fluid results in decreases the volumetric flow rate which in turn 10 times smaller turbomachinery required in case of SCO_2 cycle as rivalled with the turbomachinery of SRC system [66].

Moreover, the process of recuperation in SCO_2 Brayton cycle greatly affects to the thermal efficiency because its pressure ratio much smaller than SRC system but outlet temperature of turbine is somewhat high. Thus, to enhance the thermal efficiency, a huge quantity of heat should be recuperated [66]. Figure 1.29. shows the principle of SCO_2 cycle power conversion system.

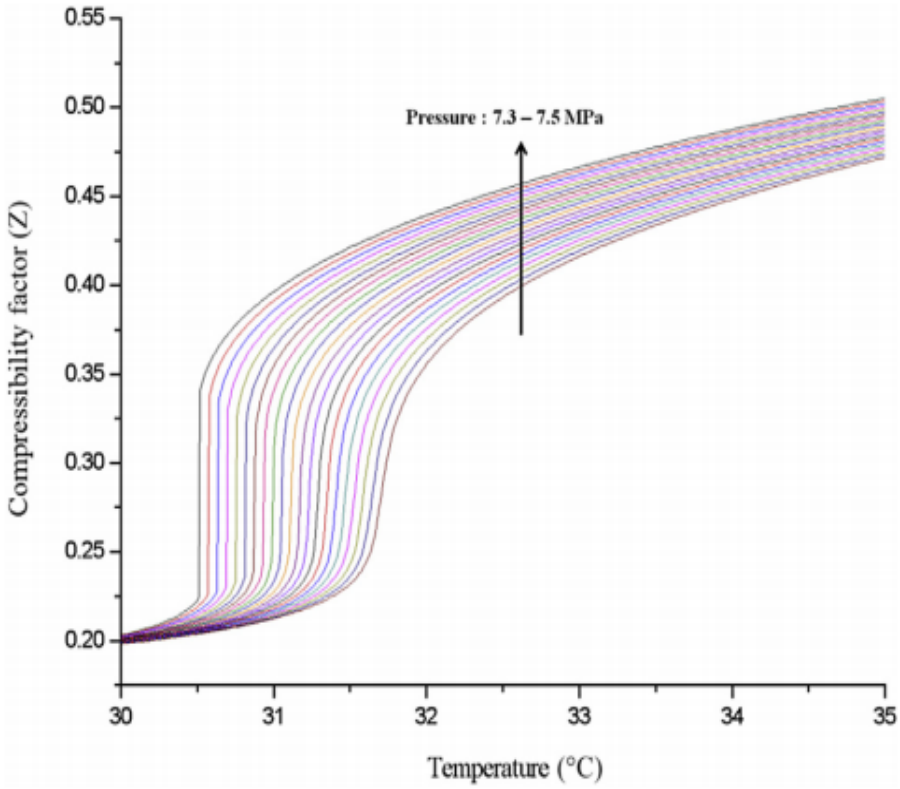

Figure 1.28. Compressibility factor of CO_2 near the critical point [66].

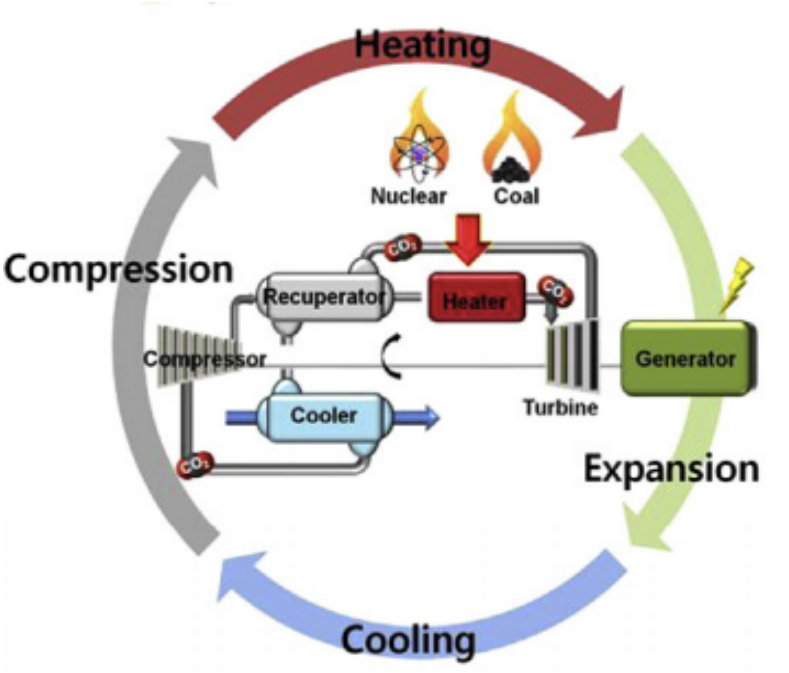

Figure 1.29. Principle of SCO_2 cycle power conversion system [66].

1.11. Organic Rankine cycle (ORC) technology

The gas or steam cycles are not technically and economically viable solution for a large variety of heat sources with respect to electric power generation, and this situation will be arising when availability of temperature and thermal power from the energy source is limited. Then, a different class of prime mover which is universally known as ORC becomes an attractive option. In case of limited capacity heat sources along with temperature lies between low to medium range (below 400℃-500℃), ORC is the unrivalled technical solution for the generation of electricity [67]. The ORC systems have a quite long history, starting in the first half of 19th century, about one hundred years after the invention of the steam engine [67].

An ORC machine is alike to steam cycle except it uses refrigerants and hydrocarbon like organic fluids instead of water. The usage of water as a working fluid has some advantages such as thermal and chemical stability is very good which means that no need of decomposition, viscosity is very low that requires less pumping work, latent and specific heat is very high means good energy carrier, ozone depletion potential (ODP) & global warming potential (GWP) is zero means no threat to the environment, and also it is non-toxic and non-flammable, it present almost everywhere on earth which means that it is cheap and abundant [68]. However, there are some problems occur with the use of water such as to avoid the condensation during the expansion requires superheating, erosion risk could be there for blades of turbine, there could be a surplus pressure in the evaporator, the turbines used are expensive and complex [68,69]. Due to these mentioned causes water is appropriate for high temperature applications as well as large centralized arrangements [68]. Figure 1.30. illustrates the Temperature-entropy (T-s) graph for water and other selected organic fluids.

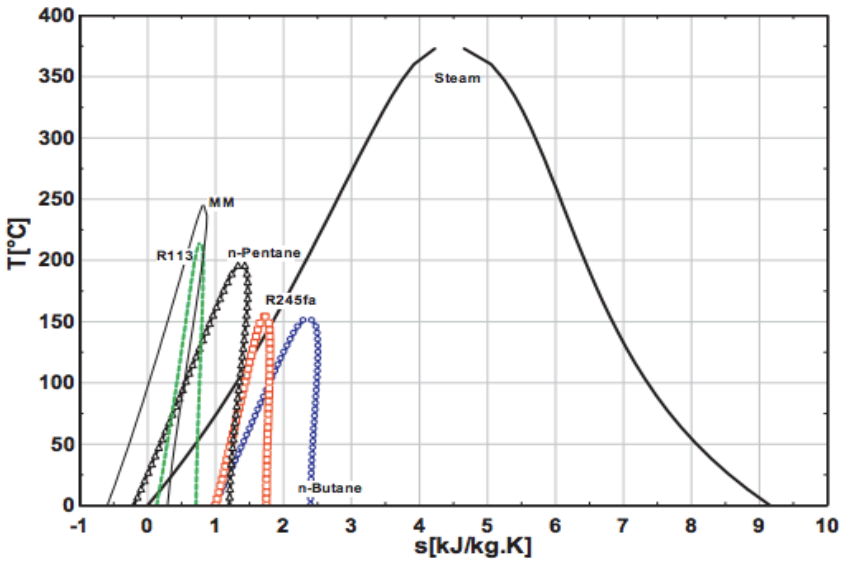

Figure 1.30. Temperature-entropy (T-s) graph for water and other selected organic fluids [68].

As compared to water, molecular mass of organic compounds will be high and ebullitions/critical temperature will be low, which have been proposed as working fluid in ORC [68]. ORC is also known as clausius Rankine cycle and it is also environment friendly small size system alongside no emission of exhaust gases such as CO, CO_2, NO_X, SO_X, and other atmospheric contaminants [70]. Also, ORC system has some advantages as compared to steam based conventional power plants [68]:

1. During the evaporation process, it requires less heat.
2. Process of evaporation yields at lower pressure and temperature.
3. Superheating is not required due to the ending of expansion process in vapor region, therefore, blades erosion risk can be avoided.
4. Pressure drop/ratio will be much lesser because of lesser temperature change amongst evaporation and condensation, and hence simple single stage turbine can be utilized.

Table 1.1. Comparison between fluid property of conventional steam cycle and ORC system [68]

Information	Steam cycle	ORC system
Fluid used	Water	Organic compound
Critical pressure	High	Low
Critical temperature	High	Low
Boiling point	High	Low
Condensing pressure	Low	Acceptable
Specific heat	High	Low
Viscosity	Low	Relatively high
Flammability	No	Yes, and depends on fluid
Toxicity	No	Yes
Environmental impact	No	High and depends on fluid
Availability	Available	Supply problem
Cost	Cheap	Expansive

Since 1880s, the ORC had studied for the first time did not attracts much attention till the world had faced first fossil fuel depletion and destruction of environment which now turned the interest of research towards low-grade energy recovery systems. ORC can recuperate heat from different sources, for example solar energy, heat of geothermal, biomass, & industrial waste heat which is due to its low operating temperature [68]. Apart from this, CSP technology such as SPTC system shows its capability to function under commercialized atmosphere [68],

and assumed as the most established sort of CSP but it could face competition in future from LFR system [49,68].

Modular ORC solar power plants run on the similar principle as conventional SRC arrangement except instead of steam it uses organic fluid [68]. Since 1990s, investigations have been carried out for small ORCs but due to absence of lesser and efficient expansion devices, it was not implemented widely. Among ORC solutions, ORC-WHR (waste heat recovery) is the rapidest rising business alongside boundless potential in industry and power plants based on combined cycle. Climate change related environmental concern and increasing prices of oil are the causes backup the explosive development of this efficient, clean, and reliable approach to generate the electricity [68]. Lastly, basic components of ORC system are similar to conventional Rankine cycle and Figure 1.31 displays the arrangement of components of ORC system utilizing thermal source.

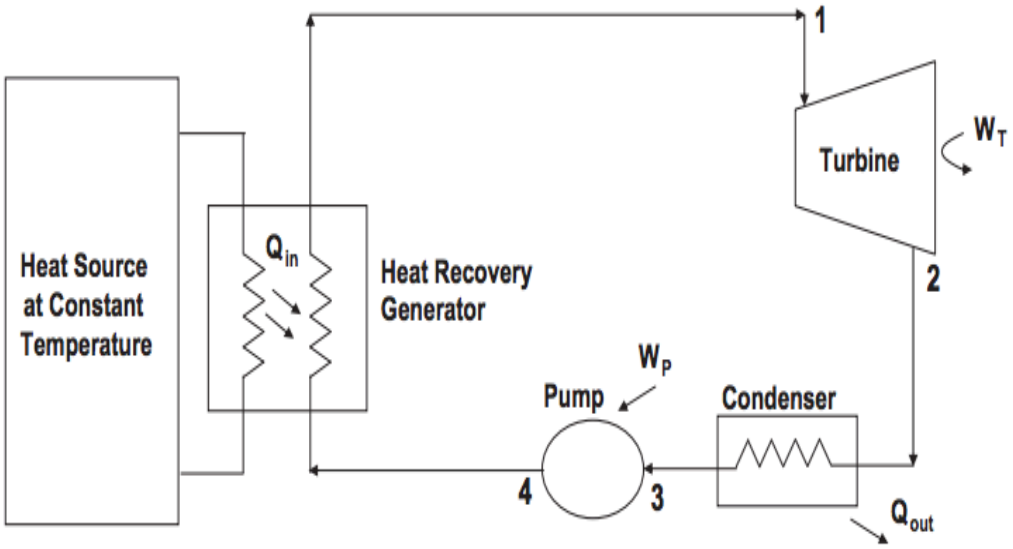

Figure 1.31. Basic components of ORC system [70].

1.12. Selection of working fluids for a ORC system

The working fluid selection has been treated in many published research papers. Mostly these research studies present the comparison in respect of thermodynamic performance and grounded on a cycle prototypical between a set of working fluids [71]. There are some guideline and indicators that should be taken in to account during the selection of most appropriate fluid:

1. Thermodynamic performance of working fluid: with regards to given heat source and sink temperature, efficiency and power output should be high as possible. Also, critical point,

acentric factor, specific heat, and density are some inter-reliant thermodynamic properties of working fluid on which performance depends [71].

2. Saturation vapor curve: A negative saturation curve for wet fluid such as in case of water prompts droplets in the expansion's following stages. To avoid any kind of turbine damage, the vapor needs to be in superheated state at turbine inlet. In case of dry fluid where positive saturation vapor curve will be formed, a recuperator could be utilized for the purpose of cycle efficiency enhancement [71].
3. High vapor density: For a fluid such as silicon oils, whose condensing pressure is very low, this parameter has kay importance. A low density prompts higher volume flow rate, consequently, so as to limit the pressure drops, heat exchanger size must be augmented which results in a non-negligible influence on the system cost. However, in case of turbo expanders for which dimension is not an essential parameter, simpler design can be allowed with the larger volume flow rates [71].

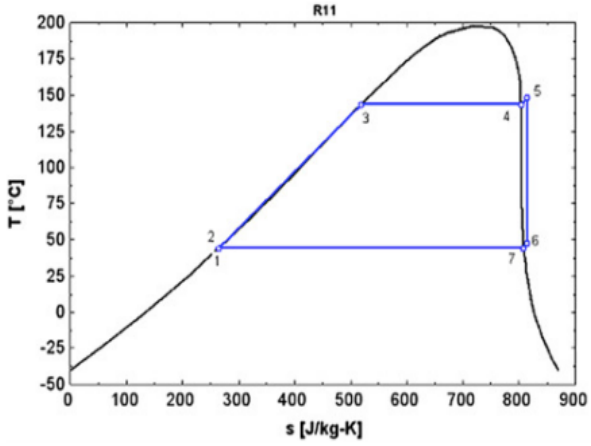

Figure 1.32 (a). Isentropic working fluid [71].

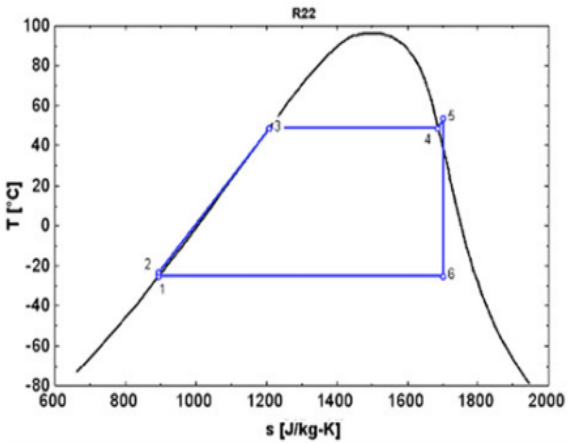

Figure 1.32 (b). Wet working fluid [71].

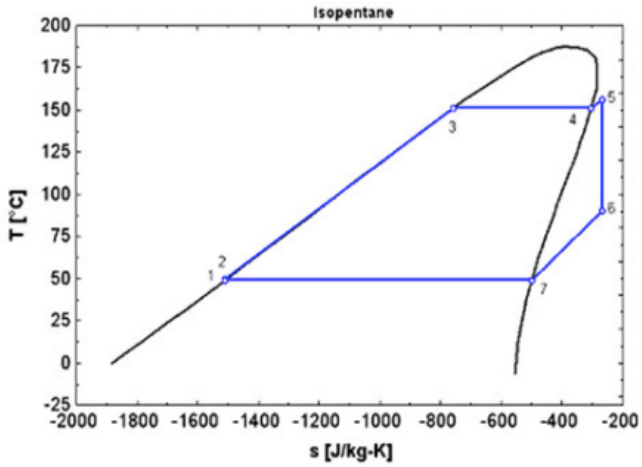

Figure 1.32 (c). Dry working fluid [71].

4. Low viscosity: Heat transfer coefficients will be high and friction losses will be low in the heat exchangers which can be as a result of low viscosity in both the liquid and vapor phase [71].
5. In the heat exchangers, high heat transfer coefficient results in high conductivity [71].
6. Acceptable evaporating pressure: Investment cost can be high and complexity can be increased as a result of higher pressure likewise in situation of water used as a working fluid [71].
7. Positive condensing gauge pressure: To circumvent air infiltration into the cycle, low pressure should be upper than the atmospheric pressure [71].
8. High temperature stability: The uppermost temperature of heat source could be restricted by the working fluid's chemical stability because at higher temperatures, organic fluids frequently undergo from chemical deterioration and decomposition unlike water [71].
9. To avoid freezing of working fluid, melting point should be lesser than the lowest temperature of ambient across the year [71].
10. High safety level: Toxicity and flammability are involved in safety constraints. Refrigerants in safety group are classified under ASHRAE Standard 34 and it can be used to evaluate particular working fluid [71].
11. Low ODP: The ODP is stated in terms of ODP of R11 which is set to unity. Under the Montreal Protocol, the non-null ODP fluids are gradually being phased out. The current refrigerants are available ODP is either null or very adjacent to zero [71].
12. Low Greenhouse Warming Potential (GWP): It is estimated as for the GWP of CO_2 which is taken as unity. There are some refrigerants whose GWP has a high value such as 1000 but to restrict use of high GWP fluids, there are not such kind of direct legislations currently available [71].
13. Good availability and low cost: Fluids that are currently used by industries such as refrigeration and chemical, are easier to achieve and also have less pricy [71].

1.13. Conclusion

On the basis of this chapter, it is clearly understood that in order to compete with the issue of energy security, environment, and increasing energy demand in near future, the RES can definitely improve the situation. It has been pointed out that solar thermal electricity can be established as a forthcoming potential choice for the generation of electricity in India. As a

most mature technology, SPTC can be used to generate the heat with the maximum temperature of 400℃ which can further be used to generate the solar thermal electricity [55]. Furthermore, RES especially the CSP systems will be developed as a promising source soon for the SCO_2 cycle.

By keeping these important aforementioned points in mind, this work is focused on find out the performance of SPTC integrated SCO_2 cycle for purpose of power generation. Moreover, ORC can be employed as the low-grade energy recovery systems. Therefore, this research study aims to examine the combined effect of these two aforementioned cycles on the energy and exergy performance in which SCO_2 cycle can be exploited as a topping cycle, whereas, the ORC and VAR as a bottoming cycle can be used to recover waste heat of SCO_2 cycle as per research objectives.

1.14. Organization of thesis

This thesis is divided into six chapters. All the chapters have been discussed sequentially as listed below:

Chapter 1 begins with the introduction that gives an overview on the continuous and rapid diminution of fossil fuels and the necessity of RES in order to avoid both the energy crisis and environmental concerns in near future. Then, energy scenario that discusses about the shares of different fuels including conventional and non-conventional in the primary energy supply, distribution of fossil fuels, and production and consumption of energy in the world. In addition, it also explains that how an interruption in energy supply can affects to the economic growth especially according to Indian scenario and how RES can help to meet the energy demand so as to achieve the energy security.

Apart from this, various issues related to conventional resources, for instance coal, oil and natural gas, large hydro plants, and nuclear power plants have been discussed along with their adverse effects on the ecosystem have also been identified. Later on, RES scenario along with their use in energy conversion have been included in this chapter and then further discussions have been made on the solar energy and solar thermal power systems which includes solar collector and concentrator.

Furthermore, pros and cons of concentrating collector over the FPC system have been considered that can little bit clarify the reason to choose the concentrating collector (i.e. SPTC system) as a heat source to drive the combined cycle. Besides, the description and status of

various CSP systems such as SPTC, LFR, PDR, and central receiver have been chatted. Moreover, the significance and benefits of SCO_2 cycle and ORC over the SRC system for various heat source, for instance CSP systems have been reviewed. Finally, a selection criteria of working fluids for the ORC system has been discussed so as to choose the most appropriate fluid for the analysis.

Chapter 2 starts with the literature review, which is basically concentrates on the two aspects such as power generation and waste heat recovery (WHR) by thermal cycles especially SCO_2 cycle and ORC system which have been operated by the CSP system. Further this chapter also discusses the literature outcomes which are then used to prepare the research gaps and on the behalf of this, research objectives have been decided.

The literature review is split into different portions in which first section is deals with the applications of SCO_2 cycle which is further divided into subsections that discusses the use of SCO_2 cycle in power production and WHR, recent studies on the recompression SCO_2 (R-SCO_2) cycle, and utilization of RES for SCO_2 cycle. The second section mainly reviews the applications of ORC system for power generation and WHR which is also divided into subsections such as utilization of RES for ORC system and studies available on SORC system. The third section discuss the application of combined cycle which have a one subsection such as utilization of RES for combined cycles.

Chapter 3 has discussed the detailed description of each model in the different sections. The first section gives the brief description of SPTC integrated combined SCO_2 cycle and ORC system along with its temperature-entropy (T-s) diagram. Further, a short discussion about the effect of pressure and temperature conditions on the density and specific heat, and variations in thermal conductivity with respect to density at different temperatures has been made which is necessary to explains some fundamental facts regarding the technology of SCO_2 cycle. Further, the operating temperature range of SCO_2 cycle for various heat source has been discussed. In the second section, description on the SPTC coupled with combined recompression SCO_2 cycle and ORC system along with its T-s diagram has been made. In the third section, description on the SPTC coupled with combined recompression SCO_2 cycle and VAR cycle has been presented, and fourth chapter discuss the description on SPTC integrated SORC system. Moreover, the parametrical values for all the selected combined cycles have been listed in the tabulated form in this section.

Chapter 4 deals with the thermodynamic modelling, which is based on the mathematical energy and exergy equations that have been programmed into the form of a computer code in order to solve these equations with the help of computational numerical technique also known as engineering equation solver software. This chapter is split into five parts in which first part deals with the modelling of SPTC system. The second section presents the modelling of combined cycle (SCO_2-ORC system) that has been discussed on the basis of important assumptions. Further, important equations for exergetic factors, for instance improvement potential (IMP), irreversibility ratio (Y*), fuel depletion ratio (Y_{DEP}), and expansion ratio (φ) also has been mentioned in this section. The third section discuss the modelling of combined recompression cycle (R-SCO_2-ORC). The fourth section deals with the modelling of combined cycle (SCO_2-VAR) for the purpose of power generation, cooling and heating effect. In the same way, the fifth section discuss the modelling of SORC system in which mainly the equations for net work output, exergy input, exergy destruction rate, exergy and thermal efficiency have been listed.

Chapter 5 describes the results and discussions, which actually analyses the results of the solar driven cycles that have been computed by computational numerical technique and then the discussion on these results have been made in various sections. First section deals with the analysis of SPTC integrated with combined cycle (SCO_2-ORC system) and the effect of various operating parameters such as solar direct normal irradiance (DNI), inlet pressure of SCO_2 turbine, inlet temperature of SCO_2 turbine, and inlet temperature of compressor have been investigated in the subsections with the help of different organic fluids. Furthermore, outcomes of the exergy analysis in the form of exergetic parameters such as exergy destruction rate, IMP, Y_{DEP}, and Y* for various system components have been evaluated in the last subsection and listed in the tabulated form. Moreover, the validation of SPTC system and SCO_2 cycle, ORC system, and combined cycle have been discussed in this section.

The second section examines the performance of SPTC integrated with combined recompression cycle (R-SCO_2-ORC system) and in addition to upper mentioned parameters, the effect of some extra parameters mass flow rate and effectiveness of HTR and LTR also have been analysed on the system's exergy and thermal efficiency, and net work output. Also, a comparative analysis has been performed between the simple and recompression based combined cycle. In the last subsection, validation of the system with and without bottoming ORC has been presented.

The third section assesses the performance of SPTC integrated combined cycle (SCO_2-VAR cycle) and the effect of functioning parameters such as local apparent time (LAT), DNI, turbine and compressor's inlet temperature, compressor pressure ratio, generator temperature, and absorber and condenser temperature on the system's exergy and thermal efficiency, COP of cooling and heating have been examined. In the last subsection, the validation of SCO_2 cycle and VAR has been presented. Final section investigates the performance of SPTC coupled with SORC system.

Chapter 6 is the last chapter of thesis, which discusses the conclusion from the research work in which the important outcomes of each objective have been discussed in subsequent sections.

Chapter-2

Literature review

2.1. Introduction

Numerous researches are available in the literature on the utilization of thermal cycles such as SCO_2 cycle and ORC system with respect to their performance evaluation in order to produce power as well as waste heat recovery (WHR). The literature has been conducted in a comprehensive way and comprised from different sections:

The first part considers the various research work related to the use of SCO_2 cycle according to the aspects of power generation and WHR, which is followed by second part that also examines the previous research work available on the ORC in the same way. Then, the third part reviews the performance studies available in the field of combined cycles especially concentrates on the combination of SCO_2 cycle and ORC system. Lastly, the fourth part discusses the research pertaining to the utilization of renewable energy sources to operate the combined cycles.

Moreover, after completing the above-mentioned targets, the important outcomes have been encountered and listed in the further corresponding section followed by the research gaps which are identified based on the scope available in past literature. Finally, the organization of thesis available in the last portion of this chapter that defines how this thesis work structurally divided in the different sections.

2.2. Applications of SCO_2 cycle

In the late nineteen-sixties, power cycles based on CO_2 at supercritical pressure and temperature were introduced. But in the past era, the global awareness in SCO_2 cycle has increased steadily. From the worldwide viewpoint, it has no doubt that SCO_2 cycle attain the attention of energy industry for stationary power production, either for stand-alone applications, combined heat and power or recovery of waste heat. A range of applications and fuels such as fossil, nuclear, or renewable defines its versatility. Also, the remarkable performance of SCO_2 power cycle at moderate temperature makes it apart from the competitors that right now rule the market (Crespi et al. [72]). In a variety of applications, SCO_2 power cycle

has an ability to achieve high efficiency amongst other, when it is operating with intermediate temperature levels: CSP (Bauer [73] and Osorio et al. [74]), WHR process (Wright at al. [75]), Gen IV nuclear reactors (Abram and Ion [76]).

2.2.1. Utilization of SCO_2 cycle in power production and WHR

Yoon et al. (2012) [77] stated that SCO_2 Brayton cycle be able to employed for the next generation nuclear reactors and its major benefits are: (i) at low turbine inlet temperature, it shows high thermal efficiency (ii) turbo-machineries and heat exchangers have compact structure (iii) simple layout cycle at a superior thermal efficiency compared to other Brayton cycle. Apart from this, these welfares could be used in water reactor technologies and they also motioned that system-integrated modular advanced reactor with a capacity of $300MW_{th}$ can be potentially utilized with SCO_2 Brayton cycle. Lastly, their proposed cycle analysis results indicate that the maximum cycle efficiency was 30.05% under temperature of 310℃, compressor outlet pressure of 22 MPa, and flow split ratio of 36% with total heat exchanger volume of $82m^3$.

Heo et al. (2017) [78] completed a thermodynamic investigation of SCO_2 power cycle layouts (i.e. simple recuperated, recompression, and partial heating Brayton cycle) using isothermal compressor. They assessed the cycle performance through the sensitivity examination of cycle design parameters such as pressure ratio and flow split ratio. Finally, their findings reveal that with the utilization of isothermal compressor, the cycle net efficiency of simple recuperated and recompression cycle was enhanced by 0.5% point and 1-3% points, respectively. Also, they found that partial heating cycle layout produced 15-18% more work net work as compared to the reference cycle.

Kim et al. (2016) [79] discussed that SCO_2 Rankine cycle has a simplicity and compact structure, and also it can achieve the high efficiency when it was utilized for WHR from a gas turbine as compared to steam/water cycle. They stated that the net output power from a specified source of waste heat can be maximized by incorporating the waste heat utilization efficiency in conjunction with the thermal efficiency of cycle.

However, they argued that simple SCO_2 Rankine cycle cannot utilize the full waste heat when it is equipped with high-temperature source due to preheating of fluid in recuperator to a high temperature that results in increases cycle efficiency. As a result, a cascade system with

low-temperature loop can be added to high-temperature loop to recover the remaining waste heat from a simple cycle or a split cycle can be used. Lastly, a comparison between the three cycles have been carried out to analyse the energy and exergy performance and their results reveal that over a wide range of operating conditions, a split cycle has an ability to produce the highest power of the three considered systems.

Khadse et al. (2017) [80] stated that SCO_2 has some advantages for the application of WHR like compactness, low capital cost, and it can be applicable to a wide range of heat source temperatures. Besides, for exhaust WHR from a next generation heavy duty simple cycle gas turbine, they performed a thermodynamic modelling and optimization of SCO_2 Brayton cycle's configurations such as recuperative cycle (RC) and recuperative recompression cycle (RRC) by using genetic algorithm and the main aim of their optimization study was to maximize the power out.

Furthermore, their results reveal that RRC configuration shows more power output than RC for the selected exhaust gas mass flow rate. Moreover, they concluded that best cycle choice for WHR highly depends on hot waste gas characteristics. Lastly, their cost analysis results showed that as comparison to SRC system, there was a total reduction in cost found to be approximately 28% for WHR applications.

Muto and Kato (2007) [81] discussed that SCO_2 turbine cycle at medium inlet turbine temperature of 500-650℃ can attain extreme cycle thermal efficiency at a pressure of 20MPa which is too high to even consider producing a reactor pressure vessel inside existing points of confinement of fabrication and this issue can be tackle by a dual expansion cycle.

Their results reveal that in case of fast reactor, for the 12.5 MPa cycle, dual expansion cycle, and the 20 MPa cycle, the thermal efficiency of cycle was found to be as 42.6%, 44.0%, and 45.1%, respectively. However, they found that in case of high-temperature gas-cooled reactor, for the 8 MPa cycle, dual expansion cycle, and 20 MPa cycle, the thermal efficiency was found to be as 47.5%, 48.5%, and 50.3%, respectively.

Cardemil and da Silva (2016) [82] presented a thermodynamic study on the CO_2 centred power cycles and they mentioned the various aspects such as cycle type (i.e. Rankine or Brayton), with or without recuperator configurations, and operational conditions like temperature of heat source, and CO_2's upper and lower operating pressure. In addition, they selected four working fluids, for instance ethane, toluene, D4 siloxane, and water for the assessment of relative performance of energy conversion cycles.

Furthermore, their results suggested that it is possible that the first law efficiency of CO_2 could be lower than the other fluids but its exergy efficiency can be significantly higher. Lastly, their findings reveal that for the certain operational conditions, the needed global conductance of CO_2 is potentially lower than competing fluids.

Mecheri et al. (2016) [83] investigates the thermodynamic performance of SCO_2 cycle for coal power plant applications. Their findings revealed that recompression cycle was mandatory even with the low temperature heat available in coal combustion flue gas and also it had a difference of more than 4.5%pt efficiency with that of standard Brayton cycle. Furthermore, they found that single reheat was an effective configuration with increase in efficiency of 1.5%pt as compared to no-reheated cycle. Moreover, they concluded that there was a 6% LHV relative efficiency improvement in the performance of SCO_2 coal-fired power plant which was from about 45% to 48% with existing material at present operating conditions.

Lastly, there were some technological challenges regarding the design of all components (for e.g. recuperator, turbomachinery, boiler wind box, surfaces of heat transfer, and air preheater) of power plant which had comes during the integration of SCO_2 power cycle with a coal-fired boiler. Finally, they had listed two main issues such as pressure drop management in boiler and boiler enclosure's cooling, therefore, an industrial compatible solution should be proposed to make this technology an authenticity for constructing more efficient, cleaner, and coal-fired power plant.

Park et al. (2018) [84] analysed the thermodynamic performance and economic investigation of coal-fired power plant integrated with SCO_2 Brayton power cycle. Finally, their results concluded that as compared to SRC system applied to the exiting coal-fired power plant, SCO_2 power cycle coupled with coal-fired power plant showed an improvement in power generation efficiency of 6.2%-7.4% and levelized cost of electricity was reduced by about 7.8%-13.6%.

Neises and Turchi (2019) [85] examines the design, cost, and performance of the various configurations of SCO_2 cycle. They found that recompression cycle can attain higher thermal efficiency and partial cooling cycle because of its necessity of higher turbomachinery capacity, it is the costliest cycle. At last, they reveal that the partial cooling cycle operated by the power tower produces more net electricity and also an inexpensive option.

Li et al. (2018) [86] carried out an experimental investigation and compared the functioning of trans-critical CO_2 (TCO_2) power cycle and R245fa based ORC for low-grade heat power generations. In addition, for these power generation configurations, they utilized the exhaust flue gases from the 80 kWe micro-turbine CHP unit as a heat source. Also, they analysed the effect of important operational constraints such as working fluid's mass flow rate and heat source input etc. at ambient on system performance. Findings of this study demonstrates that the power generation of turbine and overall efficiency could be improved significantly in case of TCO_2 system and R245fa based ORC with a fixed heat source input and at higher mass flow rate.

It was noticed from their study that when the rate of mass flow increases from 0.2 kg/s to 0.26 kg/s and from 0.23 kg/s to 0.27 kg/s for working fluids such as CO_2 and R245fa respectively, the corresponding power generation of turbine was increased by 88.2% and 27.3%, and overall efficiency of turbine was increased by 35.4% and 7.5%. However, when the working fluid's mass flow rate was fixed, both the power generation and overall efficiency of turbine were increased variably for the R245fa based ORC and TCO_2 system with higher heat source input.

Song et al. (2018) [87] discussed that SCO_2 power system is a promising way to recover the waste heat of engine due to its well characteristics such as compact structure, system safety level, and environmental friendly. They explore the potential of preheating SCO_2 power system for the WHR from a diesel engine and mentioned that for preheating of the SCO_2 fluid, a low temperature jacket cooling water was used in the original system.

Their thermodynamic evaluation concluded that with the maximum preheating temperature, the system showed the maximum net power output of 63.7 kW. Then, they included a regeneration branch in the improved preheating SCO_2 system that results in a considerable increment on the regeneration heat load and the maximum net power output of 68.4 kW were reported in the improved system which was 7.4% higher than that of the original system. Lastly, they concluded that the engine output power (996 kW) for the improved preheating system for WHR could be increased by 6.9%.

Banik et al. (2016) [88] performed a parametric optimization and also developed a thermodynamic model of a recompression TCO_2 power cycle alongside a waste heat source of 2000 kW and at a temperature of 200℃. They analysed the energetic and exergetic performance of power cycle with the variations in pressure and mass recompression ratio. Their study results

found that the thermodynamic performance such as energetic and exergetic performance can be improved with the higher-pressure ratio.

On the other side, study also reveals that exergetic efficiency of cycle increases with the higher recompression ratio but energy efficiency can be enhanced only if the inlet temperature of precooler remains constant. Lastly, they concluded that with a recompression ratio of 0.26, the maximum thermal efficiency of TCO_2 power cycle was found to be as 13.6% and also an optimum ratio of 0.48 was found to be suitable to minimize the total irreversibility of the power cycle.

2.2.2. Recent studies on recompression SCO_2 (R-SCO_2) cycle

Sarkar (2009) [89] performed the exergetic investigation and optimization of SCO_2 cycle in order to inspect the impact of operating parameters on optimum pressure ratio, energy and exergy efficiency and irreversibilities in components. Also, they analysed the effect of isentropic efficiency, effectiveness of recuperator, and pressure drop in component on the second law efficiency.

Furthermore, their study results reveal that as compared to maximum operating temperature, the minimum operating temperature has a more predominant effect on the optimum pressure ratio as well as efficiency of cycle. Moreover, they found that the effect of turbine's isentropic efficiency has a about 2.5 times more predominant effect than that of isentropic efficiency of compressor and also mentioned that the HTR effectiveness has a more predominant effect (about twofold) than that of LTR effectiveness on second law efficiency.

Ma et al. (2017) [90] investigated the performance of R-SCO_2 cycle with the main compression intercooling and also developed a mathematical model. They optimized the compressor pressure ratio and pressure ratio distribution amongst two main compression stages, and also performed a comparison between cycles with and without main compression intercooling in four typical conditions from both design and off-design perspective. Their results show that the pressure ratio distribution between two main compression stages has more predominant effect on cycle efficiency as compared to compressor pressure ratio. They reported that with the integration of main compression intercooling effects in reference conditions, the efficiency improvement of 2.65% can be obtained. At last, they found that in the design conditions, the integration of main compression intercooling cannot only improve the efficiency of cycle but

also drops the temperature difference across primary heat exchanger that tends to bring cost savings.

Kim et al. (2018) [91] utilized the effectiveness and pinch point temperature difference analysis to evaluate the irreversibility of recuperators so as to optimize the performance of SCO_2 recompression cycle. Their finding reveal that in the optimal conditions, the efficiency of recompression cycle was found to be as 44.67% when compression ratio was 2.6, inlet pressure of turbine was 19.24 MPa, and split ratio was 0.307. They stated that the practical performance of heat exchanger can be expressed with the pinch point temperature rather than the effectiveness. Lastly, they mentioned that the performance and optimal functioning state could be altered through the assistance of pinch point temperature difference of HTR and LTR.

Gkountas et al. (2017) [92] states that thermal efficiency can be increased by recompressing a fraction of the flow without heat rejection, however, the heat transfer majorly occurs in the recuperators. They studied the thermodynamic performance of 600 MWth power cycle with the help of two different simulation tools used to model the recompression system. Also, they performed a comparative analysis between the results of two simulation tools and reference cycle and found that prediction of coefficient of overall heat transfer and effectiveness of recuperator between the developed code and reference model was maximum of 4% deviation, however, the deviation between the commercial software and reference model was about 2.8%.

Padilla et al. (2015) [93] performed a thermodynamic and exergy analysis of R-SCO_2 cycle and discovered that first law and exergy efficiencies can be improved by adding reheating to R-SCO_2 cycle. They reveal that maximum exergy efficiency was found to be at 600℃ due to internal and external loss of exergy in the solar receiver.

Also, their results evaluate that with the high temperature of the cycle, the first law efficiency increases monotonically and maximum value for reheating configuration was found to be as 52% at 850℃. Lastly, they disclosed that maximum exergy loss was happen in solar collector and cooler, and also suggest that a bottoming cycle so as to improve the exergy efficiency could be implemented.

Yari (2012) [94] proposed a R-SCO_2 cycle based novel cogeneration cycle in order to exploit the WHR from a nuclear power plant. So as to augment the overall performance of cycle, the TCO_2 power cycle & $LiBr/H_2O$ absorption heat transformer was used to construct the cycle.

Results of study reveal that the new SCO_2 cycle's energy and exergy efficiencies were about 5.5–26% upper than that of simple SCO_2 cycle.

Wołowicz et al. (2018) [95] investigated the SCO_2 cycle layouts such as pre-compression, partial cooling and recompression cycle. They created a model of the R-SCO_2 cycle by using GateCycle software. Their simulation results found that for the inlet CO_2 turbine conditions of 550℃ and 20 MPa, the cycle efficiency was found to be as 44%.

Atif and Al-Sulaiman (2018) [96] analyses the energy & exergy performance of SPT incorporated R-SCO_2 cycle along with two-tank thermal storage system. Their results reveal that rate of destruction of exergy in heliostat field and solar tower was found to be as 1,295,605 and 156,254 kWh/day, respectively, for the June month. In addition, they found that the combined exergy destruction of all the components of SCO_2 cycle was 138,432 kWh/day and the rate of exergy destruction for thermal storage was 4,735 kWh/day.

Furthermore, for the month of June, March, and December, the whole system's net energy efficiency at solar noon was found to be as 6.93, 5.71, and 4.45%, respectively. Finally, they found that for the months of June, March, and December, the electrical second law efficiency was found to be as 7.44, 6.14, and 5.04%, respectively.

2.2.3. Utilization of RES for SCO_2 cycle

Garg et al. (2013) [97] inspected the performance of SCO_2 Brayton cycle for CSP applications and also compared with the trans-critical and sub-critical operations and they found that in the supercritical regime, thermal efficiency attains a maximum value at approximately 85 bar after which it starts to diminishes. However, thermal efficiency of trans-critical and sub-critical cycle enhances almost linearly with low-side pressure. Also, they demonstrate that even at low source temperature 820 K, the SCO_2 cycle is capable of power production alongside a thermal efficiency of >30%.

In a different study, **Garg et al. (2014)** [98] conducted a comparative study amongst condensing TCO_2 cycle (i.e. high temperature and pressure) and trans-critical steam cycle for CSP generation. They discovered that temperature variations did not influence the performance of TCO_2 cycle and it needs only single HTF loop as competed to trans-critical steam cycle coupled with two HTF loops in series. Their results also reveal that under the same operating conditions, both cycles yields camparable value of thermal efficiency and trans-critical CO_2 plant was

significantly compact as compared to trans-critical steam cycle due to large specific volume of steam which was responsible for bulky system.

Turchi et al. (2013) [99] discussed that at temperatures pertinent to CSP applications, the closed-loop SCO_2 Brayton cycle gives superior cycle efficiency potential as competed to superheated or supercritical steam cycles. They stated that due to higher density of fluid and simple design of cycle, the SCO_2 Brayton cycle has lesser weight and volume, lower thermal mass, and power blocks will be less complex as compared to Rankine cycle. In addition, the system's cost of installation, maintenance, and operation may be reduced due to the SCO_2 process's simpler machinery and compact size.

Moreover, from the outlook of a CSP use, they explored the SCO_2 Brayton cycle configurations' ability to accommodate dry cooling and can attain >50% efficiency as stated for the U.S. Department of Energy SunShot goal. Lastly, their outcomes reveal that the recompression cycle merged with intercooling and turbine reheat seems capable to hit this efficiency aim, notwithstanding when merged with dry cooling.

Chacartegui et al. (2008) [100] analysed the diverse arrangements of combined cycles in which closed cycle CO_2 gas turbine was a topping cycle to solve the problems linked with the solar power plant receiver design and size: lower intake temperature of turbine and higher pressure drop in heat exchanger as compared to conventional gas turbine. Also, they discussed that CO_2 Brayton cycle has high net shaft work to expansion work ratio which was in the range of 0.7-0.85 at intake pressure of supercritical compressor that was very nearer to the Rankine cycle, as a result, negative effects of pressure drops will be reduced.

Moreover, their study reveals that the use of CO_2 in topping cycle can increase the global efficiency of combined cycle by 3 percentage points with respect to the air cycle. Lastly, they stated that instead of wet fluids, the use of dry fluid gives the advantage of better performance of Rankine cycles, when working with saturated vapors. Due to this, superheated vapors at the end of expansion process will be produced that results in problem with condensation in the vapor turbine can be avoided, thus, increases the internal efficiency.

AlZahrani and Dincer (2018) [101] proposed a SPTC based power plant that employs an SCO_2 power cycle so as to convert the heat to power. They conducted an analysis based on thermodynamic and heat transfer to calculate losses of heat, exergy destructions, and energy and exergy efficiencies. Furthermore, they explore the impacts of changing some operating parameters such as intensity of beam radiation, beam incidence angle, and receiver emittance

on the energy and exergy performance of SPTC and SCO_2 power cycle. Lastly, their results reveal that the SPTC's energy and exergy efficiencies were uncovered to be as 66.35% and 38.51%, respectively.

Osorio et al. (2016) [102] done an investigation to analyze the dynamic behavior of SCO_2 power cycle incorporated with a CSP (i.e. central receiver), hot and cold energy storage, heat exchange scheme, recuperator, and multi-stage compression-expansion subsystem accompanied by the intercooler and reheater as an integral segment engaged between the compressor and turbine. Their study conclusions disclosed that the process efficiency and maximum power output were 21% and 1.6 MW, correspondingly.

Also, they presumed that the SCO_2 cycle's operating time after optimization was expanded from 220 to 480 minutes in view of thermal storage purpose. At last, their results suggested that CSP system using SCO_2 cycle could be viable substitute to fulfilling the energy needs in the areas of desert where the availability of water and fossil fuel resources are present in scarce amount.

Niu et al. (2013) [103] done an optimal arrangement of the solar collectors with a SCO_2 centred solar Rankine cycle system alongwith three distinct methods of collector arrangement, i.e. five units only in series, parallel and cascade plus individually five units in series. Their outcomes uncovered that the collectors in a cascade arrangement can deliver extensive quantity of electric power. Lastly, they also mentioned that to get more power production and heat utilization, more collector units should be installed because collection area has a significant effect on the solar Rankine cycle system.

Yamaguchi et al. (2006) [104] proposed a SCO_2 using Rankine cycle powered by solar energy in order to produce both electricity & thermal energy, and system consist of evacuated solar collectors, power producing turbine, heat recuperation system based on high-temperature and low-temperature, and feed pump. They designed and constructed an experimental prototype that has been tested under the typical summer conditions of the Kyoto, Japan. Finally, their experimental results showed that by selective absorbing surface in the evacuated solar collector, SCO_2 can be heated effectively and the proposed system works stably in trans-critical region. In addition, the estimated efficiency of power generation and heat recovery were 0.25 and 0.65, respectively.

Iverson et al. (2013) [105] discussed the way to improve the efficiency of solar-thermal power plants and they mentioned that as increase in working temperature keep on being sought, the SCO_2 Brayton cycles start to look more appealing regardless of the improvement expenses of this innovation. Their study also illustrates the response of fluctuating thermal input on the behaviour of developmental turbomachinery. Finally, they interrogated the specific improvements to the cycle with a benchmarked model to recognize the resulting impact on the efficiency of cycle which was expected to increase up to 15%, and also with minor modifications to improve insulation, it would approach approximately 24%.

Padilla et al. (2015) [106] performed an energy and exergy analysis of with and without reheat based four distinctive setups of SCO_2 Brayton cycle such as simple and recompression, partial cooling with recompression, and recompression with main compression intercooling. In addition, they replaced the heater and reheater by a solar receiver which was utilized to give the heat input to conventional Brayton cycle. Furthermore, their results reveal that with the temperature of the cycle, thermal efficiency of SCO_2 Brayton cycle increases monotonically and also found that recompression cycle with main compression intercooling has best thermal efficiency of 55.2% at 850℃.

Moreover, their exergy analysis results found that the highest exergy destructions were present in solar receiver (>68%), however, turbine and compressor have minimum exergy destructions (less than 3%). Lastly, the exergy efficiency coming to at most extreme value between 700℃-750℃ relying on the setup of cycle and also it acquires bell shaped curve.

Wang et al. (2017) [107] proposed the solar and biomass energy driven cascaded SCO_2 system and performed the energy and exergy analysis to evaluate the feasibility. Their results found that energy efficiency changes with time and the thermal efficiency reaches to 40%. They stated that the efficiency value will be minimum where the direct normal irradiance (DNI) will have the maximum value which can be due to improper utilization of surplus energy that was collected by solar receiver. Also, they found the maximum amount of exergy destructions in the solar field.

Chapman and Arias (2009) [108] discussed that the SCO_2 Brayton cycle has a high potential for use in CSP system, and mentioned that higher temperature and simplified plumbing in case of power tower configuration makes it very successful which will lead to high efficiencies and

low upfront costs. They also assessed the SCO_2 Brayton cycle for the future SPTC plants incorporating higher output temperature and a thermal storage system.

Luu et al. (2017) [109] performed a comprehensive parametric study for concentrated solar thermal plant integrated SCO_2 Brayton cycle with the main focus on development of operational strategies to adapt the fluctuations in availability of solar energy. They carried out that in terms of thermal efficiency, combined cycle comprised with recompression, reheat, and intercool feature has the most efficient cycle as compared with other layouts. In addition, the parameters like circulation rate of SCO_2 and splitting fraction are sensitized, and the cycle can adapt to input variations in heat by manipulating these two parameters without affecting net shaft power output which further leads to flexible temperature mode (FTM) and constant temperature mode (CTM).

Finally, their findings reveal that with these two modes such as FTM and CTM, the solar-assisted cycles have an ability to attain the utmost savings in fossil fuel of 28.9% and 31.2%, respectively as competed to the conventional cycles without solar.

Heo et al. (2018) [110] discussed that SCO_2 cycle has many benefits for the CSP applications such as high cycle efficiency, reduced sizing of components, and dry cooling option. They carried out a study in which an isothermal compressor was used to lessen the compression work in to layout of SCO_2 cycle. Their study results demonstrate that under the varying inlet conditions of compressor, compression work was reduced up to 50% for the isothermal compressor as compared to the conventional compressor.

Also, they evaluated the SCO_2 based simple recuperated and recompression Brayton cycle for the CSP applications. Results of their study revealed that as competed to the reference cycle, recompression Brayton cycle with the isothermal compressor shows 0.2-1.0% point higher thermal efficiency of cycle at what time the inlet temperature of compressor lies nearer to critical point. Moreover, SCO_2 cycle layout with the isothermal compressor can suggest larger area of heat exchange for the compressor that further requires development.

Enrıquez et al. (2017) [111] assessed the performance of three configurations such as recompression cycle, partial cooling with recompression cycle, and recompression with main compression intercooling cycle accompanied by one reheating stage. Also, they studied the performance of solar collector such as parabolic troughs and linear Fresnel with the different working fluids used as heat transfer medium.

Their results found that the efficiency could increase by adapting the existing SPTC with Rankine power cycles to the innovative SCO_2 Brayton cycle which results in a solar field aperture area and cost for a fixed power output could be optimized. Lastly, they pointed out that by adopting the therminol oil as a heat transfer fluid, the cost of solar field reduces which can be due to low unitary price of pipes and receivers' materials.

Reyes-Belmonte et al. (2016) [112] suggested that SCO_2 can be utilized as an alternative working fluid for the next generation power plant due to its outstanding thermo-physical properties at medium-to-moderate range of temperature. Further, they optimized the R-SCO_2 cycle for an application of solar central particles receiver and found that net efficiency of cycle was close to 50%.

Also, they pointed out that small change in parameters such as working temperatures, efficiencies of recuperator or distribution of mass flow between LTR and HTR were found to extremely modify the overall efficiency of system. Finally, they performed a recuperator effectiveness based optimization analysis and found that for medium to moderate temperature range which was around 630℃ to 680℃, the power cycle efficiency could lie between 43%-49%.

Al-Sulaiman and Atif (2015) [113] compared the thermodynamic performance of five SCO_2 Brayton cycles united with SPT, and preferred cycle forms were simple, regenerative, recompression, pre-compression, & split expansion cycle in the location of Dhahran, Saudi Arabia. They conducted an optimization analysis for the layout of heliostat field on a twelve-monthly basis by means of differential evolution technique known as evolutionary algorithm which was then incorporated with the SCO_2 Brayton cycles.

Furthermore, their optimization results reveal that recompression Brayton cycle will have the utmost thermal efficiency at June noon-time. Also, the maximum thermal efficiency of integrated system was 40%. However, the highest thermal efficiency of the cycle alone was 52%. Moreover, they found that regeneration cycle has a simple configuration and its thermal efficiency and power output results occupy second position.

Neises and Turchi (2014) [114] discussed that SCO_2 Brayton cycle at temperatures appropriate for CSP uses offers potential for higher cycle efficiency as competed to supercritical and superheated steam cycles. They also investigate the performance of simple, recompression, and partial-cooling cycles and found that partial cooling and recompression cycle were performed similarly when requiring an effectiveness to modelled the recuperator. Furthermore, they

concluded that the cycle of partial cooling was better than the recompression cycle when requiring a conductance to modelled the recuperator.

Moreover, their results pointed out that conductance model contains interpretations whose impact need to be understood but it was a better alternative for the size of physical heat exchanger than the model of effectiveness. Lastly, they found that a superior temperature differential through the primary heat exchanger occurred in case of partial-cooling cycle for CSP uses which was beneficial in the sense that it allows extra cost efficient storage systems to store sensible thermal energy as well as more thermally efficient receiver.

Singh et al. (2013) [115] investigates the dynamics of a direct-heated SCO_2 based closed Brayton cycle. They presented a simulation of the dynamic response of considered system to changes in temperatures of ambient air and input of solar energy from SPTC system on the summer and winter days. Their findings reveal that fluctuations in solar input heat triggers mass movement of CO_2 amongst the hot and cold-sides of the system which results in deviations in CO_2 mass flow rate, pressures, temperatures, and net-power output.

At last, they demonstrate that the system keeps a relatively unchanging net-power output whilst functioning under conditions descriptive of an average day in summer with capped heat input. It was noticed that because of reductions in CO_2 mass flow rates, input temperature of turbine rise well above the nominal values. In addition, they mentioned that due to subcritical conditions at inlet of compressor, a power output penalty was incurred on a winter day significantly.

Singh et al. (2013) [116] carried out a study to analyse the effect of the relative hot-to-cold side volume ratios on the dynamic characteristics of SCO_2 based closed Brayton cycle. They conducted an analysis of considered cycle by using a control oriented model in the perspective of power production in a direct heated and dry-cooled SPTC power plant. Their results found that CO_2 mass movement can be influenced by hot-to-cold side volume ratios which further affects to the power output.

Finally, they also found that when there are variabilities in input solar heat and temperatures of ambient air, increasing hot-to-cold side volume ratio results in more gradual and dynamic response.

Milani et al. (2017) [117] designed a solar-assisted R-SCO_2 Brayton cycle for net power output of 10 MWe. They found that the right combination of operating conditions (i.e. SCO_2

circulation rate and inlet temperature of turbine) can achieve the highest thermal efficiency. Also, they mentioned that for the specific thermal energy supply, higher inlet temperature of turbine was needed since it helps to minimize the working fluid's circulation rate and work of compression which in turn improves the overall thermal efficiency.

They reveal that for both indirect and direct configurations of solar heat input, the proposed set-up to supply the desirable thermal energy during the operation of 24 hours was extremely flexible, and also reliable due to auxiliary fossil-fuelled back-up heating system that stabilizes the operational settings after solar thermal input and at the turbine inlet.

Moreover, they mentioned that performance of cycle can be augmented by evolving a good control scheme aiming the minimal dispatch of fossil fuel. Lastly, their results also reveal that as compared to direct cycle, an indirect cycle consumes 19.5% less fossil fuel for a specific day which was chiefly attributed to the thermal energy storage's usage in the indirect cycle.

Chacartegui et al. (2011) [118] studied the application of CO_2 Brayton to CSP plants with central receiver. They found that layout 2 which was a recompression cycle and possess more complex layout working with the supercritical conditions at the inlet of compressor along with improved heat recovery can achieve higher cycle efficiency among the stand-alone closed recuperative Brayton cycle and this improvement can be high as 7-12 percentage point depending upon the inlet temperature of turbine.

Also, their results reveal that the combined cycle (i.e. SCO_2-ORC) use in solar power plants based on central receiver operating with 1000 K maximum temperature can increase the power of almost 7 percentage points with respect to the reheat and five feed water heaters integrated superheated steam cycles (i.e. at 850 K) for the same incident radiation. Lastly, they mentioned that as compared to steam cycle with reheat and feed water, the proposed combined cycle was simpler and more compact.

Cheng et al. (2017) [119] developed a thermodynamic model of SCO_2 cycle with recompression. They performed the optimization of global parameters based on sensitivity analysis and found that the final cycle efficiency was highly influenced by the maximum pressure and efficiency of turbo expander followed by the efficiency of recompressor, split ratio, and efficiency of main compressor.

Also, their outcomes reveal that by adjusting the split ratio (i.e. 0.687) and maximum pressure (i.e. 27.75 MPa), the cycle efficiency could be maximized to 0.447, however, the other

parameters such as temperature of heat source was 600℃, the compressor and recompressor efficiency was 0.8, and the turbine efficiency was 0.9.

Wang et al. (2018) [120] proposed a system which consists of solar island, biomass burner and power block. Their results indicate that at the design point, the system's solar-to-electric efficiency can reach to 27.85%, and the ratios of solar heat supply in the power cycle was in the range of 15.7–36.4% in the four representative days. At last, they carried out the economic evaluations so as to check the feasibility of proposed system and reveal that levelized cost of electricity of the system was 0.085 $/kW h.

2.3. Applications of ORC system for power generation and WHR

Mago et al. (2007) [121] carried out a second-law investigation for utilization of ORC system to transform low grade heat source's waste energy to power. They inspect the effect of boiling point temperature of fluid on the ORC performance with the help of organic fluids such as R134a, R113, R245ca, R245fa, R123, isobutane, and propane. Also, their results have been compared with water under similar conditions.

Moreover, they found that R113 based ORC system has the maximum efficiency amongst the fluids assessed for temperatures greater than 430 K while, for the temperatures between 380 and 430K, the fluid like R123, R245ca, and R245fa illustrate the best efficiencies, and isobutane demonstrate the best efficiency for the temperatures less than 380K. Finally, they mentioned that boiling point of organic fluid has a solid influence on the thermal efficiency of system.

Mago (2012) [122] presented an exergy analysis of medium-grade waste heat based ORC and selected the numerous organic working fluids such as R245fa, R123, R142b, isobutane, R113, and R141b with critical temperatures in the range of 407.7 to 524.9 K so as to study the effect of fluid's critical temperature on the functioning of ORC. It was concluded that at a temperature of 503 K, ORC can generate between 13.8 and 30 kW and the system can generate between 48.8 and 73 kW for a higher exhaust temperature of 713 K.

Lastly, study stated that the critical temperature of organic fluid has to be considered during the selection of fluid because if the critical temperature will be nearer to the exhaust temperature that can achieve smaller pinch point temperature difference and better exergy performance.

Wang et al. (2017) [123] stated that for the energy recuperation from the waste heat rejected by the internal combustion engines, the ORC system is a promising technology. They proposed a ORC system with dual loop which was made up of two cascaded ORCs that helps in energy recovery from the coolant and exhaust gases of engine, as a result, the energy recovery's overall efficiency could be improved substantially. Their study examines the R1233zd and R1234yf based regenerative dual loop ORC system to recover energy from compressed natural gas engine's waste heat. Moreover, they analysed the effect of a regenerative heat exchanger and other key operating constraints on the functioning of proposed dual loop cycle.

Also, they inspected the integrated engine-ORC system's performance under the actual operating conditions of engine and further investigates the proposed system's performance under the off-design conditions. Finally, their outcomes reveal that the proposed dual loop ORC system has an ability to achieve the better performance than the other ORC system employed in alike applications.

Tchanche et al. (2009) [124] comparatively assessed the thermal performance along with the thermodynamic and environmental properties of some fluids for the utilization in low-temperature solar ORC system. Their results reveal that for the small scale solar applications, the R134a fluid was the most appropriate for the low-temperature applications driven by heat source with the temperature beneath 90℃, which was followed by R152a, R600, R600a, and R290 fluid gives attractive performance but due to their flammability, it needs safety precautions.

Besides, they found that high boiling point of fluids such as ammonia, methanol, ethanol, and water makes them very efficient from the efficiency point of view but there was also a drawback exists which was occurrence of droplets during the process of expansion. At last, they mentioned that R12, R500, RC318, R114, and R113 were harmful for the environment according to the international regulations for example Kyoto and Montreal Protocols.

Xia et al. (2018) [125] found that at lower pinch point temperature variance in the evaporator, the ORC can achieve better comprehensive performance and its best value produces by the butane due to its low global warming potential for the exhaust temperature range of 443–483 K, and in range of exhaust temperature, i.e. 483–513 K, the R1233zd(E) gives the highest value of comprehensive evaluation index. Moreover, for the exhaust temperature lower than 443 K, the R1234yf was recommended.

Ahmadi et al. (2012) [126] conducted a thermodynamic modelling of the trigeneration system, which was comprises with gas turbine cycle, ORC system, a single effect absorption chiller, and a household water heater for the purpose of cooling, heating, and electricity generation. Further, they carried out the exergy and energy analysis plus assessment of environmental influence. They found that trigeneration system has a superior exergy efficiency than the combined heat and power systems or gas turbine cycles. In addition, their outcomes found that the combustion chamber has the utmost amount of exergy destruction because of irreversible nature of chemical reactions and high difference amongst the temperature of both working fluid and flame.

Moreover, their parametric examinations reveal that the compressor pressure ratio, inlet temperature and isentropic efficiency of gas turbine considerably affect the trigeneration system's exergy efficiency and environmental influence. Finally, they demonstrate that by enhancing the inlet temperature of turbine along with the reduction of combustion chamber mass flow rate can decrease the cost of environmental impact.

Roy et al. (2011) [127] analysed the performance of a regenerative ORC with the aid of working fluids, for instance R-12, R-123, R134a, and R-717. They found that R-123 shows the maximum efficiency of system, availability ratio, work output of turbine, and second law efficiency with minimum irreversibility, however, it requires the lowest system mass flow rate at the constant heat source temperature of 550 K. Their results also reveal that the system's irreversibility rate increases for a variable heat source temperature which results in a larger irreversibility with a higher source temperature and also concludes that the highest value of second law efficiency and availability ratio alongside lowest irreversibility were found to be with fluid R-123. Lastly, they assessed that the work output of turbine decreases linearly with larger slopes alongside the increase in mass flow rate of system.

Baral and Kim (2014) [128] assessed the thermodynamic performance of fifteen organic fluids in an ORC based cogeneration system. They conducted a thermodynamic modelling for a scroll expander of 1 kW, two heat exchangers of compact structure, a diaphragm pump and a solar collector. Their study investigates that out of 15 fluids, the most appropriate working fluids were R134a and R245fa for the low and medium-temperature solar ORC cogeneration systems, correspondingly. At last, they noticed that RC318 and R123 have attractive performance but it also needs the environmental safeguards because of their high ODP and high GWP.

Guo et al. (2016) [129] stated that selection of best working fluid depends on heat source and heat sink profile. They also mentioned that performance of pure fluids can be better than mixtures when inlet temperature of heat source will be high and temperature gradient will be low. Furthermore, their study illustrates that the mixtures perform better when inlet temperature of heat source becomes lower, as a result, temperature gradient of both heat source and heat sink become higher.

Moreover, they found that heat sources with small temperature gradients requires fluids with high critical temperatures and heat sources with large temperature gradients requires fluids with low critical temperatures. Lastly, they mentioned that recuperator generally utilized to augment the efficiency of cycle. Furthermore, efficiency can be decreases with the utilization of a recuperator at what time inlet temperature of heat source will be low and temperature gradient will be high.

Fu et al. (2016) [130] examined a 250-kW ORC system with the support of working fluid, for instance R245fa and a turbine expander, and it was reported that the average net power output of 242.5 kW and system thermal efficiency of 8.3% at evaporation temperature of 104.4°C and condensation temperature of 32.3°C. They also noticed that the fluctuation in the net power output was ±1.7 kW, and their results found an improvement in stability of system and developed the system's high potential for on-site WHR applications.

Moreover, they observed that as the pressure ratio of the turbine rises from 5.74 to 7.22 results in a slight decrease in the isentropic efficiency, i.e. from 63.7% to 62.2%.

2.3.1. Utilization of RES for ORC system

Li et al. (2016) [131] recommended a novel solar ORC system alongside direct vapor generation. They discussed the technical feasibility of system and analysed the functioning by using 17 dry and isentropic working fluids. Then, they studied the effect of fluid on the ORC, collectors, and whole system efficiency. Their study outcomes demonstrate that efficiency of collector generally declines, while the efficiency of both ORC and system enhances with the enhancement in critical temperature of fluid.

Finally, they concluded that the thermal efficiency of ORC, collector, and overall system for R236fa were found to be as 10.59, 56.14, and 5.08%, respectively which was found to be at evaporation temperature of 120℃ and solar radiations of 800 W/m^2. Moreover, their

findings indicate that the R123 shows the highest overall performance and also suitable for the system as proposed in this study in short term.

Nafey and Sharaf (2010) [132] stated that the ORC system has unique properties that are well suited for the generation of solar power. They utilized the solar thermal collectors for input heat, expansion turbine for the calculation of work output, condenser for the rejection of heat, pump, and reverse osmosis unit in the cycle. Then, they selected the various working fluids like butane, isobutane, propane, R134a, R152a, R245ca, and R245fa, which have been tested for the flat plate collector. While, for the compound parabolic concentrator, the fluids such as R113, R123, hexane, and pentane have been inspected. Further, for the SPTC system, the fluids namely dodecane, nonane, octane, and toluene were assigned.

Moreover, they performed an exergy and cost analysis for the DVG process under the operating conditions like saturated and superheated. Finally, their study found that for the solar collector area, specific total cost, and exergy destruction rate, the fluids such as toluene and water attained the minimum results.

Delgado-Torres and García-Rodríguez (2010) [133] carried out a study in which they coupled the low-temperature ORC and reverse osmosis unit for the desalination of seawater and brakish water. For this purpose, they chose four different working fluids, for instance butane, isopentane, R245fa, and R245ca. They found that in the configuration of DVG, the ORC's working fluid was directly heated inside the solar collector's absorber and in the second configuration, a HTF was heated without a change in phase inside the solar collector's absorber which transfer its thermal energy to the water and it was then utilized as a working fluid of ORC during the cooling process in the heat exchanger unit.

Also, they analysed the effect of temperature of condensation in ORC and process effectiveness of regeneration over system productivity. Moreover, they choose the R245fa working fluid for the solar ORC and parametric values of preliminary design of the solar thermal driven reverse osmosis and finally, concluded that the maximum increase in the solar desalination systems' productivity was below 2% if the thermal energy rejected by solar ORC was used to preheat the feed water.

Al-Sulaiman et al. (2012) [134] assessed the functioning of a novel system based on SPTC and ORC for united cooling, heating, and power. They utilized a portion of waste heat in heating by the heat exchanger and other portion was used in single-effect absorption chiller for cooling. Also, they considered three modes of setup such as solar, solar and storage, and storage mode

alongside three cases such as electrical power, cooling-cogeneration, and heating-cogeneration were considered to assess the improvement in performance of present system and a system for 500 kW electricity production has been designed in this research study.

Finally, their results indicate that for the solar, solar and storage, and storage mode, the highest electrical efficiency was found to be as 15%, 7%, and 6.5%, respectively. However, the highest combined cooling, heating, and power efficiency was around 94%, 47%, and 42%, respectively.

Gao et al. (2015) [135] reported a method for the working fluid selection and preliminary design of solar energy driven ORC, and based on inlet pressure and temperature of turbine, the performance of nine working fluids were inspected under the various working conditions. They performed a comparison between thermal efficiency of both superheated and saturated cycle, and found that superheated cycle has the higher efficiency than the saturated cycle.

Also, they stated that inlet pressure of turbine has more complicated than the temperature and found that when inlet temperature of turbine is lower or nearer to its critical temperature then with the rise in inlet pressure of turbine, the efficiency can be decreases; however, as the inlet temperature of turbine is very much higher than its critical temperature then with the rise in inlet pressure of turbine, the efficiency will be increases.

Moreover, their study reveals that in the saturated cycle, working fluid with higher critical temperature can illustrate the higher thermal efficiency. At last, they demonstrate that the MM (hexamethyldisiloxane) as a working fluid is the optimal choice for the system which is stable with the material of the system up to 300℃.

Tunc et al. (2012) [136] performed exergy analysis of ORC system integrated with geothermal power plant. They chose four unlike working fluids such as isobutene, HCFC123, R134a, and R12 for ORC. Their results demonstrate that isobutene has the highest efficiency among others which was around 30% and the electrical power was found to be as 6626 kWe. Finally, they concluded that depending upon the working fluid used, the cycle efficiency can vary between 8% and 30%.

Calise et al. (2016) [137] performed an energetic, exergetic, & exergoeconomic examination of a novel solar-geothermal polygeneration system. They used medium-enthalpy geothermal energy and SPTC field to operate the ORC system integrated with multi effect distillation unit. They found that the solar radiations affect the exergy production rate which means that it increases during daylight hours.

Further, their findings illustrate that the lower value of global exergetic efficiency found to be in summer as compared to winter and they also evaluate the annual performance on the basis of weekly and annual simulations that has been performed throughout the year. Results reveal that highest exergy destructions were detected in ORC module, secondary heat exchanger, and SPTC field.

In addition, they found that for the thermal recovery mode, global exergy efficiency varies between 40% and 50%, however, it varies between 16% and 20% for the cooling mode. At last, their exergoeconomic results found that the electricity cost varies in the range of 0.1475-0.1722 €/kWh.

He et al. (2012) [138] carried out a study on SPTC integrated ORC system. They inspected the influence of several factors on the functioning of SPTC field such as interlayer pressure amongst absorber and glass tube, high temperature oil's flow rate in the absorber tube, intensity of solar radiation, and angle of incidence. Their study shows that the solar collector's heat loss enhances sharply as the interlayer pressure amongst the absorber and glass tube rises at the initiation and then reaches to a constant value, and similarly deviation of heat collecting efficiency with the high temperature oil's flow rate in the absorber tube followed the same variation trend. While, the intensity of solar radiation and angle of incidence has the contrary influence on the heat collecting efficiency.

Bryszewska-Mazurek et al. (2011) [139] experimentally investigated R245fa working fluid based ORC system powered by solar energy as well as compared the thermodynamic efficiency of cycle with and without an internal heat exchanger. Their findings reveal that with the heat regeneration, the maximum value of thermodynamic efficiency of ORC was around 9%. At last, they pointed out the efficiency can slightly increase and condenser operation can be rationalized with the use of internal heat exchanger.

Gang et al. (2010) [140] designed a low temperature solar thermal electric production accompanied by the regenerative ORC. Based on the distributed parameters, they carried out a mathematical simulation of processes associated with heat transfer and power conversion. They also analysed that the regenerative cycle has a positive influence over efficiency of ORC system but negative influence over collector's efficiency due to the enhancement of first stage collectors' average working temperature.

Moreover, they found that the maximum regenerative ORC efficiency was 9.2% higher than that without regenerative cycle. Lastly, their results show that for the irradiance of 750

W/m^2, the electrical efficiency of system with regenerative ORC was about 8.6% which was relatively 4.9% higher than that without the regenerative cycle.

Yu¨ksel (2018) [141] performed the thermodynamic analysis of SPTC integrated modified ORC along with a single effect absorption cooling system and a PEM electrolyzer for the hydrogen production. Their results reveal that solar radiation is a crucial factor that affecting exergy efficiency of system and production rate of hydrogen. Finally, they found that exergy efficiency of the system upsurges from 58%-64% and production rate of hydrogen rises from 0.1016 kg/h to 0.1028 kg/h with the rise in solar radiation from 400 W/m^2 to 1000 W/m^2.

Reddy et al. (2012) [142] carried out an energetic and exergetic analysis for the components of the SPTC/receiver and Rankine heat engine along with evaluation of energy & exergy losses and efficiencies for the typical SPTC concentrating thermal power plant. They found that by enhancing the pressure from 90 to 105 bar, the energetic and exergetic efficiencies of SPTC concentrating thermal power plant also enhanced by 1.49% and 1.51%, respectively. Their results reveal that an increase in average year-round energetic efficiency for the location of Jodhpur was found from 22.01% to 22.62%, and it can be enhanced from 20.98% to 21.50% for the location of Delhi. Whereas, the average year-round exergetic efficiency for the location of Jodhpur can be enhanced from 23.66% to 24.32%, and it can be enhanced from 22.56% to 23.11% for the location of Delhi under the progression of the solar thermal power plant from the conditions of variable load to full load.

Bellos et al. (2018) [143] investigates an energetic, exergetic, & financial performance of a solar driven trigeneration system. They stated that SPTC combined to a storage tank can be used so as to feed an ORC which discards heat to an absorption heat pump. They also optimized the system performance based on the exergy and energy method, and optimization parameters were the temperature of heat source in the inlet of system for heat recovery, the turbine inlet pressure, & temperature of discarded heat of ORC to absorption chiller. In addition, they chose the various organic fluids such as toluene, n-octane, MDM, and cyclohexane, and further assessed that the toluene has the most suitable choice.

Moreover, their results reveal that during the operation of optimum system yearly, the heating, cooling, and electricity production were found to be as 995 kWh, 232 kWh and 154 kWh, respectively. At last, they found 5.33 years' payback period and internal return rate of 20.02% that shows a feasible system.

Bellos and Tzivanidis (2018) [144] carried out a study on the solar energy (i.e. SPTC) and waste heat (i.e. temperature varies from 150℃-300℃) driven hybrid ORC. They selected four different fluids such as toluene, cyclohexane, MDM, and n-pentane. Their results disclosed that toluene has the ability of highest electricity production, i.e. ranges from 479 kW to 845 kW followed by cyclohexane, MDM and n-pentane. Also, they found that in case of toluene, the system efficiency varies from 11.6% to 19.7%.

Bellos et al. (2017) [145] investigated the performance of a commercial SPTC (Eurotrough ET-150) according to the energetic and exergetic point of view for a temperature range from 300 K to 1300 K. They selected working fluids such as Pressurized water, Therminol VP-1, nitrate molten salt, sodium liquid, air, CO_2, and helium to examine the SPTC performance. Their results prove that for the inlet temperature of 800 K, the liquid sodium shows the global maximum exergy efficiency of 47.48% followed by the helium, CO_2, and air, i.e. 42.21%, 42.06%, and 40.12%, respectively.

Moreover, they concluded that for the temperature levels up to 550 K, the pressurized water is the best working medium, whereas, for the temperatures greater than 1100 K, the best suited fluids are CO_2 and helium.

Lizarte et al. (2017) [146] analysed the performance of combined toluene based ORC and NH_3/CO_2 based cascade refrigeration system for the applications of low-evaporation-temperature, i.e. 55℃ to 30℃. Then, they found with the help of both parametric study and regression analysis that corresponding to the ORC evaporation temperatures of 315℃ and 255℃, the highest overall system coefficient of performance and exergetic efficiency were 0.79 and 31.6%, respectively.

2.3.2. Recent studies on the Supercritical ORC (SORC) system

Zhou (2014) [147] discussed that as compared to conventional ORC, the SORC has the higher conversion efficiency due to better thermal match as a result of obscured liquid-to-vapor boundary of organic fluid at supercritical state presented in the heat exchanger unit which means that irreversibility will be reduced. Apart from this, they examined the capability of power generation from the hybridization of solar and geothermal energy based SORC, and then performance was assessed by utilizing the technical, economical, and figure of merit analysis

which was further compared the performance with those of subcritical hybrid plant, stand-alone solar and geothermal plants.

Their technical analysis results thermodynamically reveal that the SORC based hybrid plant outperforms the subcritical ORC based hybrid plant (i.e. produces 4-17% more electricity by employing same energy resources) if at least 66% its input exergy was encountered by the solar energy. Moreover, their exergy analysis shows that the exergetic efficiency of a supercritical hybrid plant was around 27-34% and for the sub-critical hybrid plant, it was around 23-32%.

In addition, their figure of merit analysis reveals that as compared to the two stand-alone plants, the hybrid plant utilizing sub-critical ORC generates a maximum of 15% and hybrid plant by using SORC produces 19% more annual electricity. Last but not least, their economic analysis results found that the solar-to-electricity cost of almost 1.5-3.3% was found to be in SORC based hybrid plant which was less than subcritical scenario.

Kalra et al. (2012) [148] reviewed the performance of SORC, subcritical ORC, and trilateral flash cycle. They mentioned that SORC has an advantage of better thermal match between the cooling curve and heating curve of working fluid as compared to the subcritical ORC. They also stated that as compared to the baseline subcritical cycle, the SORC system offers significant improvement in net power output.

Chen et al. (2010) [149] carried out a performance study on ORC systems and supercritical Rankine cycles for a low-grade heat conversion into power. They discussed that unlike supercritical Rankine cycle, the ORC system does not have a good thermal match with the heat source, however, supercritical Rankine cycle normally operated at the higher pressure. Furthermore, they found that the high unit turbine work output can be achieved by using working fluids with the high density and high latent heat.

Also, their study demonstrates that due the requirement of superheating in case of wet fluids in ORC system, isentropic and dry fluids can be preferred. While, with respect to the cycle efficiency, superheating in case of dry fluids could play a negative role. Moreover, they mentioned that for the supercritical Rankine cycle, fluids with the low critical temperatures and pressures can be potentially employed.

Pan et al. (2012) [150] discussed that ORC system has categorized in to the subcritical ORC and SORC system on the basis of critical temperature of fluid and temperature of heat source. They

stated that the HFC125, HFC143a, and HF218 can be used in both subcritical ORC and SORC for heat source temperature of 90℃ & the performance of these three substance especially in near critical conditions with the inlet temperature of expander (i.e. 85℃) and mass flow rate of hot water (i.e. 1 kg/s) has been carried out. Their results reveal that the thermal efficiency varies continuously as the fluids drive in SORC from the subcritical ORC. Also, subcritical ORC has a higher value of maximum net power generation in near-critical conditions as compared to SORC.

Furthermore, they found that when the HF218 used as a working fluid in subcritical ORC, outlet temperature of water in heater enhances firstly and then decreases as the heating pressure rises. Therefore, they concluded that the better performance can be achieved in near critical-conditions of ORC than in supercritical conditions.

Xu et al. (2015) [151] evaluated the performance of direct vapor generation SORC system driven by LFR concentrators. They discussed that the complex two-phase problem in the receiver evaporator can be avoided by supercritical process. Also, they compared the considered system with the conventional subcritical ORC system and uncovered that cyclohexane has an utmost overall efficiency of 19.65% with lower mass flow rate as rivalled with other chosen working fluids. Their findings illustrate that as the inlet temperature of turbine upsurges, the ORC efficiency increases at much faster rate than the decreasing rate of LFR efficiency that results in overall efficiency increases.

Mocarski and Borsukiewicz-gozdur (2015) [152] carried out a review study and mentioned that the adjustment of working fluid in terms of critical temperature to the heat source's temperature should take into account during the selection of fluid in the SORC power plant. They concluded that supercritical parameters of ORC power plant can increase its efficiency but in some cases a decrease in power plant rating efficiency was found through the application of supercritical cycle. Also, they stated that in supercritical cycle, larger heat exchangers are required that impact directly on the investment costs.

Yaglı et al. (2016) [153] designed a subcritical ORC and SORC in order to waste heat recovery of combined heat and power engine which was fuelled by the biogas. They used R245fa as a working fluid, and found that with enhancing the inlet turbine temperature and constant inlet pressure of turbine, three different changes were noticed in net power, thermal and exergy efficiency. Their results reveal that up to inlet pressures of turbine of 12 bar, the net power,

thermal and exergetic efficiency shows the almost linear decreasing trend and an increase has been observed with the increasing temperature until a certain point and then results start to decline between the inlet pressure of turbine, i.e. 12 and 24 bar, then, results always increase with increasing temperature over the constant inlet turbine pressure of 24 bar.

Lastly, they found that the SORC has the better performance in contrast to subcritical ORC, and concludes that for the subcritical ORC and SORC, the net power, thermal and exergy efficiency were found to be as 79.23 kW, 15.51% and 27.20% and 81.52 kW, 15.93% and 27.76%, respectively.

Wang et al. (2018) [154] examined the influence of inlet temperature of cooling water in condenser over the functioning of SORC system. They found that as soon as inlet temperature of cooling water upsurges from 20°C to 30°C, ORC's net power output decreases by 30%, 21%, 16%, respectively and thermal efficiency decreases by 19%, 11%, 11% individually with the designed temperatures of flue gas, i.e. 120/150/180°C in the SORC system. They also found that the effect of the increment in the inlet temperature of cooling water on the performance of system was much greater than the decrement under the off-design condition with the same amount on contrast to the design condition.

In addition, their results reveal that in Beijing, Shanghai and Guangzhou, the ORC system's optimal design condensation temperatures were about 30–34 °C, 34–38 °C and 38–42 °C individually.

Javanshir and Sarunac (2017) [155] investigates the thermodynamic performance of a simple subcritical and SORC so as to evaluate the influence of working parameters on functioning of cycle and selection of best working fluid. Their results showed that by using a dry working fluid in ORC, a decline in thermal efficiency was found with an upsurge in inlet temperature of turbine because of the merging of isobaric lines with the temperature. Lastly, they observed that as compared to the dry and wet fluids, the efficiency of an ORC using isentropic working fluids was higher and also found a higher cycle net power output in case of working fluids with higher specific heat capacity.

Braimakis et al. (2015) [156] investigates the WHR potential of the ORC and found that the working fluids' critical temperature can affect to the system exergy efficiency. In addition, they found that for the medium and high waste heat temperatures, the SORC has an ability to show the improvement in exergy efficiency mainly for the low critical temperature fluids as

compared to the subcritical ORC. Their results reveal that in the case of propane, the maximum increase in efficiency was 18%. Furthermore, they stated that for both the subcritical and supercritical conditions, the use of zeotropic binary mixtures as a substitute to pure fluids can potentially enhance the cycle performance.

Moreover, depends on the heat source temperature, they assessed that the mixtures instead of their pure component shows the increase in second law efficiency and it exceeds 60% in case of supercritical cyclo-pentane-propane.

Moloney et al. (2018) [157] stated that the SORC has more efficient than an ORC for low-temperature resources such as geothermal energy. They performed a parametric analysis for the different pressures & temperatures at inlet of the turbine and also analysed the various environmental and nontoxic fluids. Finally, they concluded that the best performing fluid was R1233zd(E) with a plant efficiency and second law efficiency of 16.2% and 52.3%, respectively for the inlet temperature of turbine, i.e. 240°C.

2.4. Applications of combined cycles

Khaliq et al. (2009) [158] proposed a novel cogeneration system, which was a grouping of Rankine power cycle & absorption refrigeration cycle for recovery of industrial waste heat in order to produce combined power and refrigeration. They implemented an energy and exergy based thermodynamic analysis and parametric study to analyse the influence of inlet temperature of exhaust gas, pitch point, and composition of gas on power to cold ratio, component's destruction of exergy and cogeneration cycle's energy and exergy efficiency. Their results revealed that with upsurge in gas inlet temperature, power to cold ratio increases while first law efficiency decreases. However, with increase in pitch point, exergy efficiency and power to cold ratio decreases while first law efficiency increases.
In addition, they found that maximum exergy destructions which was around 40% of the total exergy destructions found to be in steam generation process followed by 20% in steam turbine, 18% in condenser, and 10% in the generator of absorption system.

Wang and Dai (2016) [159] examines the two cogeneration cycles in which waste heat was recuperated by either TCO_2 cycle or ORC from a R-SCO_2 Brayton cycle in order to generate electricity. They selected the organic fluids such as R123, R245fa, toluene, isobutane, isopentane, and cyclohexane as working fluids. Further, they developed thermodynamic and exergoeconomic models based on conservations of mass & energy, exergy balance as well as

cost equations for the cycles. Also, their study carried out the parametric investigations to examine the effect of decision variable on the functioning of SCO_2/TCO_2 and SCO_2/ORC cycles, and then optimized and compared the performance. Their findings indicate that at lesser compression pressure ratio, the SCO_2/TCO_2 cycle perform superior than the SCO_2/ORC, and also found that a higher inlet temperature of TCO_2 turbine improves the exergoeconomic performance of the SCO_2/TCO_2 cycle.

Moreover, their optimization results reveal that the second law efficiency of SCO_2/TCO_2 cycle has comparable values along with SCO_2/ORC. Lastly, they conducted a exergoeconomics based optimization and found that the SCO_2/ORC has somewhat lesser total product unit cost than that of SCO_2/TCO_2 cycle.

Akbari and Mahmoudi (2014) [160] executed an exergoeconomic evaluation for a combined R-SCO_2 Brayton cycle/ORC. They considered different eight working fluids for the ORC and investigated the effect of pitch point temperature variance in pre-cooler1 and in condenser, compressor pressure ratio, and inlet temperature of ORC turbine over the functioning of combined cycle and R-SCO_2 Brayton cycle. They optimized the functioning of combined cycle thermodynamically and economically by using EES software.

Their outcomes revealed that exergy efficiency of combined cycle superior than that of R-SCO_2 Brayton cycle by up to 11.7% and total product unit cost for combined cycle was 5.7% lesser than that of simple recompression cycle. Finally, they concluded that the isobutane and RC318 as a working fluid shows the maximum exergy efficiency & lowest product unit cost for the combined cycle.

Saleh (2016) [161] investigated the performance of a low-grade thermal energy based combined ORC-vapor compression refrigeration system. They selected some hydrocarbons and hydrofluorocarbons, and hydrofluoroolefins as a proposed working fluid and examined the effect of temperatures of evaporator, condenser, boiler performance, and isentropic efficiencies of compressor and expander on the performance of system. They found that as the temperature of evaporator and boiler as well as isentropic efficiencies of compressor and expander increase, the COP of overall system improves while the working fluid's total mass flow rate for each kW cooling capacity decreases.

Their results concluded that the fluids such as R600 and R245fa have the highest value of overall system COP and also recommended that the R600 is a superior candidate for the

combined system because of environmental issues of R245fa. Lastly, they found that the maximum COP of overall system by using R600 was 0.718.

Polyzakis et al. (2008) [162] stated that as compared to steam, gas turbine power plant has comparatively low capital cost. Also, they optimized the functioning of power plant based on combined cycle and compared the different configurations of gas turbine cycles such as simple, intercooled, reheated, and intercooled and reheated. Their outcomes indicate that combined cycle would produce 300 MW power in which gas turbine produces 200 MW and steam turbine produces 100 MW.

Their study showed that the most desirable configuration was a reheated gas turbine due to the high exhaust gas temperature of turbine that results in thermal efficiency of bottoming steam cycle could be high. Finally, they mentioned that optimal gas turbine cycle could lead to a more efficient combined cycle power plant that results in great savings.

Ersayin and Ozgener (2015) [163] performed an investigation of power plant grounded on combined cycle on behalf of first & second law thermodynamics. They uncovered that energy and exergy efficiency of combined cycle power plant were found to be as 56% and 50.04%, respectively, and also revealed that among other components, the combustion chamber possesses utmost exergy destruction rate.

In addition, they mentioned that by adjusting the air-fuel ratio of mixture entering into the combustion chamber and by reducing surplus air so as to realize the ideal combustion, the high energy and exergy rate losses in the combustion chamber can be reduced which results in first and second law efficiency of combined cycle power plant can be enhanced.

Njoku et al. (2018) [164] analysed the performance of a combined gas and steam turbine cycle power plant coupled by a ORC and VAR cycle. They performed energy, exergy, and environment sustainability index analysis and their results reveal that through the R113 based ORC which has been operated by the waste exhaust heat of a combined cycle power plant was generated extra 7.5 MW of electricity and additional 51.1 MW electricity was produced with the utilization of VAR cycle so as to cool inlet air stream to 15℃ in the gas turbine plants. In addition, they determined that the net power output, sustainability index, thermal and exergy efficiency were increased by 9.1%, 8.4%, 8.7% and 8.8%, respectively in the integrated power plant by integrating ORC and VAR cycle with the combined cycle power plant. However, they found that both the rate of total exergy destruction and specific fuel utilisation were diminished by 13.3% and 8.4%, correspondingly.

Wu et al. (2017) [165] performed energy, exergy and exergoeconomic analysis of combined R-SCO_2 Brayton cycle and absorption refrigeration cycle. They conducted a parametric analysis to investigate the functioning of combined cycle, which was optimized and further compared on the basis of first law, second law, and exergoeconomic perspective. Also, they concluded that by combining the recompression SCO_2 Brayton cycle with the absorption refrigeration cycle cannot not only enhance its first and second law efficiencies as well as improve the exergoeconomic performance.

Their results reveal that utmost rate of exergy destruction was occur in reactor, while less exergy destruction was occurred in the constituents of absorption refrigeration cycle. Also, their exergoeconomic based optimization found that as competed with R-SCO_2 Brayton cycle, the combined cycle possesses 26.12% higher first law efficiency and 2.73% higher second law efficiency, and 2.03% lower total product unit cost.

Moreover, they pointed out that both thermodynamic and exergoeconomic performances of the combined cycle can increase with the increase in outlet temperature of reactor. At last, their study demonstrates that in contrast to recompression SCO_2 Brayton cycle, the combined cycle utilized only 0.36 MW of power to produce the cooling capacity of 71.76 MW and cooling exergy of 6.57 MW.

Hou et al. (2018) [166] performed the thermodynamic analysis for a novel combined R-SCO_2 cycle and regenerative ORC by means of zeotropic mixture. They applied a genetic algorithm based multi objective optimization and their results revealed that R236fa/R227ea (0.46/0.54) was an optimal zeotropic mixture. Furthermore, they found that optimized exergy efficiency and total product unit cost were evaluated to be as 73.65% and 10.93 $/GJ, correspondingly.

Song et al. (2018) [167] evaluated the effect of SCO_2 cycle's dissimilar recuperative ratios, effect of initial temperature of heat source and total heat load on the ORC act as a bottoming cycle. They presented two configurations of combined cycle (i.e. SCO_2-ORC) with or without pre-cooler. They also state that thermal efficiency of system could increase by the residual heat recovery with the help of a bottoming cycle. Their results found a higher evaporation temperature in ORC by using combined cycle system with a pre-cooler.

Furthermore, they reveal that with the parametric optimization, the SCO_2-ORC cycle performance could be considerably improved. Moreover, they observed that the ORC could

successfully recover the residual heat of SCO_2 cycle, thus, thermal efficiency of system increases.

Javanshir et al. (2018) [168] found that R141b using ORC has the greatest thermal efficiency for lower than the 300℃-cycle maximum temperature. Their results also revealed that combined Rankine/ORC and CO_2 regenerative Brayton cycle with recompression were the best options for the between the 300-650℃ medium range of cycle maximum temperature. Moreover, they observed highest thermal efficiency in the combined Brayton/ORC and regenerative Brayton cycle with recompression depending upon the maximum pressure and for the cycle maximum temperature higher than 650℃.

2.4.1. Utilization of RES for the combined cycles

Al-Sulaiman (2014) [169] conducted an exergy analysis of SPTC driven thermal power system. In this direction, SRC or a combined cycle, which was made up from SRC used as a topping and ORC as a bottoming cycle was selected to produce power. They selected refrigerants such as R134a, R152a, R290, R407c, R600, R600a, and ammonia were used for the ORC. Exergetic constraints like exergetic efficiency, rate of exergy destruction, Y_{DEP}, Y*, and IMP were also assessed in this research. It was found that exergy efficiency increases as the solar irradiation increases and also noticed that the combined cycle based on R134a indicates the maximum exergy efficiency of 26% after that combined cycle based on R152a along with 25% exergy efficiency. However, the lowest exergy efficiency of 20-21% was found to be in R600a combined cycle.

In addition, present study concludes that the solar collector has maximum exergy destructions which were more than 70% of total exergy destructions. Lastly, the results reveal that combined cycles based on R290, R407c, R600, and ammonia have a marginal difference between their exergetic performance.

Gao et al. (2017) [170] conducted a parameter and layout optimization analysis on the novel high temperature solar SCO_2 and ORC combined power system alongside storage device to store the low temperature thermal energy. Their results reveal that the ratio of ORC power output to the overall system and inlet turbine temperature in ORC enhances with the inlet temperature of compressor, however, the overall thermal efficiency of system decreases. Also, they uncovered that siloxanes have the best performance in the combined cycle. Furthermore,

they mentioned that the overall thermal efficiency of system can be kept as 38% when for D5, D4, MDM, and MM, the ratio of ORC power output to overall system reaches 50%, meanwhile, inlet turbine temperature in ORC was in the range of 220∼230℃. The temperature range was far lower than the temperature at high pressure SCO_2 turbine inlet, therefore, thermal storage was avoided at the high temperature. Moreover, they stated that the reheating, non-cooling and non-recompression layout was the optimum layout.

Sánchez et al. (2013) [171] carried out a performance analysis of different types of the combined cycles such as SCO_2-ORC, conventional gas turbine and ORC, and ORC-ORC systems and these were evaluated for a tower-type central receiver CSP plant. They used isopentane in the bottoming system in all cases showing favourable results for the proposed combined cycle. Also, they mentioned that with the use of CO_2, economic benefits must be expected because of the lower footprints of the heat transfer equipments and these features can be achieved by transport properties of the CO_2 when it was used at very high pressure and reduced the size of turbomachinery due to the decreased volumetric flows. At last, their results reveal that the favourable properties of SCO_2 will significantly reduce the footprint and capital costs.

Besarati and Goswami (2014) [172] examined the different configurations and found that the recompression and partial cooling configurations are the promising option for CSP applications. They indicate that with these configurations and at the same operating conditions as that of central receiver tower, the SCO_2 Brayton cycle can achieve more than 50% efficiency and it can further be improved with the utilization of bottoming cycle.

They also reported that the added bottoming cycle can upsurge the overall efficiency of cycle by 3-7%. They conclude that recompression based combined SCO_2 and ORC cycle can achieve the maximum efficiency and their results reveal that based on the global efficiency and expansion ratio, butene and cis-butene were the most appropriate fluids for every configuration of combined cycle.

Wang et al. (2017) [173] performed an exergy and exergoeconomic investigation for R-SCO_2/TCO_2 cogeneration cycle. They evaluated that energy and exergy efficiency accompanied by exergoeconomic performance of R-SCO_2 cycle can be improved by combined configuration. Also, they concluded that reactor has highest amount of exergy destruction rate, however, the components of TCO_2 has the lowest amount of exergy destructions. From the exergoeconomic based optimization, it was revealed that the overall exergoeconomic factor, total and exergy destruction cost rate assessed to be as 53.52%, 11243.15 $/h and 5225.17 $/h,

correspondingly. At last, their optimization results conclude that a decrease in both total and exergy destruction cost rate could be achieved with an enhancement in outlet temperature of reactor.

AlZahrani and Dincer (2018) [174] investigates the energy and exergy based thermodynamic performance of SPT integrated SCO_2 Brayton cycle which is cascaded by an ORC. They found that energy conversion efficiency of CO_2 Brayton cycle was about 40% and exergy efficiency was about 69%, however, the total power produced was about 102.7 MWe with the utilization of 450,000 m^2 total mirror area in the case of CO_2 Brayton cycle only. Their results also showed that a noteworthy amount of exergy destruction was found in the solar heliostats and receiver, i.e. around 81%.

Also, they reveal that the energy and exergy efficiencies achieved by overall plant was 26.9% and 28.8%, respectively and these can enhance to 30.4% and 32.6%, respectively by integration of ORC.

Garcıa et al. [175] executed a study on the ammonia–water power and cooling cycle based on exergy and statistical analysis. They used the response surface technique for the combined cycle in order to calculate the optimal operating conditions and they chose the ratio between exergetic efficiency and destruction as the response variable. Their outcomes reveal that concentration of ammonia, pressure ratio, efficiency of turbine, and temperature of pinch point in the heat exchanger have highly influence on the response variable.

Also, they observed that best functioning of the combined cycle was achieved with ammonia composition at absorber outlet and pressure ratio of around 0.47 and 14, respectively. Lastly, they concluded that LFR collector field with 40% more of mirror area attained comparable thermal performance in contrast to the SPTC field.

Kizilkan [176] assessed the energy and exergy performance for SPTC driven combined CO_2 power-refrigeration system. They evaluated that energy efficiency of SCO_2 cycle and ORC was 12.9% and 4.47%, respectively and COP of refrigeration was 3.35%. Their result also reveal that for the SPTC length of 2020.78 m, the required total aperture area of SPTC was found to be as 9801 m^2.

Furthermore, they found that exergy efficiency and exergy destruction rate were 12.95% and 4891 kW, respectively. Moreover, they uncovered that the chief contributor of exergy destruction was SPTC because of its huge area.

2.5. Outcomes of the literature review

1. RES, for instance high temperature fuel cells, CSP systems, and geothermal power plants can be utilized as a source of energy for function of SCO_2 cycle [66].
2. SPTC system shows its capacity to work in a commercialized environment and measured as the most mature sort of CSP system but it could face competition in future from LFR system [49,68].
3. In SCO_2 cycle, compactness and simplicity can make it more cost-effective than SRC even among the temperature range of 400℃-650℃ [61,83].
4. In SCO_2 cycle, if CO_2 will be compressed around its critical point, the specific volume will be reduced which results in decreases the compression work. Thus, the efficiency of cycle will be higher [62].
5. In comparison to SRC, the recuperation of waste heat from gas turbine cycle by SCO_2 cycle is practically feasible [66].
6. So as to improve the thermal efficiency, the SRC could be replaced by SCO_2 cycle [66].
7. Under the low turbine input temperature, SRC can attain high efficiency which is because of the compression of working fluid at liquid state or less compression work required in this case because liquid water is incompressible. However, gas turbine cycle required large compression work because air is a compressible fluid which means that it requires high inlet turbine temperature, consequently, raises the material issues in the gas turbine cycle. Due to these factors, its thermal efficiency is not significantly higher than the SRC. Apart from this, SCO_2 cycle has the advantages of both gas turbine cycle and SRC. Which means that SCO_2 will be compressed in incompressible region and as compared to SRC, large turbine inlet temperature could be supplied with fewer material concerns [66].
8. The CO_2 becomes incompressible at critical condition which is 30.98℃ and 7.38 MPa, and its compressibility factor falls to 0.2-0.5. As a result, compression work can be reduced [66].
9. In SCO_2 cycle, the system works above the critical point and minimum pressure will be upper than the SRC and gas Brayton cycle, which means that fluid remains dense in the entire cycle. Due to higher fluid density, the volumetric flow rate decreases in SCO_2 cycle that results in 10 times smaller turbomachinery needed as compared to the SRC [66].
10. As compared to SRC, pressure ratio in the SCO_2 cycle is much smaller and the outlet temperature of turbine is relatively higher which means that heat in large amount must be recuperated, therefore, thermal efficiency of cycle rises [66].

11. In recuperator of SCO_2 cycle, the cold side flow's specific heat is 2 to 3 times superior than the hot side flow. Therefore, in the recompression layout, CO_2 flow is split to compensate the difference between the specific heat in LTR unit and to maximize the recuperation of heat. Finally, the thermal efficiency of recompression cycle could be enhanced due to reduction of waste heat [66].
12. Heat sources with limited capacity along with the temperature lies below 400℃-500℃, the ORC is the unrivalled technical solution for the generation of electricity [67].
13. ORC can recover heat from the different sources, for instance solar energy, heat of geothermal, biomass, and industrial waste heat, which is due to its low operating temperature [68].
14. In the solar based ORC, with increment in the inlet turbine temperature, the efficiency upsurges and at above the critical temperature, thermal efficiency upsurges additionally with the rise in inlet turbine pressure [135].
15. Recuperator in ORC could be utilized to preheat the working fluid after the pump with the help of superheat available after the expansion process. This process increases the efficiency of cycle [148].
16. The advantage of supercritical ORC (SORC) over subcritical ORC is the better match between resource cooling curve and heating curve of working fluid [148].
17. As compared to subcritical ORC, the SORC offers significant improvement in net power output [148].
18. Process of heating in SORC doesn't go through the diverse two phase region such as occurs in subcritical ORC that outcomes in better thermal match in the evaporator unit, in this manner, less irreversibilities happen in SORC [149].
19. When the working fluid's critical temperature is extremely lesser than the heat source temperature, the SORC can be utilized. However, both the SORC and subcritical ORC are viable when the fluid's critical temperature is somewhat lower than the heat source temperature [150].
20. In terms of electricity production, the thermodynamic functioning of hybrid plant utilizing SORC surpasses than the utilizing subcritical ORC [147].
21. For the recuperation of exhaust discarded heat of combined heat and power engine, the SORC has the best performance in contrast to the subcritical ORC in terms of exergy & thermal efficiency, and net power [153].
22. In SORC system, radial inward flow turbine is the prominent alternative, and furthermore lower flow ratio along with higher pressure ratio in the turbine makes it appealing [177].

23. SCO_2 Brayton cycle has a few points of interest such as simplicity, compactness, superior economy, sustainability, small capital cost because of little size of equipment and plant footprint, improved safety, and high cycle efficiency, in this manner, it is an appealing alternative for power production plants [89,178].
24. CO_2 is a promising and conspicuous choice as a working fluid in light of its little cost, plenitude in nature, non-flammability, non-hazardous nature, and capacity to resist at higher temperature [117].
25. The concentrated solar systems like SPTC, LFR, and solar dish are the most standard high temperature devices so as to operate the recompression combined cycle rather than simple setup of an SCO_2 cycle [179-182].
26. In an extensive range of pressure ratios, a CSP system incorporated R-SCO_2 cycle has an utmost thermal efficiency among the different setups [183].
27. R-SCO_2 cycle's functioning at a temperature apropos to CSP application gives higher cycle efficiency as opposed to supercritical steam cycles [184].
28. In recompression cycle, extra heat can be recuperated than that by the simple configuration because of splitting of flow after the LTR that diminishes the heat capacity of high-pressure stream in LTR unit, and thus the issue of pitch point could be evaded in the recuperator [172].
29. In both SORC and subcritical ORC, if the vapours of the organic fluid at the turbine outlet is hot enough, the internal heat exchanger is used to preheat the liquid before evaporation, however, vapors are cooling down before entering in condenser. Due to this process, the overall efficiency of cycle can be enhanced [185].
30. For the source with temperature range varying from 90℃ to 350℃, the ORC can be employed to recover the heat [185].
31. The internal heat exchanger called as recuperator or regenerator can be used in ORC system especially with dry or isentropic fluids. The use of this component can reduce the amount of thermal energy extracted from the heat source, which is further relaxing the pinch limitation of evaporator. Thus, working fluids with higher flow rates allows in the ORC till the pinch conditions are re-established which enables high thermal efficiency & power output for the same heat input conditions [186].
32. Pressure should be below the critical pressure in subcritical cycle but it will be above the critical pressure in supercritical cycle. However, in trans-critical cycle, low pressure will be below the critical pressure and high pressure will be above the critical pressure [187].

33. At a similar temperature, SCO_2 observed to be less corrosive than steam which can successfully enhance the turbine inlet temperature in case of SCO_2 cycle [66,188,189].
34. In case of SCO_2 cycle, much smaller cycle pressure ratio and relatively high exit temperature of turbine has been detected as compared to SRC, as a result, thermal efficiency enhances because of the recuperation of large amount of heat [66].
35. Exergy and energy analysis help us to uncover the concept regarding heat transfer quality in a specific process as well as to check the system's sustainability level [190,191].
36. The density of CO_2 is 60% of water density at the inlet of compressor which could lessen the necessity of compression power in SCO_2 cycle [192].
37. SRC mainly appropriate for a heat source whose high temperature should be greater than 500℃ and it can employ water as well as high pressure steam as the circulating working fluid. To summarize, because it requires high operational temperature and pressure, SRC is not suitable for low temperature and pressure condition [193].
38. The ORC's power generating capacity is greater than that of the Steam-ORC and SRC when the temperature of heat source lies between 150–210℃, and when it to reaches 200℃, the rising trend of ORC generating capacity is clearly less than SRC, and when the temperature of heat source reaches to 350℃, the ORC and SRC's power generation capacity is very close [193].

2.6. Research gaps in literature

A vast literature work available in the field of solar thermal collectors, power cycles, and WHR process that have been further reviewed. In this context, there are some important points which have been pointed out from the past literature and the results of their outcomes in the form of gaps in research work are discussed below:

1. It has been found that very limited studies are available with regard to the performance evaluation of solar driven combined cycle especially in which SCO_2 cycle is acting as a topping configuration and ORC as a bottoming setup.
2. It has been noticed that mostly available studies are concentrated on the SPT integrated SCO_2 cycle because of high temperature range of SPT system. But after reassessing the literature, it becomes clear that the SPTC can be effectively utilized as a heat source because of its capacity to do work in a commercialized environment and its high maturity level [49,68].

3. In addition, there is a performance study of SPTC incorporated combined SRC-ORC system already available in the literature [169], but the energy and exergy based parametric performance analysis of SPTC incorporated combined SCO_2-ORC system has not been performed yet. Apart from this, evaluation of exergetic performance parameters of each component for this kind of configuration, for instance rate of exergy destruction, Y_{DEP}, Y*, and IMP is a matter of investigation.
4. As can be observed, R-SCO_2 cycle layout can possess high thermal efficiency which can be justified by the statement that in recuperators, cold side flow's specific heat is two to three times upper than that of specific heat of hot side flow and further the difference between specific heat in LTR could be compensated and heat recuperation in recompressing layout could be maximized with the help of splitting of CO_2 flow, as a result, waste heat could be reduced and thermal efficiency could be improved [66]. Therefore, parametric analysis based on energy and exergy performance of recompression combined cycle (R-SCO_2-ORC system) need to be performed. Moreover, a comparison with regards to efficiency of both SCO_2-ORC system and R-SCO_2-ORC system can be conducted.
5. Furthermore, in the combined configuration, the vapour absorption cycle (VAR) can be employed as a bottoming cycle instead of ORC so as to generate combined power, cooling and heating effect.
6. Lastly, it has been found that energy and exergy investigation of SORC operated by high temperature heat source (i.e. SPTC with its higher temperature range) need to be performed. Because as per literature, SRC mainly appropriate for a heat source whose high temperature should be greater than 500℃ [193].

2.7. Objectives of research work

The goals of the research work have been listed below:

1. Thermodynamic modeling of the combined supercritical carbon dioxide and organic Rankine cycle (SCO_2-ORC system) integrated with the solar parabolic trough collector (SPTC).
2. Thermodynamic modeling of the combined recompression supercritical carbon dioxide and organic Rankine cycle (R-SCO_2-ORC system) integrated with the solar parabolic trough collector (SPTC) along with comparison from simple configuration of combined cycle (SCO_2-ORC).

3. Thermodynamic modeling of the combined supercritical carbon dioxide and vapor absorption refrigeration cycle (SCO_2-VAR cycle) integrated with the solar parabolic trough collector (SPTC).
4. Thermodynamic modeling of the supercritical ORC (SORC) directly integrated with the solar parabolic trough collector (SPTC).

Chapter-3

Description of Systems

In this chapter, attempts have been made in order to describe the all necessary figures of the selected thermodynamic cycles & their temperature-entropy (T-s) diagrams. Firstly, the description of SPTC incorporated with combined SCO_2 cycle and ORC system has been discussed, which is followed by T-s diagram of combined system. Further, the variations in both density and specific heat of CO_2 at various temperature and pressure conditions has been illustrated, and then trend of variations in thermal conductivity along with the density at different temperatures also has been revealed.

Secondly, the description of SPTC driven combined recompression SCO_2 (R-SCO_2) cycle and ORC system along with T-s diagram of both topping R-SCO_2 cycle and bottoming ORC has been discussed. Thirdly, the description on SPTC driven combined SCO_2 cycle and VAR system has been made. Lastly, the description on SPTC integrated with supercritical ORC (SORC) along with its T-s diagram has been presented in a consecutive way.

3.1. SPTC integrated with combined SCO_2 cycle and ORC system

Figure 3.1 displays the schematic of combined cycle (i.e. SCO_2-ORC system). In this arrangement, the SCO_2 cycle act as a topping configuration, while the ORC is directly attached to SCO_2 cycle in order to recovered its waste heat, which is known as a bottoming cycle. In topping cycle, CO_2 as a working fluid has been utilized at the critical states, i.e. critical temperature of 30.98^{o}C and critical pressure of 7.38 MPa and adjacent to the critical point, it becomes incompressible [66,199].

In addition, combined cycle has a benefit over simple structure in a way that it can lessen the design complexity of system because of condensation at atmospheric pressure not upon vacuum pressure as in basic design [169]. A heat source i.e. multiple rows of solar thermal collectors (i.e. SPTCs) have been selected for the functioning of the combined cycle. In the SPTC field, there are 50 modules which are organised in series per collector row and each having 12.27 m length [134,169,194,199] and an efficient tracking system based on single axis can be engaged with the solar collector so as to track the sun movement for the purpose of efficiency improvement. Moreover, a thermal storage facility can be attached with the solar

loop so as to avoid the sun set situation or blocking of sunrays due to clouds, however, there are some type of costs associated with this facility of heat storage, for instance operating cost, storage medium cost, pipes' cost, and cost of containers and insulating materials, as a result of which operational cost of whole plant can be increases. Table 3.1 lists the geometrical parameters' data chosen for a SPTC plant and Table 3.2 lists the geometrical parameters' data chosen for a combined cycle [199].

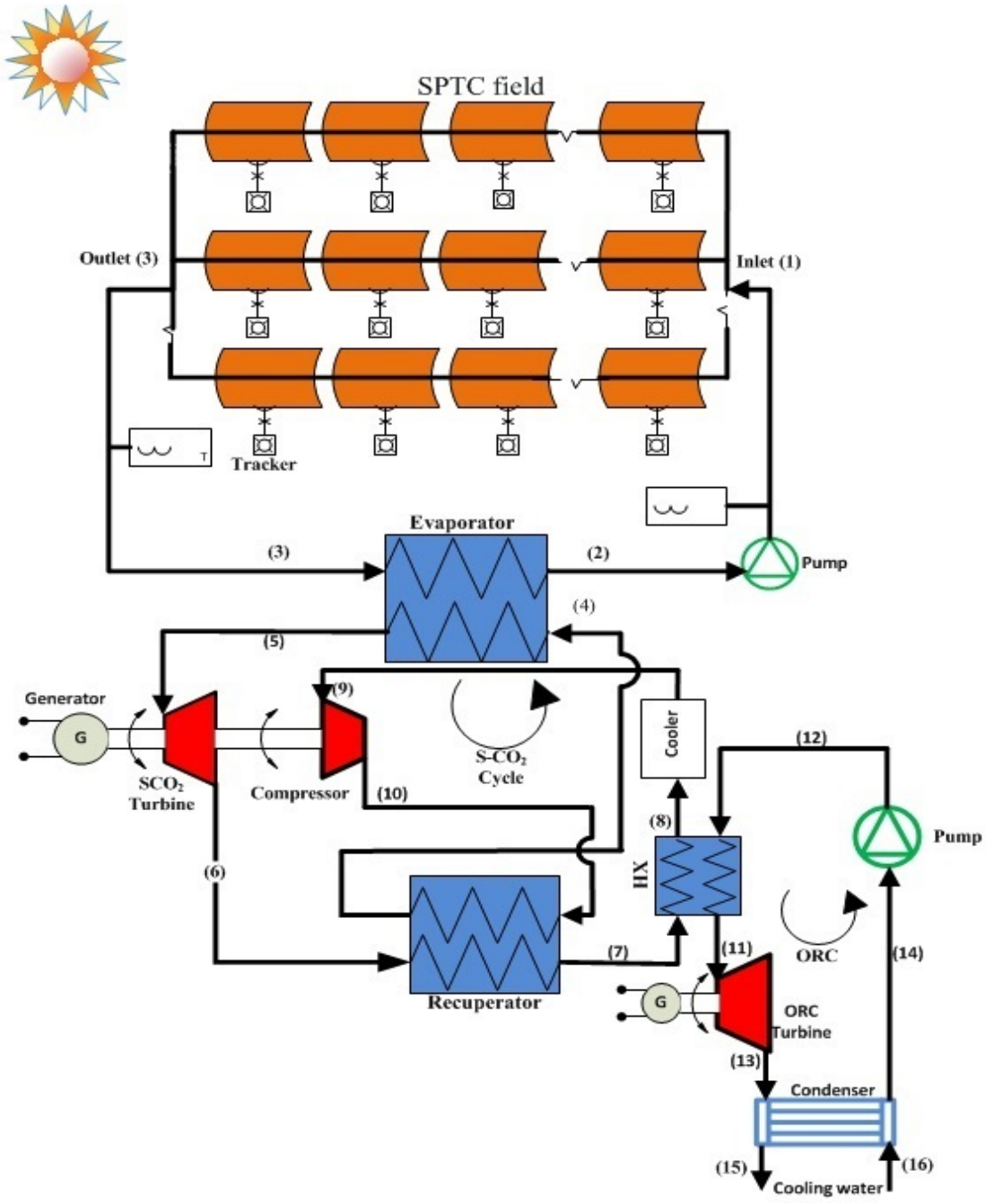

Figure 3.1. Schematic of the SPTC integrated with combined SCO_2 cycle and ORC [199]

Table 3.1. Input data adapted for the SPTC system from Ref. [169,194,196]

SPTC's parameters	**Values**
Collector row length	500 m
Collector type	Modified LS-3
Collector width	5.76 m
Collector length (single)	12.27 m
Total mirror surface	2760 m^2
Inner diameter of absorber tube	0.05 m
Outer diameter of absorber tube	0.07 m
Inner diameter of cover	0.115 m
Outer diameter of cover	0.121 m
Emittance of the cover	0.86
Emittance of the absorber tube	0.15
Reflectance of mirror	0.94
Intercept factor	0.93
Transmittance of glass cover	0.96
Absorbance of absorber tube	0.96
Shading loss	0.97
Structural loss	0.95
Concentration ratio	82:1
Intensity of direct irradiation	0.5-0.9 kW/m^2
Incidence angle modifier	1
Number of collector in series (col_s)	50 [134]
Number of parallel collector rows (Col_p)	7 [134]
Row orientation	North-South
Mirror optical efficiency	73.27%
Maximum outlet pressure	100 bar
Maximum outlet temperature	400℃
Ambient conditions	**Values**
Ambient temperature	298.15 K
Ambient pressure	101.3 kPa

Source: Singh and Mishra (2018) [199]

However, the thermal properties of working fluid (i.e. Syltherm 800) running through the collector have been listed in Table 3.3. The Syltherm 800 fluid has a uppermost working temperature range of 420^oC [195,199], therefore, it has been chosen as the HTF for the collector field (i.e. SPTC) because of its suitability in this application amongst the other available working fluids. Besides, HTF's mass flow rate value lies between 0.35-0.8 kg/s per single row

of SPTCs (it is fixed at 0.575 kg/s for this study) plus operative pressure of around 100 bar also has been kept in the SPTC field [196,199].

Table 3.2. Input data adapted for the combined SCO_2 cycle and ORC system

Combined cycle's parameters	Values
SCO_2 turbine efficiency	90% [172,200]
Compressor efficiency	89% [106,200]
Organic pump efficiency	85% [172,200]
Organic turbine efficiency	87% [172,200]
Mass flow rate of SCO_2	10 kg/s [199]
SCO_2 cycle high pressure	25 MPa [106,172,200]
Baseline ORC turbine inlet pressure	3 MPa [199]
Mass flow rate of ORC	2 kg/s [199]
Recuperator effectiveness	95% [172,200]
HX effectiveness	92% [199]

Source: Singh and Mishra (2018) [199]

There are other available options for HTF such as Therminol 55 and Therminol VP1 for SPTC. However, Therminol 55 can achieve maximum temperature of 573K which makes it usuable for small solar power plants. Whereas Downtherm A and Therminol VP1 can be used in modern solar thermal electric plants because of its highest tempertaure limit i.e. 671 K. Because of some limitations, there are some alternatives such as water/steam, pressurized gases, and molten salts available for SPTC [241].

Table 3.3. Thermal properties of Syltherm 800 at various temperatures [203]

Temperature [K]	Specific heat capacity (c_p) [J/kg K]	Density (ρ) [kg/m^3]	Thermal conductivity (λ) [W/m K]	Viscosity (μ) [Pa s]
650	2218.26	577.70	0.067833	0.000284
550	2047.318	696.0074	0.086661	0.000555
400	1791.43	840.06	0.114845	0.002163

Luz third generation trough collector, i.e. modified LS-3 considered as a modern design of SPTC plant alongside the exit temperature of collector row which is nearby 400^{o}C (i.e. 673.15 K) has been preferred from the category of solar electric generating system (SEGS) [196,199]. Whereas, the purpose to choose LS-3 collector instead of LS-2 is that LS-3 has a larger

aperture, which in turn in respect of LS-2 collector field, 15% more receivers are required. Also, when contrasted with LS-2, the LS-3 collector has a lesser mirror expenditure on a per square meter [197,199]. It should be noted that dry cooling is preferred over the wet cooling because CSP plants are generally positioned in those regions where water reserves are restricted. However, dry bulb temperature is higher than the wet bulb temperature, therefore, as compared to wet cooling, dry cooling is less effective and more expansive, and suitable for arid areas [172]. It has been assumed that direct normal irradiance (DNI) approaching upon SPTC area differs from 0.5 kW/m^2 to 0.95 kW/m^2 ordinarily fit to the region of Indian subcontinent. Based on the literature review, few organic fluids were chosen for examining the low-temperature ORC integrated with in combined cycle. Therefore, five refrigerants for the low temperature ORC such as R134a, R407C, R1234yf, R1234ze, and R245fa have been nominated for a specific heat source conditions in the first objective. These refrigerants should be well suited to the bottoming cycle ORC coupled in combined cycle and the process of fluid chosen is mainly depends on the thermodynamic and heat transfer properties, safety data, environmental and economy aspects [198,199]. Lastly, the important data related to the thermo-physical properties for various organic fluids has been listed in Table 3.4.

Table 3.4. Physical, environmental properties and security data of the selected working fluids for the ORC adapted from Ref. [124,161,198,204-209]

Working substance	**Physical properties data**					**Security Group**	**Environmental properties**		
	Type[a]	Weight (kg/kmol)	T_b[b] (℃)	T_c[c] (℃)	P_c[d] (MPa)		Lifetime (years)	ODP[e]	GWP[f]
R134a	I	102.03	-26.1	101	4.059	A1	14	0	1430
R407C	W	86.20	-43.6	86.79	4.597	A1	n.a.	0	1800
R1234yf	D	114.04	-29.5	94.7	3.38	A2L	0.029	0	4.4
R1234ze(E)	D	114.04	-19.0	109.4	3.64	A2L	0.045	0	6
R245fa	D	134.05	15.1	154.1	3.65	B1	7.7	0	1050
R123	D	152.93	27.8	183.7	3.668	B1	1.3	0.020	77
R290	W	44.10	-42.1	96.68	4.247	A3	0.041	0	~20
Toluene	D	92.138	110.6	318.6	4.1263	n/a	n/a	0	<6
Cyclohexane	D	84.16	80.7	280.5	4.075	A3	n/a	n/a	n/a
Isobutane	D	58.1	-11.7	134.7	3.63	A3	0.016	0	20
Isopentane	D	72.1	27.8	187.2	3.38	A3	0.009	0	20
n-Hexane	n.a.	86.17	69.18	234.7	3.058	n.a.	n.a.	0	<6
n-Pentane	D	72.149	36.06	196.55	3.370	n.a.	n.a.	0	~20

[a]W = Wet; D = Dry; I = Isentropic; [b]T_b = normal boiling temperature; [c]T_c = critical temperature; [d]P_c = critical pressure; [e]ODP = potential of ozone depletion (ODP) relative to R11; [f]GWP = potential of global warming (GWP) relative to CO_2

Depending upon the saturation curve's slope in T-s diagram, mainly organic fluids are categorized into three forms, i.e. wet, isentropic, and dry. The wet fluid such as water has a negative slope and requires superheating process so as to avoid the impact of liquid droplets on the blades of turbine through the process of expansion [149,172]. However, author considers more dry fluids aimed at the low-temperature ORC in order to examine the functioning of considered combined cycles, for instance isopentane and the reason behind its selection is that it has a positive slope and also enters the turbine in saturated vapour state [172]. Environmental factors such as GWP, ODP, and atmospheric lifetime are other crucial parameters which have also been taken into account during the selection of organic fluids and these have direct effect on the environment. After considering these parameters, fluids such as R-11 and R-115 already have been phased out and other fluids are planned to be phased out soon, like R141b and R142b. Apart from this, many fluids are considered to be flammable but if proper precautions will be taken, it does not bring any problem [172]. The main components of a SCO_2-ORC system are evaporator, SCO_2 turbine, recuperator, heat exchanger (HX), cooler, compressor, ORC turbine, condenser, and pump. In this combined cycle, SCO_2 stream after extracting heat in evaporator starts expanding in turbine along with inlet high pressure and temperature condition of SCO_2 (state 5-6) up to an exit condition of small temperature and pressure. Which is then enters in recuperator so as to extract the thermal energy from the hot stream by cold stream as a purpose of preheating (state 6-7). After this, the SCO_2 stream reaches to HX unit and here it gives sufficient energy input to the organic fluid flowing in the ORC (state 7-8). Then, SCO_2 stream after cooled down in cooler unit (state 8-9) up to an certain temperature (i.e. but it should be always above the critical temperature) reaches to a compressor driven directly by turbine (state 9-10), which is responsible for an increase in pressure and temperature of stream again. At that point stream after passing through recuperator comes to the evaporator (state 4-5) and completes the cycle, where process of heat extraction again take palce by SCO_2 steam from the flowing fluid (i.e. syltherm 800) through the SPTC field. Finally, it arrives the SCO_2 turbine and same process will always continue. So as to augment the cycle efficiency, two stages of compression with an intercooler between them, two stages of expansion, and a reheater can be effectively used [3,199].

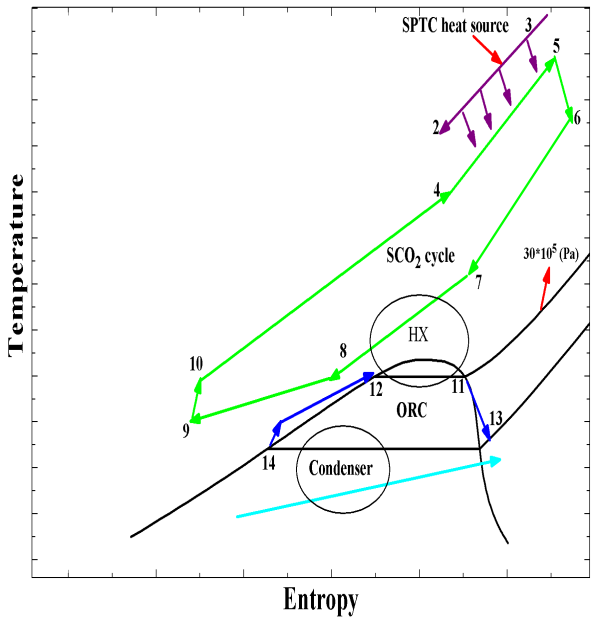

Figure 3.2. T-s diagram of SPTC integrated with combined cycle (SCO_2-ORC) [199].

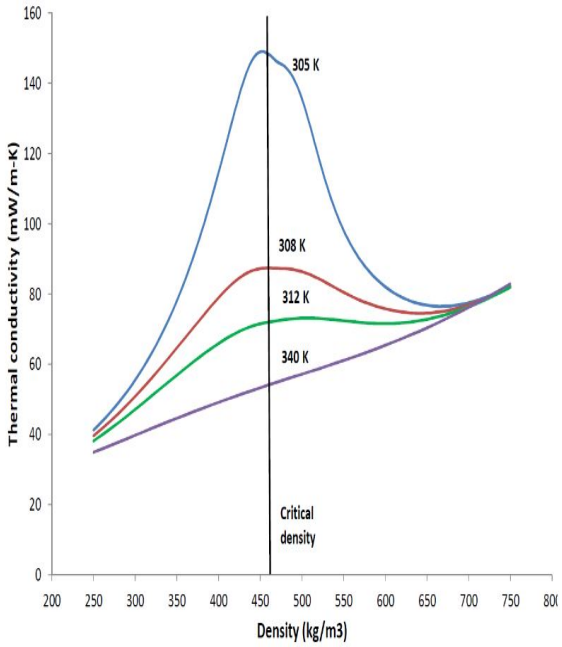

Figure 3.4. Variations in thermal conductivity of CO_2 with respect to density at different temperatures [200].

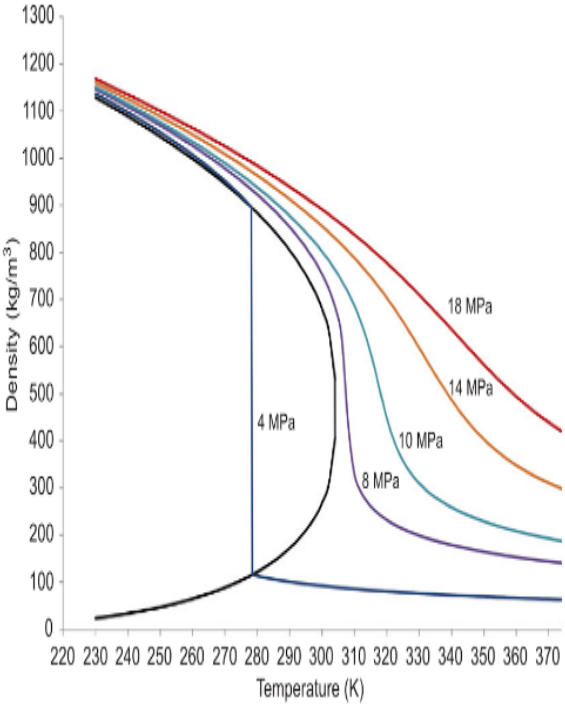

Figure 3.3. Variations in density of carbon dioxide at the different conditions of pressure and temperature [192,200].

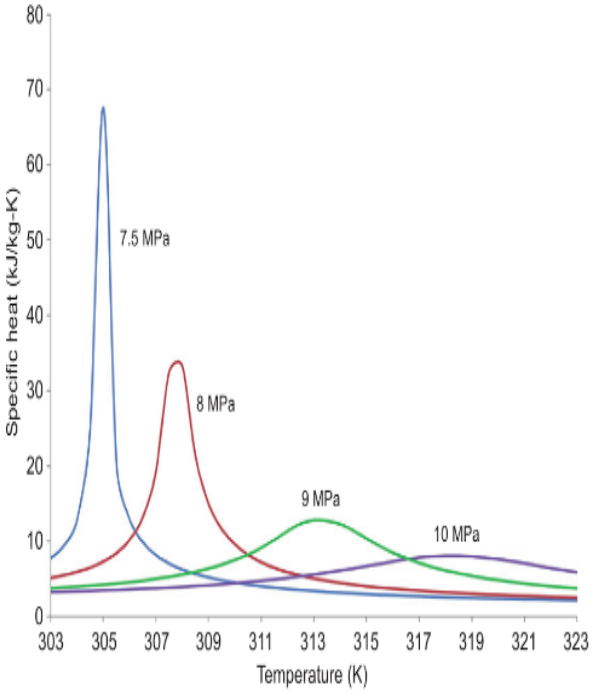

Figure 3.5. Variations in specific heat of carbon dioxide at the different conditions of pressure and temperature [192,200].

While in bottoming ORC, selected organic fluid after recovery of waste heat passes through the turbine (state 12-11) where fluid expands up to a low pressure and then it goes to condensor (state 13-14), where fluid discards its excess heat to the cooling water and pumped over up to HX unit (state 14-12), therefore completes the cycle. Additionally, power is produced by the combined cycle can be conceivable through the assistance of a generator as the rotor of turbine is directly associated to the shaft of turbine as illustrated in Figure 3.1. In fact, all the processes of combined cycle are completely understood from T-s diagram which is displayed in Figure 3.2.

In the past research, density of SCO_2 was contrasted with the water density which was investigated by Wright et al. [201] and it was discovered that at compressor inlet, the density of CO_2 is 60% of the water density that can further successfully lessen the requirement of compression power [192].

Now Figure 3.3 demonstrates the fluctuation in CO_2 density at various pressure and temperature states and a very high density can be seen nearby the critical point, hence compression work significantly diminished when contrasted with different fluids [192].

Aside from density, it was uncovered that the CO_2 thermal conductivity similarly occupies the uppermost value at the critical states, which is about 148.95 $\frac{\mathrm{mW}}{\mathrm{m-K}}$ at 305 K as depicted in Figure 3.4 [192]. Besides, CO_2 specific heat differs radically alongside the fluctuations in pressure and temperature as described in Figure 3.5, and it was observed that the temperature difference between fluids fluctuates broadly inside the recuperator unit that straightforwardly influences the recuperator design as for the location of pitch point [192].

It has likewise been seen that CO_2 specific heat is high at a critical point that outcomes in builds the need of vast amount of cooling water's mass flow rate in cooler that in turns parasitic loss augments in the topping cycle [192]. Figure 3.6 represents the heat source's operating temperature range for SCO_2 cycle accompanied by its power conversion efficiency.

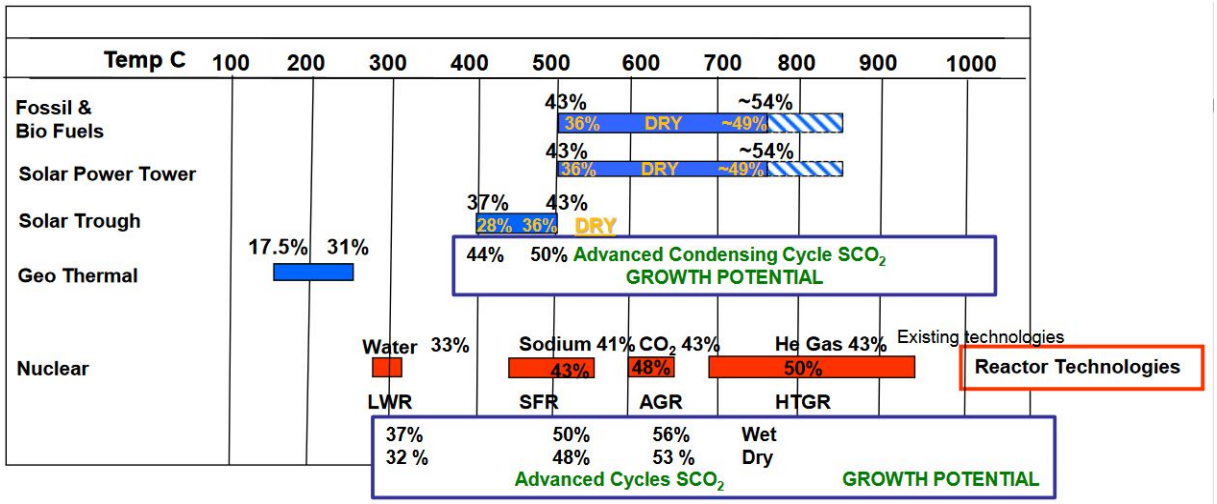

Figure 3.6. Operating temperature range of heat source for SCO_2 cycle along with its efficiency of power conversion [200,202].

3.2. SPTC integrated with combined R-SCO_2 cycle and ORC system

The arrangement of R-SCO_2 cycle (i.e. topping structure) and ORC (i.e. bottoming structure) recognised as combined recompression cycle as described in Figure 3.7. The modified LS-3 is a type of SPTC system, which has been utilized as a heat source to operate the combined recompression cycle (R-SCO_2-ORC system). In addition, SPTC technology has a huger potential to produce electric power because of its greater commercial performance & reliability features, and of course its appropriateness in Indian sunny weather, which means that the accessible solar energy potential in the country is 20 MW/km^2 and the solar intensity is around 6 kwh/m^2/day [210,211].

CSP driven SCO_2 cycle also has certain key merits, for instance at conditions of dry cooling, the SCO_2 cycle possess superior functioning as competed to the SRC, and it can run with a thermal storage system cost-effectively [114]. In addition, geometrical data for considered SPTC system and data related to thermal properties of Syltherm 800 working fluid has already been shown in Table 3.1 & Table 3.3, correspondingly. However, geometrical data for the combined recompression cycle has been registered in Table 3.5.

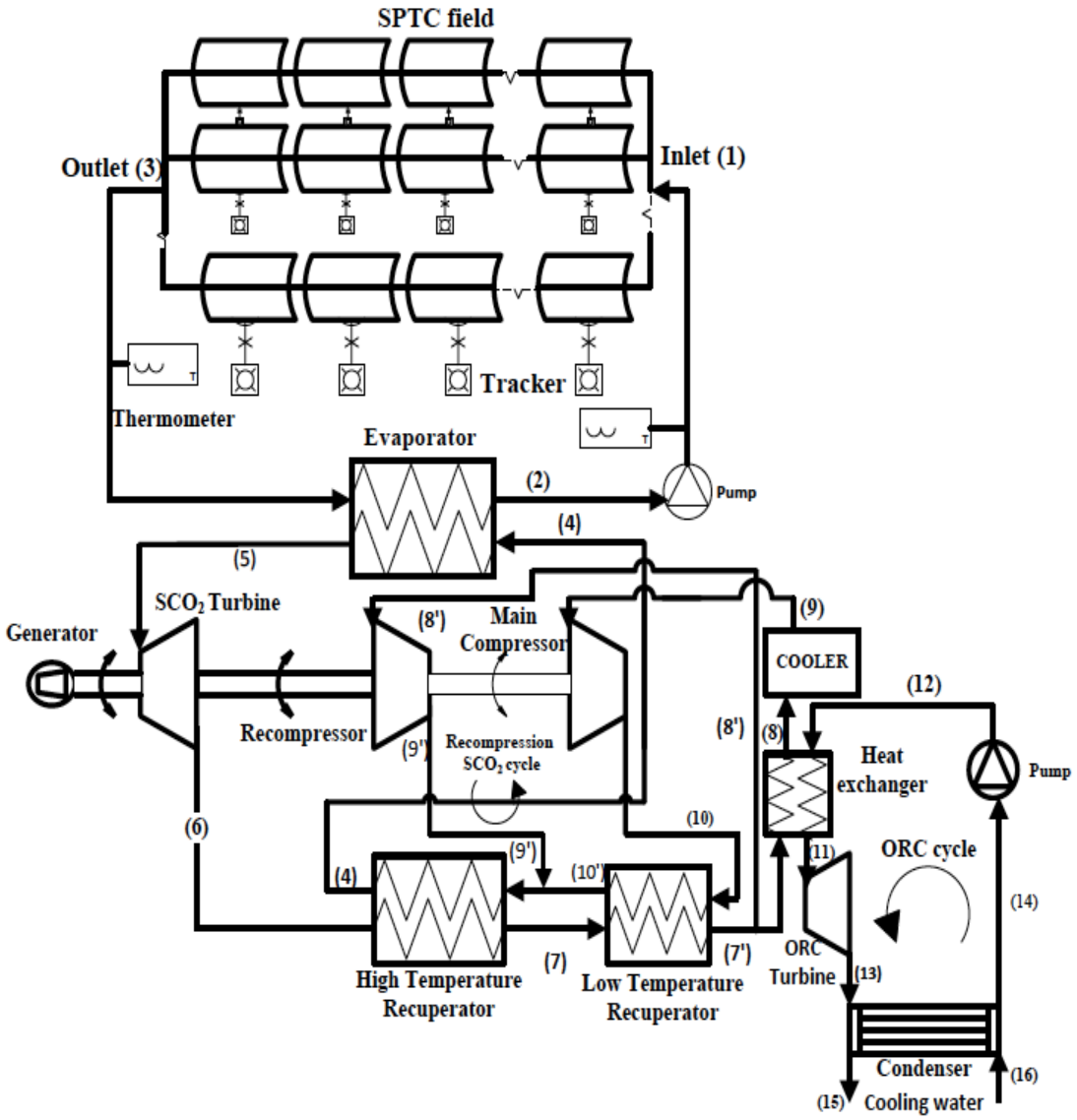

Figure 3.7. Schematic of the SPTC integrated with combined R-SCO_2 cycle and ORC [211].

It was observed that recompression configuration diminishes the heat losses from the R-SCO_2 cycle and augments the thermal efficiency with the assistance of flow splitting so as to compensate the specific heats' differences in LTR [66]. However, simple configuration of SCO_2 cycle has less efficient although it can attract to the commercial market potentially because of its design easiness. Instead, a simple design also has been possessed by recompression cycle which could be commissioned in those applications that need high thermal efficiencies [114]. One more preferred standpoint of R-SCO_2 cycle is that extra heat can be recovered than the simple setup which is because of the flow splitting after LTR that diminishes the heat capacity of high pressure stream in LTR and therefore, the issue of pitch point can be kept away from the recuperator [172,211].

Table 3.5. Input data adapted for the combined R-SCO_2 cycle and ORC system

Combined recompression cycle's parameters	Values
SCO_2 turbine's isentropic efficiency	90% [90,212]
Main compressor's isentropic efficiency	89% [90,212]
Recompressor's Isentropic efficiency	89% [90,212]
Pump efficiency in ORC unit	85% [172]
Turbine efficiency in ORC unit	87% [172]
SCO_2 fluid's mass flow rate	10 kg/s [211]
Split mass flow rate	4 kg/s [211]
ORC's working fluid mass flow rate	5 kg/s [211]
High or maximum pressure SCO_2 cycle	25 MPa [106]
Turbine inlet pressure in ORC unit	3 MPa [211]
Effectiveness of HTR	95% [90,112]
Effectiveness of LTR	95% [90,112]
Effectiveness of HX unit	95% [172]

Source: Singh and Mishra (2018) [211]

The main components of a R-SCO_2-ORC system are evaporator, SCO_2 turbine, high temperature recuperator (HTR), low temperature recuperator (LTR), HX, main compressor, recompressor, ORC turbine, condenser, and pump. The SCO_2 stream after getting heat in evaporator unit (state 4-5) reaches to SCO_2 turbine, where it expands from heat temperature and pressure conditions to a low temperature and pressure conditions but remain above the critical conditions of CO_2 (state 5-6). Then, SCO_2 stream goes to the HTR where it transfers its energy to the mixed jet enters in HTR from the opposite side (state 6-7), which is sum of two different streams coming out from recompressor and LTR. After HTR, stream passes through the LTR and transfer its excess energy to the stream comes out from main compressor (state 7-7′). Now from the LTR, exited stream is divided upstream of the HX unit (state 7′) from which main stream along with high mass flow rate is flowing through the HX unit (state 7′-8) where it gives its excess heat to the bottoming ORC and then it cooled down in the cooler (state 8-9). Following this, main stream compressed in the main compressor up to a high pressure at exit point (state 9-10) and ultimately, this part of stream arrives again in LTR (state 10) where exchange of energy take place with the inward stream of LTR (state 7). This main stream that passes through the cooler unit and main compressor is an essential constraint that directly affects the functioning of cycle [172]. On the opposite side, another part of the split stream along with low mass flow rate drives straightforwardly to the recompressor that compressed this

stream up to a higher pressure (state 9′) and blended it with the main stream came back from the LTR (state 10′) before the HTR. It ought to be noticed that flow splitting should be balanced in such a way that the outlets for recompressor and exiting cold stream of LTR always remain same [89]. Basically, high pressure SCO_2 stream can be preheated through the utilization of HTR & LTR. Lastly, the sufficient thermal energy is added to mixed stream in HTR (state 9-4′) as well as in evaporator (state 4-5) so as to attain the mandatory inlet temperature of turbine, therefore, completes the cycle [211].

Furthermore, heat recovery unit or HX has been placed prior to the cooler and main compressor which means that a portion of total mass flow rate of SCO_2 stream arrives to the HX. As can be observed, if HX unit placed prior to the splitting of mass flow rate or immediately just afterward the LTR lessens the temperature of stream entering the recompressor which results in temperature at exit point 9′ declines that damagingly affects to the cycle functioning [172]. After recovery of waste heat in HX, the organic fluid expands in the ORC turbine (state 11-13) up to condenser pressure. Then, fluid passes through the condenser where it discards its excess heat to the cooling water (state 13-14) and then pumped up to the inlet of HX unit (state 14-12), which completes the cycle.

For the analysis, organic fluids such as R123, R1290, R1234yf, R1234ze, toluene, cyclohexane, isobutane, and isopentane have been chosen for the ORC and the thermo-physical properties data for all these fluids already have been registered in Table 3.4. Moreover, in the combined recompression cycle, Power can be delivered through the assistance of a generator as the turbine rotor is directly associated with the turbine shaft [211]. Lastly, Figure 3.8 and Figure 3.9 represents the T-s diagrams of R-SCO_2 cycle & ORC.

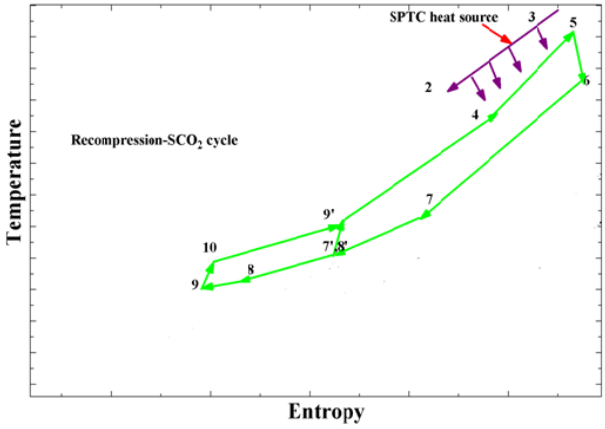

Figure 3.8. T-s diagram of R-SCO_2 cycle [211]

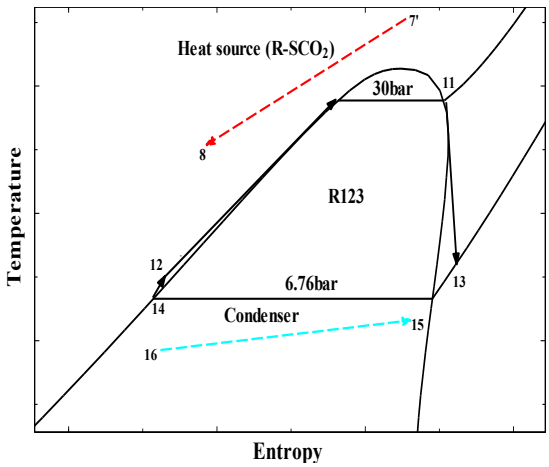

Figure 3.9. T-s diagram of R123 fluid based ORC system [211]

3.3. SPTC integrated with combined SCO_2 cycle and VAR cycle

This combined cycle used in this study has a combination of SCO_2 cycle (i.e. topping structure) & VAR cycle (i.e. bottoming structure) with the aim to produce combined power, cooling as well as heating effect. The working procedure of SCO_2 cycle has already been discussed in section 3.1, however, the description on VAR cycle has been made in the next paragraph. Also, the geometrical data for the parameters of SPTC and SCO_2 cycle has already been registered in Table 3.1 and Table 3.2, correspondingly.

In bottoming VAR cycle, after getting heat from the hot water in evaporator (EV2) (state 19-11), ammonia vapours at low-pressure (LPAV) arrives to the absorber in which ammonia vapours absorbed by a great quantity of cold water (state 11-12), and like this made a well-known aqua-ammonia solution. Besides, pressure inside the absorber can be declined as the absorption of ammonia vapours by water take place that results in extra vapour draws from the evaporator and subsequently, temperature of solution rises. Apart from this, water cooling arrangement has been engaged so as to eliminate the heat evolved in absorber and to improve the water absorption capacity. Then absorber's strong solution pumped to the SHE unit (state 13) and here it is heated by weak solution turning out from the generator (state 14′). The strong solution then inserts in the generator (state 13′) where it is heated by heat swapped from SCO_2 stream and in the wake of getting heat at high pressure, solution separates ammonia vapours from hot weak ammonia solution that instantly flows back toward the absorber (state 15). Further at this point, ammonia vapours at high-pressure (HPAV) goes to the condenser (state 16) and alter here into high pressure liquid ammonia that runs toward the receiver (state 17). Eventually, liquid ammonia at low pressure enters in to the EV2 after going through the expansion valve (EXV) (state 18-19) [214]. Lastly, some important functioning and design parameters for VAR cycle were taken for the analysis such as high pressure of 10.8 bar, low pressure of 1.4 bar, effectiveness of solution heat exchange (SHE) was 70% [213], condenser and absorber temperature was 303.12 K [214].

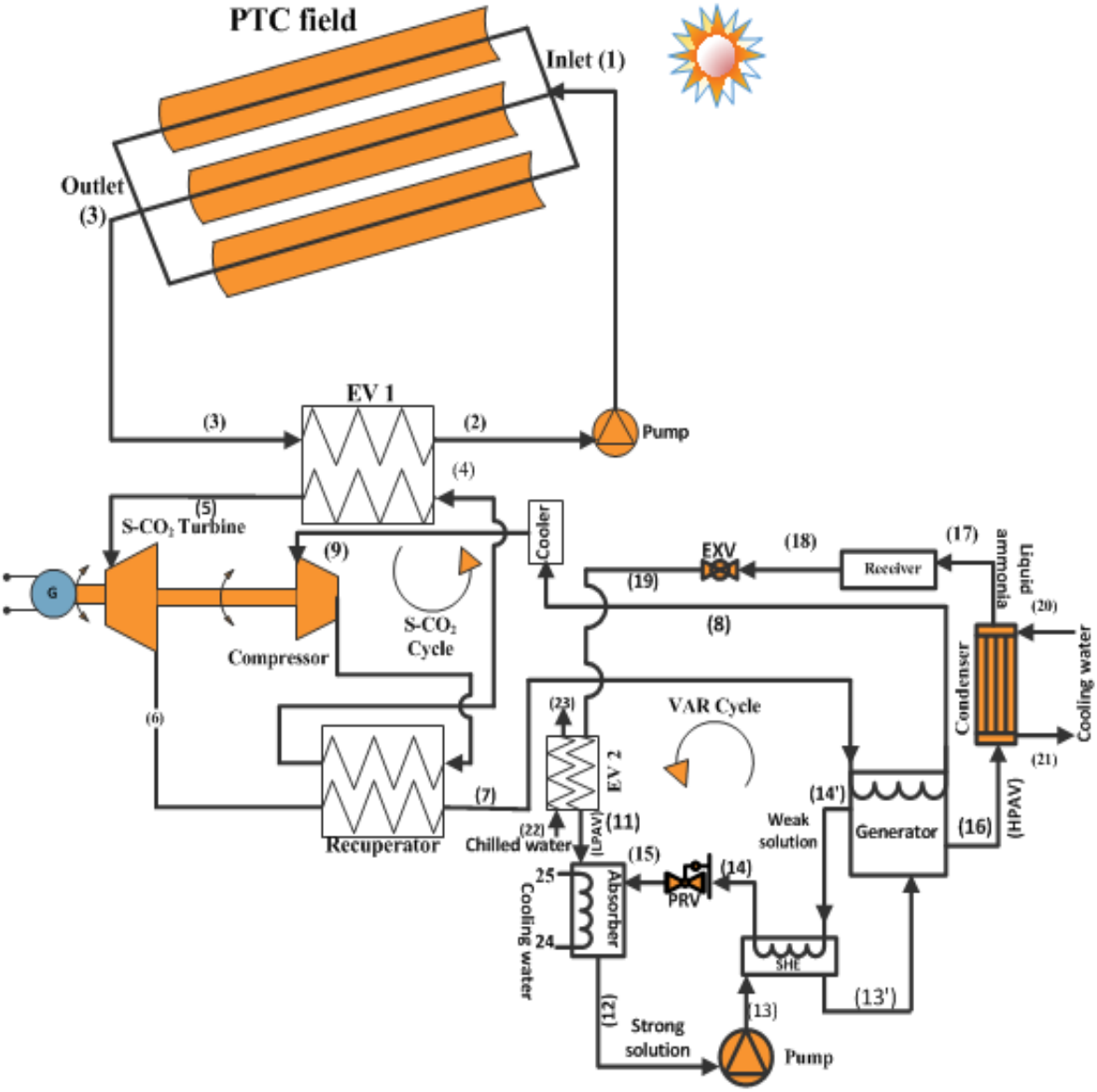

Figure 3.10. Schematic of the SPTC integrated with combined SCO_2 cycle and VAR cycle [214].

3.4. SPTC integrated with SORC system

It has been noted that ORC is an unrivalled technical solution for electricity generation from heat sources with limited capacity whose temperature varies from low to medium range say below 400-500°C [67]. Due to its low operating temperature, ORC can recover waste heat from solar & geothermal energy, biomass and industrial source. Also, CSP such as SPTC shows its capacity to operate in a commercialized environment [68]. Therefore, SPTC has chosen as a heat source for the SORC system in this study.

As compared to SRC, the ORC has a simple layout which means that no water-steam drum associated to the boiler and to implement the three evaporation phases such as preheating, vaporization, and superheating, one single heat exchanger is required [71]. But a recuperator or internal heat exchanger can be used in ORC system especially with dry or isentropic fluids that can further reduce the amount of thermal energy extracted from the heat source [186].

In ORC, heat can be recuperated at much lower temperature which is because of lesser boiling point of preferred organic working fluid and there is no need of superheating because organic fluids at the end of expansion are remain in superheated state. Also, pressure in ORC does not exceed 30 bar in contrast to steam cycle in which pressure of about 60-70 bar that increases the thermal stress, thus, more complexity and cost of steam boiler [71].

The ORC technology is relying upon the same principle as that of conventional SRC except that instead of water, it utilizes organic fluid as a working fluid. In many respects, water is a perfect fluid because of its characteristics such as it is neither toxic nor flammable, thermodynamic and chemically stable, quite inexpensive as well as environmental friendly such as ODP and GWP equal to zero. However, organic fluids could have low availability and costly in contrast to water, and some could have negative effect on the environment, for instance CFC already been phased out by the Montreal protocol due to their high ODP and some HCFC are being phased out by Kyoto protocol due to their high GWP. In order to replace CFC and HCFC, the HFC with lower GWP are now concerned such as R1234yf and R1234ze and R32 fluids [185].

The SORC is different from classical cycle in respect of pressure and temperature conditions. In SORC cycle, fluid enters the supercritical state which means that distinction between gas and liquid phases disappear [185].

The SORC system involves six processes in their operation: pump raises the pressure of fluid above the critical pressure (process 10 to 11). Then, the temperature of fluid is raises by getting heat in recuperator (process 11 to 4) as well as evaporation of fluid take place in HX unit above the critical temperature (process 4 to 5) which is done at constant pressure. After this, vapours are expanded in the turbine up to its initial pressure (process 5 to 6) and passes through the recuperator where exchange of heat take place (process 6 to 7).

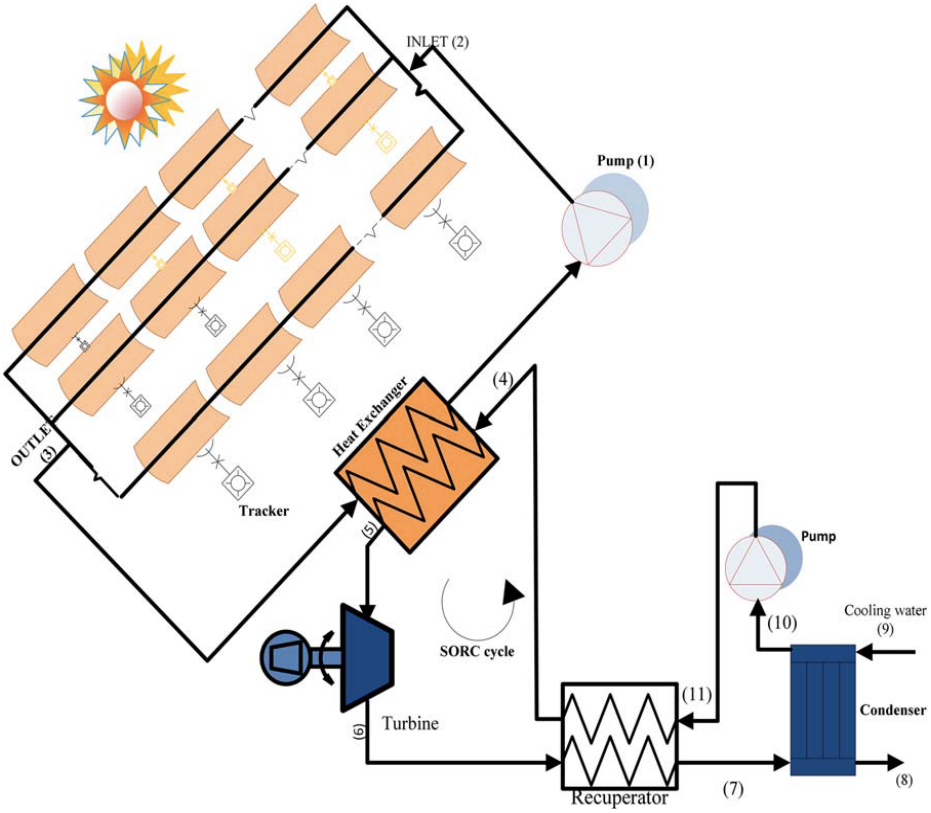

Figure 3.11. Schematic of SPTC integrated with SORC [237].

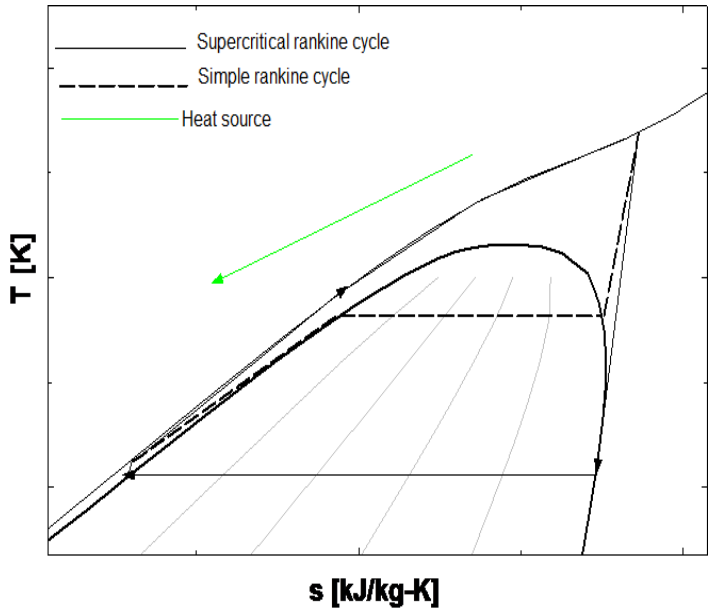

Figure 3.12. T-s diagram of the SORC [237].

Noted that an internal recuperator can be used when the working fluid at the turbine outlet is still superheated which is then enhance the cycle performance as in subcritical cases [185]. Finally, fluid is cooled down until condensation in condenser (process 7 to 10) and

then, it reaches to pump again which completes the cycle. Lastly, the Figure 3.11 shows the schematic of SPTC integrated with SORC and Figure 3.12 displays the basic T-s diagram of SORC.

Table 3.6. Input data adapted for the SORC system

SORC parameters	Values
Efficiency of SORC turbine	87% [172]
Efficiency of SORC pump	85% [172]
Mass flow rate in SORC	2 kg/s
High pressure of SORC	8 MPa
Pressure ratio in SORC	2.8
Effectiveness of HX unit	95%
Effectiveness of recuperator	95%

Organic fluids instead of water can be utilized owing to the interesting properties, for example low boiling point or high molecular mass that renders them conceivable to utilize when water can't be- technically or economically and this is eminently the situation when the heat source is at very low temperature (i.e. below 300℃) [185]. Therefore, for the analysis of SORC, we have fixed the temperature of heat source (i.e. SPTC system) at 300℃. In addition, the range of HTF's mass flow rate per single row of SPTCs was 0.35-0.8 kg/s [169,196], which is fixed at 0.8 kg/s for the present study. All other parametrical data of SPTC has already been listed in Table 3.1. While the important parameters of SORC have listed in Table 3.6.

Chapter-4

Thermodynamic modelling

In this chapter, thermodynamic modelling of considered cycles based on mathematical equations has been conducted. First, the mathematical modelling of SPTC has been discussed, which is followed by the modelling of combined SCO_2 cycle and ORC system (SCO_2-ORC), combined R-SCO_2 cycle and ORC system (R-SCO_2-ORC), combined SCO_2 cycle and VAR cycle (SCO_2-VAR cycle), and SORC system. Further, the mathematical equations have been programmed into a computer code which is then solved by a computational numerical technique.

4.1. Modelling of the SPTC system

This area discusses the modelling of SPTC based on the standard equations as presented in the literatures [169,199,215,216].

Useful energy gathered by the SPTCs per unit time ($\dot{Q}_u$) is characterized as:

$$\dot{Q}_u = \dot{m}_a . Cp_a . (T_{a_o} - T_{a_i}) \quad (4.1.1)$$

Where specific heat and mass flow rate of flowing liquid inside absorber tube has been expressed by Cp & $\dot{m}_a$, correspondingly. The subscripts a_o and a_i denotes the outlet and inlet of absorber.

Besides, useful heat gain can likewise be assessed from another equation which is described as:

$$\dot{Q}_u = A_{ap} \cdot F_R \cdot \left(S - \frac{A_a}{A_{ap}} U_L (T_{a_i} - T_0) \right) \quad (4.1.2)$$

Where F_R is a heat removal factor of collector, S is an absorbed heat flux via absorber tube, A_{ap} is an aperture area, U_L is a SPTC's overall heat loss coefficient, and T_0 is a atmospheric temperature.

In a different way, the useful heat gain may be written as [218]:

$$\dot{Q}_u = \dot{Q}_s . \eta_{en,SPTC} \quad (4.1.3)$$

Where $\eta_{en,SPTC}$ is the energy efficiency of SPTC and $\dot{Q}_s$ is a overall quantity of solar flux directed upon the SPTC.

Absorbed heat flux (S) can be outlined as:

$$S = \eta_a \cdot G_b \quad (4.1.4)$$

Where η_a is an absorber or receiver's efficiency and G_b is a solar DNI.

Aperture area (A_{ap}) can be written as:

$$A_{ap} = (W - D_{co,o}) \cdot L \quad (4.1.5)$$

Where W is a collector's width, $D_{co,o}$ is an cover's outside diameter, and L is a length of collector.

Efficiency of an absorber (η_a) can be stated as:

$$\eta_a = \rho_r \cdot \alpha \cdot \gamma \cdot \tau \cdot K_m \quad (4.1.6)$$

Where ρ_r is a reflectance of mirror, τ is a transmittance of glass cover, K_m is a incident angle modifier that can be find out by dividing the instantaneous thermal efficiency (η_i) at a known value of incidence angle to the SPTC's peak efficiency [217], η_a can be evaluated by the ratio of S to G_b which is designated as absorber tube's efficiency, γ is a intercept factor, and α is a absorber tube's absorbance. All the important information related with these parameters has been mentioned in Table 3.1.

Now, SPTC's heat removal factor (F_R) can be defined as below:

$$F_R = \frac{\dot{m}_a \cdot C_{Pa}}{A_a \cdot U_L}\left(1 - \exp\left(-\frac{F \cdot A_a \cdot U_L}{\dot{m}_a \cdot C_{Pa}}\right)\right) \quad (4.1.7)$$

Area of the absorber (A_a) can be defined as:

$$A_a = \pi D_{a,O} L \quad (4.1.8)$$

Collector efficiency factor (F) can be expressed as below:

$$F = \frac{U_o}{U_L} \quad (4.1.9)$$

Coefficient of overall heat loss (U_o) amongst surrounding & fluid running inside the absorber tube can be illustrated as:

$$U_o = \left[\frac{1}{U_L} + \frac{D_{a,o}}{h_{coa,i} D_{a,i}} + \left(\frac{D_{a,o}}{2K_a} \ln\left(\frac{D_{a,o}}{D_{a,i}}\right)\right)\right]^{-1} \quad (4.1.10)$$

Now the coefficient of heat loss ($h_{coa,i}$) amongst absorber & glass cover has been described as under:

$$h_{coa,i} = \frac{Nu_a \cdot k_a}{D_{a,i}} \quad (4.1.11)$$

Further, the coefficient of heat loss of SPTC (U_L) amongst ambient and absorber tube has been expressed as:

$$U_L = \left[\frac{A_a}{(h_{c,amco} + h_{r,amco}) A_{co}} + \frac{1}{h_{r,coa}}\right]^{-1} \quad (4.1.12)$$

Where subscript a refers to absorber & co refers to cover, $h_{c,amco}$ is a coefficient of convection heat loss amongst ambient & cover, $h_{r,amco}$ is a coefficient of radiation heat loss, and $h_{r,coa}$ is a coefficient of radiation heat loss amongst absorber and glass cover and these can be expressed as under:

$$h_{c,amco} = \frac{Nu \cdot K_{air}}{D_{co,o}} \quad (4.1.13)$$

$$h_{r,amco} = \epsilon_{co} \cdot \sigma \cdot (T_{co}^2 + T_{am}^2)(T_{co} + T_{am}) \quad (4.1.14)$$

$$h_{r,coa} = \frac{\sigma \cdot (T_{co} + T_{a,avg})(T_{co}^2 + T_{a,avg}^2)}{\frac{1}{\epsilon_a} + \frac{A_a}{A_{co}}\left(\frac{1}{\epsilon_{co}} - 1\right)} \quad (4.1.15)$$

Where subscripts am & avg denotes the ambient & average, respectively, K_{air} is an air's thermal conductivity, Nu & σ is an Nusselt number & Stefan–Boltzmann constant, respectively, ϵ_{co} & ϵ_a is an emittance of the cover & absorber, correspondingly.

Cover's temperature (T_{co}) can be described as:

$$T_{co} = \frac{h_{r,coa}\, T_{a,am} + \frac{A_{co}}{A_a}(h_{c,amco} + h_{r,amco}) T_{am}}{h_{r,coa} + \frac{A_{co}}{A_a}(h_{c,amco} + h_{r,amco})} \quad (4.1.16)$$

The total quantity of solar flux focussed in the form of beam radiation upon the SPTC ($\dot{Q}_s$) that can be supposed as a total accessible heat on behalf of combined cycle.

$$\dot{Q}_s = A_{ap} \cdot F_R \cdot S \cdot Col_s \cdot Col_p \quad (4.1.17)$$

Where Col_s is the total number of SPTCs in series per single row and Col_p is the total number of parallel SPTC rows.

SPTC's energy efficiency ($\eta_{En,SPTC}$) as given below [218]:

$$\eta_{En,SPTC} = \eta_o - c_1\frac{(T_m - T_a)}{G_b} - c_2\frac{(T_m - T_a)^2}{G_b} \quad (4.1.18)$$

Where η_o is the SPTC optical efficiency, c_1 & c_2 is the first order and second order coefficient measured in [W/m^2°C] & [W/m^2°C^2], respectively.

HTF's mean temperature (T_m) can be written as:

$$T_m = \frac{(T_1 + T_3)}{2} \quad (4.1.19)$$

Beside, the exergy term can be expressed as the maximum theoretical work attained from system as it interacts with the surrounding in a state of equilibrium.

So, exergy balance of control volume at steady state for every component engaged in combined cycle on the basis of physical boundary approach can be expressed as:

$$\sum_Q \left(1 - \frac{T_o}{T_Q}\right) \dot{Q}_Q - \dot{w}_{c.v.} - \sum_i (\dot{m}_i Ex_i) - \sum_e (\dot{m}_e Ex_e) - \dot{E}x_d = 0 \quad (4.1.20)$$

Where $\dot{E}x_d$ is the rate of exergy destruction, subscripts O and Q refers to the value of physical property at surrounding or dead state (i.e. T_0 = 298.15 K and P_0 = 101.3 kPa) and for a particular state, subscripts e and i refers to the exit and inlet state. Further, the Ex is the exergy per unit mass flow rate and chemical exergy value assumed to be negligible in the system.

Fluid's total exergy (Ex_{Total}) is a summation of physical exergy (Ex_{ph}) & chemical exergy (Ex_{ch}) may be stated as [223]:

$$Ex_{Total} = Ex_{ph} + Ex_{ch} \quad (4.1.21)$$

Therefore, physical exergy per unit mass flow rate subsequent to ignoring both velocity and elevation changes may be assessed as [169,219,223]:

$$Ex_{ph} = \dot{m}.[(h - h_0) - T_0 (s - s_0)] \quad (4.1.22)$$

Where h signifies specific enthalpy & s denotes specific entropy.

Point to be noted: with regards to CO_2, the change in chemical exergy presumed to be negligible & also has been considered that from one point to another, it will not change [223].

Apart from this, exergy at the system inlet (Ex_{inl}) also considered to be as maximum useful work accessible from sun radiations that can be further determined by utilizing Petela's formula as mentioned beneath [169,220,221,222]:

$$Ex_{inl} = A_{ap} \cdot G_b \cdot \left[1 + \frac{1}{3}\left(\frac{T_o}{T_{sun}}\right)^4 - \frac{4}{3}\left(\frac{T_o}{T_{sun}}\right)\right] \quad (4.1.23)$$

Where, temperature of sun's superficial surface (T_{sun}) also assumed to be as black body, which is nearby 5800 K [169].

However, solar energy directed upon the solar field ($\dot{Q}_s$) can be written as [218]:

$$\dot{Q}_s = A_{ap}.G_b \quad (4.1.24)$$

Therefore, the Petela's formula aimed at solar radiation's exergy ($\dot{E}x_s$) may be modify as [220,222]:

$$\dot{E}x_s = \dot{Q}_s \left[1 + \frac{1}{3}\left(\frac{T_0}{T_{sun}}\right)^4 - \frac{4}{3}\left(\frac{T_0}{T_{sun}}\right)\right] \quad (4.1.25)$$

Now exergy gain ($\dot{E}x_u$) by working fluid from the SPTC field can be stated as [218]:

$$\dot{E}x_u = \frac{\dot{Q}_u}{T_3 - T_1}\left[(T_3 - T_1) - \left(T_o \ln \frac{T_3}{T_1}\right)\right] \quad (4.1.26)$$

The SPTC's exergy efficiency can be described as:

$$\eta_{Ex,SPTC} = \frac{\dot{Ex}_u}{Ex_{inl}} \quad (4.1.27)$$

Or

In other words, SPTC's exergy efficiency may be expressed as [218]:

$$\eta_{Ex,SPTC} = \frac{\dot{Ex}_u}{\dot{Ex}_s} \quad (4.1.28)$$

Furthermore, LAT can be utilized to determine the hour angle (ω), which can further be attained by employing the two corrections in the standard time spotted from clock. Therefore, the relation for LAT can be termed as [1,214]:

$$LAT = ST \pm 4\ (ST\ longitude - LOL) + (E) \quad (4.1.29)$$

Noted that standard time, longitude of location, & equation of time correction has been denoted by ST, LOL, & E, respectively.

Where the first correction can be calculated as a result of difference amongst the meridian on which ST is centred and LOL. As can be seen in the equation 4.1.29, negative & positive symbol has been valid for the first correction with regards to eastern & western hemisphere, correspondingly. Likewise, in the correction, a magnitude of 4 minutes for every degree difference in longitude has been applied.

Moreover, second correction has been designated as E, which is because of occurrence of small variations in the earth's orbit and rate of rotation, and it has been calculated on the basis of experimental observations [1,214].

Last but not least, the empirical formula for the E (in minutes) may defined as below [1,214]:

$$E = 229.18(0.000075 + 0.001868 \cos B - 0.032077 \sin B - 0.014615 \cos 2B - 0.04089 \sin 2B) \quad (4.1.30)$$

&

$$B = (n - 1)\frac{360}{365} \quad (4.1.31)$$

Where n denotes the days of a year.

4.2. Modelling of combined SCO_2 cycle and ORC system

In this section, mathematical modelling of SCO_2-ORC system has been discussed. Energy and exergy based mathematical equations for each component involved in topping cycle (SCO_2 cycle) as well as bottoming cycle (ORC) has been derived on the basis of literature [89,167,172,199]. Apart from this, some important exergetic parameters for the combined cycle such as rate of exergy destruction, Y_{DEP}, Y*, and IMP also have been evaluated.

Few assumptions have been taken into consideration during the modelling which are given below:

1. System's pressure drop considered to be neglected excluding in case of pump and turbine
2. The steady state condition assumed for the system that means it should be unchanged even when transformation take place.
3. For all the organic fluids, efficiency of pump and turbine is considered to be as constant as revealed in Table 3.2.

Total input heat delivered by SPTC (Q_{inl}) to the combined cycle through the evaporator may be calculated as:

$$Q_{inl} = \dot{m}_{SCO_2} \cdot (h_5 - h_4) \quad (4.2.1)$$

Where $\dot{m}_{SCO_2}$ is a SCO_2 mass flow rate.

In SCO_2 turbine, thermodynamic process (state 5 to 6) can be termed as:

$$W_{SCO_{2,Turbine}} = \dot{m}_{SCO_2} \cdot (h_5 - h_{6s}) \cdot \eta_{SCO_{2,Turbine}} \quad (4.2.2)$$

Where $W_{SCO_{2,Turbine}}$ is the power output by SCO_2 turbine, h_{6s} is an isentropic enthalpy at the SCO_2 turbine's outlet, & $\eta_{SCO_{2,Turbine}}$ is a SCO_2 turbine's isentropic efficiency.

In recuperator, thermodynamic balance (state 6 to 7) may be stated as:

$$Q_{Recuperator} = \dot{m}_{SCO_2} \cdot (h_6 - h_7) = \dot{m}_{SCO_2} \cdot (h_4 - h_{10}) \quad (4.2.3)$$

Factor of effectiveness and recuperative ratio (ε) can be formulated as:

$$\varepsilon = \frac{h_6 - h_7}{h_6 - h_7(T_{10}, P_7)} \quad (4.2.4)$$

Where $h_7(T_{10}, P_7)$ is an enthalpy at point 7 that depends on the hypothesis that the SCO_2 stream's temperature exited from the recuperator at point 7 approaches to the SCO_2 stream's temperature, which is originating from the compressor at point 10.

Straightway, the waste heat delivered by SCO_2 cycle to ORC ($Q_{inl,ORC}$) within the HX (state 7 to 8) can be written as:

$$Q_{inl,ORC} = \dot{m}_{SCO_2} \cdot (h_7 - h_8) \quad (4.2.5)$$

In HX unit, thermodynamic relation (state 6 to 7) can be written as:

$$Q_{HX} = \dot{m}_{SCO_2} \cdot (h_7 - h_8) = \dot{m}_f \cdot (h_{11} - h_{12}) \quad (4.2.6)$$

Where $\dot{m}_f$ is an working fluid's mass flow rate in bottoming ORC.

In cooler unit, thermodynamic process (state 8 to 9) can be defined as:

$$Q_{Cooler} = \dot{m}_{SCO_2} \cdot (h_8 - h_9) \quad (4.2.7)$$

In SCO_2 compressor, thermodynamic process (state 9 to 10) is shown as:

$$W_{SCO_2,Compressor} = \frac{\dot{m}_{SCO_2} \cdot (h_{10s} - h_9)}{\eta_{SCO_2,Compressor}} \quad (4.2.8)$$

Where $W_{SCO_2,Compressor}$ is the power consumed by SCO_2 compressor which is directly driven by turbine, h_{10s} is an isentropic enthalpy at the compressor outlet & $\eta_{SCO_2,Compressor}$ is an isentropic efficiency of SCO_2 compressor.

Now for the ORC turbine, the thermal process (state 11 to 13) can be written as:

$$W_{ORC,Turbine} = \dot{m}_f \cdot (h_{11} - h_{13s}) \cdot \eta_{ORC,Turbine} \quad (4.2.9)$$

Where $W_{ORC,Turbine}$ is the power output by ORC turbine, h_{13s} is an isentropic enthalpy at the ORC turbine's outlet, and $\eta_{ORC,Turbine}$ is the isentropic efficiency of ORC turbine.

In condenser unit, thermodynamic process (state 13 to 14) can be described as:

$$Q_{Condenser} = \dot{m}_f \cdot (h_{13} - h_{14}) \quad (4.2.10)$$

In pump, thermodynamic process (state 14 to 12) can be given as:

$$W_{ORC,Pump} = \frac{\dot{m}_f \cdot (h_{12s} - h_{14})}{\eta_{ORC,Pump}} \quad (4.2.11)$$

Where h_{12s} is an isentropic enthalpy at the pump outlet and $\eta_{ORC,Pump}$ is the ORC pump's isentropic efficiency.

Further for the combined cycle (SCO_2-ORC), the thermal efficiency may be formulated as:

$$\eta_{Combined} = \frac{W_{Net,SCO_2\ cycle} + W_{Net,ORC}}{Q_{inl}} \quad (4.2.12)$$

Net power output from SCO_2 cycle ($W_{net,SCO_2\ cycle}$) can be evaluated as:

$$W_{Net,SCO_2\ cycle} = W_{SCO_2,Turbine} - W_{SCO_2,Compressor} \quad (4.2.13)$$

Net power output from ORC ($W_{net,ORC}$) can be calculated as:

$$W_{Net,ORC} = W_{ORC,Turbine} - W_{ORC,Pump} \quad (4.2.14)$$

Now the SPTC's outlet temperature can be presumed as a constant. Consequently, the total input exergy to the cycle (Ex_{inl}) can be evaluated as:

$$Ex_{inl} = Q_{inl} \cdot \left[1 - \frac{T_O}{T_3}\right] \quad (4.2.15)$$

For the combined cycle, overall electrical exergy efficiency ($\eta_{Elec,Ex}$) may be expressed as ratio of net electrical output to input exergy, and it can be expressed as:

$$\eta_{Elec,Ex} = 1 - \frac{Ex_{DES_{Total}}}{Ex_{inl}} \quad (4.2.16)$$

Therefore, in the combined cycle, total exergy destruction rate ($Ex_{DES_{Total}}$) may be written as:

$$Ex_{DES_{Total}} = Ex_{DES_{SCO_2,Turbine}} + Ex_{DES_{Recuperator}} + Ex_{DES_{Evaporator}} + Ex_{DES_{HX}} + Ex_{DES_{compressor}} + Ex_{DES_{ORC,Turbine}} + Ex_{DES_{Condensor}} + Ex_{DES_{ORC,Pump}} \quad (4.2.17)$$

Now the difference of input and output exergy recognized as a fraction of total exergy destruction of a component.

Therefore, in the SCO_2 turbine, the fraction of total exergy destruction ($Ex_{DES_{SCO_2,Turbine}}$) may be written as:

$$Ex_{DES_{SCO_2,Turbine}} = \frac{((Ex_5 - Ex_6) - W_{SCO_2,Turbine})}{Ex_{inl}} \quad (4.2.18)$$

In the recuperator, the fraction of total exergy destruction ($Ex_{DES_{Recuperator}}$) may be defined as:

$$Ex_{DES_{Recuperator}} = \frac{((Ex_6 - Ex_7) - (Ex_4 - Ex_{10}))}{Ex_{inl}} \quad (4.2.19)$$

In the evaporator, the fraction of total exergy destruction ($Ex_{DES_{Evaporator}}$) may be given as:

$$Ex_{DES_{Evaporator}} = \frac{(Ex_{inl} - (Ex_5 - Ex_4))}{Ex_{inl}} \quad (4.2.20)$$

In the HX unit, the fraction of total exergy destruction ($Ex_{DES_{HX}}$) as shown below:

$$Ex_{DES_{HX}} = \frac{((Ex_7 - Ex_8) - (Ex_{11} - Ex_{12}))}{Ex_{inl}} \quad (4.2.21)$$

In compressor, the fraction of total exergy destruction ($Ex_{DES_{compressor}}$) may be formulated as:

$$Ex_{DES_{compressor}} = \frac{(W_{Compressor} - (Ex_{10} - Ex_9))}{Ex_{inl}} \quad (4.2.22)$$

In the ORC turbine, the fraction of total exergy destruction ($Ex_{DES_{ORC,Turbine}}$) may be given as:

$$Ex_{DES_{ORC,Turbine}} = \frac{((Ex_{11} - Ex_{13}) - W_{ORC,Turbine})}{Ex_{inl}} \quad (4.2.23)$$

In the condenser, the fraction of total exergy destruction ($Ex_{DES_{Condensor}}$) may be expressed as:

$$Ex_{DES_{Condensor}} = \frac{((Ex_{13} - Ex_{14}) - (Ex_{15} - Ex_{16}))}{Ex_{inl}} \quad (4.2.24)$$

In the pump, the fraction of total exergy destruction ($Ex_{DES_{Pump}}$) may be calculated as:

$$Ex_{DES_{Pump}} = \frac{(W_{Pump} - (Ex_{12} - Ex_{14}))}{Ex_{inl}} \quad (4.2.25)$$

Anyways, few significant exergetic terms, for instance Y_{DEP}, Y*, IMP for each individual component, and φ are described in this section below.

So as to improve the system's functioning, fuel depletion ratio (Y_{DEP}) is an essential exergetic constraint, which may be expressed as ratio of exergy destruction rate to complete inlet exergy. The fuel depletion ratio for the different components of SCO_2-ORC system has been shown below [169,199]:

In the SCO_2 turbine, fuel depletion ratio ($Y_{DEP\ (SCO_2,Turbine)}$) can be written as:

$$Y_{DEP\ (SCO_2,Turbine)} = \frac{Ex_{DES_{SCO_2,Turbine}}}{Ex_{Total,inl}} \quad (4.2.26)$$

In the recuperator, fuel depletion ratio ($Y_{DEP\ (Recuperator)}$) can be defined as:

$$Y_{DEP\ (Recuperator)} = \frac{Ex_{DES_{Recuperator}}}{Ex_{Total,inl}} \quad (4.2.27)$$

In the evaporator, fuel depletion ratio ($Y_{DEP\ (Evaporator)}$) can be given as:

$$Y_{DEP\ (Evaporator)} = \frac{Ex_{DES_{Evaporator}}}{Ex_{Total,inl}} \quad (4.2.28)$$

In the HX unit, fuel depletion ratio ($Y_{DEP\ (HX)}$) can be written as:

$$Y_{DEP\ (HX)} = \frac{Ex_{DES_{HX}}}{Ex_{Total,inl}} \tag{4.2.29}$$

In the compressor, fuel depletion ratio ($Y_{DEP\ (Compressor)}$) can be defined as:

$$Y_{DEP\ (Compressor)} = \frac{Ex_{DES_{compressor}}}{Ex_{Total,inl}} \tag{4.2.30}$$

In the ORC turbine, fuel depletion ratio ($Y_{DEP\ (ORC,Turbine)}$) can be given as:

$$Y_{DEP\ (ORC,Turbine)} = \frac{Ex_{DES_{ORC,Turbine}}}{Ex_{Total,inl}} \tag{4.2.31}$$

In the condenser, fuel depletion ratio ($Y_{DEP\ (Condenser)}$) can be expressed as:

$$Y_{DEP\ (Condenser)} = \frac{Ex_{DES_{Condensor}}}{Ex_{Total,inl}} \tag{4.2.32}$$

In the pump, fuel depletion ratio ($Y_{DEP\ (Condenser)}$) can be calculated as:

$$Y_{DEP\ (Pump)} = \frac{Ex_{DES_{Pump}}}{Ex_{Total,inl}} \tag{4.2.33}$$

Apart from this, another vital constraint which is also known as irreversibility ratio (Y*) may be stated as ratio of destructed exergy to rate of overall exergy destruction in a system. Therefore, irreversibility ratio for the different components of SCO_2-ORC system has been illustrated below [169,199]:

In the SCO_2 turbine, irreversibility ratio ($Y*_{(SCO_2,Turbine)}$) can be written as:

$$Y*_{(SCO_2,Turbine)} = \frac{Ex_{DES_{(SCO_2,Turbine)}}}{Ex_{DES_{Total}}} \tag{4.2.34}$$

In the recuperator, irreversibility ratio ($Y*_{(Recuperator)}$) can be defined as:

$$Y*_{(Recuperator)} = \frac{Ex_{DES_{Recuperator}}}{Ex_{DES_{Total}}} \tag{4.2.35}$$

In the evaporator, irreversibility ratio ($Y*_{(Evaporator)}$) can be given as:

$$Y*_{(Evaporator)} = \frac{Ex_{DES_{Evaporator}}}{Ex_{DES_{Total}}} \tag{4.2.36}$$

In the HX unit, irreversibility ratio ($Y^*_{(HX)}$) can be written as:

$$Y^*_{(HX)} = \frac{Ex_{DES_{HX}}}{Ex_{DES_{Total}}} \quad (4.2.37)$$

In the compressor, irreversibility ratio ($Y^*_{(Compressor)}$) can be defined as:

$$Y^*_{(Compressor)} = \frac{Ex_{DES_{compressor}}}{Ex_{DES_{Total}}} \quad (4.2.38)$$

In the ORC turbine, irreversibility ratio ($Y^*_{(ORC,Turbine)}$) can be given as:

$$Y^*_{(ORC,Turbine)} = \frac{Ex_{DES_{ORC,Turbine}}}{Ex_{DES_{Total}}} \quad (4.2.39)$$

In the condenser, irreversibility ratio ($Y^*_{(Condenser)}$) can be expressed as:

$$Y^*_{(Condenser)} = \frac{Ex_{DES_{Condensor}}}{Ex_{DES_{Total}}} \quad (4.2.40)$$

In the pump, irreversibility ratio ($Y^*_{(Pump)}$) can be calculated as:

$$Y^*_{(Pump)} = \frac{Ex_{DES_{Pump}}}{Ex_{DES_{Total}}} \quad (4.2.41)$$

Now again a significant exergetic constraint which is known as improvement potential (IMP) and it could be utilized to identify that how much improvement can be conceivable in the combined system. Therefore, IMP for the various components of SCO_2-ORC can be calculated as [169,199]:

In the SCO_2 turbine, improvement potential ($IMP_{(SCO_2,Turbine)}$) can be written as:

$$IMP_{(SCO_2,Turbine)} = \left(1 - \frac{\eta_{Elec,Ex}}{100}\right) Ex_{DES_{(SCO_2,Turbine)}} \quad (4.2.42)$$

In the recuperator, improvement potential ($IMP_{(Recuperator)}$) can be defined as:

$$IMP_{(Recuperator)} = \left(1 - \frac{\eta_{Elec,Ex}}{100}\right) Ex_{DES_{Recuperator}} \quad (4.2.43)$$

In the evaporator, improvement potential ($IMP_{(Evaporator)}$) can be given as:

$$IMP_{(Evaporator)} = \left(1 - \frac{\eta_{Elec,Ex}}{100}\right) Ex_{DES_{Evaporator}} \quad (4.2.44)$$

In the HX unit, improvement potential (IMP $_{(HX)}$) can be written as:

$$\text{IMP}_{(HX)} = \left(1 - \frac{\eta_{Elec,Ex}}{100}\right) \text{Ex}_{\text{DES}_{HX}} \quad (4.2.45)$$

In the compressor, improvement potential (IMP $_{(Compressor)}$) can be defined as:

$$\text{IMP}_{(Compressor)} = \left(1 - \frac{\eta_{Elec,Ex}}{100}\right) \text{Ex}_{\text{DES}_{Compressor}} \quad (4.2.46)$$

In the ORC turbine, improvement potential (IMP $_{(ORC,Turbine)}$) can be given as:

$$\text{IMP}_{(ORC,Turbine)} = \left(1 - \frac{\eta_{Elec,Ex}}{100}\right) \text{Ex}_{\text{DES}_{ORC,Turbine}} \quad (4.2.47)$$

In the condenser, improvement potential (IMP $_{(Condenser)}$) can be expressed as:

$$\text{IMP}_{(Condenser)} = \left(1 - \frac{\eta_{Elec,Ex}}{100}\right) \text{Ex}_{\text{DES}_{Condenser}} \quad (4.2.48)$$

In the pump, improvement potential (IMP $_{(Pump)}$) can be calculated as:

$$\text{IMP}_{(Pump)} = \left(1 - \frac{\eta_{Elec,Ex}}{100}\right) \text{Ex}_{\text{DES}_{Pump}} \quad (4.2.49)$$

Lastly, the ORC cycle's expansion ratio may be formulated as:

$$\varphi = \left[\frac{\dot{V}_{13}}{\dot{V}_{11}}\right] \quad (4.2.50)$$

Where $\dot{V}$ is the volume flow rate.

4.3. Modelling of combined R-SCO_2 cycle and ORC system

In this section, mathematical modelling of combined recompression cycle (R-SCO_2-ORC) has been discussed on the basis of each component's exergy and energy balance associated with system. In this direction, the modelling of R-SCO_2-ORC has been carried out with the help of mathematical equations that have been acquired from literature [89,211] and their outcomes have been figured through the application of computational numerical method.

For the analysis, the subsequent needed assumptions have been considered:

1. In the combined cycle, processes should be in steady state.
2. System's pressure drop considered to be neglected excluding in case of pump and turbine.
3. For all the organic fluids, efficiency of pump and turbine is considered to be as constant.
4. Exchange of heat should be negligible with the surrounding excepting in cooler.

Total specific heat delivered in the R-SCO_2-ORC system from the SPTC through the evaporator unit (q_{inl}) can be defined as:

$$q_{inl} = (h_5 – h_4) \quad (4.3.1)$$

Now, the specific work output from SCO_2 turbine of recompression cycle has been described as:

$$w_{R-SCO_{2,Turbine}} = (h_5 – h_{6S}).\ \eta_{R-SCO_{2,Turbine}} \quad (4.3.2)$$

Thermodynamic relations for the specific enthalpy balance in HTR & LTR have been expressed as:

$$(h_4 – h_{9'}) = (h_6 – h_7) \quad (4.3.3)$$

$$(1–y).\ (h_{10'} – h_{10}) = (h_7 – h_{7'}) \quad (4.3.4)$$

Where y is the recompression mass fraction.

It was noticed that heat capacity of hot side is somewhat lower than that of cold side, consequently, the HTR effectiveness has been described as:

$$\varepsilon_{HTR} = \frac{(T_6 - T_7)}{(T_6 - T_{9'})} \quad (4.3.5)$$

Besides, effectiveness closely relies on the heat capacity that means product of mass flow rate & specific heat capacity. Hence, LTR effectiveness can be determined as:

$$\varepsilon_{LTR} = \frac{(T_7 - T_{7'})}{(T_7 - T_{10})} \quad \text{if minimum in hot side} \quad (4.3.6)$$

Or

$$\varepsilon_{LTR} = \frac{(T_{10'} - T_{10})}{(T_7 - T_{10})} \quad \text{if minimum in the cold side} \quad (4.3.7)$$

In case of total hot stream, the effectiveness factor & recuperative ratio (ε) can be formulated as [172,224]:

$$\varepsilon_{hot\ stream} = \frac{h_6 - h_{7'}}{h_6 - h_{7'}(T_{10}, P_{7'})} \quad (4.3.8)$$

In the downside term, enthalpy at point 8 can be estimated on the basis of hypothesis that the SCO_2 hot stream's temperature exiting the LTR approaches to the point 10 temperature. It has been noted that the iteration procedure has been utilized to formulate the mass fraction of SCO_2 stream that goes to LTR in recompression configuration until the temperature

at LTR outlet (state 10′) and recompressor outlet (state 9′) become almost equal. Apart from this, constant isentropic efficiency has been used to determine the output conditions of compressors and turbines [172].

The specific work consumed by main compressor ($w_{\text{Main Compressor}}$) and it can be expressed as:

$$w_{\text{Main Compressor}} = \frac{(1-y).(h_{10s}- h_9)}{\eta_{\text{Main Compressor}}} \quad (4.3.9)$$

Where $\eta_{\text{Main Compressor}}$ is the isentropic efficiency of main compressor.

The specific work consumed by recompressor which is directly driven by R-SCO_2 turbine ($w_{\text{Recompressor}}$) and it can be defined as:

$$w_{\text{Recompressor}} = \frac{(y).(h_{9's} - h_{8'})}{\eta_{\text{Recompressor}}} \quad (4.3.10)$$

Where $\eta_{\text{Recompressor}}$ is the isentropic efficiency of recompressor.

The specific work output of ORC turbine ($w_{\text{ORC,Turbine}}$) is given as:

$$w_{\text{ORC,Turbine}} = (h_{11}–h_{13s}) \cdot \eta_{\text{ORC,Turbine}} \quad (4.3.11)$$

The specific work consumed by ORC pump ($w_{\text{ORC}_{\text{Pump}}}$) is shown below:

$$w_{\text{ORC}_{\text{Pump}}} = \frac{(h_{12s}- h_{14})}{\eta_{\text{ORC,Pump}}} \quad (4.3.12)$$

Net specific work output of R-SCO_2 cycle as a topping cycle ($w_{\text{Net,R}-SCO_2\text{ cycle}}$) can be evaluated as:

$$w_{\text{Net,R}-SCO_2\text{ cycle}} = w_{\text{R}-SCO_{2,\text{Turbine}}} - w_{\text{Main Compressor}} - w_{\text{Recompressor}} \quad (4.3.13)$$

Net specific work output of ORC as a bottoming cycle ($w_{\text{Net,ORC}}$) can be expressed as:

$$w_{\text{Net,ORC}} = w_{\text{ORC,Turbine}} - w_{\text{ORC}_{\text{Pump}}} \quad (4.3.14)$$

Further in the combined recompression cycle (R-SCO_2-ORC system), the thermal efficiency can be described as:

$$\eta_{\text{combined}} = \frac{w_{\text{Net,R}-SCO_2\text{ cycle}}+w_{\text{Net,ORC}}}{q_{\text{inl}}} \quad (4.3.15)$$

Now in the SCO_2 turbine of recompression cycle, the fraction of total exergy destruction ($Ex_{DES_{R-SCO_{2,Turbine}}}$) can be written as:

$$Ex_{DES_{R-SCO_{2,Turbine}}} = \frac{[(Ex_5 - Ex_6) - w_{R-SCO_{2,Turbine}}]}{Ex_{inl}} \quad (4.3.16)$$

In the HTR, the fraction of total exergy destruction ($Ex_{DES_{HTR}}$) may be described as:

$$Ex_{DES_{HTR}} = \frac{[(Ex_6 - Ex_7) - (Ex_4 - Ex_{9'})]}{Ex_{inl}} \quad (4.3.17)$$

In the LTR, the fraction of total exergy destruction ($Ex_{DES_{LTR}}$) may be expressed as:

$$Ex_{DES_{LTR}} = \frac{[(Ex_7 - Ex_{7'}) - (1-y).(Ex_{10'} - Ex_{10})]}{Ex_{inl}} \quad (4.3.18)$$

In the evaporator, the fraction of total exergy destruction ($Ex_{DES_{Evaporator}}$) can be given as:

$$Ex_{DES_{Evaporator}} = \frac{[Ex_{inl} - (Ex_5 - Ex_4)]}{Ex_{inl}} \quad (4.3.19)$$

In the HX unit, the fraction of total exergy destruction ($Ex_{DES_{HX}}$) as shown below:

$$Ex_{DES_{HX}} = \frac{[((1-y).(Ex_{7'} - Ex_8)) - (Ex_{11} - Ex_{12})]}{Ex_{inl}} \quad (4.3.20)$$

In main compressor, fraction of total exergy destruction ($Ex_{DES_{Main\ Compressor}}$) can be defined as:

$$Ex_{DES_{Main\ Compressor}} = \frac{[w_{Main\ Compressor} - ((1-y)(Ex_{10} - Ex_9))]}{Ex_{inl}} \quad (4.3.21)$$

In the recompressor, the fraction of total exergy destruction ($Ex_{DES_{Recompressor}}$) can be written as:

$$Ex_{DES_{Recompressor}} = \frac{[w_{Recompressor} - (y(Ex_{9'} - Ex_{8'}))]}{Ex_{inl}} \quad (4.3.22)$$

In the ORC turbine, the fraction of total exergy destruction ($Ex_{DES_{ORC,Turbine}}$) can be given as:

$$Ex_{DES_{ORC,Turbine}} = \frac{[(Ex_{11} - Ex_{13}) - w_{ORC,Turbine}]}{Ex_{inl}} \quad (4.3.23)$$

The fraction of total exergy destruction in condenser ($Ex_{DES_{Condensor}}$) is expressed as:

$$Ex_{DES_{Condensor}} = \frac{[(Ex_{13} - Ex_{14}) - (Ex_{15} - Ex_{16})]}{Ex_{inl}} \quad (4.3.24)$$

The fraction of total exergy destruction in pump ($Ex_{DES_{Pump}}$) is calculated as:

$$Ex_{DES_{Pump}} = \frac{[W_{Pump} - (Ex_{12} - Ex_{14})]}{Ex_{inl}} \quad (4.3.25)$$

Therefore, in the R-SCO_2-ORC system, the total exergy destruction may be determined as:

$$Ex_{DES_{Total}} = Ex_{DES_{R-SCO_{2,Turbine}}} + Ex_{DES_{HTR}} + Ex_{DES_{LTR}} + Ex_{DES_{Evaporator}} + Ex_{DES_{HX}} + Ex_{DES_{Main\ Compressor}} + Ex_{DES_{Recompressor}} + Ex_{DES_{ORC,Turbine}} + Ex_{DES_{Condensor}} + Ex_{DES_{Pump}} \quad (4.3.26)$$

Lastly, in the R-SCO_2-ORC system, the second law efficiency may be formulated by ratio of net exergy output to the exergy input by the SPTC.

$$\eta_{Ex} = \frac{W_{Net,R-SCO_2\ cycle} + W_{Net,ORC}}{Ex_{inl}} = 1 - \frac{Ex_{DES_{Total}}}{Ex_{inl}} \quad (4.3.27)$$

4.4. Modelling of combined SCO_2 cycle and VAR cycle

In this section, mathematical modelling of the SCO_2-VAR cycle has been performed on the basis of energy and exergy equations which are then utilized to calculate the results through the application of computational numerical technique.

Furthermore, key assumptions that should be reasonable and do not affects the outcomes so much, have been prepared beneath in the current work and these are essential for the growth of thermodynamic models.

(a) The steady state condition assumed for the system that means it should be unchanged even when transformation take place [199,214].

(b) Variations in kinetic & potential energy must be ignored [214,223].

(c) In the system components, drop in pressure & losses of heat are assumed to be as negligible as in evaporator 1 & 2 (i.e. EV1 & EV2), recuperator, pipelines, refrigerant solution, & valves excluding in the area of pump & turbine. It has been pointed out that both pressure and heat loss in the actual HX and pipelines can produce insignificant decline in the efficiency & net power output that has minute influence on the thermodynamic examination [214,223].

(d) The refrigerant exiting the condenser and EV2 ought to be as saturated liquid & saturated vapour, correspondingly [214,223].

(e) From the absorber & generator, strong & weak solutions are exiting as saturated liquids [214,223].

Exergy examination is an important tool that can be utilized to assess system's overall exergy destruction. Exergy balance dependent on the steady state of every component incorporated in the control volume and it can be described as [169,199,214]:

$$\sum_Q \left(1 - \frac{T_o}{T_Q}\right) \dot{Q}_Q - \dot{w}_{c.v.} - \sum_i (\dot{m}_i Ex_i) - \sum_j (\dot{m}_e Ex_e) - \dot{E}x_d = 0 \quad (4.4.1)$$

Total exergy (Ex_{Total}) of a fluid is a summation of physical & chemical exergy that has been stated below [214,223]:

$$Ex_{Total} = Ex_{ph} + Ex_{ch} \quad (4.4.2)$$

Fluid's physical exergy (Ex_{ph}) at each state point after avoiding the changes in velocity and elevation, and it has been outlined as [214,223]:

$$Ex_{ph} = \dot{m}.[(h - h_0) - T_0 (s - s_0)] \quad (4.4.3)$$

As mentioned earlier with regards to CO_2, the change in chemical exergy presumed to be negligible & also has been considered that from one point to another, it will not change [214,223].

Rate of heat loss in SPTC ($\dot{Q}_{loss,SPTC}$) can be mentioned as [214,218]:

$$\dot{Q}_{loss,SPTC} = \dot{Q}_s.(1 - \eta_{En,SPTC}) \quad (4.4.4)$$

Where $\eta_{En,SPTC}$ is the energy efficiency of SPTC.

Likewise, rate of heat transfer in EV1 ($\dot{Q}_{EV1}$) from the SPTC to $SCO_2 - VAR$ cycle and it has been formulated as [214]:

$$\dot{Q}_{EV1} = \dot{m}_{oil}.(h_3 - h_1) = \dot{m}_{SCO_2}.(h_5 - h_4) \quad (4.4.5)$$

Where $\dot{m}_{oil}$ is an oil's mass flow rate, which is running in the SPTC field.

So as to perform the modelling, the energy & exergy balance to the distinct components of SCO_2-VAR cycle has been applied.

Heat input to SCO_2 cycle (state 4 to 5) from the SPTC through the EV1, which can be stated as [167,199]:

$$Q_{inl} = \dot{m}_{sco_2}.(h_5 - h_4) \quad (4.4.6)$$

In the SCO_2 turbine, thermodynamic process (state 5 to 6) can be written as [167,199]:

$$W_{SCO_{2,Turbine}} = \dot{m}_{SCO_2} \cdot (h_5 - h_{6s}) \cdot \eta_{SCO_{2,Turbine}} \quad (4.4.7)$$

In the recuperator unit, thermodynamic relation for heat transfer rate can be expressed as [167,199]:

$$\dot{Q}_{Recuperator} = \dot{m}_{SCO_2}(h_6 - h_7) = \dot{m}_{SCO_2}(h_4 - h_{10}) \quad (4.4.8)$$

Factor of effectiveness & recuperative ratio (ε) can be formulated as [167,199]:

$$\varepsilon = \frac{h_6 - h_7}{h_6 - h_7(T_{10}, P_7)} \quad (4.4.9)$$

In the SCO_2 compressor, thermodynamic process (state 9 to 10) is given by [167,199]:

$$W_{SCO_{2,Compressor}} = \frac{\dot{m}_{SCO_2} \cdot (h_{10s} - h_9)}{\eta_{SCO_{2,Compressor}}} \quad (4.4.10)$$

In the EV2, heat transfer equation ($\dot{Q}_{EV2}$) can be expressed as [214]:

$$\dot{Q}_{EV2} = [(\dot{m}_W.h_{22}) + (\dot{m}_{NH_3}.h_{19})] - [(\dot{m}_W.h_{23}) + (\dot{m}_{NH_3}.h_{11})] \quad (4.4.11)$$

In the EV1, heat transfer equation ($\dot{Q}_{EV1}$) can be defined as [214]:

$$\dot{Q}_{EV1} = [(\dot{m}_{sco_2}.h_5) + (\dot{m}_{oil}.h_2)] - [(\dot{m}_{sco_2}.h_4) + (\dot{m}_{oil}.h_3)] \quad (4.4.12)$$

The specific exergy ($\dot{E}x$) at each state can be stated as [214]:

$$\dot{E}x = \dot{m}.(h - T_0.s) \quad (4.4.13)$$

Noted that value of entropy and enthalpy is zero at T_0. Besides, chemical exergy may be defined as the maximum work achieved from the system when it is brought in a reaction by a substance existing in the atmosphere at a reference state [213,214].

Therefore, for the mixture of ammonia-water (NH_3-H_2O), the chemical exergy ($\dot{E}x_{ch}$) can be computed through the equation as shown under [214,223]:

$$\dot{E}x_{ch} = \dot{m}\left[\left(\frac{X}{M_{NH_3}}\right)Ex^0_{ch,NH_3} + \left(\frac{1-X}{M_{H_2O}}\right)Ex^0_{ch,H_2O}\right] \quad (4.4.14)$$

Where Ex^0_{ch,NH_3} and Ex^0_{ch,H_2O} are the usual value of chemical exergy for the fluids like NH_3 & H_2O, correspondingly.

Now after considering SPTC's outlet temperature as a constant value, input exergy to the SCO_2-VAR cycle (Ex_{inl}) can be described as [214]:

$$Ex_{inl} = Q_{inl}\left[1 - \frac{T_O}{T_3}\right] \quad (4.4.15)$$

In the EV2, exergy rate for the cooling ($\dot{E}x_{cooling}$) can be computed by the relation as shown under [214]:

$$\dot{E}x_{cooling} = \dot{Q}_{EV2}\left[\frac{T_0}{T_{EV2}} - 1\right] \quad (4.4.16)$$

In the EV1, the exergy destruction ($Ex_{DES_{EV1}}$) may be written as [214]:

$$Ex_{DES_{EV1}} = [(Ex_3 - Ex_2) - (Ex_5 - Ex_4)] \quad (4.4.17)$$

In the SCO_2 turbine, the exergy destruction ($Ex_{DES_{SCO_{2,Turbine}}}$) can be expressed as [214]:

$$Ex_{DES_{SCO_{2,Turbine}}} = \left[(Ex_5 - Ex_6) - W_{SCO_{2,Turbine}}\right] \quad (4.4.18)$$

In the SCO_2 compressor, the exergy destruction ($Ex_{DES_{SCO_{2,Compressor}}}$) can be defined as [214]:

$$Ex_{DES_{SCO_{2,Compressor}}} = \left[W_{SCO_{2,Compressor}} - (Ex_{10} - Ex_9)\right] \quad (4.4.19)$$

In the recuperator, the exergy destruction ($Ex_{DES_{Recuperator}}$) can be given as [214]:

$$Ex_{DES_{Recuperator}} = [(Ex_6 - Ex_7) - (Ex_4 - Ex_{10})] \quad (4.4.20)$$

In EV2, exergy destruction ($Ex_{DES_{EV2}}$) may be defined as [214]:

$$Ex_{DES_{EV2}} = [(Ex_{22} - Ex_{23}) - (Ex_{11} - Ex_{19})] \quad (4.4.21)$$

In EV_2, mass flow rate of NH_3 vapours may be formulated as [214]:

$$\dot{m}_{11} = \frac{\dot{Q}_{EV2}}{(h_{11} - h_{19})} \quad (4.4.22)$$

In the absorber, balance of mass & material for NH_3 may be stated as [214]:

$$\dot{m}_{11} + \dot{m}_{15} = \dot{m}_{12} \quad (4.4.23)$$

and

$$(\dot{m}_{11}.X_{11}) + (\dot{m}_{15}.X_{15}) = \dot{m}_{12}.X_{12} \quad (4.4.24)$$

or

$$(\dot{m}_{11}.X_{11}) + (\dot{m}_{15}.X_{15}) = (\dot{m}_{11}+\dot{m}_{15}).X_{12} \quad (4.4.25)$$

Noted that the rejection of heat in the absorber & condenser to the cooling water that may be further utilized for heating uses.

Therefore, in the absorber, heat loss ($\dot{Q}_{Absorber}$) can be evaluated as [214]:

$$\dot{Q}_{Absorber} = [(\dot{m}_{11} \times h_{11}) + (\dot{m}_{15} \times h_{15})] - (\dot{m}_{12} \times h_{12}) \quad (4.4.26)$$

In the condenser, heat loss ($\dot{Q}_{Condenser}$) can be written as [214]:

$$\dot{Q}_{Condenser} = [(\dot{m}_{16} \times h_{16}) - (\dot{m}_{17} \times h_{17})] = \dot{m}_{11} \times (h_{16} - h_{17}) \quad \{\because \dot{m}_{16} = \dot{m}_{17} = \dot{m}_{11}\} \quad (4.4.27)$$

In the SHE, heat loss ($\dot{Q}_{SHE}$) can be expressed as [214]:

$$\dot{Q}_{SHE} = [(\dot{m}_{14'} \times h_{14'}) + (\dot{m}_{13} \times h_{13})] - [(\dot{m}_{13'} \times h_{13'}) + (\dot{m}_{14} \times h_{14})] \quad (4.4.28)$$

In absorber, exergy destruction ($Ex_{DES_{Absorber}}$) may be written as [214]:

$$Ex_{DES_{Absorber}} = [(Ex_{11} + Ex_{15}) - Ex_{12}] - \dot{Q}_{Absorber} \cdot \left[1 - \left(\frac{T_o}{T_{Absorber}}\right)\right] \quad (4.4.29)$$

In condenser, exergy destruction ($Ex_{DES_{Condenser}}$) may be expressed as [214]:

$$Ex_{DES_{Condenser}} = [(Ex_{16} - Ex_{17}) - (Ex_{21} - Ex_{20})] \quad (4.4.30)$$

In SHE, exergy destruction ($Ex_{DES_{SHE}}$) may be defined as [214]:

$$Ex_{DES_{SHE}} = [(Ex_{14'} - Ex_{14}) - (Ex_{13'} - Ex_{13})] \quad (4.4.31)$$

Heat loss & exergy destruction in pressure reducing valve (PRV) & expansion valve (EXV) can be described as [214]:

$$\dot{Q}_{PRV} = [(\dot{m}_{14}.h_{14}) - (\dot{m}_{15}.h_{15})] = \dot{m}_{15}.(h_{14}-h_{15}) \quad \{\because \dot{m}_{14}=\dot{m}_{15}\} \quad (4.4.32)$$

$$\dot{Q}_{EXV} = [(\dot{m}_{18}.h_{18}) - (\dot{m}_{19}.h_{19})] = \dot{m}_{11}.(h_{18}-h_{19}) \quad \{\because \dot{m}_{18}=\dot{m}_{19}=\dot{m}_{11}\} \quad (4.4.33)$$

$$Ex_{DES_{PRV}} = [Ex_{14} - Ex_{15}] \quad (4.4.34)$$

$$Ex_{DES_{EXV}} = [Ex_{18} - Ex_{19}] \quad (4.4.35)$$

In the pump, exergy destruction ($Ex_{DES_{Pump}}$) can be written as [214]:

$$Ex_{DES_{Pump}} = \left[W_{Pump} - (Ex_{13} - Ex_{12})\right] \quad (4.4.36)$$

Heat supplied ($\dot{Q}_{Generator}$) and exergy destruction ($Ex_{DES_{Generator}}$) in generator can be expressed as [214]:

$$\dot{Q}_{Generator} = (\dot{m}_{16}.h_{16}) + (\dot{m}_{14'}.h_{14'}) - (\dot{m}_{13}.h_{13}) \quad (4.4.37)$$

$$Ex_{DES_{Generator}} = [(Ex_{16} + Ex_{14'}) - Ex_{13'}] + \dot{Q}_{Gen}.\left[1 - \left(\frac{T_o}{T_{Gen}}\right)\right] \quad (4.4.38)$$

In the SCO_2-VAR cycle, the net work output ($W_{Net,SCO_2-VAR\ cycle}$) may be calculated as [214]:

$$W_{Net,SCO_2-VAR\ cycle} = W_{SCO_2,Turbine} - (W_{SCO_2,Compressor} + W_{Pump}) \quad (4.4.39)$$

In the SCO_2-VAR cycle, the thermal efficiency (η_{Th}) may be stated as [214]:

$$\eta_{Th} = \frac{W_{Net,SCO_2-VAR\ cycle}}{Q_{inl}} \quad (4.4.40)$$

In the SCO_2-VAR cycle, the exergy efficiency (η_{Ex}) may be termed as ratio of net exergy output to the input exergy delivered by the SPTC, and its relation may be expressed as [214,223]:

$$\eta_{Ex} = \frac{W_{Net,SCO_2-VAR\ cycle} + \dot{E}x_{cooling}}{Ex_{inl}} \quad (4.4.41)$$

Or

In the SCO_2-VAR cycle, exergy efficiency can also be termed as [214]:

$$\eta_{Ex} = 1 - \frac{Ex_{DES_{Total}}}{Ex_{inl}} \quad (4.4.42)$$

Furthermore, in the VAR cycle, the actual COP so as to produce cooling may be expressed as [213,214]:

$$COP_{cooling} = \frac{\dot{Q}_{EV2}}{\dot{Q}_{Generator} + W_{Pump}} \quad (4.4.43)$$

Where $\dot{Q}_{EV2}$ is the amount of heat absorption through the ammonia vapours in order to generate the effect of cooling, $\dot{Q}_{Generator}$ is the amount of supplied heat in the generator, and W_{Pump} is considered to be as negligible in contrast to supplied heat in the generator, and therefore it could be neglected during calculations.

Consequently, net refrigeration effect may be described as the ratio of heat transfer to the refrigerant in evaporator to the total heat delivered to the generator, which may be stated as [213,214]:

$$COP_{cooling} = \frac{\dot{Q}_{EV2}}{\dot{Q}_{Generator}} \quad (4.4.44)$$

Finally, heat rejection in the process of absorption and condensation could be consumed for heating applications. Therefore, in the VAR cycle, the actual COP for the heating may be written as [213,214]:

$$COP_{heating} = \frac{\dot{Q}_{Condenser} + \dot{Q}_{Absorber}}{\dot{Q}_{Generator}} \quad (4.4.45)$$

Where $\dot{Q}_{Condenser}$ and $\dot{Q}_{Absorber}$ is the rejected heat through the convection cooling in the condenser & absorber, correspondingly.

4.5. Modelling of SORC system

In this section, modelling of the SORC system has been discussed based mathematical equations which have been programmed into a computer code and then solved by a computational numerical technique. Some assumptions have been considered such as that pressure change is negligible excluding the pump & turbine, and the system operates in steady state conditions.

Total input heat delivered by SPTC to the SORC through the heat exchanger unit (Q_{inl}) may be written as:

$$Q_{inl} = \dot{m}_f \cdot (h_5 - h_4) \quad (4.5.1)$$

Where $\dot{m}_f$ is an organic fluid's mass flow rate.

In the SORC turbine, thermodynamic process can be described as:

$$W_{SORC,Turbine} = \dot{m}_f \cdot (h_5 - h_{6s}) \cdot \eta_{SORC,Turbine} \quad (4.5.2)$$

Where $\eta_{SORC,Turbine}$ is the isentropic efficiency of turbine in SORC system.

In the recuperator, thermodynamic balance can be stated as:

$$Q_{Recuperator} = \dot{m}_f \cdot (h_6 - h_7) = \dot{m}_f \cdot (h_4 - h_{11}) \quad (4.5.3)$$

In the condenser unit, thermodynamic process can be described as:

$$Q_{Condenser} = \dot{m}_f \cdot (h_7 - h_{10}) \quad (4.5.4)$$

In the SORC pump, thermodynamic process can be written as:

$$W_{SORC,Pump} = \frac{\dot{m}_f \cdot (h_{11s} - h_{10})}{\eta_{SORC,Pump}} \quad (4.5.5)$$

In the SORC system, the net work output may be computed as:

$$W_{Net,SORC} = W_{SORC,Turbine} - W_{SORC,Pump} \quad (4.5.6)$$

Further, in the SORC system, the thermal efficiency ($\eta_{Th,SORC}$) may be expressed as:

$$\eta_{Th,SORC} = \frac{W_{Net,SORC}}{Q_{inl}} \quad (4.5.7)$$

Where Ex_{inl} is the exergy input to SORC system, which can be computed by considering the outlet temperature of SPTC as a constant value, and it may be expressed as [199]:

$$Ex_{inl} = Q_{inl}\left[1 - \frac{T_O}{T_3}\right] \quad (4.5.8)$$

Now for the SORC system, total exergy destruction may be determined as:

$$Ex_{DES_{Total}} = Ex_{DES_{SORC,Turbine}} + Ex_{DES_{Recuperator}} + Ex_{DES_{Evaporator}} + Ex_{DES_{Condensor}} + Ex_{DES_{Pump}} + Ex_{DES_{SPTC}} \quad (4.5.9)$$

Apart from this, the difference of input and output exergy recognized as a fraction of total exergy destruction of a component.

Therefore, in the SCO_2 turbine, the fraction of total exergy destruction is written as:

$$\mathrm{Ex_{DES_{SORC,Turbine}}} = \frac{[(\mathrm{Ex_5} - \mathrm{Ex_6}) - \mathrm{W_{SORC,Turbine}}]}{\mathrm{Ex_{inl}}} \quad (4.5.10)$$

The fraction of total exergy destruction in recuperator is defined as:

$$\mathrm{Ex_{DES_{Recuperator}}} = \frac{[(\mathrm{Ex_6} - \mathrm{Ex_7}) - (\mathrm{Ex_4} - \mathrm{Ex_{11}})]}{\mathrm{Ex_{inl}}} \quad (4.5.11)$$

The fraction of total exergy destruction in evaporator is given by:

$$\mathrm{Ex_{DES_{Evaporator}}} = \frac{[\mathrm{Ex_{inl}} - (\mathrm{Ex_5} - \mathrm{Ex_4})]}{\mathrm{Ex_{inl}}} \quad (4.5.12)$$

The fraction of total exergy destruction in condenser is expressed as:

$$\mathrm{Ex_{DES_{Condensor}}} = \frac{((\mathrm{Ex_7} - \mathrm{Ex_{10}}) - (\mathrm{Ex_8} - \mathrm{Ex_9}))}{\mathrm{Ex_{inl}}} \quad (4.5.13)$$

The fraction of total exergy destruction in pump is calculated as:

$$\mathrm{Ex_{DES_{Pump}}} = \frac{(\mathrm{W_{Pump}} - (\mathrm{Ex_{11}} - \mathrm{Ex_{10}}))}{\mathrm{Ex_{inl}}} \quad (4.5.14)$$

Moreover, the exergy efficiency of SPTC integrated SORC ($\eta_{\mathrm{Ex,SORC}}$) may be termed as the ratio of net exergy output to the exergy input delivered by the SPTC [199].

$$\eta_{\mathrm{Ex,SORC}} = \frac{\mathrm{W_{Net,SORC}}}{\mathrm{Ex_{inl}}} = 1 - \frac{\mathrm{Ex_{DES_{Total}}}}{\mathrm{Ex_{inl}}} \quad (4.5.15)$$

Chapter-5

Results and discussion

In this chapter, discussion have been made on the results comes out from the energy and exergy analysis of considered cycles such as SPTC integrated with combined SCO_2 cycle and ORC (SCO_2-ORC) system, SPTC integrated with combined R-SCO_2 cycle and ORC (R-SCO_2-ORC) system, SPTC integrated with combined SCO_2 cycle and VAR cycle (i.e. SCO_2-VAR cycle), and SPTC integrated with SORC system in the different sections. The computer programs have been prepared through the use of engineering equation solver (EES) software so as to modelled the selected systems and their computed results have been discussed in this chapter in a comprehensive way under the different sections.

5.1. SPTC integrated with combined SCO_2 cycle and ORC system

In this section, the energetic & exergetic performance of a SPTC driven SCO_2-ORC system has been inspected against the variations of solar direct normal irradiance (solar DNI or G_b), inlet pressure & temperature of SCO_2 turbine, and inlet temperature of compressor with the assistance of EES software in a detailed way in the subsections below. Then, the exergetic performance parameters for individual components of the considered system has been presented in a separate section.

Presently, the SPTC has been designed on the premise of the average solar DNI of 850 W/m^2 following strictly to the Indian sunny climate in which SCO_2-ORC system is presumed to be operated.

Besides, the effect of solar DNI on the performance of SCO_2-ORC system with and without the implication of SPTC has been assessed throughout the daytime between the selected range of solar DNI, i.e. 500 W/m^2 to 950 W/m^2. In addition, organic working fluids such as R407c, R1234ze, R1234yf, R245fa, and R134a have been chosen for low-temperature ORC to analyse the system performance [199].

5.1.1. Effect of the variation in solar DNI on the system performance

The exergetic performance of SCO_2-ORC system is clearly influenced by the fluctuations in solar DNI as illustrated in Figure 5.1. From the Figure 5.1, it has been detected that the exergy efficiency of SCO_2-ORC system rises with the rise in solar DNI, which has been examined on the basis of simulation conditions of high pressure & mass flow rate of SCO_2 (i.e. 25 MPa & 10 kg/s). Also, noted that the rising solar DNI upon the SPTC field provides the better and efficient exploitation of specific range of the SPTC rows accessible in the overall solar field that further improves the exergetic performance. Among all the nominated refrigerants for the SCO_2-ORC system, the R407c fluid has exhibited a maximum value of exergetic efficiency followed by the R1234ze, R1234yf, R245fa, and R134a fluids [199].

Figure 5.1 implies that the exergy efficiency of R407c fluid based combined cycle rises uninterruptedly from 54.93% at 500 W/m^2 to 78.07% at 950 W/m^2. Apart from this, R1234ze and R1234yf fluid based combined cycle has a maximum exergetic efficiency of 77.37% and 76.74% at 950 W/m^2, correspondingly, which is lies between the R407c and R134a fluid based combined cycle. Whereas the study also disclosed that R134a and R245fa fluid based cycles have the minor differences amongst their values of exergetic efficiency, i.e. 75.87% & 76.07% at 950 W/m^2, correspondingly [199].

Figure 5.2 demonstrates that the R407c fluid based combined cycle has a highest amount of thermal efficiency in contrast to other cycles, which is upsurges from 30.6% at 500 W/m^2 to 43.49% at 950W/m^2. Otherwise, R134a fluid has a lowest amount of thermal efficiency, which is nearby 27.91% at 500 W/m^2 rises to 42.26% at 950 W/m^2. In addition, the thermal efficiency of R1234ze, R1234yf, & R245fa fluid based combined cycles lies between the R407c and R134a fluid combined cycle as shown in Figure 5.2 [199].

However, with regards to complete plant, i.e. combined cycle along with solar collector (i.e. SPTC-SCO_2-ORC system), it has been assessed from the Figure 5.3 that R407c fluid has a highest value of exergy efficiency, which is rises from 18.45% at 500 W/m^2 to 57.12% at 950 W/m^2. Instead, R245fa fluid has a lowest value of exergy efficiency, which is enhances from 8.839% at 500 W/m^2 to 52.07% at 950 W/m^2. Also, the exergy efficiency of R1234ze, R1234yf, and R134a fluid has a maximum value of 55.39%, 54.37%, and 53.07% at 950 W/m^2, correspondingly, which is lies between the R407c and R245fa fluid, and also these cycles have a marginal difference amongst their exergy efficiency values as shown in Figure 5.3.

Apart from this, Figure 5.4. clearly specifies the variations in thermal efficiency of SPTC-SCO_2-ORC system with regards to the solar DNI. Outcomes of the analysis reveal that the R407c fluid has a maximum value of thermal efficiency among other cycles as considered above, which is continuously increasing from 10.28% at 500 W/m^2 to 31.82% at 950 W/m^2

followed by the R1234ze, R1234yf, R134a, and R245fa fluid has a minimum amount of thermal efficiency, which is augments from 4.924% at 500 W/m^2 to 29% at 950 W/m^2 as clearly understood from Figure 5.4.

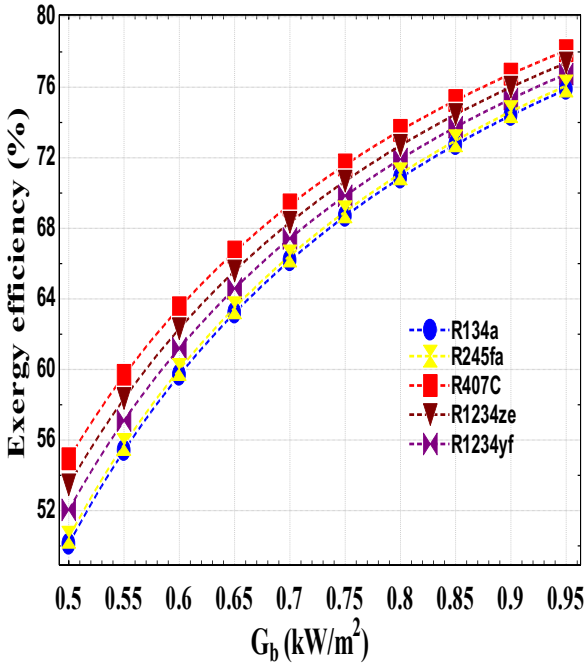

Figure 5.1. Exergy efficiency of combined cycle without solar collector (SCO_2-ORC) versus solar DNI [199]

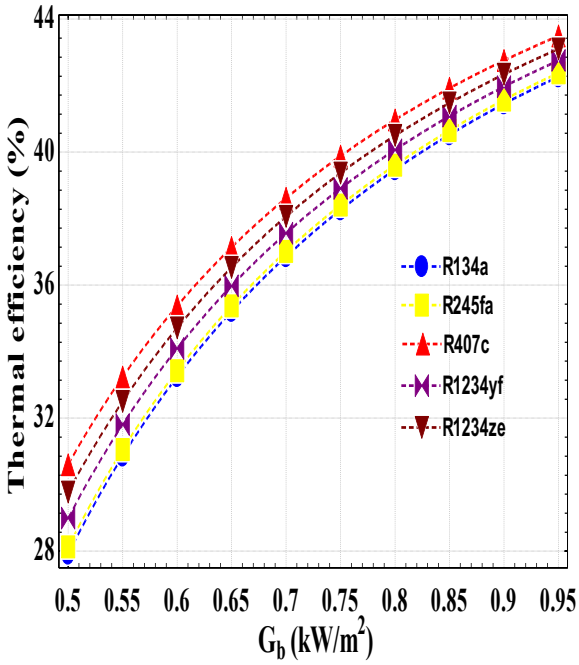

Figure 5.2. Thermal efficiency of combined cycle without solar collector (SCO_2-ORC) versus solar DNI [199]

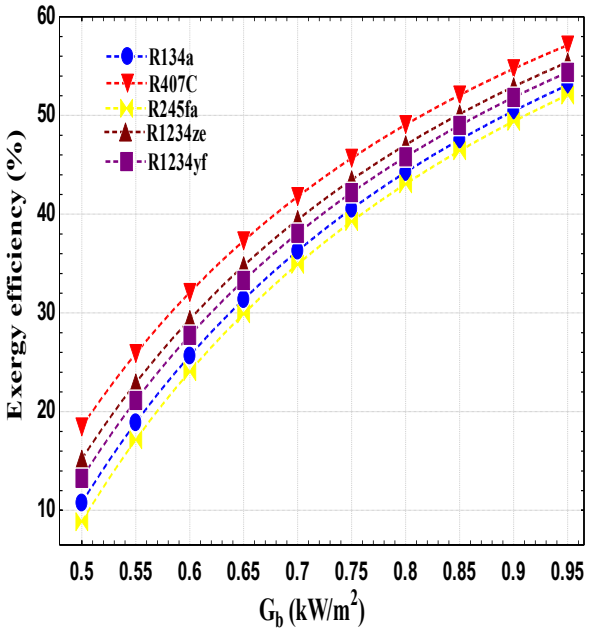

Figure 5.3. Exergy efficiency of complete plant (SPTC-SCO_2-ORC) versus solar DNI

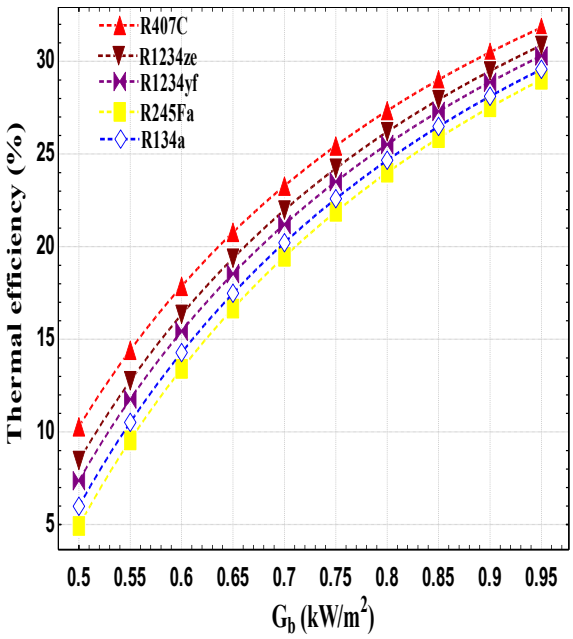

Figure 5.4. Thermal efficiency of complete plant (SPTC-SCO_2-ORC) versus solar DNI

Moreover, Figure 5.5 displays that rate of total exergy destruction for SCO_2-ORC system decreases with the augmentation in solar DNI from 500 W/m^2 to 950 W/m^2, which has been estimated on the basis of same simulated conditions as depicted previously. Additionally, the rate of exergy destruction has a reverse behaviour from the exergetic efficiency, and it has been found that the R407c fluid based combined cycle has a lowest rate of exergy destruction, which is reduces from 8412 kW at 500 W/m^2 to 4093 kW at 950 W/m^2 followed by the exergy destruction rate of R1234ze, R1234yf, and R245fa fluid based combined cycles with a maximum value of 8746 kW, 8985 kW, and 9243 kW at 500 W/m^2, respectively. Likewise, Figure 5.5 also illustrates that the R134a fluid based combined cycle has an utmost rate of exergy destruction, which is falling from 9321 kW to 4508 kW as the solar DNI rises from 500 W/m^2 to 950 W/m^2 [199].

Eventually, in the complete plant, i.e. SPTC-SCO_2-ORC system, the exergy destruction rate in the entire area of solar collector (i.e. SPTC field) observed to be comparatively much higher than the both SCO_2 cycle & ORC, which is commonly because of the fact that extensive amount of input exergy to the SPTC, however, low rate of exergy conversion to working fluid in the meantime [199,225].

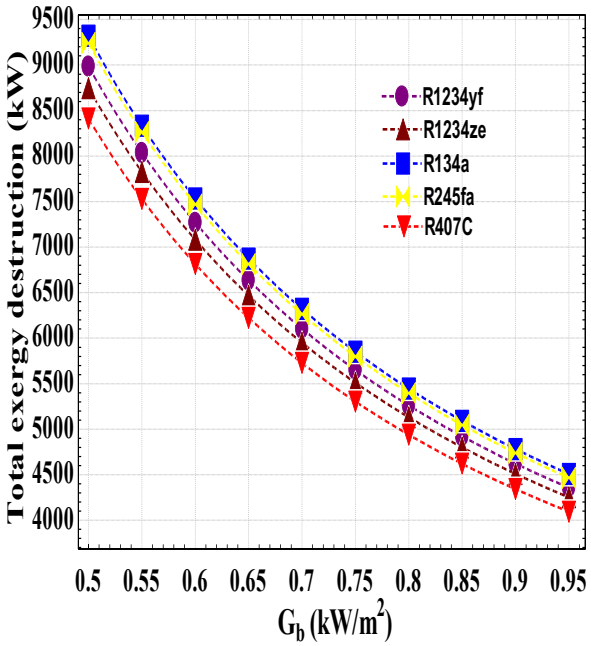

Figure 5.5. Total exergy destruction of combined cycle without solar collector (SCO_2-ORC) versus solar DNI [199]

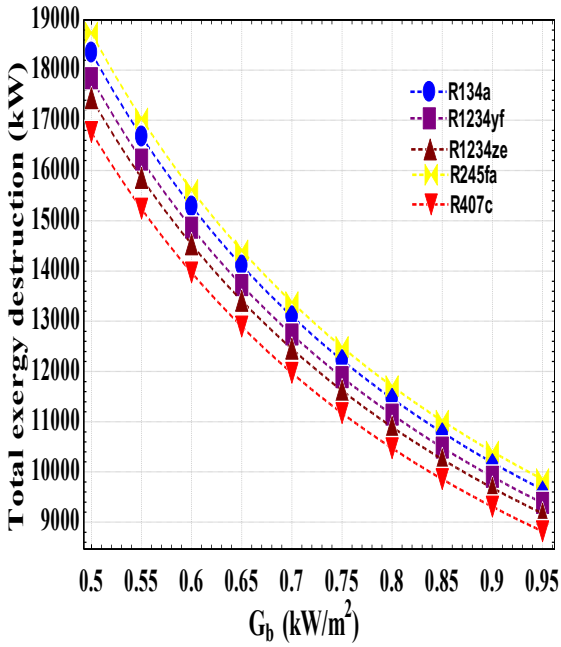

Figure 5.6. Total exergy destruction of complete plant (SPTC-SCO_2-ORC) versus solar DNI [199]

It is clear from Figure 5.6 that the exergy destruction rate in SPTC-SCO_2-ORC system diminishes step by step as the solar DNI expands, which can be because of effective utilization of the SPTC field. Clearly if the great intensity of solar irradiation falling upon the fewer SPTC rows comprise with the multiple number of SPTCs that are organised in a series and parallel arrangement in the entire SEGS plant can successfully decrease the rate of exergy destruction [199].

Regarding the Figure 5.6, it has been detected that the R245fa fluid has an utmost amount of exergy destruction rate in SPTC-SCO_2-ORC system, and it gradually declines from 18743 kW at 500 W/m^2 to 9855 kW at 950 W/m^2. Whereas, the R407c fluid has a smallest rate of total exergy destruction in contrast to other working fluids, which is reduces from 16767 kW at 500 W/m^2 to 8816 kW at 950 W/m^2. Whilst the exergy destruction rate of R134a, R1234yf, and R1234ze fluid based cycles lies between the values of these two cycles (i.e. depends on the R245fa and R407c fluid) as mentioned above.

5.1.2. Effect of the variation in inlet pressure of SCO_2 turbine on the system performance

The inlet pressure of SCO_2 turbine is a significant constraint that can be exploit to investigate the performance as well as improve the combined cycle's design. A specified range of turbine inlet pressure has been selected on the basis of concept that inlet pressure should be adjusted in such a way that the CO_2 will be remains in supercritical state before and after expansion. The influence of fluctuations in inlet pressure of SCO_2 turbine on the exergy efficiency of SCO_2-ORC system has been assessed on the basis of fixed simulated conditions like the solar DNI amount of 850 W/m^2, SCO_2 cycle's maximum temperature and mass flow rate of about 653 K & 10 kg/s, respectively [199].

Figure 5.7. exhibits that the exergetic efficiency is marginally upsurges as the inlet pressure of SCO_2 turbine rises. It has been found that the R407c fluid based SCO_2-ORC system has a greatest exergetic efficiency value that it will be rises from 75.03% at 14 MPa to 75.21% at 23 MPa. Furthermore, both the R245fa and R134a fluids have the smallest value along with the comparable value of exergetic efficiency, i.e. around 72.53% at 14 MPa increases to 72.92% at 23 MPa and 72.64% at 14 MPa increases to 72.75% at 23 MPa, correspondingly as comapred to the other considered combined cycles with the marginal changes in their exergy performance. Likewise, the R1234yf and R1234ze fluid based combined cycles indicated an incremental trend of exergy efficiency and the maximum value

of these cycles have around 73.75% and 74.44% at 23 MPa, respectively as shown in Figure 5.7 [199].

Additionaly, the Figure 5.8 demonstrates that the R407c fluid has a utmost amount of thermal efficiency, which is augments somewhat from 41.8% at 14 MPa to 41.9% at 23 MPa. However, R245fa fluid has a smallest value of thermal efficiency, i.e. around 40.4% at 14 MPa and upsurges to 40.62% at 23 MPa, which is comparable to R134a fluid along with thermal efficiency varying from around 40.47% at 14 MPa enhances to 40.53% at 23 MPa as described in Figure 5.8 [199].

Apart from this, in respect of complete cycle, i.e. combined cycle along with solar collector (i.e. SPTC-SCO_2-ORC system), it has been inspected from the Figure 5.9 that the R407c fluid has a maximum exergy efficiency value, which is increases marginally from 51.93% at 14 MPa to 52.05% at 23 MPa. However, the exergy efficiency of R245fa fluid has a minimum exergy efficiency value, which is augments from 46.11% at 14 MPa to 46.39% at 23 MPa. Also, the exergy efficiency curves of R1234ze, R1234yf, and R134a fluids with a maximum value of 50.14%, 49.02%, and 47.56% at 23 MPa, respectively lies between the R407c and R245fa fluid as shown in Figure 5.9.

On the contrary side, the influence of inlet turbine pressure on the thermal performance of SPTC-SCO_2-ORC system has been demonstrated in Figure 5.10. Study reveals that R407c fluid has an uppermost value of thermal efficiency amongst the other fluids, which is rises slightly from 28.93% at 14 MPa to 29% at 23 MPa followed by the R1234ze, R1234yf, R134a, and R245fa fluid has a minimum amount of thermal efficiency, i.e. augments somewhat from 25.69% at 14 MPa to 25.84% at 23 MPa as indicated in Figure 5.10.

Besides, it has been detected that as the inlet turbine pressure upsurges, rate of total exergy destruction in SCO_2-ORC reduces slightly as revealed in Figure 5.11, and the R407c fluid based SCO_2-ORC system has a lowest rate of total exergy destruction, which is approximately 4683 kW at 14 MPa declines to 4659 kW at 23 MPa followed by the R1234ze and R1234yf fluid. However, the R245fa and R134a fluid based combined cycles have a relatively maximum rate of total exergy destruction along with a lowest value of 5053 kW and 5088 kW at 23 MPa, correspondingly as depicted in Figure 5.11 [199].

Lastly, in the SPTC-SCO_2-ORC system, the maximum quantity of exergy destructions, which is about 50% to 60% happens in the solar collector (i.e. SPTC field) only as demonstrated in Figure 5.12, and this sort of exergy destructions are partly initiated by the temperature as well as material limits of the SPTCs deployed in the plant. Hence, it is essential to examine the amount of exergy destruction because of SPTC for the further

development in design of whole plant so as to achieve the better exergetic and energetic performance [199].

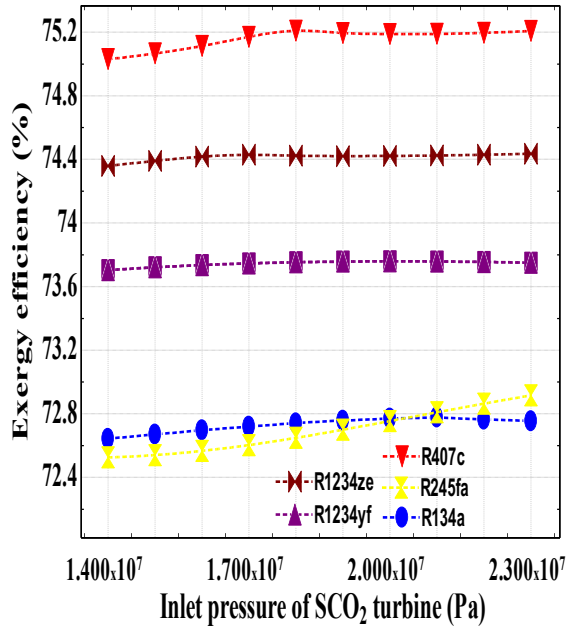

Figure 5.7. Exergy efficiency of combined cycle without solar collector (SCO_2-ORC) versus inlet pressure of SCO_2 Turbine [199]

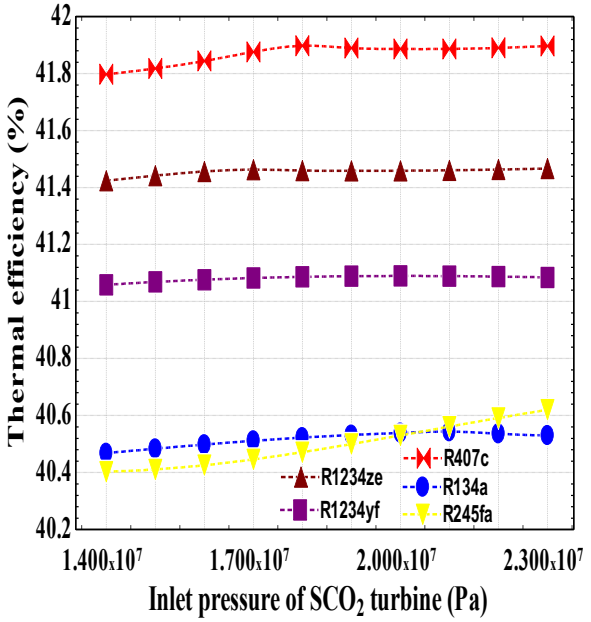

Figure 5.8. Thermal efficiency of combined cycle without solar collector (SCO_2-ORC) versus inlet pressure of SCO_2 Turbine [199]

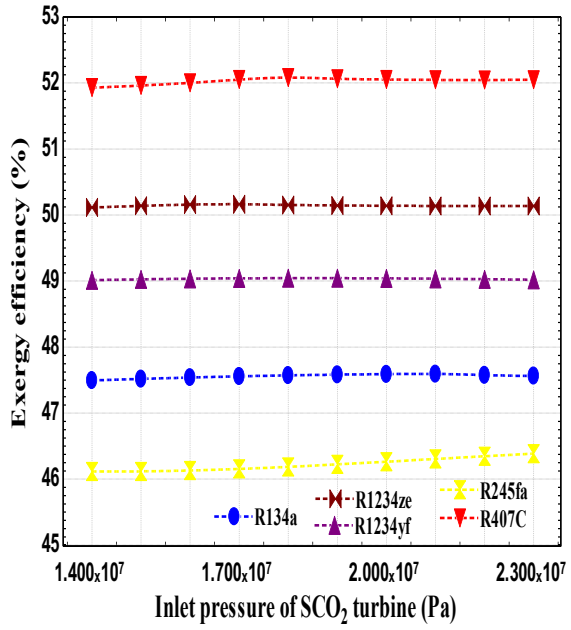

Figure 5.9. Exergy efficiency of complete plant (SPTC-SCO_2-ORC) versus inlet pressure of SCO_2 Turbine

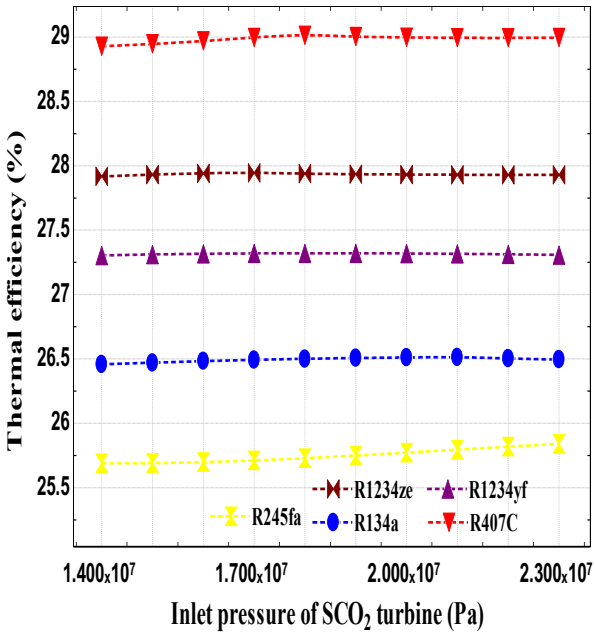

Figure 5.10. Thermal efficiency of complete plant (SPTC-SCO_2-ORC) versus inlet pressure of SCO_2 Turbine

Figure 5.12 also exhibits that the R407c fluid has a lowest exergy destruction rate in the SPTC-SCO_2-ORC system, which is decreases from 9884 kW at 14 MPa to 9859 kW at 23 MPa. Alternatively, R245fa fluid has a highest exergy destruction rate, which is declining from 11079 kW at 14 MPa to 11023 kW at 23 MPa. While the exergy destruction rate of R1234ze, R1234yf, and R134a fluid lies between these two mentioned above cycles along with a minimum value of 10252 kW, 10482 kW, and 10781 kW at 23 MPa, respectively as shown in Figure 5.12.

Ultimately, it has been determined from exergetic analysis that the major amount of exergy destruction rate is because of SPTC lone, which is nearby 6092 kW during the utilization of R245fa fluid in bottoming ORC, and this amount is exactly equal to 55.3% of the rate of total exergy destruction in the complete cycle [199].

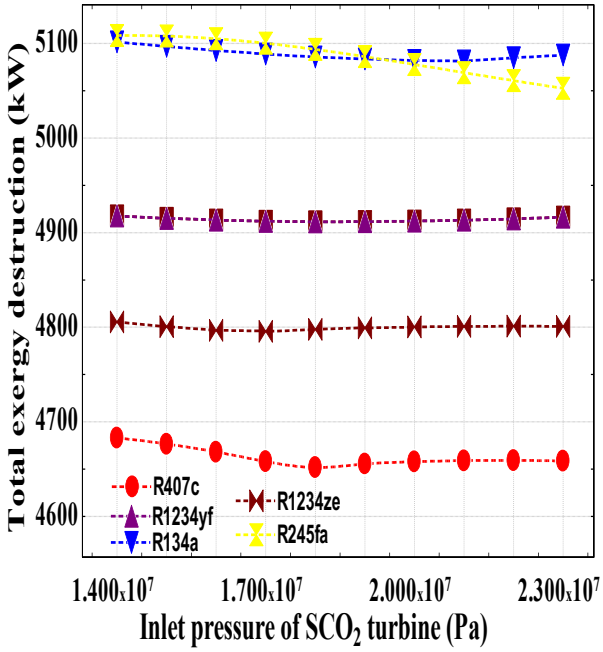

Figure 5.11. Total exergy destruction in combined cycle without solar collector (SCO_2-ORC) versus inlet pressure of SCO_2 Turbine [199]

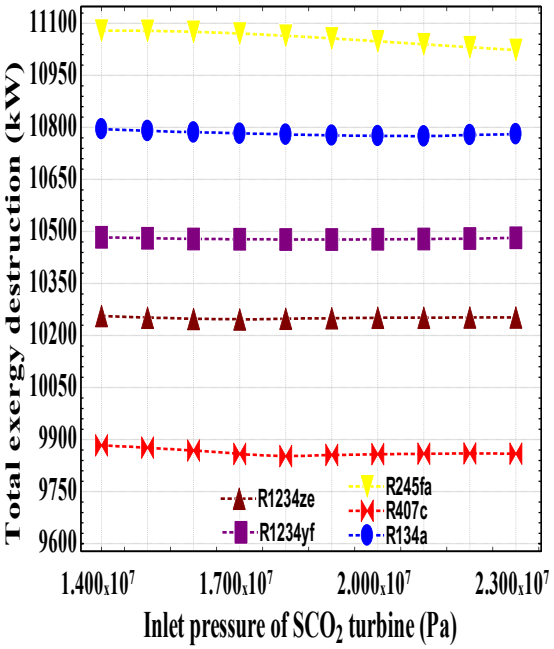

Figure 5.12. Total exergy destruction in complete plant (SPTC-SCO_2-ORC) versus inlet pressure of SCO_2 Turbine [199]

5.1.3. Effect of variation in inlet temperature of SCO_2 turbine on the system performance

The inlet temperature of SCO_2 turbine or cycle's high temperature is one of the parameter that helps us to analyse the combined cycle's energy and exergy performance. From

the literature, it has been found that the inlet or high temperature can enhance up to a specific limit, i.e. 750℃ so as to enhancement of oxide formation rate on the metal alloys could be avoided [226,227]. From the literature, it has been found that as compared to SRC, the SCO_2 cycle's compactness and simplicity makes it more economic even between the temperature range of 400℃-650℃ [61,83]. Therefore, a specified range of turbine inlet temperature (i.e. lies between the range of SPTC and SPT system) has been selected so as to check the performance of system.

In this direction, Figure 5.13 demonstrates the effect of inlet or high temperature on the exergy efficiency of a SCO_2-ORC system that has been examined under the simulated conditions such as inlet turbine pressure of 25 MPa and mass flow rate of 10 kg/s. It has been analysed that with the rise in inlet turbine temperature, the exergy efficiency also rises, and the R407c fluid based SCO_2-ORC system has an utmost exergy efficiency, which is increases from 54.96% at 600 K to 81.79% at 850 K followed by the R1234ze and R1234yf fluid along with a maximum exergy efficiency value of 80.81% and 80.43% at 850 K, respectively. However, both the R134a and R245fa fluid have a minimum and comparable value of exergy efficiency, i.e. around 49.99% at 600 K increases to 79.68% at 850 K and 50.09% at 600 K increases to 80.13% at 850 K, correspondingly as clearly indicated in Figure 5.13.

Furthermore, Figure 5.14 demonstrates the effect of inlet or high temperature of SCO_2 turbine on the thermal efficiency of SCO_2-ORC system, which has been analysed on the basis of same simulated conditions as described above. It has been assessed that thermal efficiency also upsurges as the inlet turbine temperature upsurges, and the R407c fluid has an utmost thermal efficiency, which is augments from 30.62% at 600 K to 45.57% at 850 K followed by the R1234ze and R1234yf fluid along with maximum thermal efficiency of 45.02% and 44.8% at 850 K. While the thermal efficiency of both R134a and R245fa fluid have a lowest and comparable values, i.e. 27.85% at 600 K enhances to 44.39% at 850 K and 27.9% at 600 K enhances to 44.64% at 850 K, respectively as shown in Figure 5.14.

The explanation for the increasing exergy and thermal efficiency is that with the rise in inlet or high temperature of SCO_2 turbine, there is a corresponding rise in enthalpy inflow to the turbine, as a result, turbine's work output rises. However, compressor work at the same time has a reasonable value. Hence, net work output upsurges in the SCO_2-ORC system. Accordingly, the exergy and thermal efficiency increases with the rise in turbine inlet temperature. One more cause for enhancing exergy and thermal efficiency is that with the rise in inlet turbine temperature, difference of temperature amongst the heat addition

and heat rejection also rises, consequently, an increase in cycle efficiency has been noticed [89,199].

On the contrary side, the exergy and thermal performance of SPTC-SCO_2-ORC system also has been examined under the same baseline conditions as mentioned above. Figure 5.15 shows the influence of inlet or high temperature on the exergy efficiency of SPTC-SCO_2-ORC system, and it has been detected that the R407c fluid has a highest exergy efficiency value, i.e. upsurges from 15.52% at 600 K to 64.96% at 850 K which is followed by the R1234ze, R1234yf, and R134a fluid along with a maximum exergy efficiency value of 62.88%, 62.37%, and 61.2%, respectively. Instead, R245fa fluid has a lowest exergy efficiency value, which is enhances from 6% at 600 K to 60.68% at 850 K and it also showed a marginal difference from the exergy performance of R134a fluid as displayed in Figure 5.15.

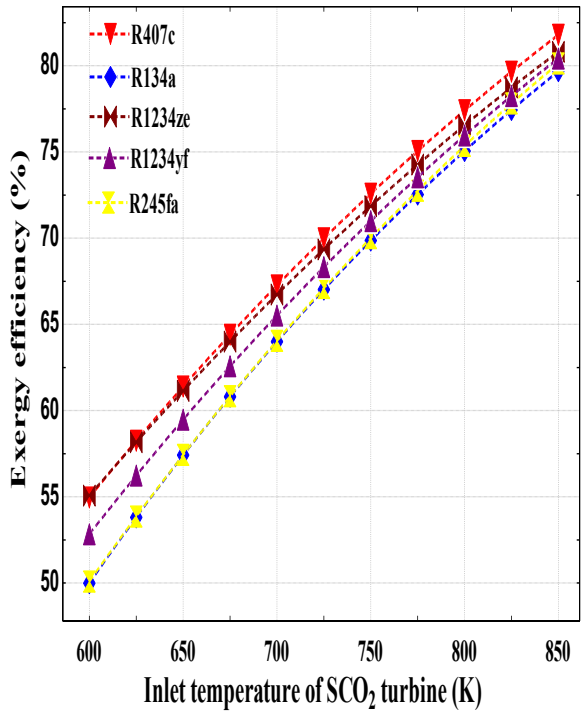

Figure 5.13. Exergy efficiency of combined cycle without solar collector (SCO_2-ORC) versus inlet temperature of SCO_2 turbine

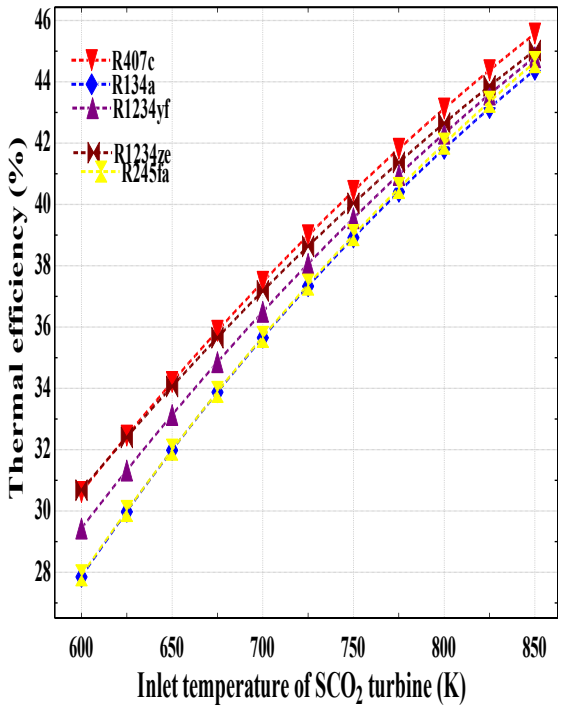

Figure 5.14. Thermal efficiency of combined cycle without solar collector (SCO_2-ORC) versus inlet temperature of SCO_2 turbine

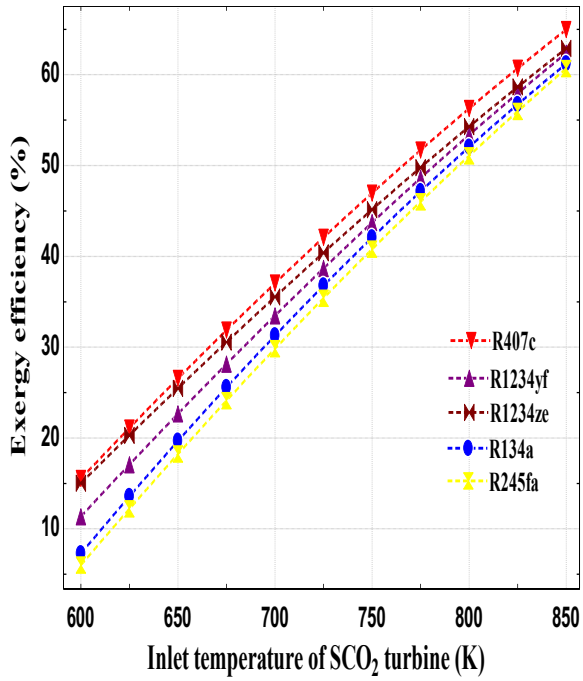

Figure 5.15. Exergy efficiency of complete plant (SPTC-SCO_2-ORC) versus inlet temperature of SCO_2 turbine

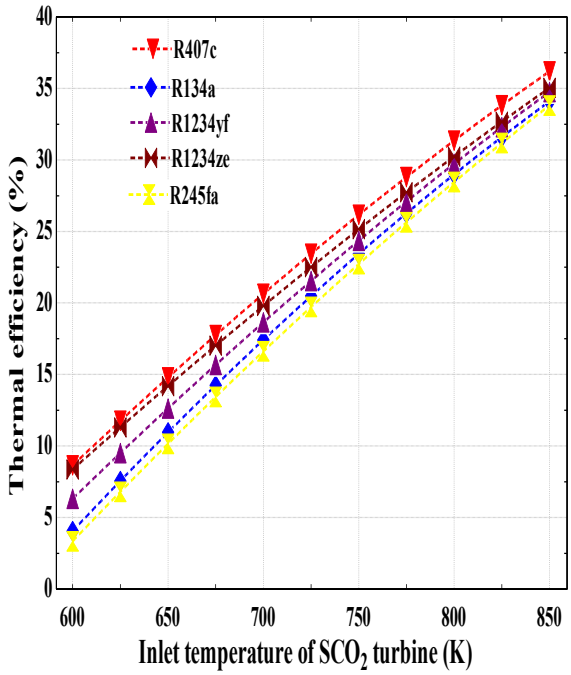

Figure 5.16. Thermal efficiency of complete plant (SPTC-SCO_2-ORC) versus inlet temperature of SCO_2 turbine

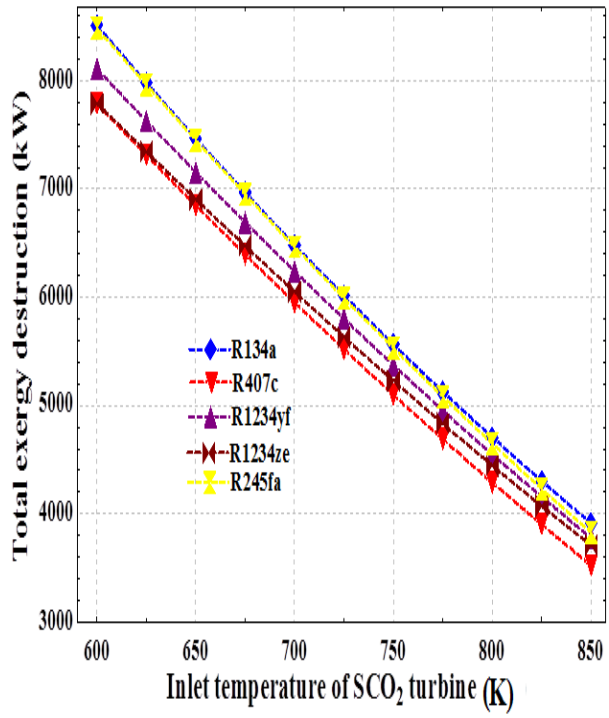

Figure 5.17. Total exergy destruction in combined cycle without solar collector (SCO_2-ORC) versus inlet temperature of SCO_2 turbine

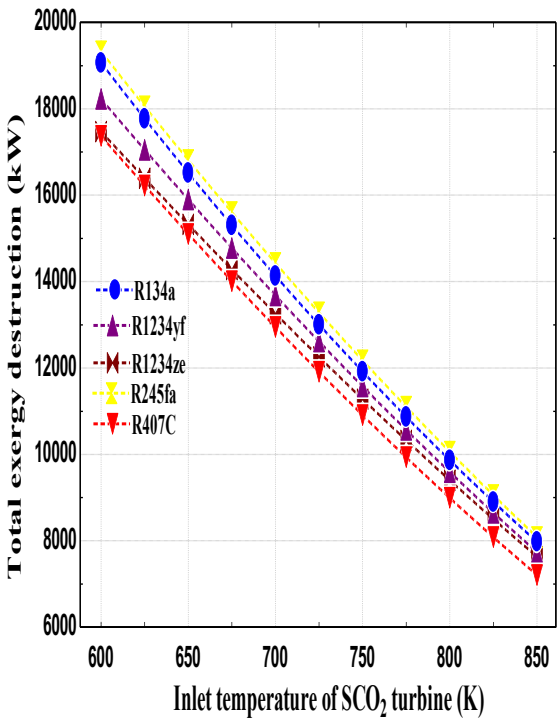

Figure 5.18. Total exergy destruction in complete plant (SPTC-SCO_2-ORC) versus inlet temperature of SCO_2 turbine

In addition, Figure 5.16 indicates the influence of inlet or high temperature on the thermal efficiency of SPTC-SCO_2-ORC system, and it has been found that the R407c fluid possess the uppermost thermal efficiency value, i.e. increases from 8.646% at 600 K to 36.19% at 850 K. Alternatively, R245fa fluid has a smallest value of thermal efficiency, i.e. enhances from 3.342% at 600 K to 33.8% at 850 K. However, the thermal efficiency curves of R1234ze, R1234yf, and R134a fluid lies between the above-mentioned fluids with a maximum thermal efficiency value of 35.03%, 34.75%, and 34.09%, correspondingly as demonstrated in Figure 5.16.

Apart from this, Figure 5.17 shows the influence of inlet or high temperature of SCO_2 turbine on the overall exergy destruction rate of SCO_2-ORC has been studied under the same baseline condition as mentioned above, and it has been found that both R134a and R245fa fluid have a highest rate of total exergy destruction, i.e. 8512 kW at 600 K decreases to 3913 kW at 850 K and 8482 kW at 600 K decreases to 3827 kW at 850 K, respectively, and these findings also shows that both the fluids have a marginal difference in their rate of exergy destruction values.

Alternatively, R407c fluid has a least exergy destruction rate due to its higher exergy performance among the other selected refrigerants, i.e. 7785 kW at 600 K decreases to 3524 kW at 850 K. However, the rate of exergy destruction for R1234ze and R1234yf fluid lies in between the curves of R134a and R407c fluid along with a maximum exergy destruction rate of 7789 kW and 8107 kW at 600 K, correspondingly as described in Figure 5.17.

Lastly, the influence of inlet or high temperature on rate of total exergy destruction for SPTC-SCO_2-ORC has been examined in Figure 5.18. It has been observed that R245fa fluid has a maximum rate of exergy destruction, which is decreases from 19327 kW at 600 K to 8084 kW at 850 K followed by the R134a, R1234yf, and R1234ze fluid with a maximum exergy destruction rate of 19067 kW, 18229 kW, and 17474 kW, respectively. On the contrary side, R407c fluid has a lowest rate of total exergy destruction, i.e. declining from 17369 kW at 600 K to 7205 kW at 850 K as indicated in Figure 5.18.

5.1.4. Effect of variation in inlet temperature of SCO_2 compressor on the system performance

The influence of inlet temperature or minimum cycle temperature of SCO_2 compressor over exergy and thermal performance of SCO_2-ORC system has been examined under the fixed simulated conditions such as solar DNI of 850 W/m^2, maximum temperature of 653 K, mass

flow rate of 10 kg/s, & turbine inlet pressure of 25 MPa. A specified range of inlet temperature of SCO_2 compressor has been decided on the basis of fact that the minimum temperature of cycle should be present nearer to the supercritical conditions. As can be spotted from Figure 5.19 that the exergy efficiency of SCO_2-ORC system reduces with the rise in inlet temperature of SCO_2 compressor, and also found that both R407c and R1234ze fluids have a highest and comparable exergy efficiency among the other nominated fluids, i.e. 69.75% at 300 K decreases to 68.67% at 327 K and 69.33% at 300 K decreases to 68.94% at 327 K, respectively, which is followed by the R1234yf, R245fa, and R134a fluid has a smallest value of exergy efficiency, i.e. 67.16% at 300 K decreases to 66.71% at 327 K as indicated in Figure 5.19.

Instead, Figure 5.20 demonstrates the influence of inlet temperature of SCO_2 compressor on the thermal efficiency of SCO_2-ORC system, and it has been reveal that both R407c and R1234ze have the highest and comparable value of thermal efficiency, i.e. 38.86% at 300 K decreases to 38.26% at 327 K and 38.62% at 300 K decreases to 38.4% at 327 K, correspondingly followed by the R1234yf, R245fa, and R134a fluid has a lowest thermal efficiency, i.e. 37.42% at 300 K decreases to 37.16% at 327 K as shown in Figure 5.20.

The explanation for the diminishing exergy and thermal efficiency is that the specific heat capacity of CO_2 declines with the rise in inlet temperature of SCO_2 compressor (i.e. far from the critical point). Thus, a decrease has been noticed in the specific enthalpy inflow to the main compressor. Consequently, the SCO_2 compressor's work rises remarkably but in the meantime, SCO_2 turbine's work do not disturbed so much. In this way, the net work output reduces, and hereafter the exergy and thermal efficiency also reduces instantaneously. In a different way, with the upsurge in inlet temperature of the SCO_2 compressor, the difference amongst the cycle's maximum temperature & minimum temperature reduces correspondingly, consequently, the cycle efficiency also reduces [89].

Furthermore, the influence of inlet temperature of SCO_2 compressor on the exergy and thermal performance of SPTC-SCO_2-ORC system has also been discussed in this section under the same simulated conditions as mentioned above. Figure 5.21 shows the influence of inlet temperature of SCO_2 compressor on the exergy efficiency of SPTC-SCO_2-ORC system, and determines that the R407c fluid has an utmost value of exergy efficiency, i.e. 47.04% at 300 K decreases to 46.06% at 327 K. Instead, R245fa fluid shows the minimum value of exergy efficiency, i.e. 41.58% at 300 K decreases to 41.52% at 327 K. However, the exergy efficiency of R1234ze, R1234yf, and R134a fluid lies in between these two above mentioned fluids along with a maximum value of 45.46%, 44.09%, and 42.47% at 300 K, respectively as shown in Figure 5.21.

Apart from this, Figure 5.22 demonstrates the influence of inlet temperature of SCO_2 compressor on the thermal efficiency of SPTC-SCO_2-ORC system, and the outcomes of study reveal that the R407c fluid has a maximum value of thermal efficiency, i.e. 26.21% at 300 K decreases to 25.66% at 327 K. Conversely, R245fa fluid has a minimum thermal efficiency value, i.e. 23.16% at 300 K decreases to 23.13% at 327 K. While the thermal efficiency of R1234ze, R1234yf, and R134a fluid lies in between these two above mentioned fluids along with a maximum value of 25.33%, 24.56%, and 23.66% at 300 K, respectively as designated in Figure 5.22.

Likewise, influence of inlet temperature of SCO_2 compressor on rate of total exergy destruction of SCO_2-ORC has been described in Figure 5.23, and it has been seen that the R134a fluid has an utmost rate of total exergy destruction, i.e. 6134 kW at 300 K increases to 6218 kW at 327 K which is followed by the R245fa and R1234yf fluid along with a maximum rate of total exergy destruction, i.e. 6052 kW and 6004 kW at 327 K, respectively. Contrariwise, the R407c and R1234ze fluid possess least and comparable amount of total exergy destruction rate, i.e. 5687 kW at 300 K enhances to 5891 kW at 327 K and 5762 kW at 300 K enhances to 5836 kW at 327 K, respectively.

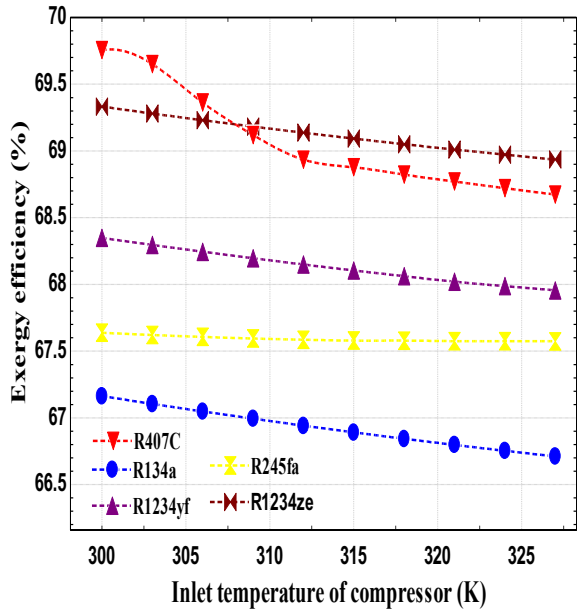

Figure 5.19. Exergy efficiency of combined cycle without solar collector (SCO_2-ORC) versus inlet temperature of compressor

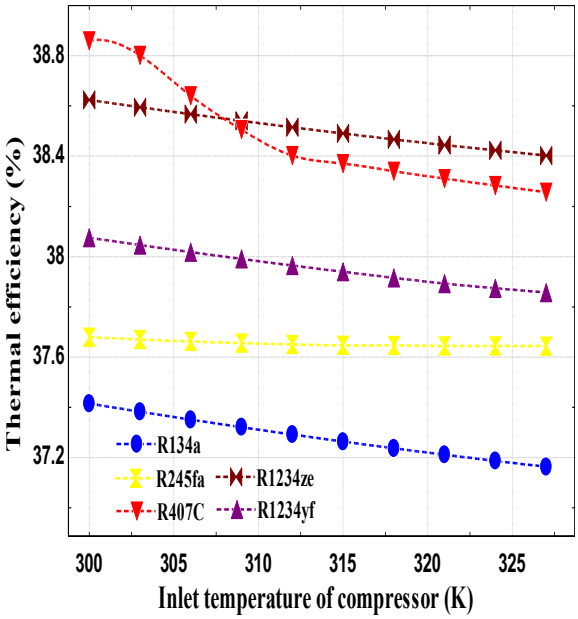

Figure 5.20. Thermal efficiency of combined cycle without solar collector (SCO_2-ORC) versus inlet temperature of compressor

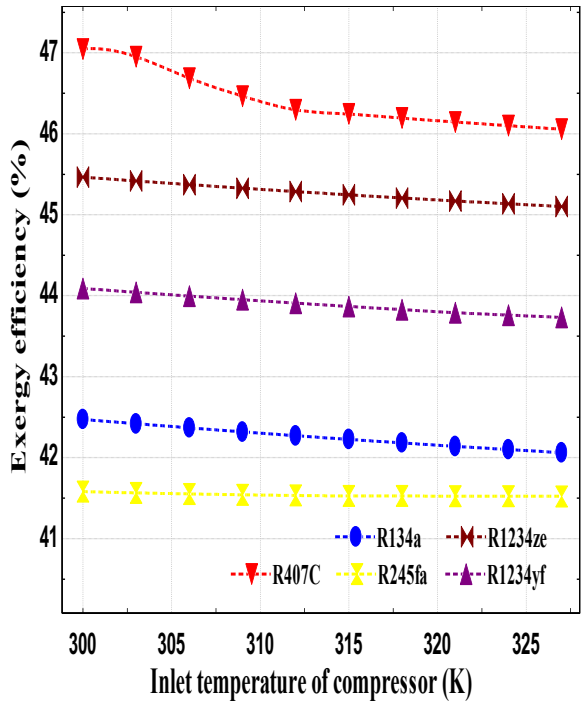

Figure 5.21. Exergy efficiency of complete plant (SPTC-SCO_2-ORC) versus inlet temperature of compressor

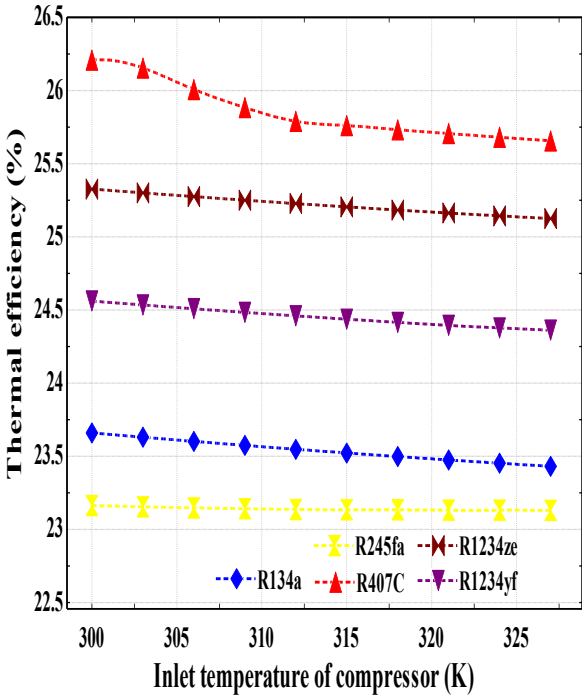

Figure 5.22. Thermal efficiency of complete plant (SPTC-SCO_2-ORC) versus inlet temperature of compressor

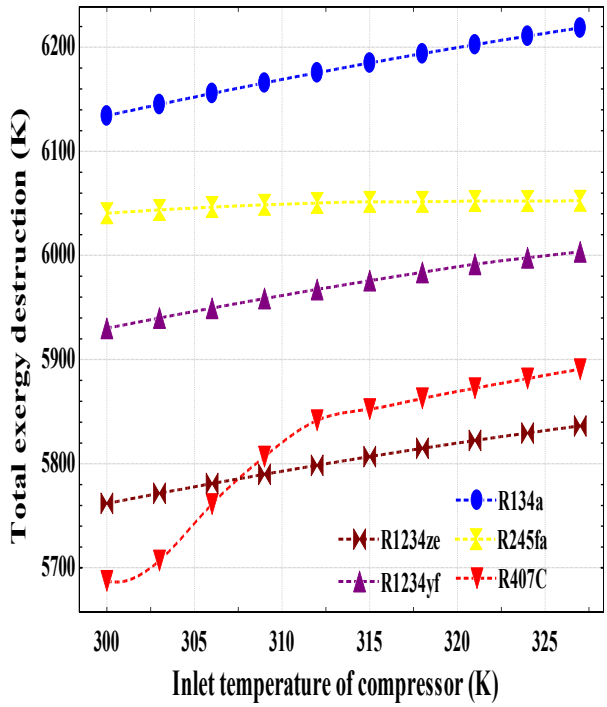

Figure 5.23. Total exergy destruction in combined cycle without solar collector (SCO_2-ORC) versus inlet temperature of compressor

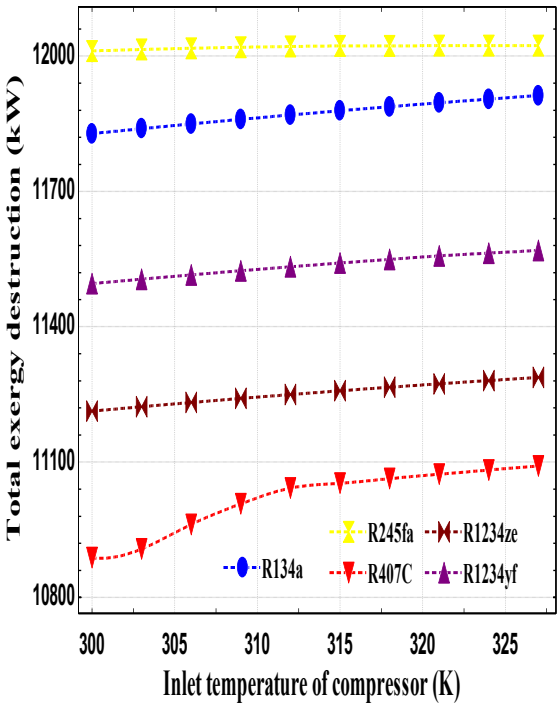

Figure 5.24. Total exergy destruction in complete plant (SPTC-SCO_2-ORC) versus inlet temperature of compressor

At last, Figure 5.24 explains the influence of inlet temperature of SCO_2 compressor on rate of overall exergy destruction of SPTC-SCO_2-ORC, and found that the R245fa fluid has a maximum rate of total exergy destruction, i.e. 12011 kW at 300 K increases to 12023 kW at 327 K. Alternatively, R407c fluid has a lowest rate of total exergy destruction, i.e. 10888 kW at 300 K increases to 11091 kW at 327 K. However, the rate of total exergy destruction of R1234ze, R1234yf, and R134a fluid lies in between these two above mentioned fluids with a maximum value of 11287 kW, 11569 kW, and 11912 kW, respectively as shown in Figure 5.24.

5.1.5. Outcomes of detailed exergy analysis of the selected combined cycle's components

In this portion, an energy and exergy based performance analysis has been conducted so as to estimate the performance of various components of a combined cycle. The purpose and motivation behind this performance study is that method of energy and exergy is helpful in evaluating both the heat transfer quality in a specific process [190] and system's sustainability level [191].

Numerical computation method also known as EES software has been employed in order to solve the equations of exergetic parameters. Also, the values of thermodynamic parameters (i.e. temperature and pressure) at various states for SPTC integrated combined cycle have been registered in Table 5.1. In addition, key exergy parameters have been examined in this study under the selected baseline conditions for each component, and these exergetic parameters are fuel depletion ratio (Y_{DEP}), improvement potential (IMP), exergy destruction rate, and irreversibility ratio (Y*).

It has been detected that major part of total exergy destruction rate was observed to be in the SPTC system, evaporator unit, and turbine of SCO_2 cycle as shown in Table 5.2. Noted that highest rate of exergy destruction may be because of huge difference amongst the temperature of incoming fluid stream and exiting fluid stream.

Furthermore, the analysis results determine that the combined cycle based on R407c organic fluid has a lowest rate of exergy destruction for the net electrical power of 3740 kW as shown in Figure 5.25. Furthermore, the values of exergetic parameters have been listed in Table 5.2, 5.3, 5.4, & 5.5, and these readings have been calculated on the basis of fixed baseline settings like inlet pressure of SCO_2 turbine, i.e. 25 MPa, solar DNI of 850 W/m^2, inlet temperature of SCO_2 turbine, i.e. 653 K, and SCO_2 mass flow rate of 10 kg/s, & all other important parameters' values are already mentioned in Table 3.1 & 3.2.

Also, R245fa organic fluid based combined cycle has an utmost exergy destruction rate which means that 6092 kW in the SPTC field followed by turbine of SCO_2 cycle (i.e. 2108 kW), & evaporator unit (i.e. 1895 kW) as listed in Table 5.2, which additionally rely on the different values of mass flow rate associated with various working fluids running in the SPTC field, SCO_2 cycle, & ORC system.

Table 5.1. Temperature and pressure at the selected states for the SPTC integrated SCO_2-ORC system [228,229]

Selected states	Type of working Fluid	P (bar)	T (K)
Inlet of SPTC (1)	Syltherm 800	100	544.6
Outlet of SPTC (3)	Syltherm 800	100	673
Inlet of SCO_2 turbine (5)	SCO_2	250	653
Outlet of SCO_2 turbine (6)	SCO_2	155.8	562.3
Outlet of recuperator (7)	SCO_2	155.8	388.3
Inlet of compressor (9)	SCO_2	155.8	327.5
Outlet of compressor (10)	SCO_2	250	362.8
Inlet of evaporator (4)	SCO_2	250	524.6
Inlet of ORC turbine (11)	R134a	30	368.9
Outlet of ORC turbine (13)	R134a	6.386	310.6
Outlet of condenser (14)	R134a	6.386	298.5
Inlet of HX (12)	R134a	30	318.8

Source: Singh and Mishra (2018) [199].

It has been found that SPTC has a maximum rate of exergy destruction as compared to other components present in the entire plant. Consequently, a careful design process should be employed to enhance the exergetic performance of system components.

Furthermore, IMP for the SPTC in the combined cycle based on R407c organic fluid was about 5282 kW followed by turbine of SCO_2 cycle (i.e. 1984 kW), and evaporator unit (i.e. 1743 kW), however, the values of IMP for other components of different selected combined cycles have been listed in Table 5.3.

Table 5.2. Rate of exergy destruction in different components of the combined cycle for all the selected working fluids [229]

Parameter	Combined Cycle's components	Selected SPTC based combined cycle				
		R134a	**R245fa**	**R1234ze**	**R407c**	**R1234yf**
Rate of total exergy destruction (kW)	SPTC area	5810	6092	5563	5310	5679
	Evaporator	1880	1895	1773	1756	1825
	Solar pump	2.576	2.368	2.478	5.515	2.404
	SCO_2 turbine	2099	2108	1987	1999	2045
	ORC turbine	565.2	505.1	529.8	516.2	517.3
	ORC pump	4.705	3.916	2.08	5.403	7.494
	Recuperator	46.56	41.4	44.6	60.37	45.21
	HX	89.4	87.19	75.34	23.47	76.23
	Condenser	0.0355	0.0382	0.0374	0.0436	0.0377
	Compressor	407.6	404.3	388.1	308	404

Source: Singh and Mishra (2018) [199].

Apart from this, IMP represents that in order to avoid the major exergy loss, the design improvement of the complete SPTC plant is necessary which can further be possible by maximizing the optical efficiency SPTC and by reducing the overall heat losses of SPTC plant.

Instead of SPTC and SCO_2 turbine, other components of the combined cycle also necessitate an excellent design so as to improve the functioning of system, for example evaporator, recuperator, and HX unit have a noteworthy quantity of exergy destruction. Hence, these components necessitate a greater area for the heat transfer for the advancement of the design.

Besides, in case of R245fa organic fluid based combined cycle, the maximum rate of exergy destruction for SPTC field was 29.6% of the solar inlet exergy (i.e. 20562 kJ), and nearly 19.4% of the solar inlet exergy has been destructed in the SCO_2 cycle's turbine & evaporator unit.

Table 5.3. Improvement potential in different components of the combined cycle for all the selected working fluids [229]

Parameter	Combined Cycle's components	Selected SPTC based combined cycle				
		R134a	R245fa	R1234ze	R407c	R1234yf
Improvement potential or IMP (kW)	SPTC area	5783	6064	5535	5282	5651
	Evaporator	1866	1881	1760	1743	1812
	Solar pump	2.564	2.357	2.465	5.487	2.392
	SCO_2 turbine	2083	2093	1973	1984	2030
	ORC turbine	561.1	501.4	525.9	511.6	513.5
	ORC pump	4.671	3.887	2.065	5.362	7.439
	Recuperator	46.23	41.1	44.27	59.92	44.88
	HX	88.75	86.56	74.78	23.29	75.67
	Condenser	0.0352	0.0379	0.0371	0.0433	0.0375
	Compressor	404.6	401.4	385.2	305.7	401

Source: Singh and Mishra (2018) [199].

From the Table 5.4, it has been observed that among all the other combined cycles, the R407c organic fluid based combined cycle has a comparatively lowest amount of fuel depletion ratio which was about 0.2583, 0.1063, & 0.0934 for the SPTC field, SCO_2 cycle's turbine, and evaporator unit, correspondingly.

Besides, the SPTC field and SCO_2 cycle's turbine has a maximum value of irreversibility ratio among all other components of the complete cycle (SPTC-SCO_2-ORC system). Likewise, evaporator unit has an accountable amount of irreversibility ratio as registered in Table 5.5 for all available fluids.

Table 5.4. Fuel depletion ratio in different components of the combined cycle for all the selected working fluids [229]

Parameter	Combined Cycle's components	Selected SPTC based combined cycle				
		R134a	R245fa	R1234ze	R407c	R1234yf
Fuel depletion ratio (Y_{DEP})	SPTC area	0.2826	0.2963	0.2705	0.2583	0.2762
	Evaporator	0.1006	0.1015	0.09437	0.0934	0.09743
	Solar pump	$1.253*10^{-4}$	$1.152*10^{-4}$	$1.205*10^{-4}$	$2.683*10^{-4}$	$1.169*10^{-4}$
	SCO_2 turbine	0.1124	0.113	0.1058	0.1063	0.1092
	ORC turbine	$3.026*10^{-2}$	$2.706*10^{-2}$	$2.82*10^{-2}$	$2.764*10^{-2}$	$2.761*10^{-2}$
	ORC pump	$2.519*10^{-4}$	$2.098*10^{-4}$	$1.107*10^{-4}$	$2.873*10^{-3}$	$4.0*10^{-4}$

	Recuperator	$2.493*10^{-3}$	$2.218*10^{-3}$	$2.374*10^{-3}$	$3.211*10^{-3}$	$2.413*10^{-3}$
	HX	$4.786*10^{-3}$	$4.671*10^{-3}$	$4.01*10^{-3}$	$1.248*10^{-3}$	$4.069*10^{-3}$
	Condenser	$1.901*10^{-6}$	$2.047*10^{-6}$	$1.994*10^{-6}$	$2.32*10^{-6}$	$2.017*10^{-6}$
	Compressor	$2.182*10^{-2}$	$2.166*10^{-2}$	$2.066*10^{-2}$	$1.638*10^{-2}$	$2.156*10^{-2}$

Source: Singh and Mishra (2018) [199].

Apart from this, fluctuation in the outcomes of thermal efficiency and expansion ratio for the different organic fluids has been described in Figure 5.26. From the study, it has been discovered that with the augment in evaporating temperature of ORC, expansion ratio also rises. Thus, the highest value of expansion ratio (i.e. 1.143) has been detected in respect of R134a organic fluid. While the R407c organic fluid has an utmost thermal efficiency value of 41.92%. Additionally, the power generation capacity per unit collection area is 1.355 kW/m^2, 1.305 kW/m^2, 1.281 kW/m^2, 1.243 kW/m^2, and 1.242 kW/m^2 for R407c, R1234ze, R1234yf, R134a, and R245fa fluid, respectively and it is also indirectly an economic indicator.

Finally, Figure 5.25 demonstrates the power produced in respect of different combined cycles at the fixed standard conditions as stated above. Also, the study discloses that R407c organic fluid based combined cycle has a greatest power generation with an amount of 3740 kW as compared to all other available organic fluids.

Table 5.5. Irreversibility ratio in different components of the combined cycle for all the selected working fluids [229]

Parameter	**Combined Cycle's components**	**Selected SPTC based combined cycle**				
		R134a	**R245fa**	**R1234ze**	**R407c**	**R1234yf**
Irreversibility ratio (Y*)	SPTC area	0.5387	0.553	0.5426	0.5388	0.5416
	Evaporator	0.1743	0.172	0.1729	0.1782	0.1741
	Solar pump	$2.388*10^{-4}$	$2.15*10^{-4}$	$2.417*10^{-4}$	$5.596*10^{-4}$	$2.293*10^{-4}$
	SCO_2 turbine	0.4121	0.4179	0.414	0.4295	0.4156
	ORC turbine	0.111	0.1001	0.1104	0.1053	0.1051
	ORC pump	$9.239*10^{-4}$	$7.761*10^{-4}$	$4.334*10^{-4}$	$1.161*10^{-3}$	$1.523*10^{-3}$
	Recuperator	$9.144*10^{-3}$	$8.205*10^{-3}$	$9.292*10^{-3}$	$1.297*10^{-2}$	$9.187*10^{-3}$
	HX	$1.756*10^{-2}$	$1.728*10^{-2}$	$1.57*10^{-2}$	$5.042*10^{-3}$	$1.549*10^{-2}$
	Condenser	$6.973*10^{-6}$	$7.573*10^{-6}$	$7.804*10^{-6}$	$9.373*10^{-6}$	$7.677*10^{-6}$
	Compressor	$8.004*10^{-2}$	$8.013*10^{-2}$	$8.084*10^{-2}$	$6.617*10^{-2}$	$8.209*10^{-2}$

Source: Singh and Mishra (2018) [199].

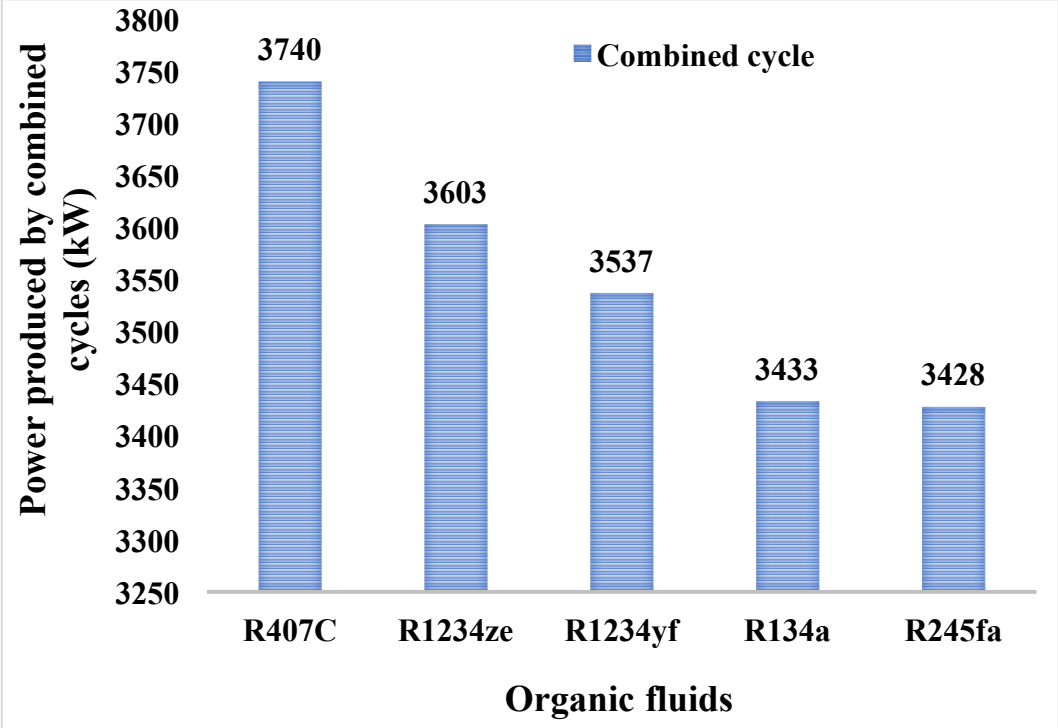

Figure 5.25. Shows the power produced in case of different combined cycles

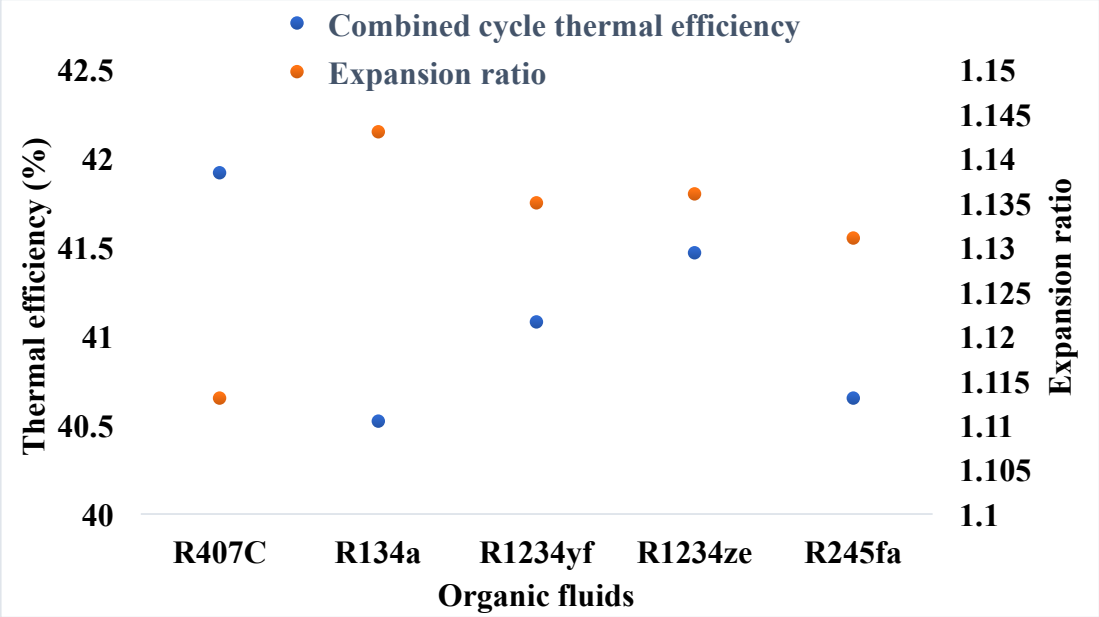

Figure 5.26. Variations in expansion ratio and thermal efficiency of combined cycles

5.1.6. Validation of collector and combined cycle

Now, the validation of modified LS-3 type of SPTC has been performed in this portion, and the outcomes have been compared with the experimental model of Dudley et al. [230] and Forristall's NREL model [231].

For both the cases such as vacuum and air, the collector efficiency has been calculated with the help of performance equations of given by Dudely et al. [230] and then, performance curves have been drawn as shown in the Figure 5.27.

Noted that the collector efficiency results have been calculated at the selected parametrical values as registered in Table 3.1 and conclusively, it has been reveal that the SPTC efficiency curves are strictly matching with the curves of earlier models as described in Figure 5.27.

So as to authenticate the considered system, i.e. SCO_2-ORC system, various researches (Song et al. (2018) [167]; Besarati et al. (2014) [172]; Clemente et al. (2013) [232]) have been chosen from the previous work. The modelling results have been computed in the current study that were compared with the outcomes of earlier researches as displayed in Table 5.6, 5.7 & 5.8, and the comparison implies that the current modelling outcomes of existing model properly agreed with that of literature work at the similar baseline conditions, which was then further utilized to investigate the combined cycle's performance.

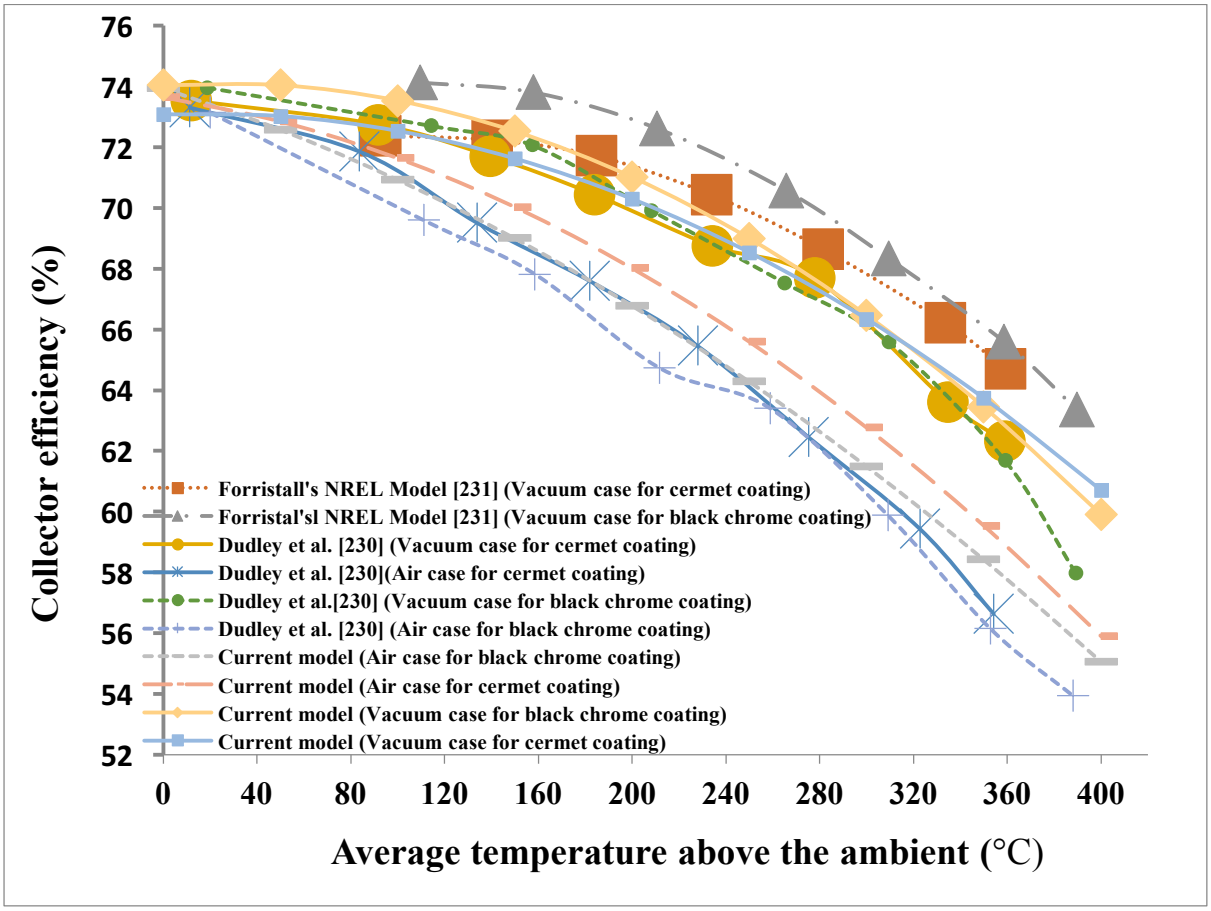

Figure 5.27. Variations in collector efficiency with the average temperature above ambient

Table 5.6. Validation results of SCO_2 topping cycle

SCO_2 topping cycle				
Working fluid of topping cycle	**Literature work**	**Thermal efficiency in literature work**	**Thermal efficiency expected**	**Error approximation**
SCO_2	Besarati et al. [172]	0.4507	0.4333	-3.8%
SCO_2	Song et al. [167]	0.491	0.482	-1.8%

Source: Singh and Mishra (2018) [199].

Table 5.7. Validation results of ORC bottoming cycle

ORC bottoming cycle				
Organic working fluid of bottoming cycle	**Literature work**	**Thermal efficiency in literature work**	**Thermal efficiency expected**	**Error approximation**
R245fa	Clemente et al. [232]	0.11	0.119	8.1%
R245fa	Song et al. [167]	0.114		4.3%

Source: Singh and Mishra (2018) [199].

Table 5.8. Validation results of combined cycle (SCO_2-ORC)

Combined cycle (SCO_2-ORC)				
Organic working fluid of bottoming cycle	**Literature work**	**Thermal efficiency in literature work**	**Thermal efficiency expected**	**Error approximation**
R245fa	Besarati et al. [172]	0.5140	0.5203	1.2%

Source: Singh and Mishra (2018) [199].

5.2. SPTC integrated with combined R-SCO_2 cycle and ORC system

In this section, the energy and exergy analysis has been conducted on the SPTC integrated combined recompression cycle (i.e. R-SCO_2-ORC system) on the basis of assumed simulated conditions as illustrated in Table 3.5. The effect of solar direct normal irradiance (solar DNI or G_b), pressure & temperature at inlet of R-SCO_2 turbine, mass flow rate of SCO_2, inlet temperature of main compressor, and HTR & LTR effectiveness on the both exergy and thermal performance has been studied in a detailed way and discussed in the subsections.

Presently, SPTC arrangement is working on an average value of solar DNI, i.e. 850 W/m^2 and the influence of solar DNI on the performance of combined cycle with and without SPTC has been inspected throughout the daytime concerning the full range of solar DNI, i.e. 500 W/m^2 to 950 W/m^2.

In addition, eight organic working fluids, for instance R123, R1234ze, R1234yf, toluene, cyclohexane, isopentane, isobutene, and R290 have been nominated for the ORC in order to examine the system performance.

5.2.1. Effect of variation in solar DNI and pressure at the inlet of R-SCO_2 turbine on the system performance

In this section, Figure 5.28 & 5.29 displays the variations in exergy and thermal efficiency with the fluctuations in solar DNI, and it has been detected that both the thermal and exergy efficiency increases with the rise in solar DNI (i.e. 500 W/m^2 to 950 W/m^2) that has been analysed depends upon the fixed simulated conditions, for instance inlet R-SCO_2 turbine pressure of 25 MPa & mass flow rate of 10 kg/s. Noted that optimum utilization of SPTC rows existing in the complete SPTC field can be attained through the enhancing solar DNI that directly focus on the whole SPTC plant.

It has been observed from the Figure 5.28 that the exergy efficiency upsurges with the rise in solar DNI, and found that the R123 fluid based R-SCO_2-ORC system has an utmost exergy efficiency that will be enhancing from 73.4% at 500 W/m^2 to 86.75% at 950 W/m^2. Instead, R290 fluid has a minimum exergy efficiency that will be rising from 72.22% at 500 W/m^2 to 86.17% at 950 W/m^2. However, the exergy efficiency of all other selected fluids such as R1234ze, R1234yf, toluene, cyclohexane, isopentane, and isobutane lies in

between these two aforementioned fluids with a maximum value of 86.65%, 86.64%, 86.53%, 86.47%, 86.32%, and 86.28% at 950 W/m^2, respectively as shown in Figure 5.28 [211].

Now Figure 5.29 shows that thermal efficiency of R-SCO$_2$-ORC system enhances as solar DNI enhances, and concludes that the thermal efficiency of R123 fluid based R-SCO$_2$-ORC system upsurges from 40.89% at 500 W/m^2 to 48.33% at 950 W/m^2. While the R290 fluid has a smallest value of thermal efficiency, which is enhances from 40.23% at 500 W/m^2 to 48% at 950 W/m^2. On the contrary side, the thermal efficiency of fluids such as R1234ze, R1234yf, toluene, cyclohexane, isopentane, and isobutane lies in between these two aforementioned fluids with a maximum value of 48.27%, 48.26%, 48.2%, 48.17%, 48.09%, and 48.06% at 950 W/m^2, respectively as illustrated in Figure 5.29 [211].

Apart from this, Figure 5.30 demonstrates that the R123 fluid based SPTC integrated combined cycle (i.e. SPTC-R-SCO$_2$-ORC system) has a maximum exergy efficiency among the other available refrigerants that will be enhancing from 44.53% at 500 W/m^2 to 70.83% at 950 W/m^2. Conversely, R290 fluid based SPTC-R-SCO$_2$-ORC system has a lowest exergy efficiency that will be enhancing from 43.47% at 500 W/m^2 to 70.28% at 950 W/m^2. However, the exergy efficiency of fluids such as R1234ze, R1234yf, toluene, cyclohexane, isopentane, and isobutane lies in between these two aforementioned fluids with a maximum value of 70.74%, 70.72%, 70.62%, 70.57%, 70.42%, and 70.38% at 950 W/m^2, respectively as described in Figure 5.30 [211].

Also, the Figure 5.31 indicated the influence of solar DNI on the thermal efficiency of SPTC-R-SCO$_2$-ORC system, and it has been estimated that the R123 fluid has an uppermost thermal efficiency value among the other available selected fluids, i.e. increases from 24.81% at 500 W/m^2 to 39.46% at 950 W/m^2. Whereas the R290 fluid based SPTC-R-SCO$_2$-ORC system has a smallest thermal efficiency that will be enhancing from 24.22% at 500 W/m^2 to 39.15% at 950 W/m^2. But the thermal efficiency of fluids such as R1234ze, R1234yf, toluene, cyclohexane, isopentane, and isobutane lies in between these two aforementioned fluids with a maximum value of 39.41%, 39.4%, 39.34%, 39.31%, 39.23%, and 39.21, respectively as shown in Figure 5.31. As can be seen, the SPTC coupled with combined recompression cycle has a relatively lower exergy and thermal efficiency than that of simple configuration (i.e. without SPTC), which is because of the greatest quantity of exergy destructions linked with the SPTC field [211].

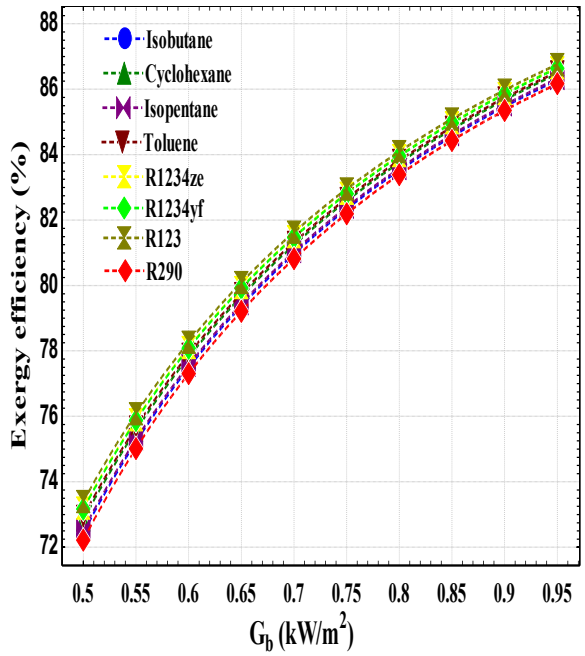

Figure 5.28. Exergy efficiency of combined recompression cycle without solar collector (R-SCO_2-ORC) versus solar DNI

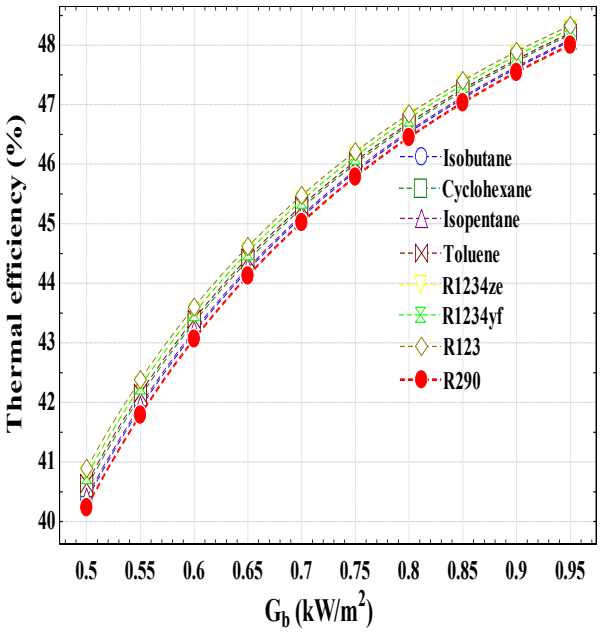

Figure 5.29. Thermal efficiency of combined recompression cycle without solar collector (R-SCO_2-ORC) versus solar DNI

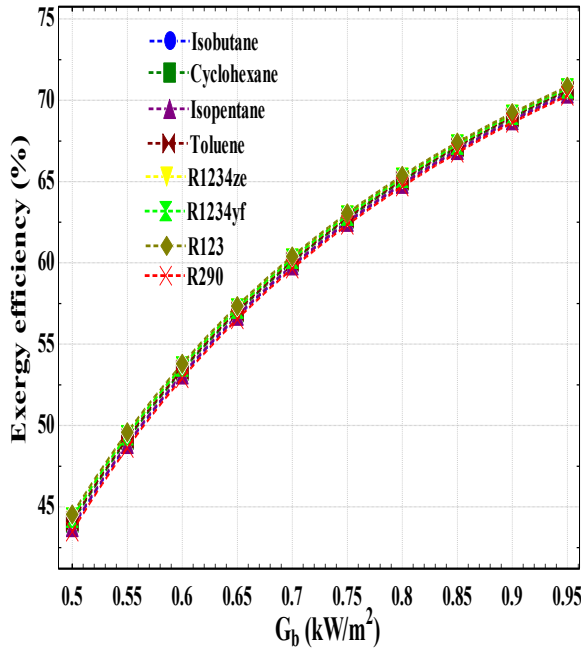

Figure 5.30. Exergy efficiency of complete plant (SPTC-R-SCO_2-ORC) versus solar DNI

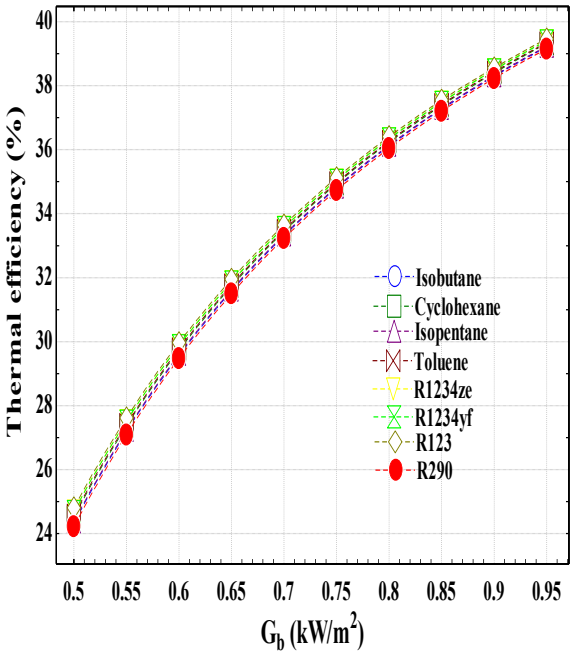

Figure 5.31. Thermal efficiency of complete plant (SPTC-R-SCO_2-ORC) versus solar DNI

Moreover, Figure 5.32 explains the influence of solar DNI on rate of overall exergy destruction of R-SCO_2-ORC, and found that R290 fluid has an utmost rate of total exergy

destruction, i.e. 5358 kW at 500 W/m^2 decreases to 2667 kW at 950 W/m^2. Conversely, R123 has a smallest rate of total exergy destruction, i.e. 5130 kW at 500 W/m^2 decreases to 2555 kW at 950 W/m^2. However, the rate of total exergy destruction of fluids such as R1234ze, R1234yf, toluene, cyclohexane, isopentane, and isobutane lies in between these two aforementioned fluids with a maximum value of 5171 kW, 5175 kW, 5217 kW, 5240 kW, 5298 kW, and 5315 kW at 500 W/m^2, respectively. Regarding the Figure 5.32, it is completely understood that rate of exergy destruction follows the opposite pattern from exergy efficiency.

Whereas, Figure 5.33 displays the effect of solar DNI on rate of overall exergy destruction of SPTC-R-SCO$_2$-ORC system (i.e. complete plant), and observed that the R290 fluid possess a maximum rate of total exergy destruction, i.e. 11623 kW at 500 W/m^2 decreases to 6111 kW at 950 W/m^2. Contrariwise, R123 fluid has a minimum rate of 11405 kW at 500 W/m^2 decreases to 5997 kW at 950 W/m^2. Also, the rate of exergy destruction of fluids such as R1234ze, R1234yf, toluene, cyclohexane, isopentane, and isobutane lies in between these two aforementioned fluids with a maximum value of 11442 kW, 11448 kW, 11489 kW, 11510 kW, 11565 kW, and 11580 kW at 500 W/m^2, respectively as demonstrates in Figure 5.33.

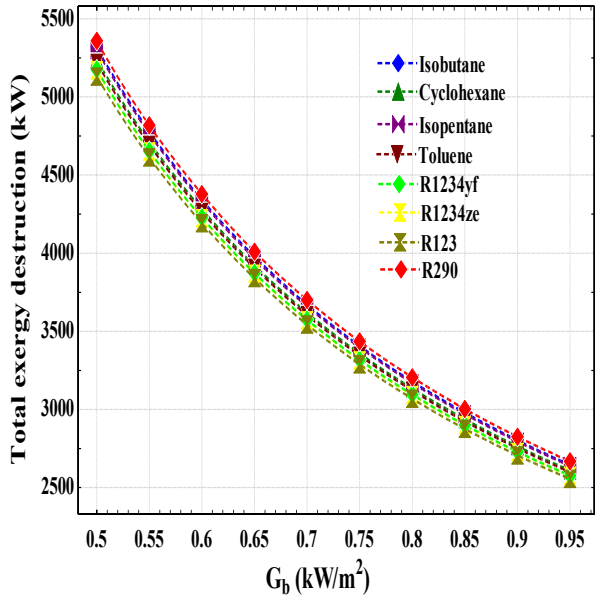

Figure 5.32. Total exergy destruction in combined recompression cycle without solar collector (R-SCO$_2$-ORC) versus solar DNI

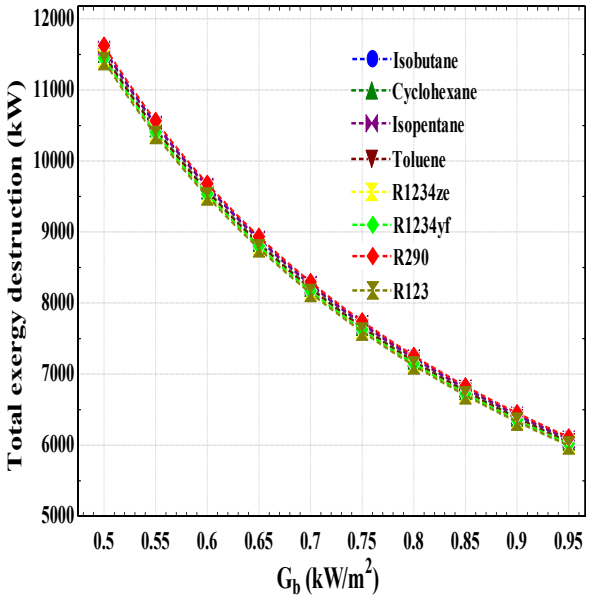

Figure 5.33. Total exergy destruction in complete plant (SPTC-R-SCO$_2$-ORC) versus solar DNI

Now the outcomes have revealed that the exergy destruction rate declines gradually with the rise in solar DNI that can be because of efficient utilization of the SPTC field. It is understandable that if a huge quantity of solar DNI falling upon the fewer number of SPTC rows that comprise with the multiple SPTCs organised in series as well as parallel arrangement in the complete SEGS plant can further successfully lessen the rate of exergy destruction [211].

Apart from this, the influence of pressure at the inlet of R-SCO_2 turbine on the combined cycle's exergy and thermal performance on the basis of baseline conditions, for example solar DNI of 850 W/m^2, R-SCO_2 turbine's inlet temperature of 652.8 K, & mass flow rate of 10 kg/s has also been analysed in this section.

Figure 5.34 demonstrates that the R123 fluid based R-SCO_2-ORC system has a highest exergy efficiency in contradiction of other combined cycles, which is around 78.8% at 14 MPa increases to 79.04% at 23 MPa. Otherwise, R290 fluid based R-SCO_2-ORC system displays the smallest efficiency, which can be undoubtedly due to the existence of great amount of exergy destructions in this cycle against the other cycles. In this way, the exergy efficiency of R290 fluid upsurges from 75.73% at 14 MPa to 76.15% at 23 MPa. Although the exergy efficiency of fluids such as R1234ze, R1234yf, toluene, cyclohexane, isopentane, and isobutane lies in between the R123 and R290 fluid as presented in Figure 5.34 [211].

Moreover, Figure 5.35 depicts that the R123 fluid based R-SCO_2-ORC system has a greatest thermal efficiency value against the other elected fluids, i.e. increases from 43.9% at 14 MPa increases to 44.03% at 23 MPa, respectively. However, the thermal efficiency for R290 fluid based R-SCO_2-ORC system enhances from 42.19% at 14 MPa to 42.42% at 23 MPa. Also, the thermal efficiency of all other fluids such as R1234ze, R1234yf, toluene, cyclohexane, isopentane, and isobutane lies in the range of R123 and R290 fluid as illustrated in Figure 5.35 [211].

Lastly, Figure 5.36 explains the influence of pressure at the inlet of R-SCO_2 turbine on rate of overall exergy destruction of R-SCO_2-ORC, and it has been detected that R290 fluid has an utmost exergy destruction rate, i.e. 4530 kW at 14 MPa decreases to 4452 kW at 23 MPa. Instead, R123 fluid has a lowest exergy destruction rate, i.e. 3957 kW at 14 MPa decreases to 3912 kW at 23 MPa. However, the exergy destruction rate of R1234ze, R1234yf, toluene, cyclohexane, isopentane, and isobutane lies in the range of R123 and R290 fluid as disclosed in Figure 5.36.

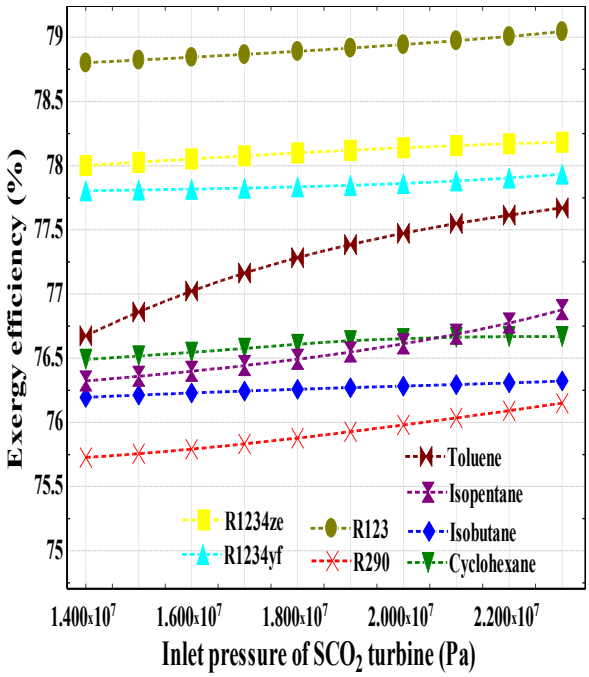

Figure 5.34. Exergy efficiency of combined recompression cycle without solar collector (R-SCO_2-ORC) versus inlet pressure of SCO_2 turbine

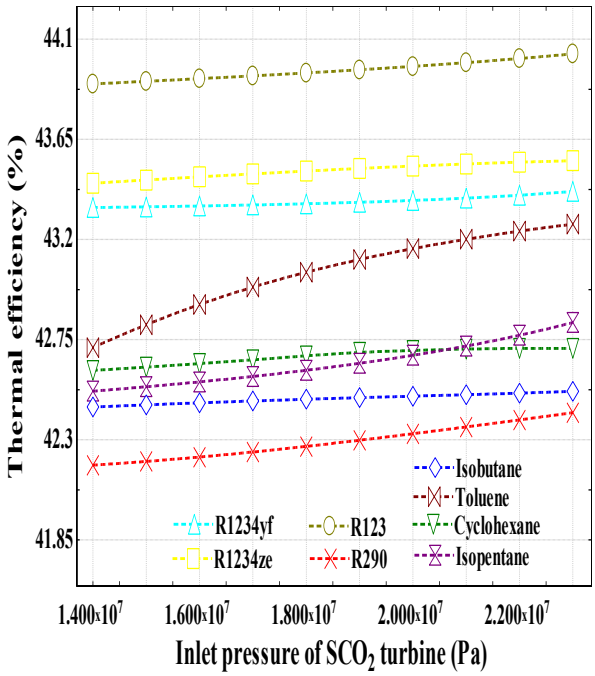

Figure 5.35. Thermal efficiency of combined recompression cycle without solar collector (R-SCO_2-ORC) versus inlet pressure of SCO_2 turbine

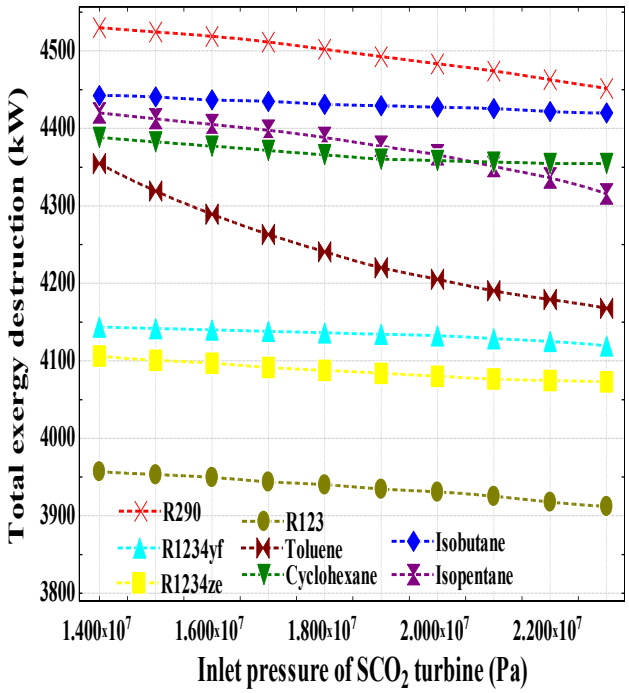

Figure. 5.36. Exergy destruction rate of combined recompression cycle without solar collector (R-SCO_2-ORC) versus inlet pressure of SCO_2 turbine

5.2.2. Effect of variation in inlet temperature at R-SCO_2 turbine and mass flow rate of SCO_2 on the system performance

Inlet R-SCO_2 turbine temperature or maximum temperature of a combined recompression cycle (i.e. R-SCO_2-ORC system) is a significant constraint used to analyse the system performance. From the literature, it was found that the inlet or high temperature may be augmented up to a definite limit of 750°C so as to oxide formation layer could be prevented over the alloys of metal [226,227].

Now the effect of inlet R-SCO_2 turbine temperature on the exergy and thermal performance of the R-SCO_2-ORC system has been examined in this section. Figure 5.37 & 5.38 concludes that with the upsurge in inlet temperature, exergy and thermal efficiency of R-SCO_2-ORC system also upsurges that has been studied on the basis of fixed baseline conditions like mass flow rate of 10 kg/s & inlet R-SCO_2 turbine pressure of 25 MPa.

The cause of rising exergy and thermal efficiency is the rising enthalpy inflow to the turbine with the rise in inlet or high temperature that results in turbine's work output rises. Whilst the work related to recompression & main compressor at the meantime will be show a reasonable amount. Consequently, the recompression cycle's net work output upsurges, therefore, augments the exergy & thermal efficiency. In a different way, the justification can be clarified by the statement that the difference of temperature amongst the heat addition & heat rejection rises with the rise in inlet temperature of turbine, which results in efficiency of cycle increases [89].

Figure 5.37 shows that the R123 fluid based R-SCO_2-ORC system has a maximum amount of exergy efficiency that will be increasing continuously from 63.86% at 650 K to 86.59% at 920 K. Otherwise, R290 fluid based R-SCO_2-ORC system has a smallest amount of exergy efficiency, i.e. enhances from 63.13% at 650 K to 85.94% at 920 K. Whereas, the exergy efficiency of fluids such as R1234ze, R1234yf, toluene, cyclohexane, isopentane, and isobutane lies in the range of these two aforementioned fluids with a maximum value of 86.48%, 86.46%, 86.34%, 86.28%, 86.11%, and 86.06% at 920 K, respectively as described in Figure 5.37. From the outcomes, it has been determined that the exergy efficiency curves for both the R1234ze and R1234yf fluids displays a marginal difference [211].

Then the Figure 5.38 explains the influence of inlet R-SCO_2 turbine temperature on the thermal efficiency, and disclosed that the R123 fluid based R-SCO_2-ORC system has an uppermost value of thermal efficiency, i.e. enhances from 35.57% at 650 K to 48.24%

at 920 K, correspondingly. Conversely, R290 fluid based R-SCO_2-ORC has a lowermost value of thermal efficiency, i.e. 35.17% at 650 K enhances to 47.87% at 920 K. In addition, the thermal efficiency of R1234ze, R1234yf, toluene, cyclohexane, isopentane, and isobutane lies in between these two aforementioned fluids with a maximum value of 48.18%, 48.17%, 48.1%, 48.06%, 47.97%, and 47.94% at 920 K, correspondingly as shown in Figure 5.38. From the outcomes, it is clearly understood that the values of exergy and thermal efficiency for both the R1234ze and R1234yf fluids have a marginal difference [211].

Apart from this, the influence of inlet or high temperature on the exergy performance of SPTC integrated combined recompression cycle (i.e. SPTC-R-SCO_2-ORC system) has been analysed in Figure 5.39. The results of analysis reveal that the R123 fluid has a greatest exergy efficiency, which is increases from 25.37% at 650 K to 70.68% at 920 K. On the contrary side, R290 fluid has a smallest exergy efficiency, i.e. increases from 24.76% at 650 K to 70.06% at 920 K. However, the exergy efficiency of fluids such as R1234ze, R1234yf, toluene, cyclohexane, isopentane, and isobutane lies in between these two aforementioned fluids with a maximum value of 70.57%, 70.56%, 70.44%, 70.38%, 70.22%, and 70.18% at 920 K, respectively as shown in Figure 5.39. From the results, it has been noticed that the exergy performance of both R1234ze and R1234yf fluids have a marginal difference [211].

Also, the Figure 5.40 demonstrates the influence of inlet or high temperature over thermal efficiency of SPTC-R-SCO_2-ORC system, & found that R123 fluid has a greatest thermal efficiency against the other fluids, i.e. enhances from 14.14% at 650 K to 39.37% at 920 K. Instead, R290 fluid has a minimum thermal efficiency, i.e. enhances from 13.79% at 650 K to 39.03% at 920 K, respectively. Whereas, the thermal efficiency of fluids such as R1234ze, R1234yf, toluene, cyclohexane, isopentane, and isobutane lies in between these two aforementioned fluids with an uppermost value of 39.31%, 39.31%, 39.24%, 39.21%, 39.12%, and 39.1% at 920 K, respectively as shown Figure 5.40 [211].

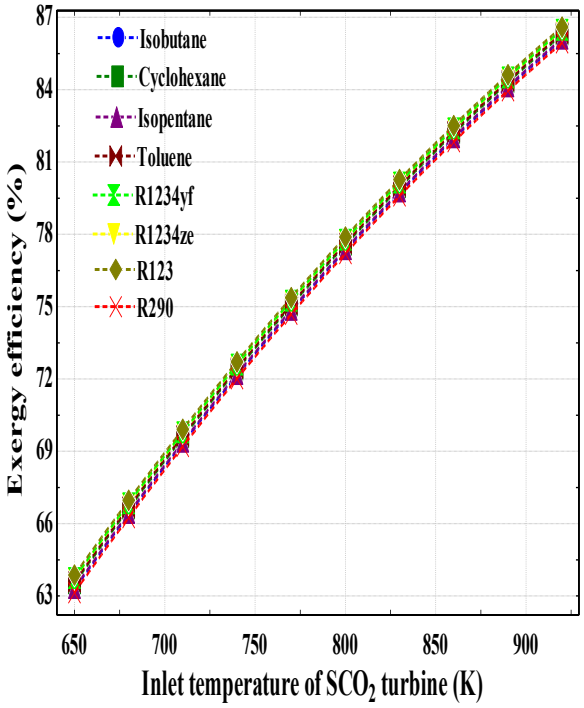

Figure 5.37. Exergy efficiency of combined recompression cycle without solar collector (R-SCO_2-ORC) versus inlet temperature of SCO_2 turbine

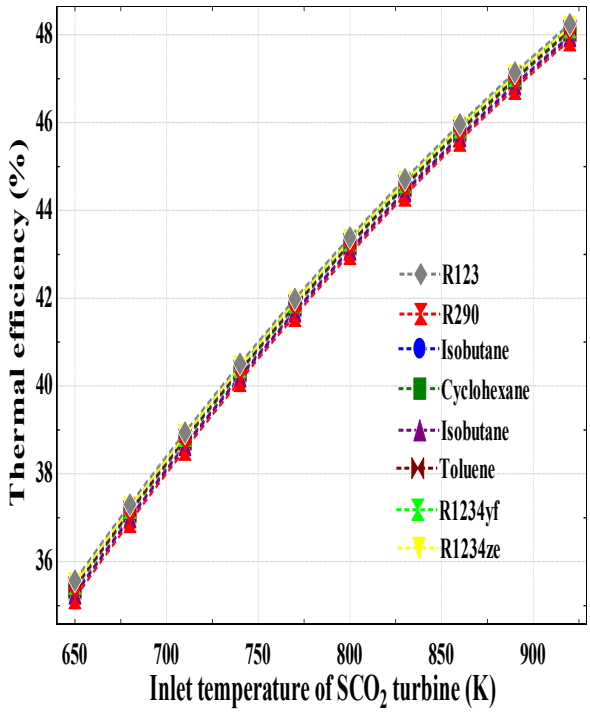

Figure 5.38. Thermal efficiency of combined recompression cycle without solar collector (R-SCO_2-ORC) versus inlet temperature of SCO_2 turbine

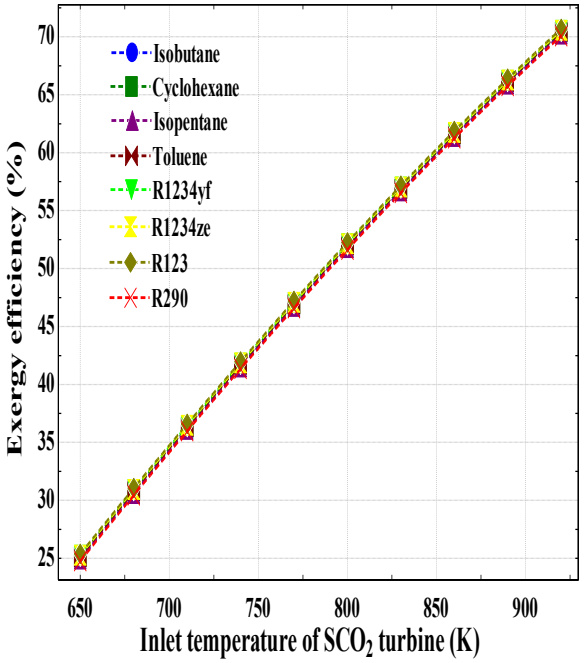

Figure 5.39. Exergy efficiency of complete plant (SPTC-R-SCO_2-ORC) versus inlet temperature of SCO_2 turbine

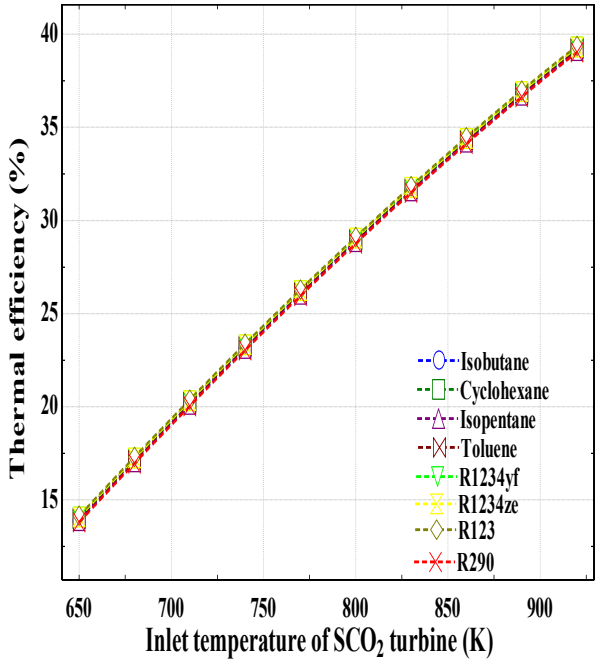

Figure 5.40. Thermal efficiency of complete plant (SPTC-R-SCO_2-ORC) versus inlet temperature of SCO_2 turbine

Furthermore, the Figure 5.41 indicates the effect of inlet temperature of SCO_2 turbine over rate of total exergy destruction of R-SCO_2-ORC system, and it has been concluded that the R290 fluid has an utmost rate of total exergy destruction, i.e. 7111 kW at 650 K decreases to 2712 kW at 920 K. Conversely, R123 fluid has a lowest rate of total exergy destruction, i.e. 6970 kW at 650 K decreases to 2586 kW at 920 K. Whereas, the exergy destruction rate of fluids such as R1234ze, R1234yf, toluene, cyclohexane, isopentane, and isobutane lies in between these two aforementioned fluids with a maximum value of 6995 kW, 6997 kW, 7024 kW, 7038 kW, 7072 kW, and 7084 kW at 650 K, correspondingly as explained in Figure 5.41.

Likewise, Figure 5.42 demonstrates the effect of inlet temperature of SCO_2 turbine over rate of total exergy destruction of SPTC-R-SCO_2-ORC system, and it has been seen that the R290 fluid has a maximum rate of total exergy destruction, i.e. 15470 kW at 650 K decreases to 6156 kW at 920 K.

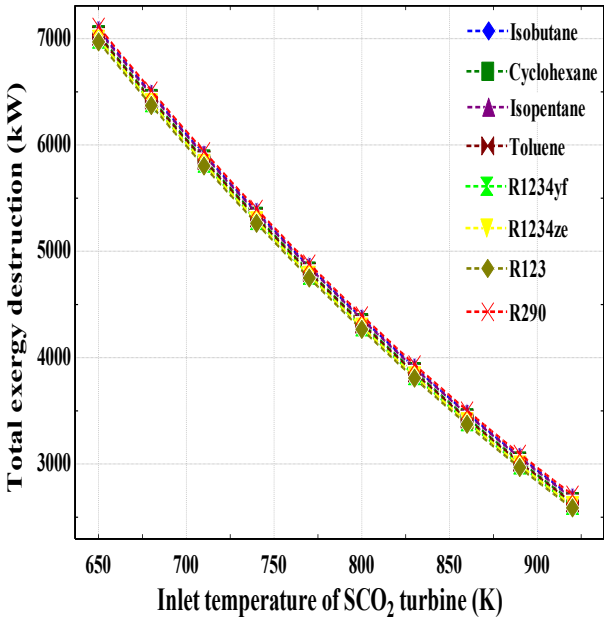

Figure 5.41. Total exergy destruction in combined recompression cycle without solar collector (R-SCO_2-ORC) versus inlet temperature of SCO_2 turbine

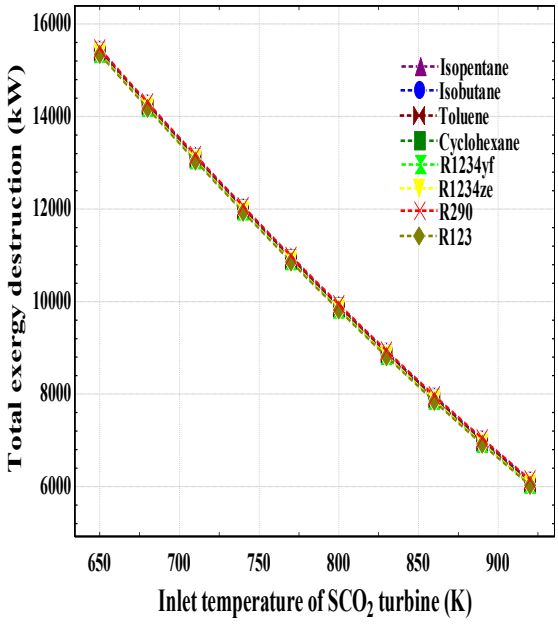

Figure 5.42. Total exergy destruction in complete plant (SPTC-R-SCO_2-ORC) versus inlet temperature of SCO_2 turbine

On the contrary side, R123 fluid has a smallest rate of total exergy destruction, i.e. 15344 kW at 650 K decreases to 6028 kW at 920 K. Whereas, the exergy destruction rate of R1234ze, R1234yf, toluene, cyclohexane, isopentane, and isobutane lies in between

these two aforesaid fluids alongside an uppermost value of 15365 kW, 15369 kW, 15391 kW, 15404 kW, 15437 kW, and 15447 kW at 650 K, respectively as shown in Figure 5.42.

Moreover, Figure 5.43 investigates the influence of inlet or high temperature turbine on the net work output of R-SCO_2-ORC system, and detected that the R123 fluid has a maximum net work output of 4594 kJ at 650 K increases to 6231 kJ at 920 K. Alternatively, R290 fluid has a smallest net work output, i.e. increases from 4542 kJ at 650 K to 6183 kJ at 920 K. While the fluids such as R1234ze, R1234yf, toluene, cyclohexane, isopentane, and isobutane have a maximum net work output of 6223 kJ, 6221 kJ, 6212 kJ, 6207 kJ, 6196 kJ, and 6192 kJ, respectively lies in between R123 and R290 fluid as shown in Figure 5.43 [211].

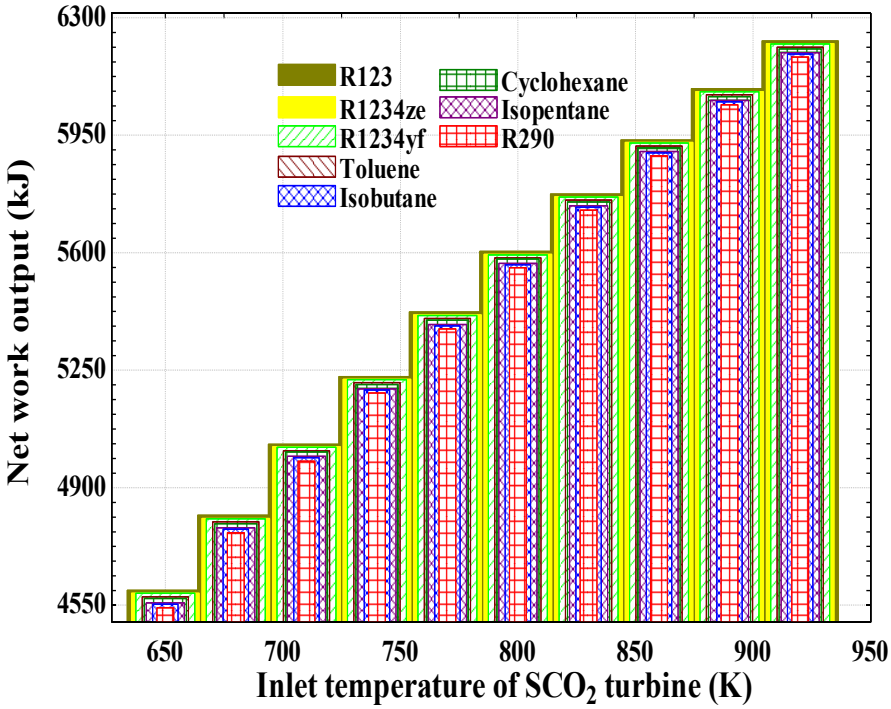

Figure 5.43. Net-work output of combined recompression cycle (R-SCO_2-ORC) versus inlet temperature of turbine

Besides, working fluid's mass flow rate also has a noteworthy influence over efficiency of R-SCO_2-ORC system because of the fact that heat transfer coefficient upsurges with the rise in fluid's mass flow rate but in meantime drop in pressure can also be rises that can further augment the necessity of pumping power [1].

Figure 5.44 displays the influence of mass flow rate of SCO_2 on exergy and thermal performance of the R-SCO_2-ORC system that has been analysed on the basis of baseline

conditions, for example inlet R-SCO_2 turbine pressure of 25 MPa and inlet R-SCO_2 turbine temperature of 652.8 K. It has been assessed that the exergy efficiency rises with the rise in mass flow rate of SCO_2, and concluded that R123 fluid based R-SCO_2-ORC system displays the greatest exergy efficiency, i.e. increases from 74.84% at 7 kg/s to 89.59% at 16 kg/s. Alternatively, R290 fluid based R-SCO_2-ORC system reveals the smallest exergy efficiency, i.e. enhances from 74.32% at 7 kg/s to 88.71% at 16 kg/s. Whereas, the exergy efficiency of fluids such as R1234ze, R1234yf, toluene, cyclohexane, isopentane, and isobutane lies in between the aforementioned fluids with a maximum value of 89.43%, 89.41%, 89.25%, 89.17%, 88.95%, and 88.88% at 16 kg/s, correspondingly as described in Figure 5.44 [211].

Now, Figure 5.45 demonstrates that the R123 fluid based R-SCO_2-ORC system has a greatest thermal efficiency, which is increases from 41.69% at 7 kg/s to 49.91% at 16 kg/s. Instead, R290 fluid based R-SCO_2-ORC system has a smallest thermal efficiency, which is enhances from 41.4% at 7 kg/s to 49.42% at 16 kg/s. Also, the thermal efficiency of R1234ze, R1234yf, toluene, cyclohexane, isopentane, and isobutane lies in between aforementioned fluids with a maximum value of 49.82%, 49.81%, 49.72%, 49.67%, 49.55%, and 49.51%, respectively as shown in Figure 5.45 [211].

Moreover, the influence of mass flow rate on exergy and thermal performance of a SPTC-R-SCO_2-ORC system has been discussed in this paragraph. Figure 5.46 indicates that the R123 fluid based SPTC-R-SCO_2-ORC system possess the utmost value of exergy efficiency, which is enhances from 58.77% at 7 kg/s to 71.41% at 16 kg/s. However, the R290 fluid based SPTC-R-SCO_2-ORC illustrates the lowest value of exergy efficiency, which is increased from 58.3% at 7 kg/s to 70.57% at 16 kg/s. Whereas, the exergy efficiency of fluids such as R1234ze, R1234yf, toluene, cyclohexane, isopentane, and isobutane lies in between aforesaid fluids alongside a maximum value of 71.26%, 71.24%, 71.09%, 71.01%, 70.8%, and 70.73%, respectively as illustrated in Figure 5.46 [211].

Besides, Figure 5.47 illustrates that the R123 fluid based SPTC-R-SCO_2-ORC system has a maximum thermal efficiency, i.e. 32.74% at 7 kg/s increases to 39.78% at 16 kg/s. Conversely, R290 fluid based SPTC-R-SCO_2-ORC system demonstrates the lowest value of thermal efficiency, i.e. increases from 32.48% at 7 kg/s to 39.31% at 16 kg/s. Furthermore, the thermal efficiency of fluids such as R1234ze, R1234yf, toluene, cyclohexane, isopentane, and isobutane lies in between aforementioned fluids with an uppermost value of 39.7%, 39.69%, 39.6%, 39.56%, 39.44%, and 39.4% at 16 kg/s, correspondingly as clearly understood from Figure 5.47 [211].

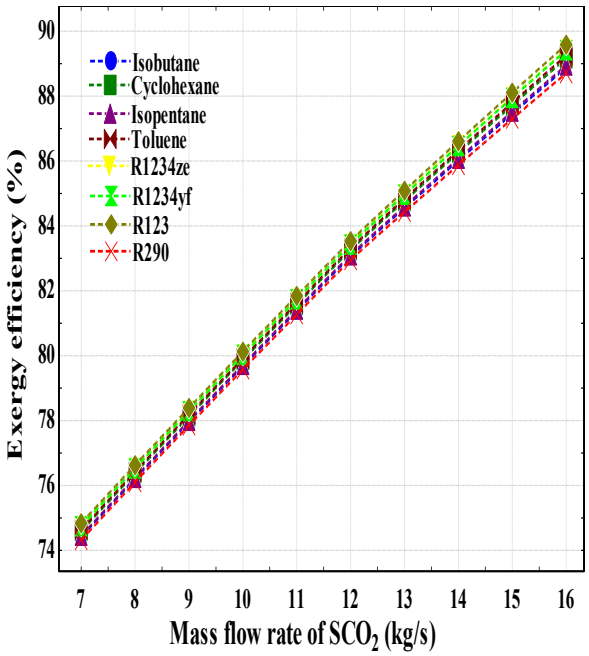

Figure 5.44. Exergy efficiency of combined recompression cycle without solar collector (R-SCO_2-ORC) versus mass flow rate of SCO_2

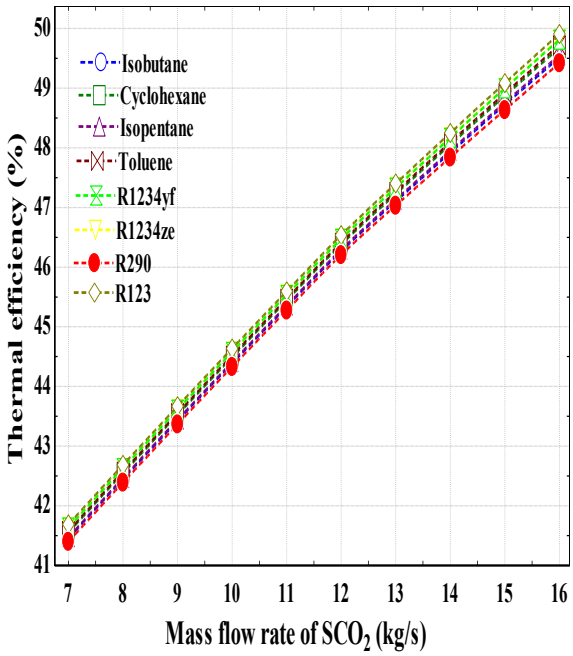

Figure 5.45. Thermal efficiency of combined recompression cycle without solar collector (R-SCO_2-ORC) versus mass flow rate of SCO_2

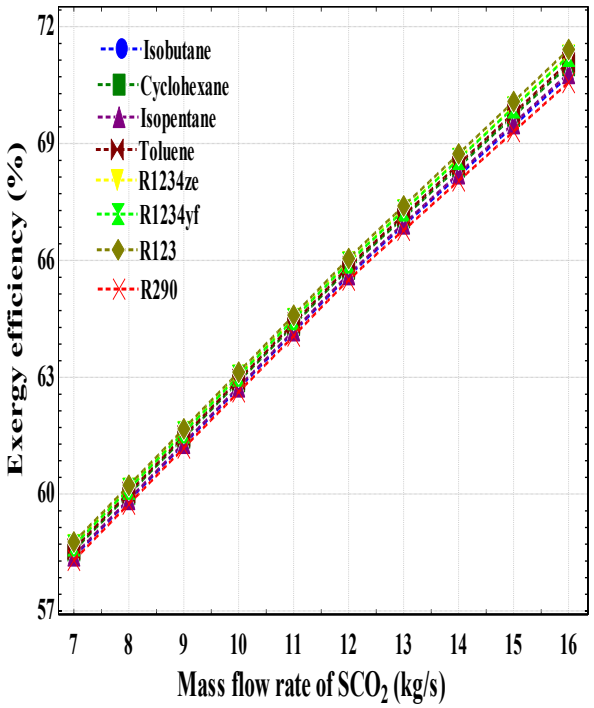

Figure 5.46. Exergy efficiency of complete plant (SPTC-R-SCO_2-ORC) versus mass flow rate of SCO_2

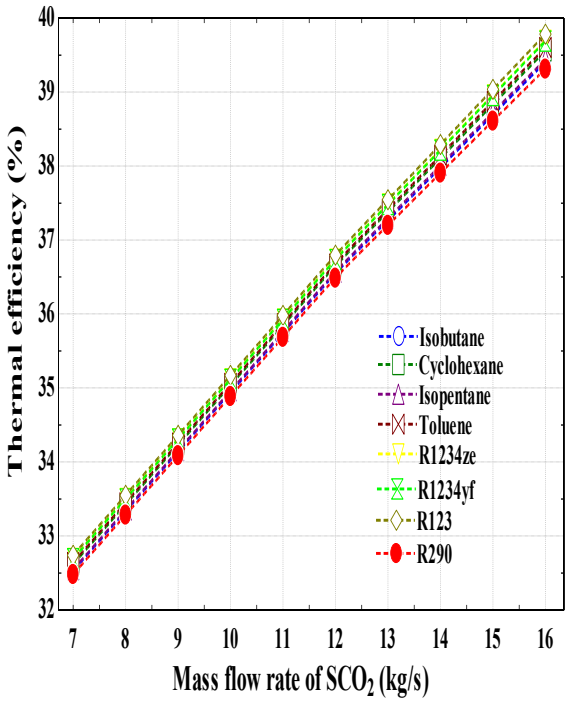

Figure 5.47. Thermal efficiency of complete plant (SPTC-R-SCO_2-ORC) versus mass flow rate of SCO_2

Apart from these, Figure 5.48 indicates influence of mass low rate of SCO_2 over total rate of exergy destruction for R-SCO_2-ORC system, and realized that the R290 fluid has an utmost rate of total exergy destruction that will be falling from 4953 kW at 7 kg/s to 2177 kW at 16 kg/s. Alternatively, R123 fluid has a lowest rate of total exergy destruction that will be diminishing from 4852 kW at 7 kg/s to 2008 kW at 16 kg/s. However, the exergy destruction rate of fluids such as R1234ze, R1234yf, toluene, cyclohexane, isopentane, and isobutane lies in between aforementioned fluids with an upmost value of 4870 kW, 4872 kW, 4891 kW, 4901 kW, 4928 kW, and 4933 kW at 7 kg/s, respectively as described in Figure 5.48.

Lastly, the Figure 5.49 expresses the influence of mass low rate of SCO_2 over total rate of exergy destruction for SPTC-R-SCO_2-ORC system, and it has been reveal that the R290 fluid has a maximum rate of total exergy destruction that will be reduces from 8574 kW at 7 kg/s to 6051 kW at 16 kg/s.

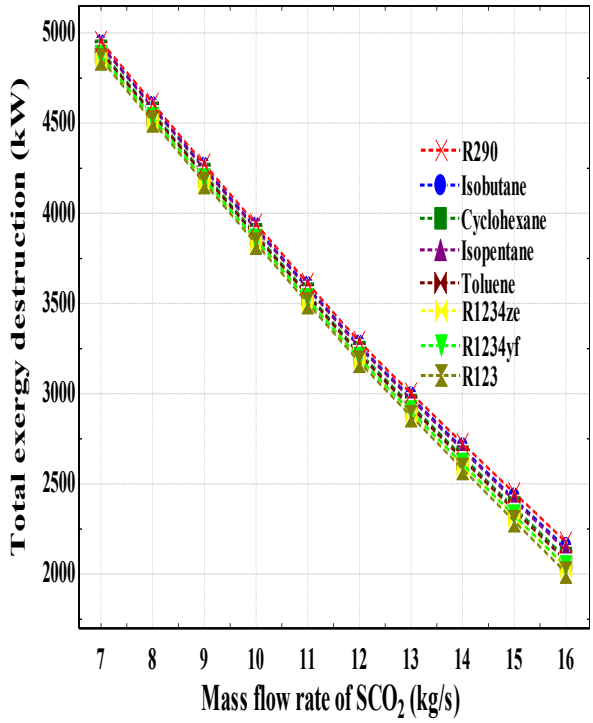

Figure 5.48. Total exergy destruction in combined recompression cycle without solar collector (R-SCO_2-ORC) versus mass flow rate of SCO_2

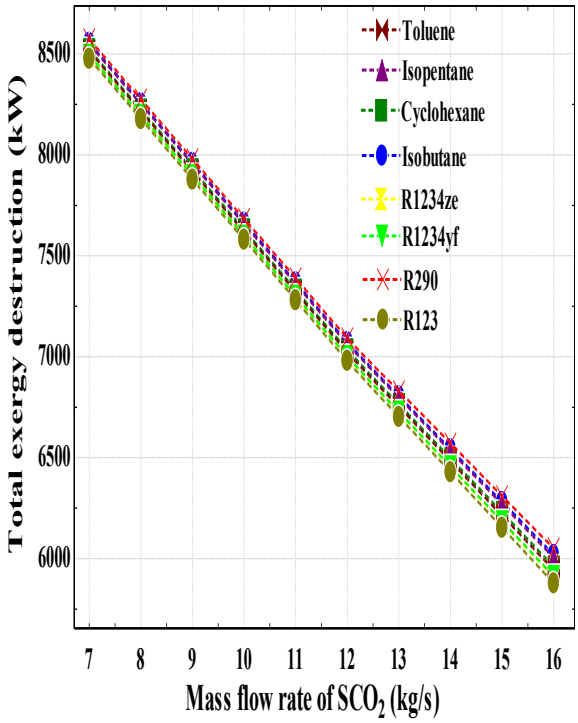

Figure 5.49. Total exergy destruction in complete plant (SPTC-R-SCO_2-ORC) versus mass flow rate of SCO_2

Alternatively, the R123 fluid has a lowest rate of total exergy destruction, which is falling from 8477 kW at 7 kg/s to 5878 kW at 16 kg/s. Furthermore, the exergy destruction rate of fluids such as R1234ze, R1234yf, toluene, cyclohexane, isopentane, and isobutane lies in between aforesaid fluids alongside a highest value of 8493 kW, 8495 kW, 8514 kW, 8522 kW, 8549 kW, and 8555 kW at 7 kg/s, respectively as indicated in Figure 5.49.

5.2.3. Effect of variation in inlet temperature of main compressor on the system performance

Present section discusses influence of main compressor's inlet temperature over exergy and thermal performance of combined recompression cycle (R-SCO_2-ORC system) has been examined. In this direction, Figure 5.50 shows that with the rise in main compressor's inlet temperature, the exergy efficiency of R-SCO_2-ORC system reduces.

The cause of reducing efficiency is that as the main compressor's inlet temperature upsurges, the specific heat capacity of CO_2 reduces (i.e. far from the critical point) which further decreases the main compressor's specific enthalpy inflow. Consequently, the main compressor's work upsurges remarkably but the work of the recompression compressor and SCO_2 turbine do not disturbed so much in the meantime which means that net work output reduces, and finally the exergy and thermal efficiency will also be reduces simultaneously [89].

This fact can be explained in other way that the difference amongst the cycle's maximum & minimum temperature reduces with the increase in main compressor's inlet temperature, consequently, cycle efficiency reduces. In addition, it has been noticed that with the rise in main compressor's inlet temperature, there will be a sharp degradation of cold fluid's specific heat capacity in contrast to hot fluid as reasonably far from the critical point in the LTR, which results in a significant decline in the recompression mass fraction [89]. On the basis of these factors as discussed above, the range of inlet temperature of compressor has been decided so as to assess the performance.

From Figure 5.50, it has been realised that exergy efficiency of R123 fluid based R-SCO_2-ORC system decreases from 85.83% at 300 K to 84.64% at 327 K. Alternatively, the R290 fluid possess the smallest exergy efficiency, i.e. decreases from 84.91% at 300 K to 84.12% at 327 K. However, the exergy efficiency of fluids such as R1234ze, R1234yf, toluene, cyclohexane, isopentane, and isobutane lies in between these aforesaid fluids with a highest value of 85.67%, 85.65%, 85.48%, 85.39%, 85.17%, and 85.09% at 300 K, respectively as illustrated in Figure 5.50 [211].

On the other side, Figure 5.51 demonstrates the thermal efficiency of R123 fluid based R-SCO_2-ORC system decreases from 47.82% at 300 K to 47.15% at 327 K, correspondingly and its amount is utmost as compared to another considered working fluids, for example R1234ze, R1234yf, toluene, cyclohexane, isopentane, and isobutane with a maximum thermal efficiency value of 47.72%, 47.71%, 47.62%, 47.57%, 47.44%, and 47.4% at 300 K, respectively, while the R290 fluid possess the lowest value of thermal efficiency, i.e. decreases from 47.3% at 300 K to 46.86% at 327 K as shown in Figure 5.51 [211].

Furthermore, the influence of main compressor's inlet temperature on the exergy and thermal performance of SPTC integrated combined recompression cycle (SPTC-R-SCO_2-ORC system) also has been investigated in this section. From the Figure 5.52, it has been assessed that the R123 fluid based SPTC-R-SCO_2-ORC system has an utmost exergy efficiency, i.e. decreases from 68.1% at 300 K to 66.98% at 327 K. While, the R290 fluid has a lowermost amount of exergy efficiency, i.e. decreases from 67.24% at 300 K to 66.49% at 327 K [211].

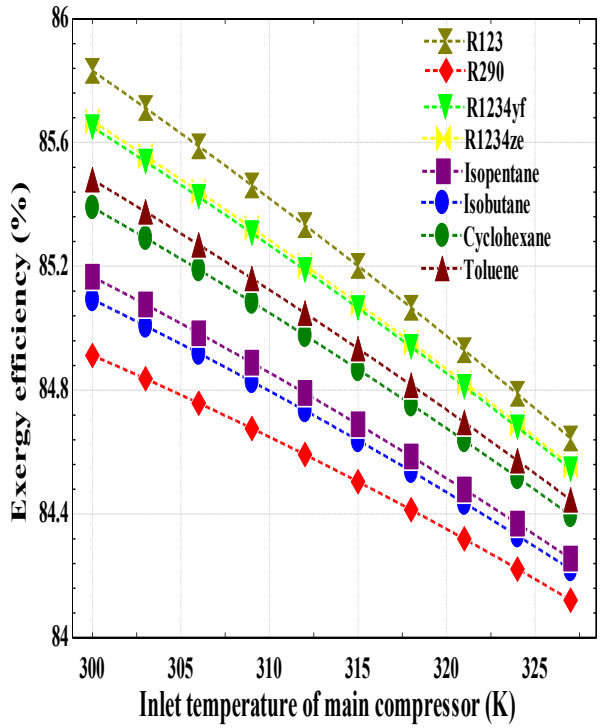

Figure 5.50. Exergy efficiency of combined recompression cycle without solar collector (R-SCO_2-ORC) versus inlet temperature of main compressor

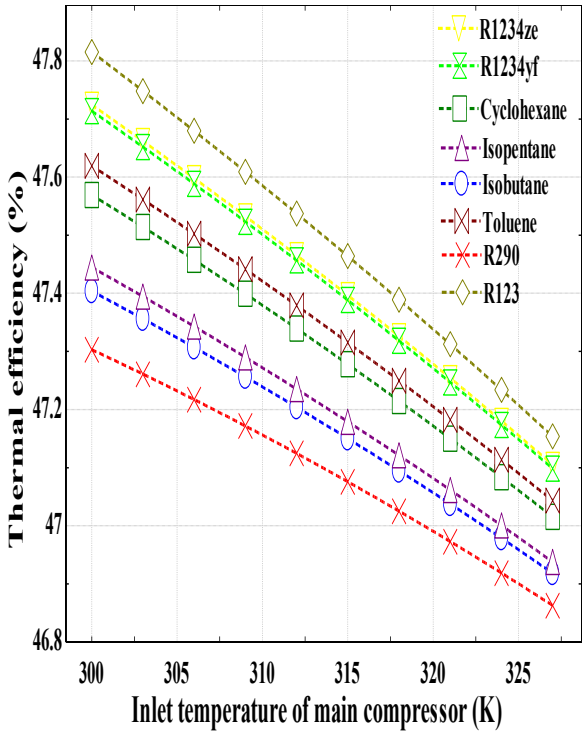

Figure 5.51. Thermal efficiency of combined recompression cycle without solar collector (R-SCO_2-ORC) versus inlet temperature of main compressor

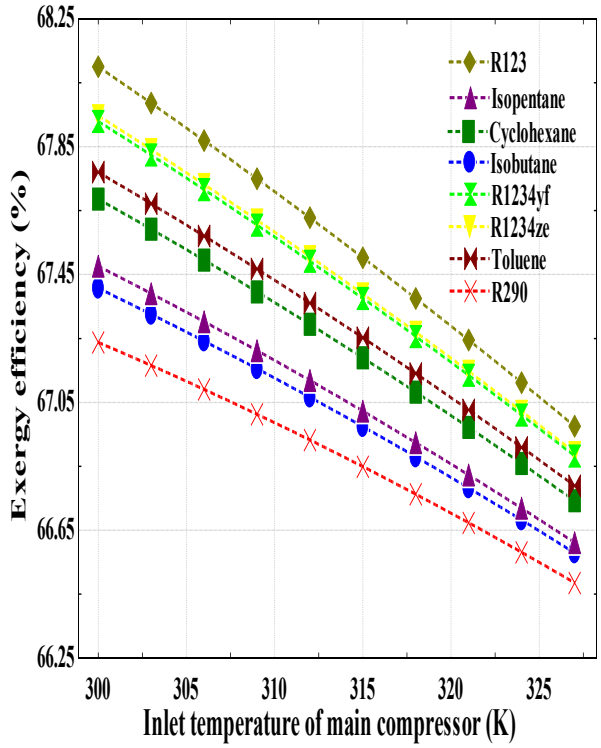

Figure 5.52. Exergy efficiency of complete plant (SPTC-R-SCO_2-ORC) versus inlet temperature of main compressor

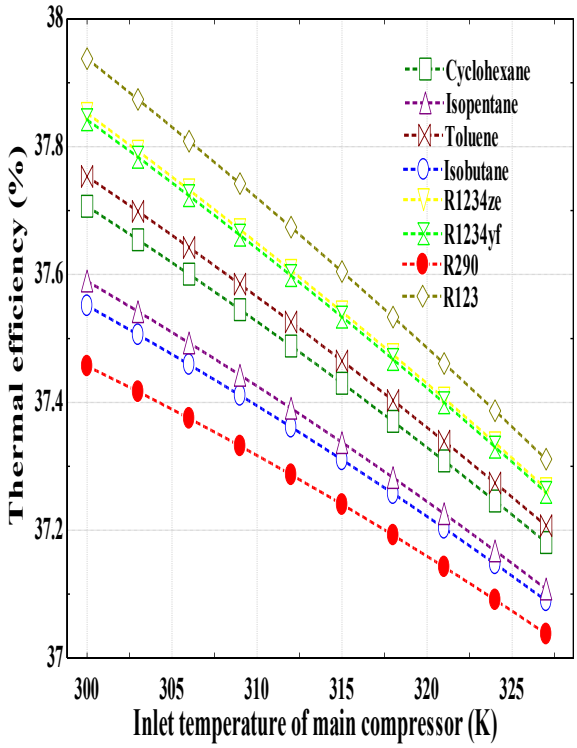

Figure 5.53. Thermal efficiency of complete plant (SPTC-R-SCO_2-ORC) versus inlet temperature of main compressor

Also, the exergy efficiency of fluids such as R1234ze, R1234yf, toluene, cyclohexane, isopentane, and isobutane lies in between these aforementioned fluids with a maximum value of 67.95%, 67.93%, 67.77%, 67.69%, 67.48%, and 67.41%, respectively as indicated in Figure 5.52 [211].

Moreover, Figure 5.53 shows that the R123 fluid based SPTC-R-SCO_2-ORC system has a maximum thermal efficiency, which is decreases from 37.94% at 300 K to 37.31% at 327 K. While, the R290 fluid has a smallest thermal efficiency, which is decreases from 37.46% at 300 K to 37.04% at 327 K. Also, the thermal efficiency for all other fluids such as R1234ze, R1234yf, toluene, cyclohexane, isopentane, and isobutane lies in between these two fluids as stated overhead with a highest value of 37.85%, 37.84%, 37.75%, 37.71%, 37.59%, and 37.55% as understood from the Figure 5.53 [211].

Apart from this, Figure 5.54 explains the influence of main compressor's inlet temperature on the rate of overall exergy destruction of R-SCO_2-ORC, and it has been concluded that the R290 fluid based R-SCO_2-ORC system has a highest rate of total exergy destruction, i.e. 2910 kW at 300 K increases to 3063 kW at 327 K. Alternatively, the R123 fluid has a lowest rate of total exergy destruction, i.e. 2733 kW at 300 K increases to 2962 kW

at 327 K. Whereas, the exergy destruction rate of fluids such as R1234ze, R1234yf, toluene, cyclohexane, isopentane, and isobutane lies in between these aforesaid fluids with a highest value of 2978 kW, 2982 kW, 2999 kW, 3009 kW, 3036 kW, and 3043 kW at 327 K as shown in Figure 5.54.

In addition, Figure 5.55 demonstrates the influence of main compressor's inlet temperature on the rate of total exergy destruction of SPTC-R-SCO_2-ORC system, and it has been reveal that R290 fluid based SPTC-R-SCO_2-ORC has a maximum rate of total exergy destruction, i.e. 6736 kW at 300 K increases to 6890 kW at 327 K. While the R123 fluid has a smallest rate of total exergy destruction, i.e. 6559 kW at 300 K increases to 6789 kW at 327 K. Also, the exergy destruction rate of fluids such as R1234ze, R1234yf, toluene, cyclohexane, isopentane, and isobutane lies in between these aforementioned fluids with an uppermost value of 6807 kW, 6810 kW, 6828 kW, 6838 kW, 6865 kW, and 6871 kW at 327 K, respectively as indicated in Figure 5.55.

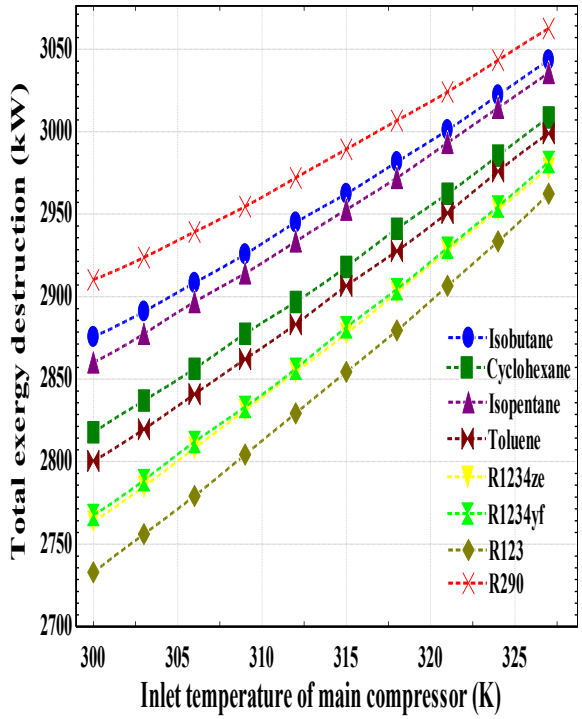

Figure 5.54. Total exergy destruction in combined recompression cycle without solar collector (R-SCO_2-ORC) versus inlet temperature of main compressor

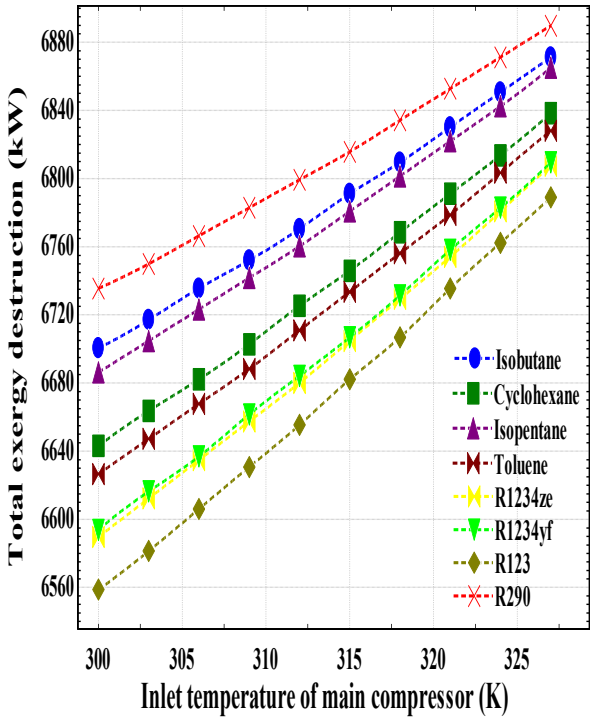

Figure 5.55. Total exergy destruction of complete plant (SPTC-R-SCO_2-ORC) versus inlet temperature of main compressor

Lastly, the influence of main compressor's inlet temperature on the net work output of combined recompression cycle (R-SCO_2-ORC system) has been studied in Figure 5.56. It has been observed that as the inlet temperature of the main compressor increases, the net work output decreases correspondingly and also found that R123 fluid has the maximum amount of net work output, which is around 6176 kJ at 300 K and 6090 kJ at 327 K. Alternatively, R290 fluid has the lowest value of net work output, i.e. around 6109 kJ at 300 K and 6052 kJ at 327 K. In addition, the net work output of all other fluids such as R1234ze, R1234yf, toluene, cyclohexane, isopentane, and isobutane lies in between these two fluids as mentioned above with a maximum value of 6163 kJ, 6162 kJ, 6150 kJ, 6144 kJ, 6127 kJ, and 6122 kJ at 300K, respectively as shown in Figure 5.56.

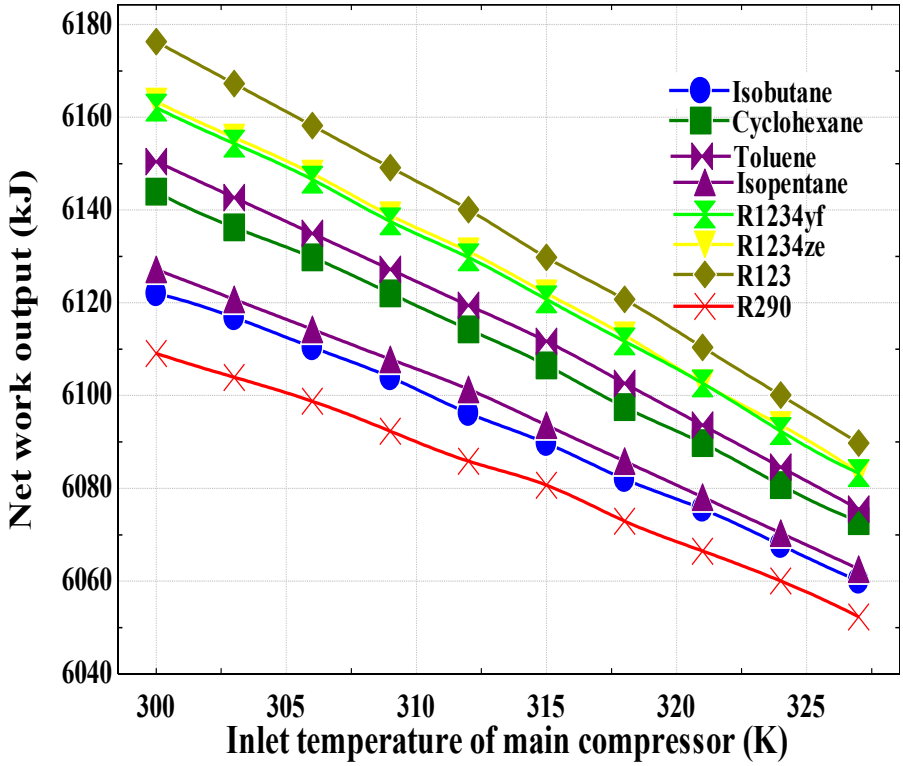

Figure 5.56. Net work output of combined recompression cycle (R-SCO_2-ORC) versus inlet temperature of main compressor

5.2.4. Effect of variation in effectiveness of HTR and LTR on the system performance

In this section, the effect of HTR and LTR effectiveness on the exergy and thermal performance of combined recompression cycle (R-SCO_2-ORC system) has been examined. It is clear that with the rise in recuperator's effectiveness, heat exchange and exergy gain can

also increase that results in recompression cycle's exergy destruction reduces, consequently, the exergy efficiency rises [89].

In a different way, as the recuperator's effectiveness increases, the input specific exergy decreases, however, the net output specific exergy stays uniform because of unaffected cycle pressure ratio, isentropic efficiencies, and other operating conditions and hence, exergy efficiency also enhances [89].

It has been observed by the Figure 5.57 that the exergy efficiency upsurges as the effectiveness of HTR (ε_{HTR}) upsurges, and uncovered that the R123 fluid based R-SCO_2-ORC system has an utmost exergy efficiency, which is around 84.57% at ε_{HTR} = 0.65 increases to 85.01% at ε_{HTR} = 0.92. Otherwise, the R290 fluid has a lowermost exergy efficiency, which is around 83.72% at ε_{HTR} = 0.65 increases to 84.32% at ε_{HTR} = 0.92. Also, the exergy efficiency of all other fluids, for instance R1234ze, R1234yf, toluene, cyclohexane, isopentane, and isobutane lies in between these two fluids as stated above with a maximum value of 84.89%, 84.87%, 84.74%, 84.67%, 84.5%, and 84.45% at ε_{HTR} = 0.92, respectively as illustrated in Figure 5.57 [211].

On the other hand, Figure 5.58 demonstrates that the thermal efficiency also enhances with the rise in effectiveness of HTR, and concluded that the R123 fluid based R-SCO_2-ORC system has a greatest thermal efficiency, i.e. around 47.11% at ε_{HTR} = 0.65 increases to 47.35% at ε_{HTR} = 0.92. Conversely, the R290 fluid has a minimum thermal efficiency, which is around 46.64% at ε_{HTR} = 0.65 increases to 46.97% at ε_{HTR} = 0.92. Whereas, the amount of thermal efficiency for all other fluids like R1234ze, R1234yf, toluene, cyclohexane, isopentane, and isobutane lies in between these two fluids as stated overhead with an uppermost value of 47.29%, 47.28%, 47.21%, 47.17%, 47.07%, and 47.04% at ε_{HTR} = 0.92, respectively as indicated in Figure 5.58 [211].

Furthermore, the Figure 5.59 displays the influence of LTR effectiveness (ε_{LTR}) on the exergy efficiency, and uncovered that the efficiency of R123 fluid based R-SCO_2-ORC system enhances as the LTR effectiveness enhances, and it possess the maximum exergy efficiency among the other fluids, which is around 85.06% at ε_{LTR} = 0.65 increases to 85.1% at ε_{LTR} = 0.92. Instead, the R290 fluid has a minimum exergy efficiency, which is around 84.39% at ε_{LTR} = 0.65 increases to 84.44% at ε_{LTR} = 0.92. While the exergy efficiency of fluids such as R1234ze, R1234yf, toluene, cyclohexane, isopentane, and isobutane lies in between these two fluids as stated overhead with an upmost value of 84.99%, 84.97%, 84.85%, 84.78%, 84.62%, and 84.57% at ε_{LTR} = 0.92, respectively as described in Figure 5.59 [211].

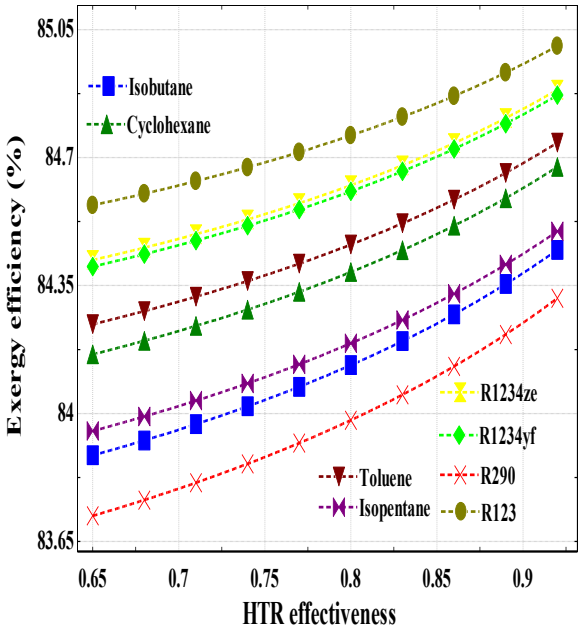

Figure 5.57. Exergy efficiency of combined recompression cycle (R-SCO_2-ORC) versus HTR effectiveness

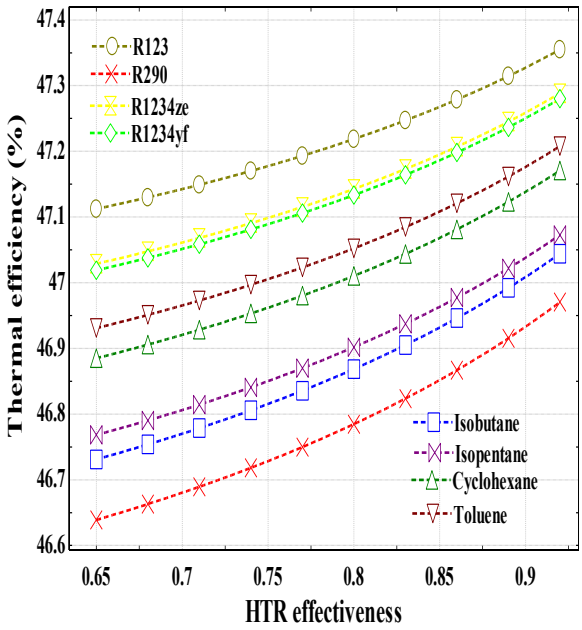

Figure 5.58. Thermal efficiency of combined recompression cycle (R-SCO_2-ORC) versus HTR effectiveness

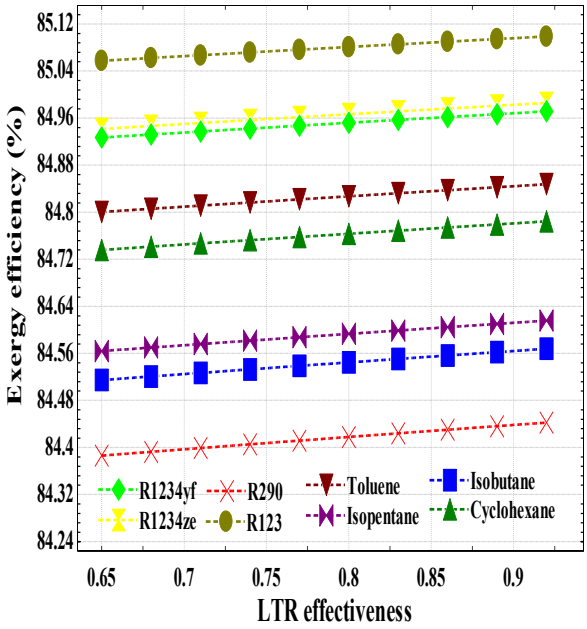

Figure 5.59. Exergy efficiency of combined recompression cycle (R-SCO_2-ORC) versus LTR effectiveness

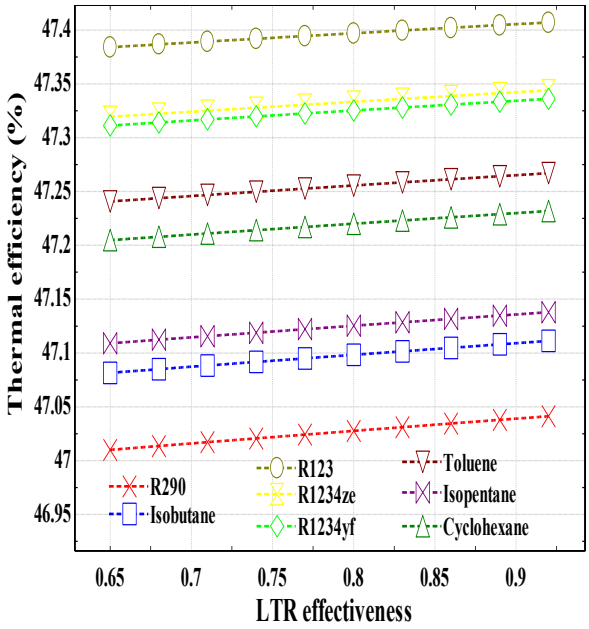

Figure 5.60. Thermal efficiency of combined recompression cycle (R-SCO_2-ORC) versus LTR effectiveness

Moreover, the effect of the LTR effectiveness on the thermal efficiency has been described in Figure 5.60, and found that the R123 fluid based R-SCO_2-ORC system has an utmost thermal efficiency value, i.e. around 47.38% at ε_{LTR} = 0.65 increases to 47.41% at ε_{LTR} = 0.92. Contrariwise, R290 fluid has a lowermost thermal efficiency, i.e. around 47.01% at ε_{LTR} = 0.65 increases to 47.04% at ε_{LTR} = 0.92. Likewise, the thermal efficiency of all other fluids such as R1234ze, R1234yf, toluene, cyclohexane, isopentane, and isobutane lies in between these two fluids as stated above with a maximum value of 47.34%, 47.34%, 47.27%, 47.23%, 47.14%, and 47.11% at ε_{LTR} = 0.92, respectively as shown in Figure 5.60 [211].

Additionally, it is completely understood from the results that the HTR effectiveness has a more prevalent effect on the efficiency in contrast to LTR effectiveness since HTR exchanges more heat and exergy [211].

Apart from these, Figure 5.61 displays the influence of HTR effectiveness on rate of overall exergy destruction of R-SCO_2-ORC, and it has been found that R290 fluid based R-SCO_2-ORC system has an utmost rate of total exergy destruction, i.e. 3140 kW at ε_{HTR} = 0.65 decreases to 3024 kW at ε_{HTR} = 0.92. Alternatively, R123 fluid has a lowest rate of total exergy destruction, i.e. 2976 kW at ε_{HTR} = 0.65 decreases to 2891 at ε_{HTR} = 0.92.

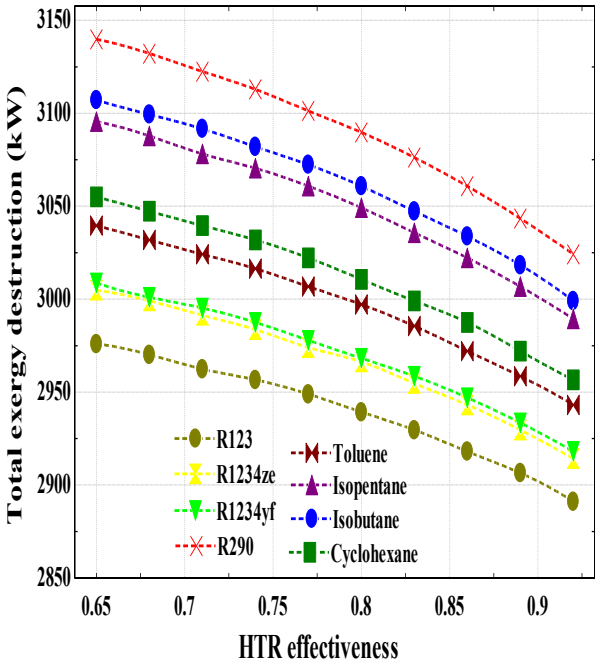

Figure 5.61. Total exergy destruction in combined recompression cycle without solar collector (R-SCO_2-ORC) versus HTR effectiveness

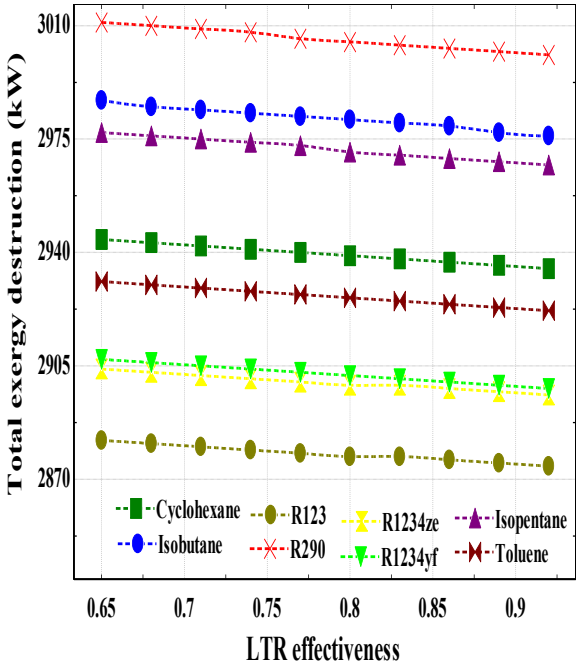

Figure 5.62. Total exergy destruction in combined recompression cycle without solar collector (R-SCO_2-ORC) versus LTR effectiveness

Also, the exergy destruction rate of other fluids such as R1234ze, R1234yf, toluene, cyclohexane, isopentane, and isobutane lies in between these two fluids as stated above with a highest value of 3005 kW, 3009 kW, 3040 kW, 3055 kW, 3095 kW, and 3107 kW at ε_{HTR} = 0.65 as illustrated in Figure 5.61.

Lastly, Figure 5.62 indicates the influence of LTR effectiveness on rate of overall exergy destruction of R-SCO_2-ORC, and it has been observed that the R290 fluid based R-SCO_2-ORC system has a maximum rate of total exergy destruction, i.e. 3011 kW at ε_{LTR} = 0.65 decreases to 3001 kW at ε_{LTR} = 0.92. Conversely, the R123 fluid has a minimum rate of total exergy destruction, i.e. 2882 kW at ε_{LTR} = 0.65 decreases to 2874 at ε_{LTR} = 0.92. Also, the total exergy destruction rate of other fluids such as R1234ze, R1234yf, toluene, cyclohexane, isopentane, and isobutane lies in between these two fluids as stated above with a maximum value of 2904 kW, 2907 kW, 2931 kW, 2944 kW, 2977 kW, and 2987 kW at ε_{LTR} = 0.65, respectively as demonstrates in Figure 5.62.

Moreover, the study investigates that the R-SCO_2-ORC system has a greater exergy and thermal efficiency than the simple structure of a combined cycle (SCO_2-ORC system), which is generally because of the SCO_2 flow splitting in a recompression cycle which further helps in compensate the difference amongst specific heat in LTR along with the maximum heat recuperation in topping R-SCO_2 cycle which in turn amount of waste heat will be dropped and consequently, the cycle thermal efficiency can be improved [66].

Therefore, a comparison has been made between cycles such as R-SCO_2-ORC system and SCO_2-ORC system under the same baseline conditions, for instance solar DNI of 850 W/m^2, inlet turbine temperature of 652.8 K, inlet turbine pressure of 25 MPa, and mass flow rate of SCO_2 as 10 kg/s, then the results demonstrate that the R123 fluid based R-SCO_2-ORC system has a maximum exergy efficiency of 85.09% and R290 fluid based R-SCO_2-ORC system has a minimum exergy efficiency of 84.43%. However, the exergy efficiency of other fluids such as R1234ze, R1234yf, toluene, cyclohexane, isopentane, and isobutane lies in between these two fluids alongside an observed value of 84.97%, 84.97%, 84.84%, 84.77%, 84.6%, and 84.55%, respectively as demonstrated in Figure 5.63.

Also, Figure 5.64 illustrates that the R123 fluid based R-SCO_2-ORC system has an uppermost thermal efficiency of 47.4% and R290 fluid based R-SCO_2-ORC system has a lowermost thermal efficiency of 47.03%. Whereas, the thermal efficiency of other fluids such as R1234ze, R1234yf, toluene, cyclohexane, isopentane, and isobutane lies in between

these two fluids alongside an estimated value of 47.34%, 47.33%, 47.26%, 47.23%, 47.13%, and 47.1%, respectively as shown in Figure 5.64.

On the contrary side, in case of SCO_2-ORC system, R123 fluid again has an utmost exergy efficiency of 83.63% and R290 fluid has a smallest exergy efficiency of 82.49%. While the exergy efficiency of other fluids such as R1234ze, R1234yf, toluene, cyclohexane, isopentane, and isobutane lies in between these two fluids with an assessed value of 83.39%, 83.35%, 82.98%, 82.88%, 82.64%, and 82.59%, respectively as indicated Figure 5.63.

Table 5.9. Temperature and pressure at the selected states for the SPTC integrated R-SCO_2-ORC at the selected stations [228,229]

Selected stations	Fluid type	P (MPa)	T (K)
SPTC Receiver outlet (3)	Syltherm 800	10	673.15
SCO_2 turbine inlet (5)	SCO_2	25	652.8
SCO_2 turbine outlet (6)	SCO_2	13.2	588.8
HTR outlet (7)	SCO_2	13.2	462.4
LTR outlet (7')	SCO_2	13.2	385.2
Heat exchanger outlet (8)	SCO_2	13.2	327.8
Main compressor outlet (10)	SCO_2	25	369.1
Recompressor outlet (9')	SCO_2	25	438.4
LTR outlet (10')	SCO_2	25	436.8
HTR outlet (4)	SCO_2	25	532.3
ORC turbine inlet (11)	R123	3	359.2
ORC turbine outlet (13)	R123	0.676	312.7
Condenser outlet (14)	R123	0.676	297.2
Heat exchanger inlet (12)	R123	3	306.9

Source: Singh and Mishra (2018) [211]

Apart from this, R123 fluid based SCO_2-ORC system has an utmost thermal efficiency of 46.59% and R290 fluid based SCO_2-ORC system has a smallest thermal efficiency of 45.95%. Likewise, the thermal efficiency of other fluids such as R1234ze, R1234yf, toluene, cyclohexane, isopentane, and isobutane lies in between these two fluids alongside a calculated value of 46.46%, 46.43%, 46.23%, 46.17%, 46.04%, and 46.01%, respectively as shown in Figure 5.64.

Therefore, it has been concluded that the combined recompression cycle has around 1.74% to 2.4% more efficiency value than the simple combined cycle. Moreover, the important thermodynamic parameters (i.e. temperature and pressure) for R-SCO_2-ORC system has been depicted in Table 5.9.

Finally, the study found that the highest amount of exergy destruction rate happens in a SPTC field, i.e. around 58.25% of the whole exergy destruction rate which can be due to temperature and material restrictions of SPTC system. In addition, total exergy destruction in the R123 fluid based SPTC-R-SCO_2-ORC system found to be as 32.59% of the inlet exergy from SPTC (i.e. 20562 kJ).

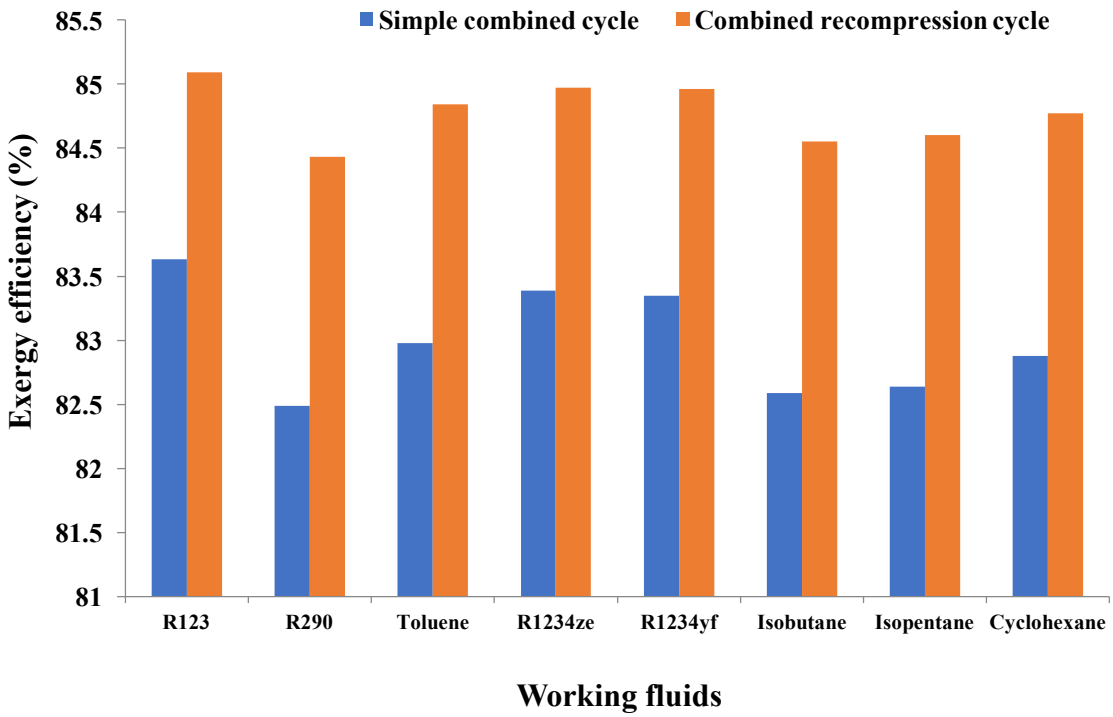

Figure 5.63. Comparison of exergy efficiency of simple combined cycle and combined recompression cycle for selected fluids

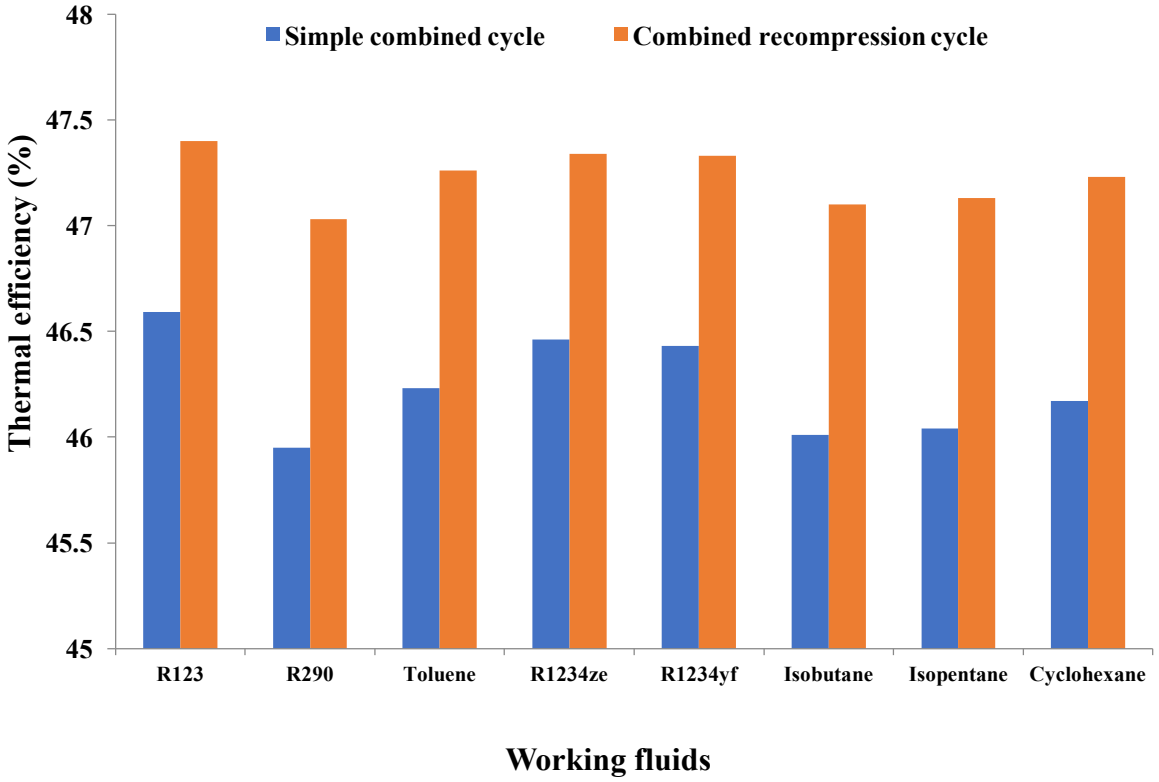

Figure 5.64. Comparison of thermal efficiency of simple combined cycle and combined recompression cycle for selected fluids

5.2.5. Validation of combined recompression cycle and R-SCO_2 cycle

In this section, the validation results of both combined recompression cycle (R-SCO_2-ORC system) and simple structure of R-SCO_2 cycle have been listed in the Table 5.10 & Table 5.11.

Table 5.10. Validation of combined recompression cycle (R-SCO_2-ORC)

Organic working fluid in bottoming cycle	Literature work	Thermal efficiency in literature work	Thermal efficiency estimated	Error approximation
Isobutane	Besarati et al. [172]	0.5357	0.517	-3.4%

Source: Singh and Mishra (2018) [211]

Outcomes have been calculated with the assistance of EES software at the same baseline conditions as that considered in the literature work and It has been found that

thermal efficiency results in the existing model matched well with the results found from all the literature work [99,106,172,233].

Table 5.11 Validation of simple R-SCO_2 cycle at the turbine inlet temperature of 500℃

Working fluid in topping cycle	Literature work	Thermal efficiency predicted in literature work	Thermal efficiency estimated	Error approximation
SCO_2	Besarati et al. [172]	0.4421	0.4377	-0.9%
SCO_2	Kulhánek and Dostál [233]	0.4419		-0.95%
SCO_2	Turchi et al. [99]	0.4441		-1.4%
SCO_2	Padilla et al. [106]	0.4424		-1.06%

Source: Singh and Mishra (2018) [211]

- **System optimization by RSM**

After examine the lot of literature, it is well-known that researchers are using mainly genetic algorithm for the performance optimization but another technique also known as response surface methodology (RSM) have been suggested for the same purpose in current study. Firstly, R1234yf fluid has been chosen from the available fluids to analyze the optimized performance. Secondly, any three independent factors have to decide, for example solar DNI, effectiveness of HTR & LTR are taken as Y_1, Y_2, and Y_3 respectively and their impact we want to analyze on the system as shown in Table 5.12. Thirdly, dependent or response variables, for example exergy & thermal efficiency have been selected and these are taken as Z_1 and Z_2, respectively. Now based on the Box-Behnken response surface design, three different levels i.e., -1, 0, & +1 have been applied for the selected range of independent parameters (suggestion: select any three process parameters), i.e. solar DNI (500, 725, & 950 W/m^2), effectiveness of HTR (65, 78.5, & 92%), and LTR (65, 78.5, to 92%) so as to inspect the influence on system performance. Design Expert 11 software used to generate the different arrangements of independent variables to find out optimized values of response variables. Computer program based modelling that has been done in EES software further applied to each arrangement made up in seventeen treatments of Bob-Behnken design matrix. The empirical statistical modelling technique known as RSM which is utilizing quantitative data obtained from the designed experiments for the multiple regression analysis so that multivariate equations could be solved simultaneously [238,239]. The design expert software 11 has been utilized to perform statistical

analysis. The analysis based on multiple regression has been applied to investigate the simulation data and F-test is utilized to evaluate the importance of regression coefficient. Throughout the modeling, quadratic model should be suggested along with linear, squared, and interaction terms. Also, the R-Squared, Adjusted R-Squared, and PRESS (prediction error sum of squares) are utilized to check the model's adequacy. Pareto analysis of variance (ANOVA) has been employed to find the important terms for each response in the model and on the behalf of this, ANOVA table can be generated.

Table 5.12. Design of Box-Behnken for the independent variables & their corresponding simulation and predicted values

Run	Y_1 (W/m^2)	Y_2 (%)	Y_3 (%)	Exergy efficiency, R1234yf (%)		Thermal efficiency, R1234yf (%)	
				Z_1 (Simulation)	Z_1 (RSM)	Z_2 (Simulation)	Z_2 (RSM)
1	725	78.5	78.5	61.18	61.18	34.08	34.08
2	950	92	78.5	70.64	70.64	39.35	39.35
3	725	78.5	78.5	61.18	61.18	34.08	34.08
4	725	65	92	60.99	60.97	33.98	33.97
5	725	65	65	60.96	60.95	33.96	33.95
6	500	78.5	65	43.65	43.66	24.32	24.33
7	950	65	78.5	70.23	70.25	39.12	39.14
8	500	78.5	92	43.7	43.71	24.35	24.36
9	950	78.5	65	70.37	70.36	39.2	39.19
10	500	92	78.5	44.16	44.13	24.6	24.59
11	725	92	92	61.53	61.54	34.28	34.29
12	725	92	65	61.49	61.5	34.25	34.26
13	725	78.5	78.5	61.18	61.18	34.08	34.08
14	725	78.5	78.5	61.18	61.18	34.08	34.08
15	500	65	78.5	43.38	43.38	24.17	24.17
16	725	78.5	78.5	61.18	61.18	34.08	34.08
17	950	78.5	92	70.4	70.38	39.22	39.21

Likewise, to check the adequacy of models, the sequential model sum of squares (SOS), degree of freedom (DOF), mean square (MS), F-value, and P-value were carried out. Results showed that for quadratic and linear model, the P-value lower than 0.0001 was estimated. Box-Behnken design along with the simulation technique was used to obtained the simulation results to fit the polynomial equation of second order. The final equations as expressions of coded factors can be utilized to create forecasts about the response for specified levels of each factor are given below:

Exergy efficiency (R1234yf), $Z_1 = 61.18 + 13.34Y_1 + 0.2825Y_2 + 0.0188Y_3 - 0.0925Y_1Y_2 - 0.0050Y_1Y_3 + 0.0025Y_2Y_3 - 4.15Y_1^2 + 0.0675Y_2^2 - 0.0050Y_3^2$

Thermal efficiency (R1234yf), $Z_2 = 34.08 + 7.43Y_1 + 0.1563Y_2 + 0.0125Y_3 - 0.0500Y_1Y_2 - 0.0025Y_1Y_3 + 0.0025Y_2Y_3 - 2.31Y_1^2 + 0.0375Y_2^2 + 0.0000Y_3^2$

The ANOVA was applied to test the model's adequacy and suitability. Their outcomes showed that the actual relationship between independent variables and responses as revealed in Table 5.13. The outcomes of ANOVA for the exergy and thermal efficiency of R1234yf showed that model F-value was 412369.50 and 390579.59, respectively which advises that model is noteworthy and there is merely 0.01% chance that due to noise, the F-value could occur large. The values of R^2, adjusted R^2, predicted R^2 for the exergy and thermal efficiency of R1234yf having the same value as 1. To assess the model's fitness as well as adequacy, the adjusted R^2 was used that also corrects the value of R^2 for the size of sample and model's number of terms, and its high-pitched value supports for a great importance the model. The value 1 for predicted R^2 is in reasonable agreement with adjacent R^2 of 1, which means that difference is less than 0.2. The adequate precision evaluates the signal to noise ratio and should be bigger than 4 which is needed [238], and adequate precision value for the exergy and thermal efficiency of R1234yf was 1768.76 and 1721.19, respectively, which signifies an adequate signal. Also, the relative diffusion of the experimental points from the guesses of polynomial models of second order can be indicated by the coefficient of variation (C.V.%) [238,240]. The value of C.V.% for the exergy and thermal efficiency of R1234yf was 0.0339 and 0.0348, respectively. The low value of C.V.% shows that the differences between simulation and predicted values are low.

Table 5.13. ANOVA for the R1234yf based simulation results of the design of Box-Behnken

Source	DOF	Exergy efficiency, R1234yf (%)				Thermal efficiency, R1234yf (%)				
		COE	SOS	MS	P-value	COE	SOS	MS	P-value	Significant
Model	9	61.18	1497.78	166.42	< 0.0001	34.08	464.51	51.61	< 0.0001	
Residual	7	-	0.0028	0.0004	-	-	0.0009	0.0001	-	
Lack of Fit	3	-	0.0028	0.0009	-	-	0.0009	0.0003	-	
Pure Error	4	-	0.0000	0.0000	-	-	0.0000	0.0000	-	
Cor Total	16	-	1497.79	-	-	-	464.51	-	-	
Std. Dev.	-	0.0201	-	-	-	0.0115	-	-	-	
Mean	-	59.26	-	-	-	33.01	-	-	-	
C.V. %	-	0.0339	-	-	-	0.0348	-	-	-	
PRESS	-	0.0452	-	-	-	0.0148	-	-	-	
Adeq. Precision	-	1768.76	-	-	-	1721.19	-	-	-	
R^2	-	1.0000	-	-	-	1.0000	-	-	-	
Adjusted R^2	-	1.0000	-	-	-	1.0000	-	-	-	
Predicted R^2	-	1.0000	-	-	-	1.0000	-	-	-	

Diagnostic of model's competence has been implemented to check the model's adequacy with the aim to find out that model would give poor or ambiguous fallouts. In order to check the normality of residuals and their normal percentage probability plots for response with respect to the internally studentized residuals were analysed in the plot no. (a) & (b), which shows that the residuals are lie reasonably close to the 45° line.

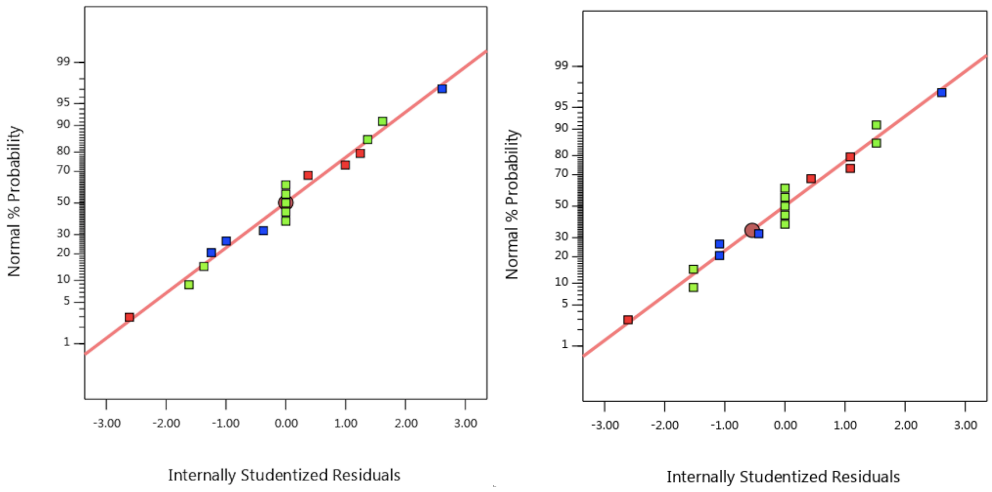

(a) (b)

Plot (a) & (b). Normal percentage probability for the exergy and thermal efficiency

Further, response surface (RS) plots are the function of two independent variables at a time that shows the main & interactive effect of these variables on the response. To identify the interaction between process variables and to determine each level's optimum level, the RS curves for exergy efficiency and thermal efficiency in case of R1234yf were plotted in plot no. (d), (e), (f) & (g). From the plots, it is clear that high value of solar DNI displays the high exergy & thermal efficiency, which has also been reported in the literature [169]. Also, it has been observed from the response plots that both HTR and LTR effectiveness illustrates a positive effect on the exergy and thermal efficiency of cycle that means efficiency augments with the enhance in effectiveness as stated in literature [89]. For the optimization and authentication of model, Derringer's desirability function method has been used to optimize the conditions of independent variables, which are as follow: solar DNI of 949.916 W/m^2, HTR effectiveness of 91.9944%, and LTR effectiveness of 88.9916%. Under these conditions, the predicted exergy & thermal efficiency was 70.6439% and 39.3561% with a desirability of 1. Through the numerical optimization technique, desirability ramps were developed for the R1234yf from the optimal points as shown in plot no. (h) & (i).

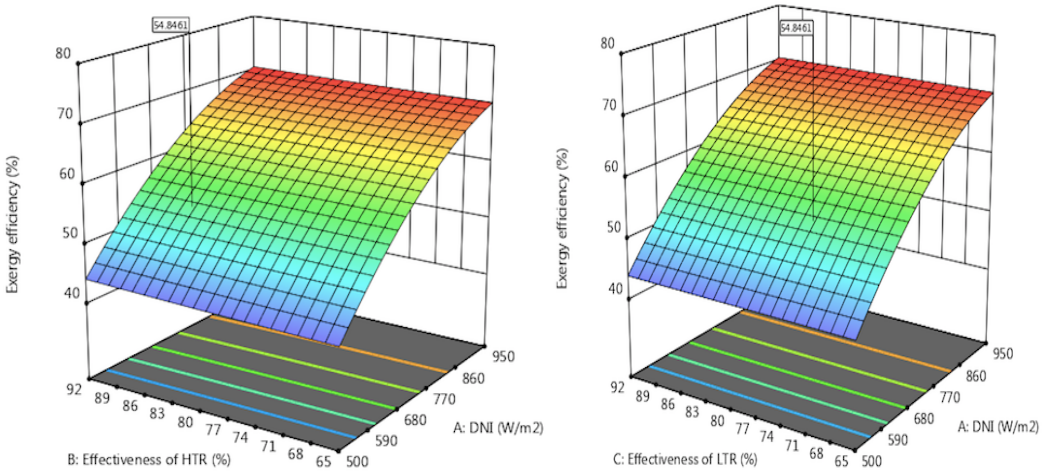

(d) (e)

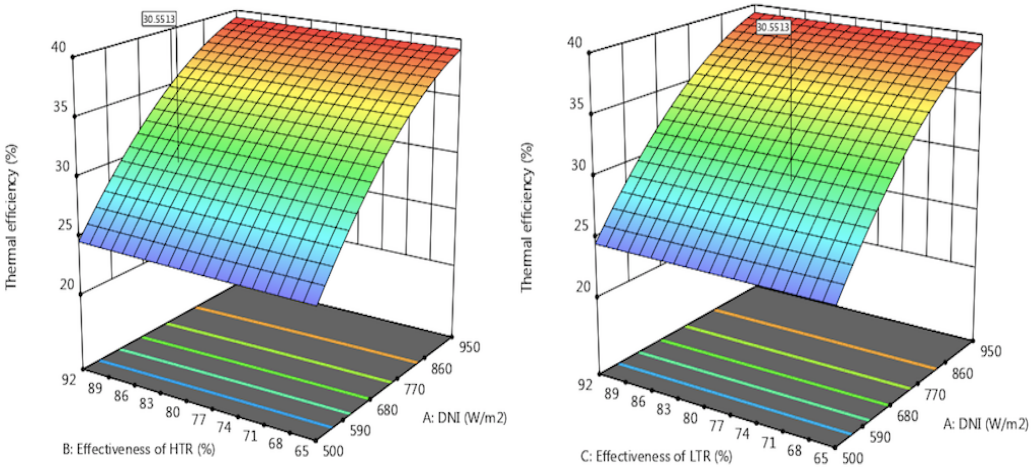

(f) (g)

Colour specifications for response surface plots

Upper maximum value of efficiency
Lower maximum value of efficiency
Middle value of efficiency
Upper minimum value of efficiency
Lower minimum value of efficiency

Plot (d), (e), (f), & (g). Response surfaces for R1234yf based exergy & thermal efficiency

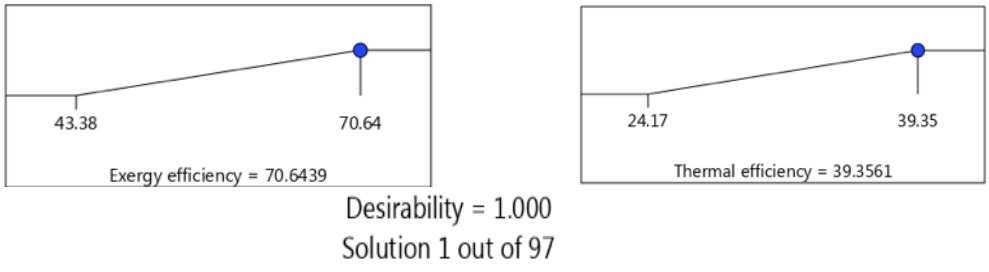

(h) **(i)**

Plot (h) & (i). Desirability ramps for optimization in case of R1234yf

5.3. SPTC integrated with combined SCO_2 cycle and VAR cycle

The energetic and exergetic based investigation has been conducted for the SPTC based combined SCO_2 cycle and VAR (i.e. SCO_2-VAR cycle) with the support of EES software. The effect of various constraints, for example local apparent time (LAT), solar DNI (G_b), maximum or inlet temperature of turbine, compressor's inlet temperature & pressure ratio, temperature of generator, and temperature of absorber & condenser on the functioning of a SCO_2-VAR cycle has been studied with the aim of power generation, cooling & heating purposes. Also, parametric analysis has been carried out so as to compute exergy & thermal efficiency, network output, COP of cooling & heating, and heat transfer rate in the evaporator.

5.3.1. Effect of variation in LAT on the system performance

To analyse system performance, solar DNI data for the location of Mumbai has been collected from the Ref. [1]. Variation in Solar DNI for the length of day or with respect to LAT for the different month and date (i.e. April 15 & December 15) has been illustrated in Figure 5.65 and 5.66. As can be seen, the solar DNI for the location Mumbai is more on the April 15 as compared to December 15.

Figure 5.65 clearly indicates that on the April 15, the highest value of solar DNI is 705 W/m^2 at LAT(h) = 1230 and the smallest amount of solar DNI is 145 W/m^2 at LAT(h) = 0730. While, Figure 5.66 also illustrates that on the December 15, the maximum amount of solar DNI is 580 W/m^2 at LAT(h) = 1130 & 1230 and smallest amount of solar DNI is 81 W/m^2 at LAT(h) = 0730 [214].

Furthermore, Figure 5.65 reveals the influence of LAT on the performance of SPTC system for the date of April 15, and it has been uncovered that the minimum value of exergy & thermal efficiency is around 17.1% & 33.31%, respectively at LAT(h) = 0730 and the greatest amount of exergy & thermal efficiency is around 32.58% and 63.46%, respectively at LAT(h) = 1230 [214].

However, Figure 5.66 depicts the effect of LAT on the performance of SPTC system for the date of December 15, and it has been observed that the lowest value of exergy & thermal efficiency is around 1.702% & 3.315%, respectively at LAT(h) = 0730 and the

uppermost value of exergy & thermal efficiency is around 31.72% & 61.78%, respectively at LAT(h) = 1130 & 1230 [214].

It has been noted that in the April, May, and June month, the energy & exergy efficiency along with solar day's length can be highest, and variation in efficiency can be small which can be because of smallest influence of incident angle in contrast to other months, for example December and January wherein energy & exergy efficiency will be lowest owing to high incident angle [142].

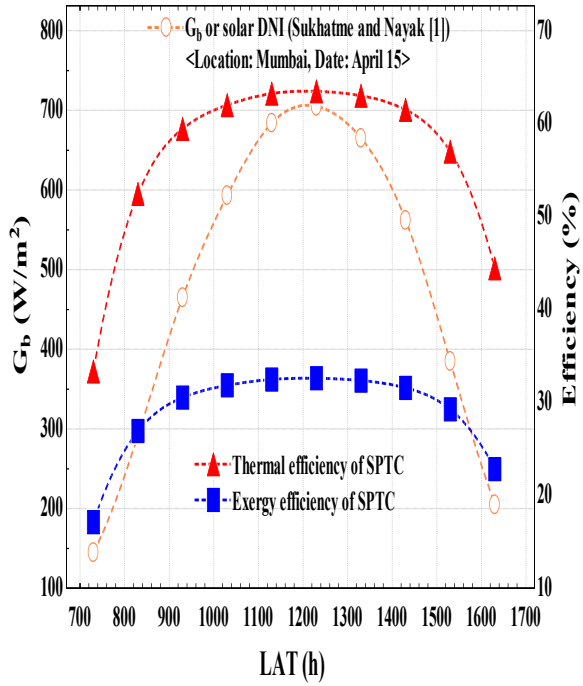

Figure 5.65. Variations in solar DNI, exergy and thermal efficiency with respect to LAT for location of Mumbai on the April 15

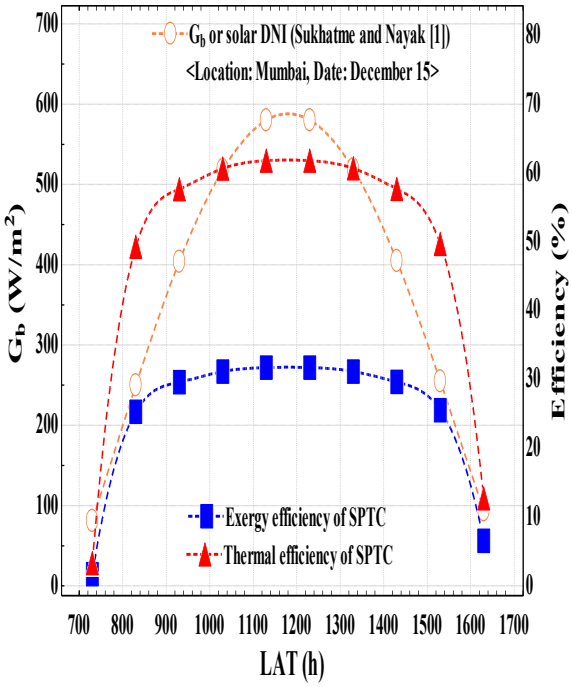

Figure 5.66. Variations in solar DNI, exergy and thermal efficiency with respect to LAT for location of Mumbai on the December 15

Furthermore, Figure 5.67 explains the influence of LAT over performance of SCO_2-VAR cycle with respect to date of April 15, and it has been concluded that the greatest amount of exergy & thermal efficiency is about 75.71% & 42.18%, respectively at LAT(h) = 1230 [214].

Also, Figure 5.68 indicates the effect of LAT on the performance of complete cycle (i.e. SPTC-SCO_2-VAR cycle) with regards to date of April 15, it has been disclosed that the greatest amount of exergy & thermal efficiency is about 61.95% and 34.51%, respectively at LAT(h) = 1230 [214].

Moreover, Figure 5.69 shows influence of LAT over functioning of SCO_2-VAR cycle for date of December 15, it has been assessed that highest value of exergy & thermal efficiency is around 70.1% and 39.05%, respectively at LAT(h) = 1130 & 1230 [214].

Lastly, the Figure 5.70 depicts the effect of LAT over the functioning of SPTC-SCO_2-VAR cycle for the date of December 15, and it has been detected that uppermost amount of exergy & thermal efficiency is around 53.73% & 29.93%, respectively at LAT(h) = 1130 & 1230 [214].

Apart from these, Figure 5.71 illustrates that for the April 15, minimum total exergy destruction rate of SCO_2-VAR cycle & SPTC-SCO_2-VAR cycle is around 4445 kW & 7823 kW, respectively at LAT(h) = 1230. In addition, Figure 5.72 shows that for the December 15, minimum total exergy destruction rate of SCO_2-VAR cycle & SPTC-SCO_2-VAR cycle is around 5471 kW & 9513 kW, respectively at LAT(h) = 1130 & 1230 [214].

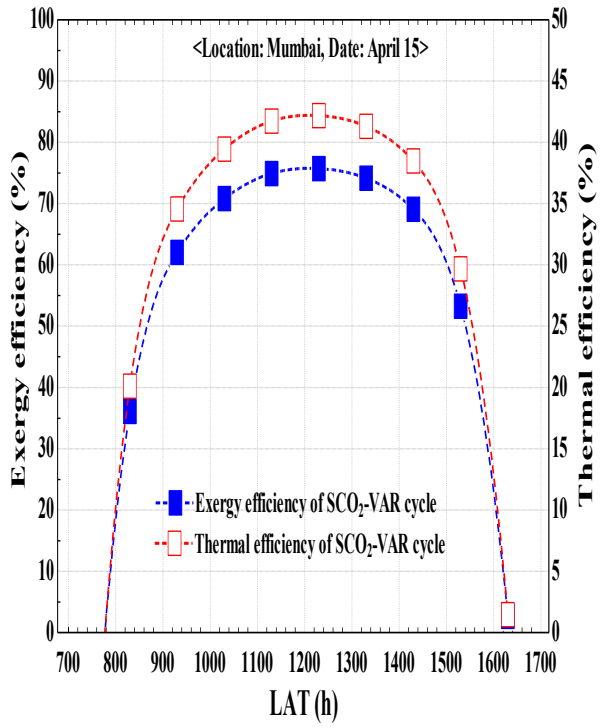

Figure 5.67. Exergy and thermal efficiency of combined cycle without solar collector (SCO_2-VAR cycle) versus LAT on the April 15

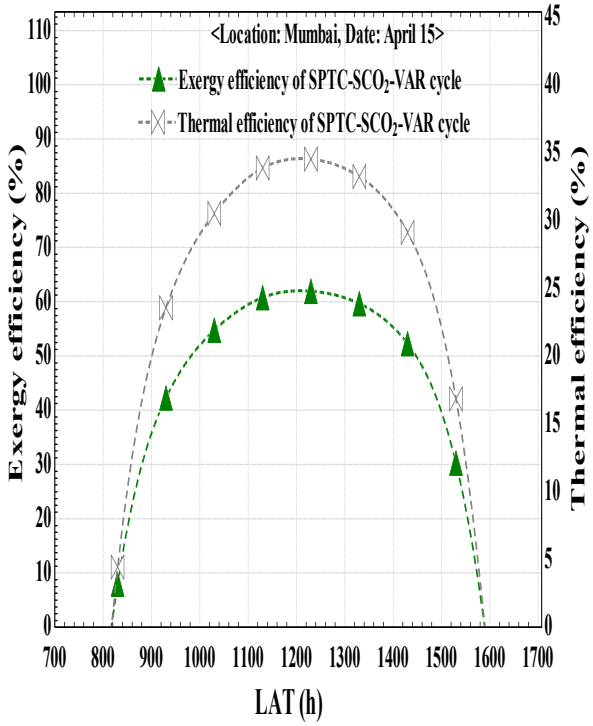

Figure 5.68. Exergy and thermal efficiency of complete plant (SPTC-SCO_2-VAR cycle) versus LAT on the April 15

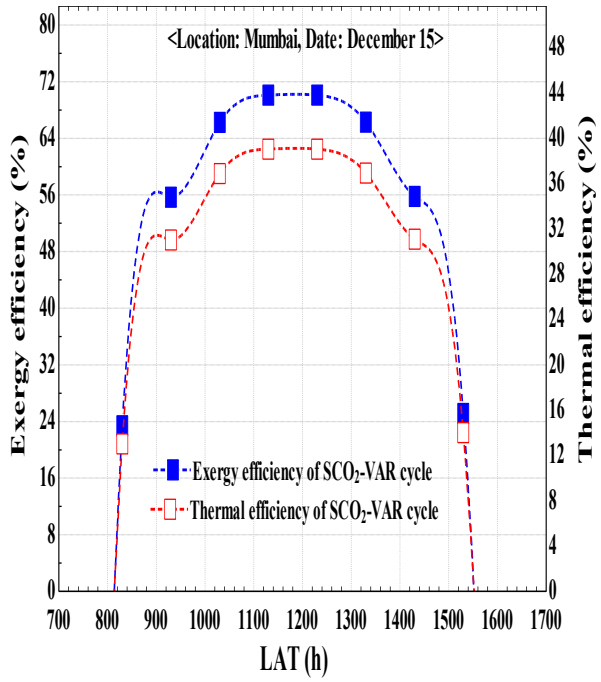

Figure 5.69. Exergy and thermal efficiency of combined cycle without solar collector (SCO_2-VAR cycle) versus LAT on the December 15

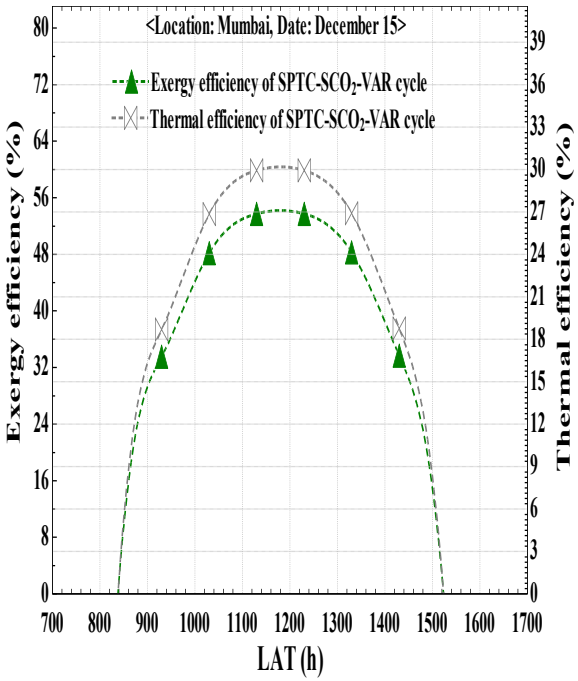

Figure 5.70. Exergy and thermal efficiency of complete plant (SPTC-SCO_2-VAR cycle) versus LAT on the December 15

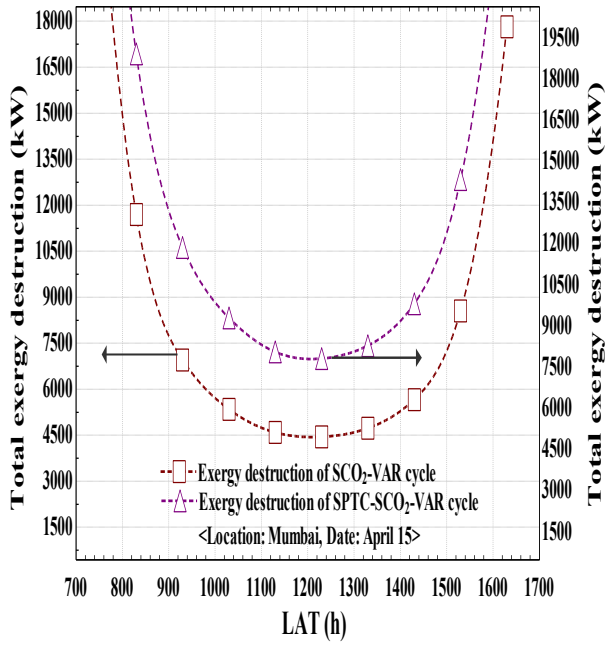

Figure 5.71. Total exergy destruction in SCO_2-VAR cycle and SPTC-SCO_2-VAR cycle versus LAT on the April 15

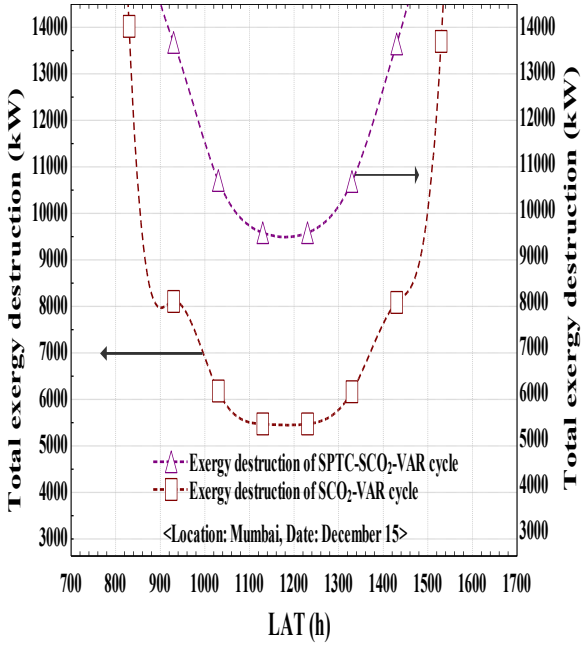

Figure 5.72. Total exergy destruction in SCO_2-VAR cycle and SPTC-SCO_2-VAR cycle versus LAT on the December 15

5.3.2. Effect of solar DNI on the system performance

In this section, Figure 5.73 demonstrates the influence of solar DNI over the exergy & thermal efficiency of SPTC field, and it has been realized that the exergy efficiency upsurges from 22.17% at 200 W/m^2 up to 33.9% at 960 W/m^2 & thermal efficiency also upsurges from 42.72% at 200 W/m^2 up to 65.32% at 960 W/m^2 [214].

It has been noted that in a solar plant which is consists of multiple rows of SPTCs organised in both series & parallel arrangement, the efficient & better utilization of SPTCs can be achieved by enhancing the solar DNI.

Also, Figure 5.74 shows the effect of solar DNI over the performance of combined cycle (SCO_2-VAR cycle), and it has been found that exergy efficiency enhances from 64.91% at 500 W/m^2 to 82.24% at 950 W/m^2 and thermal efficiency enhances from 36.16% at 500 W/m^2 to 45.82% at 950 W/m^2. Whereas, the Figure 5.75 demonstrates the effect of solar DNI on the functioning of complete plant (SPTC-SCO_2-VAR cycle), and it has been observed that exergy efficiency rises from 46.31% at 500 W/m^2 to 71.77% at 950 W/m^2 and thermal efficiency increases from 25.8% at 500 W/m^2 to 39.98% at 950 W/m^2 [214].

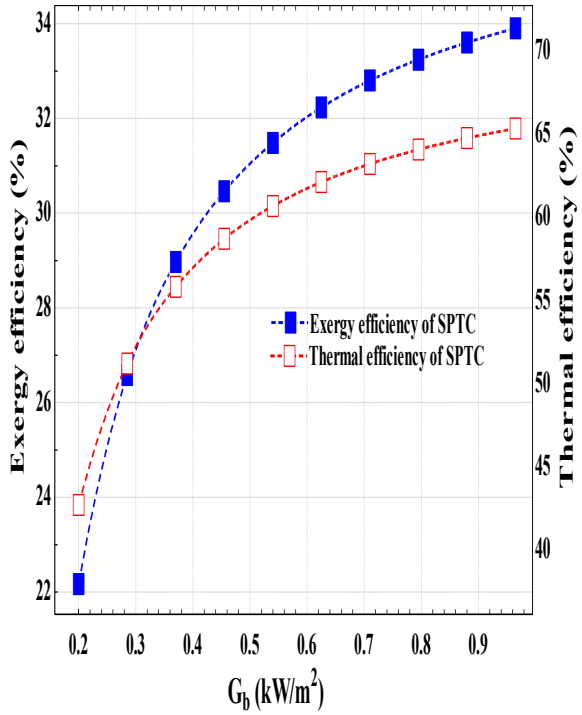

Figure 5.73. Exergy and thermal efficiency of solar collector (SPTC system) versus solar DNI

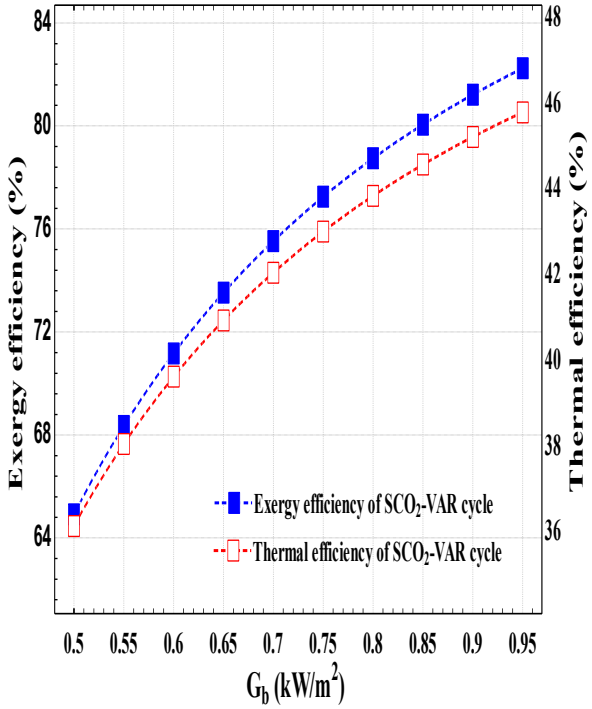

Figure 5.74. Exergy and thermal efficiency of combined cycle without solar collector (SCO_2-VAR cycle) versus solar DNI

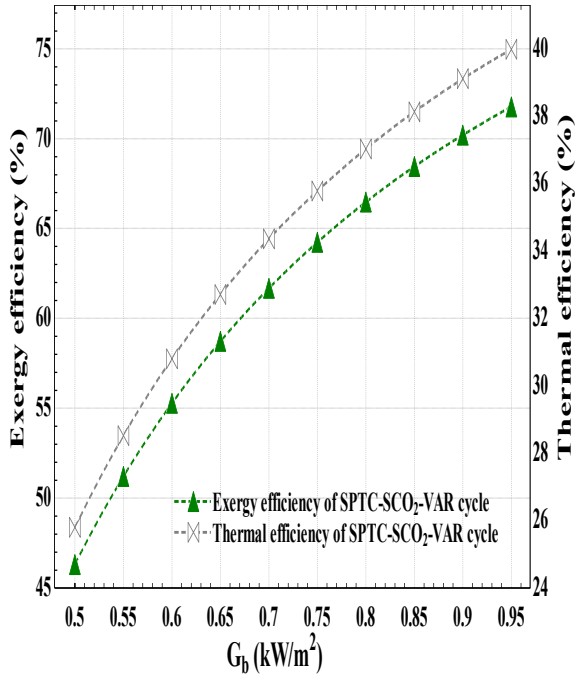

Figure 5.75. Exergy and thermal efficiency of complete plant (SPTC-SCO_2-VAR cycle) versus solar DNI

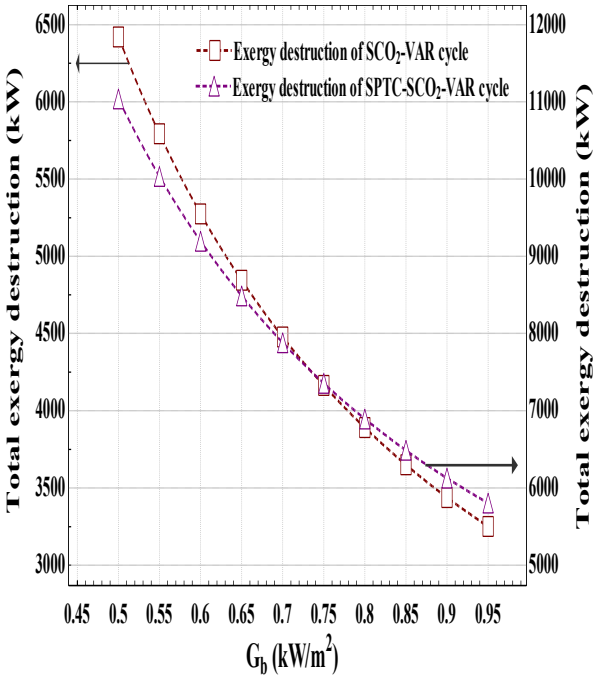

Figure 5.76. Total exergy destruction of SCO_2-VAR cycle and SPTC-SCO_2-VAR cycle versus solar DNI

It was already discussed that the rate of exergy destruction follows the reverse trend from exergy efficiency. Therefore, the Figure 5.76 illustrates that the exergy destruction rate of SCO_2-VAR cycle declines from 6421 kW at 500 W/m^2 to 3250 kW at 950 W/m^2 and exergy destruction rate of SPTC-SCO_2-VAR cycle also declines from 11039 kW at 500 W/m^2 to 5804 kW at 950 W/m^2. Lastly, it has been concluded that exergy destructions of SPTC are precisely equal to the 56.9% of total exergy destructions of complete plant. Additionally, Table 5.14 shows thermodynamic parameters (i.e. temperature, pressure, mass flow rate, & ammonia concentration) of SCO_2-VAR cycle at selected states [214].

5.3.3. Effect of variation in turbine inlet temperature on the system performance

Outlet temperature of SPTC enhances as soon as solar DNI enhances, which can be because of more heat exchanged by the sun rays to heat transfer fluid within the absorber tube that further exchanged to the SCO_2 cycle across the EV1 unit. Finally, the turbine inlet or maximum cycle temperature augments with the solar DNI simultaneously.

Table 5.14. Thermodynamic parameters of SCO_2-VAR cycle at the selected states [228,229]

Selected states	Fluids	Temperature (K)	Pressure (bar)	Mass flow rate (kg/s)	X (%NH_3)
5	SCO_2	653	250	10	-
6	SCO_2	547.5	139.1	10	-
7	SCO_2	428.2	139.1	10	-
8	SCO_2	377.7	139.1	10	-
9	SCO_2	357.7	139.1	10	-
10	SCO_2	398.3	250	10	-
4	SCO_2	480.6	250	10	-
11	NH_3	274.28	1.4	0.246	90.8
12	NH_3-H_2O	303.12	1.4	2	38
13	NH_3-H_2O	303.19	10.8	2	38
13′	NH_3-H_2O	358.1	10.8	2	38
14	NH_3-H_2O	321.9	10.8	1.754	30.6
14′	NH_3-H_2O	389.8	10.8	1.754	30.6
15	NH_3-H_2O	321.98	1.4	1.754	30.6
16	NH_3	389.8	10.8	0.246	90.8
18	NH_3	303.12	10.8	0.246	90.8
19	NH_3	254.83	1.4	0.246	90.8

Source: Mishra and Singh (2018) [214]

Now, Figure 5.77 demonstrates the effect of maximum or inlet temperature of turbine on the functioning of combined cycle (SCO_2-VAR cycle), and it has been observed that the exergy efficiency upsurges from 75.2% at 650 K to 80.13% at 920 K and thermal efficiency upsurges from 41.89% at 650 K to 44.64% at 920 K [214].

As can be observed, exergy inflow increases with the upsurge in turbine inlet temperature, as a result, turbine work output augments for a specific heat input rate, however, work of compressor do not alter so much, which in turn an increase in net work output has been noticed, therefore, enhances the exergy & thermal efficiency [89]. In a different way, there is a rise in temperature difference amongst the heat addition & heat rejection has been noticed alongside the rise in turbine inlet temperature which results in system efficiency increases [89].

In addition, Figure 5.78 displays the influence of maximum or inlet temperature of turbine over the performance of a complete plant (SPTC-SCO_2-VAR cycle), and also concluded that the exergy efficiency upsurges from 65.19% at 650 K to 68.5% at 920 K and thermal

efficiency upsurges from 36.32% at 650 K to 38.16% at 920 K. On the other side, Figure 5.79 depicts that exergy destruction rate of the SCO_2-VAR cycle declines from 4450 kW at 650 K to 3636 kW at 920 K and exergy destruction rate of the SPTC-SCO_2-VAR cycle also declines from 7156 kW at 650 K to 6476 kW at 920 K [214].

Furthermore, Figure 5.80 indicates the effect of maximum or inlet temperature of turbine on the thermodynamic constraints such as network output ($\dot{W}_{net}$) of the SCO_2-VAR cycle, i.e. rises from 1570 kW at 650 K to 1668 kW at 920 K and heat transfer rate in EV2 ($\dot{Q}_{EV2}$) reduces somewhat from 143.5 kW at 650 K to 116.5 kW at 920 K that further reduces the cooling exergy rate because of constant temperature of both evaporator and ambient [214].

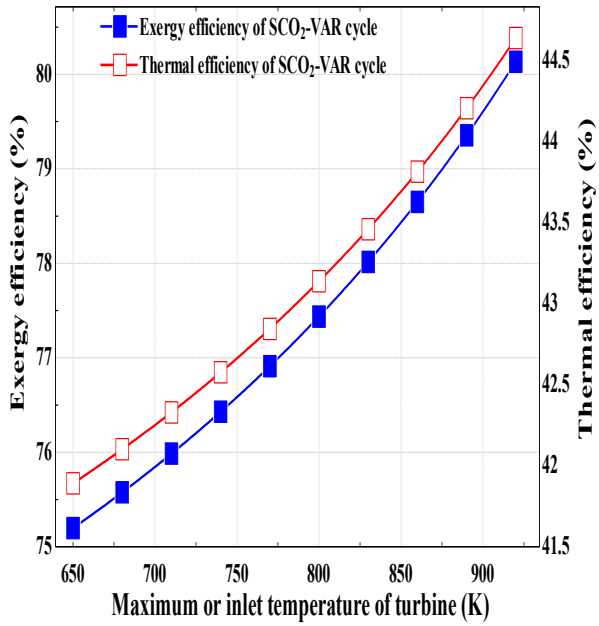

Figure 5.77. Exergy and thermal efficiency of combined cycle without solar collector (SCO_2-VAR cycle) versus turbine inlet temperature

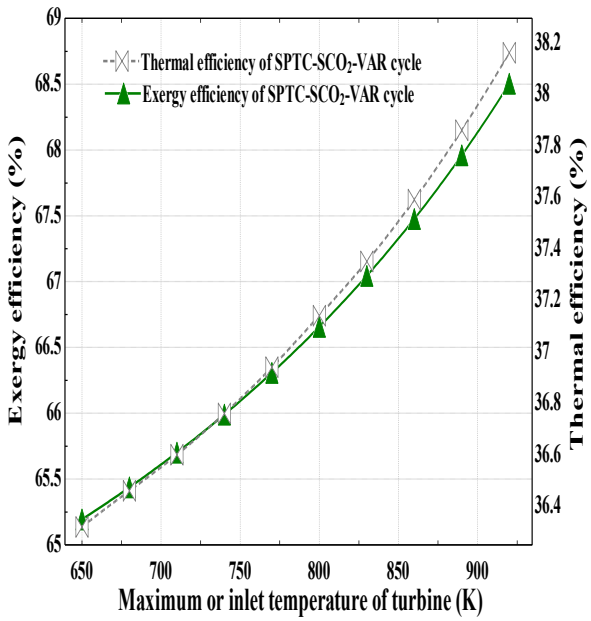

Figure 5.78. Exergy and thermal efficiency of complete plant (SPTC-SCO_2-VAR cycle) versus turbine inlet temperature

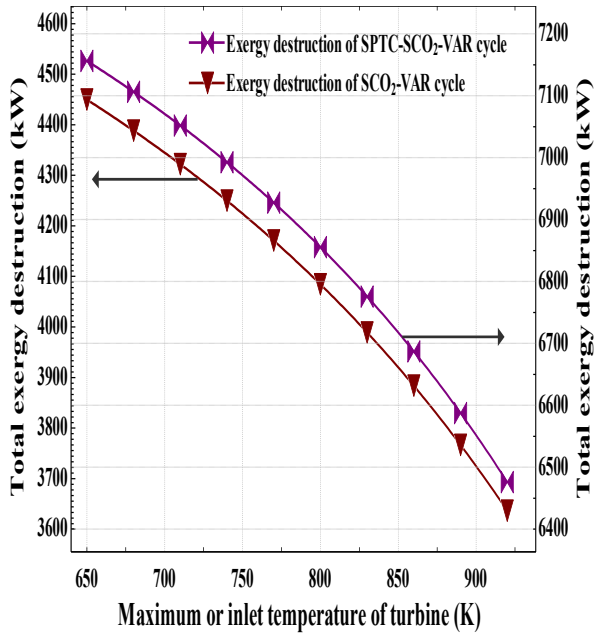

Figure 5.79. Total exergy destruction of SCO_2-VAR cycle and SPTC-SCO_2-VAR cycle versus turbine inlet temperature

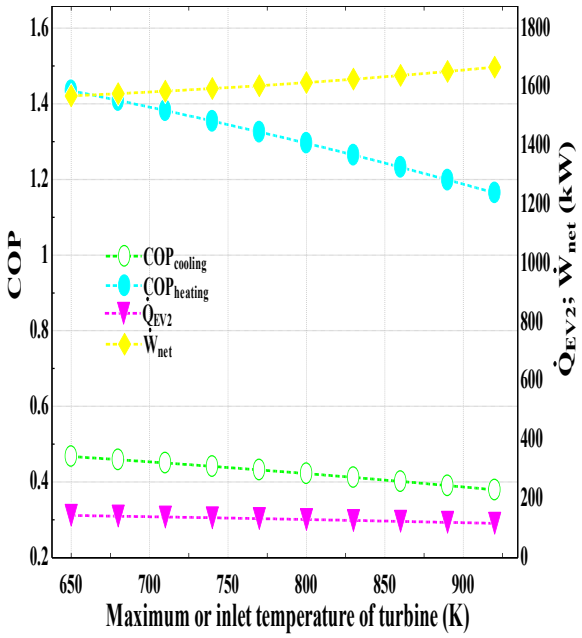

Figure 5.80. Effect of turbine inlet temperature on the $COP_{cooling}$, $COP_{heating}$, $\dot{W}_{net}$, and $\dot{Q}_{EV2}$ [214]

However, it has been noticed from the Figure 5.80 that the incremental change in $\dot{W}_{net}$ is greater than the detrimental change of $\dot{Q}_{EV2}$, which turns in both thermal and exergy efficiency continuously rises as the maximum or inlet temperature of turbine rises from 650 K to 920 K. Lastly, Figure 5.80 also depicts that the $COP_{cooling}$ decreases from 0.4675 at 650 K to 0.3794 at 920 K and $COP_{heating}$ decreases from 1.435 at 650 K to 1.164 at 920 K [214].

5.3.4. Effect of variation in compressor pressure ratio on the system performance

This section discusses influence of compressor pressure ratio over combined cycle (SCO_2-VAR cycle) performance has been discussed, and noted that at a constant turbine inlet temperature of 653 K, an increase in compressor's work consumption and turbine's work output has been seen as the compressor pressure ratio increases. In addition, work output amount of turbine is relatively much higher than that of work consumed by compressor and therefore, network output ($\dot{W}_{net}$) increases.

Figure 5.81 indicates that as the compressor pressure ratio enhances from 1.37 to 2.67, the exergy & thermal efficiency of SCO_2-VAR cycle upsurges from 78.14% to

81.51% & 43.53% to 45.41%, correspondingly. Also, Figure 5.82 depicts that as the compressor pressure ratio enhances from 1.37 to 2.67, the exergy & thermal efficiency of complete plant (SPTC-SCO_2-VAR cycle) upsurges from 66.75% to 69.74% and 37.19% to 38.85%, correspondingly [214].

Instead, Figure 5.83 demonstrates that exergy destruction rate of SCO_2-VAR cycle and SPTC-SCO_2-VAR cycle decreases from 4001 kW to 3383 kW and 6837 kW to 6221 kW, respectively as the compressor pressure ratio augments from 1.37 to 2.67 [214].

Besides, compressor outlet temperature increases as the compressor pressure ratio rises, as a result, temperature at the recuperator outlet (T_7) upsurges because of low amount heat transfer from the hot stream to cold stream of SCO_2, therefore, extra heat will be offered for a VAR cycle. Consequently, the $COP_{cooling}$ of VAR cycle upsurges from 0.3382 to 0.4722, and $COP_{heating}$ of VAR cycle upsurges from 0.9759 to 1.207, respectively with increase in compressor pressure ratio 1.37 to 2.67 as shown in Figure 5.84. But as soon as temperature of generator enhances beyond a limit, the system's COP turns to decline slowly owing to rising amount of exergy destructions in the VAR cycle [214].

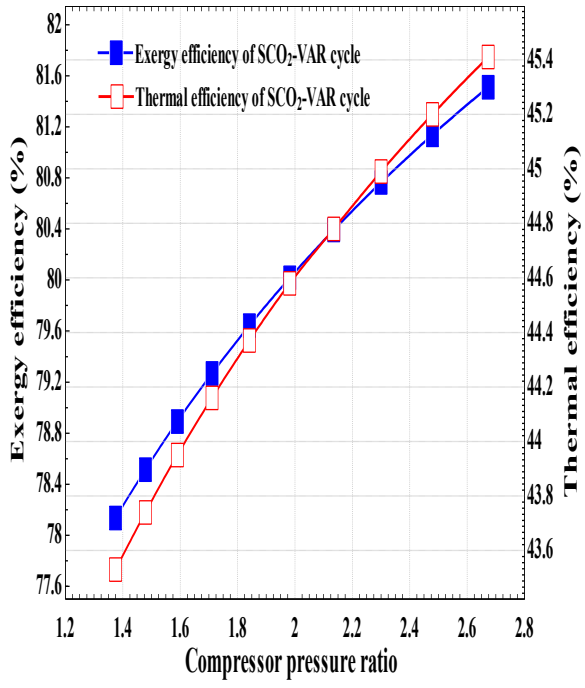

Figure 5.81. Exergy and thermal efficiency of combined cycle without solar collector (SCO_2-VAR cycle) versus compressor pressure ratio

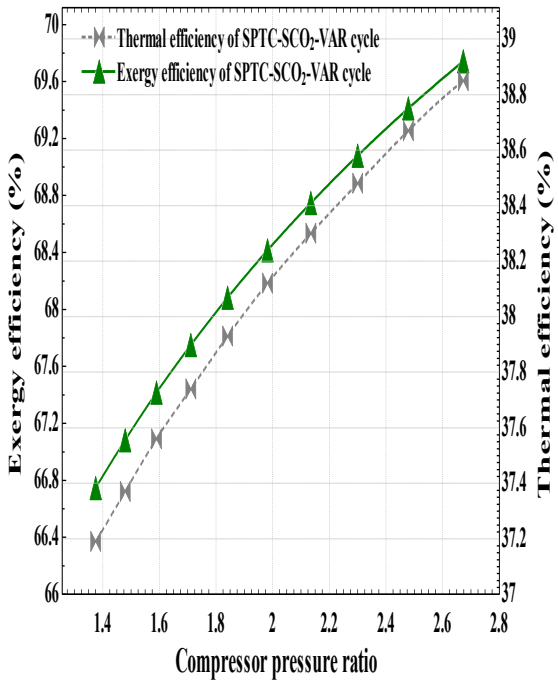

Figure 5.82. Exergy and thermal efficiency of complete plant (SPTC-SCO_2-VAR cycle) versus compressor pressure ratio

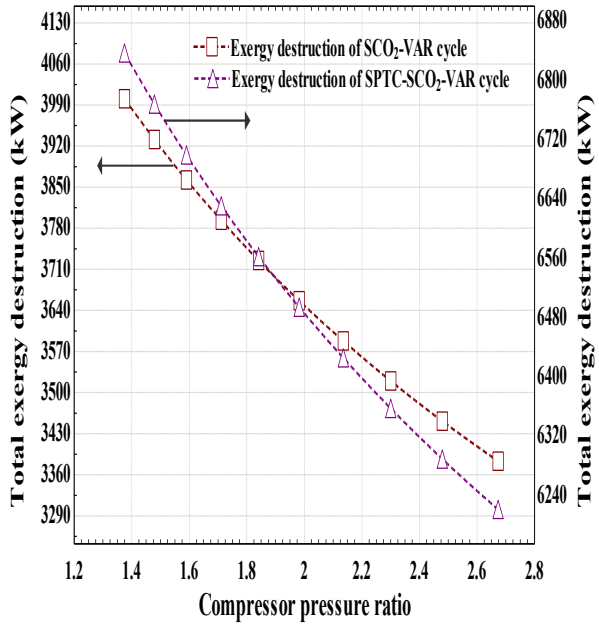

Figure 5.83. Total exergy destruction of SCO_2-VAR cycle and SPTC-SCO_2-VAR cycle versus compressor pressure ratio

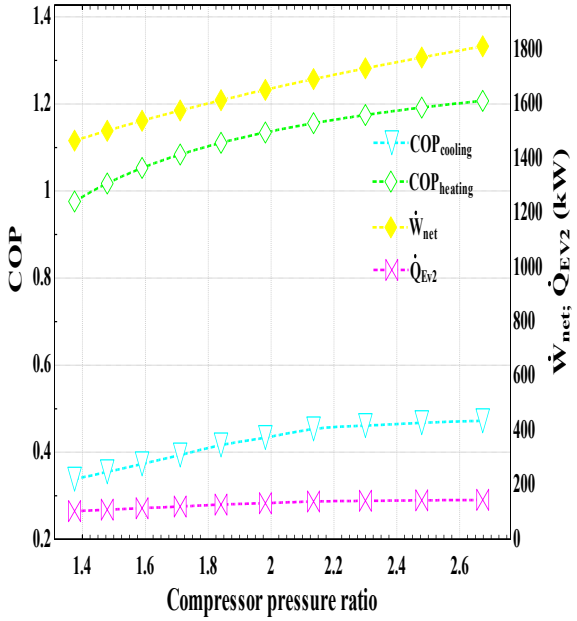

Figure 5.84. Effect of the compressor pressure ratio on $COP_{cooling}$, $COP_{heating}$, $\dot{W}_{net}$, and $\dot{Q}_{EV2}$ [214]

Moreover, Figure 5.84 demonstrates that as the compressor pressure ratio upsurges from1.37 to 2.67, the $\dot{Q}_{EV2}$ also upsurges from 103.8 kW to 145 kW, therefore, the cooling exergy rate also enhances simultaneously. However, the $\dot{W}_{net}$ increases from 1466 kW to 1813 kW. Lastly, it is understood from the Figure 5.84 that $\dot{W}_{net}$ has a dominance over $\dot{Q}_{EV2}$ which is a reason for the enhancement of thermal and exergy efficiency [214].

5.3.5. Effect of compressor inlet temperature on the system performance

In this section, the influence of inlet temperature of compressor over performance of combined cycle (SCO_2-VAR cycle) has been discussed. Figure 5.85 indicates that as the compressor inlet temperature rises from 300 K to 312 K, the exergy and thermal efficiency decreases from 81.29% to 80.39% and 45.29% to 44.78%, respectively. Whereas, the Figure 5.86 depicts that as the compressor inlet temperature increases from 300 K to 312 K, the exergy and thermal efficiency of complete plant (SPTC-SCO_2-VAR cycle) reduces from 69.54% to 68.75% and 38.74% to 38.3%, correspondingly. Alternatively, Figure 5.87 shows that rate of exergy destruction for the SCO_2-VAR cycle and SPTC-SCO_2-VAR cycle increases from 3424 kW to 3588 kW and 6262 kW to 6426 kW, correspondingly with

increase in compressor inlet temperature from 300 K to 312 K [214]. We have discussed earlier that as the inlet temperature of compressor upsurges, the specific heat capacity of CO_2 reduces (i.e. far from the critical point), which further decreases the compressor's specific enthalpy inflow. Consequently, the compressor work upsurges remarkably but SCO_2 turbine's work do not affected so much in the meantime which means that the net work output reduces, and finally exergy & thermal efficiency also reduces simultaneously. This fact can be explained in other way that the difference amongst the cycle's maximum & minimum temperature reduces as the compressor inlet temperature rises, subsequently, the cycle efficiency decreases [89].

In addition, Figure 5.88 demonstrates that with the enhancement of compressor inlet temperature from 300 K to 312 K, the net work output declines from 1788 kW to 1692 kW. However, the $\dot{Q}_{EV2}$ upsurges from 100.7 kW to 113.9 kW. Moreover, Figure 5.88 illustrates that the $COP_{cooling}$ of VAR cycle rises from 0.348 to 0.3936 and $COP_{heating}$ of VAR cycle rises from 1.207 to 1.239 with the augmentation of compressor inlet temperature from 300 K to 312 K, which can be because of the definite amount of heat extraction by compressor from the generator side that further reduces the rate of heat transfer from heating coil to generator, thus, temperature of generator decreases simultaneously [214].

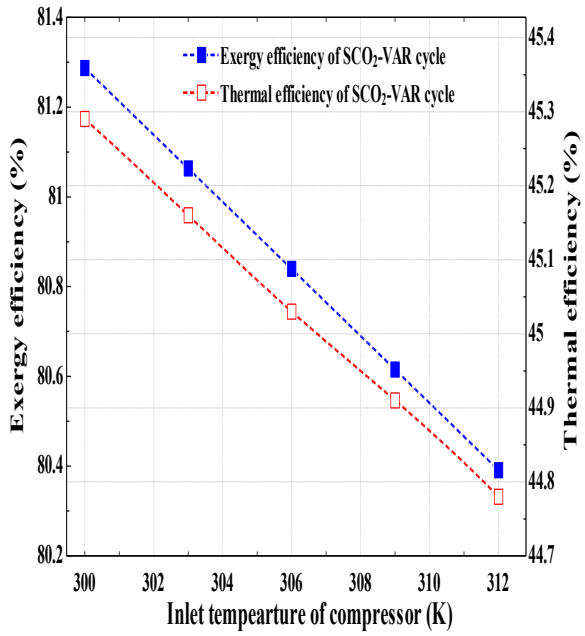

Figure 5.85. Exergy and thermal efficiency of combined cycle without solar collector (SCO_2-VAR cycle) versus inlet temperature of compressor

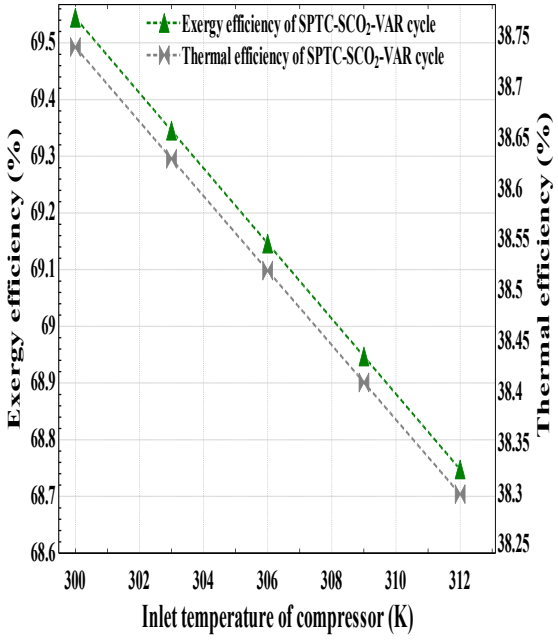

Figure 5.86. Exergy and thermal efficiency of complete plant (SPTC-SCO_2-VAR cycle) versus inlet temperature of compressor

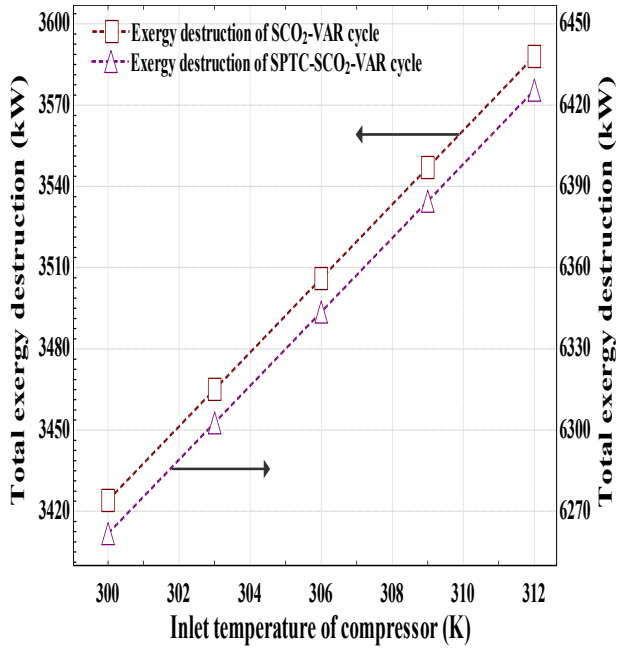

Figure 5.87. Total exergy destruction of SCO_2-VAR cycle and SPTC-SCO_2-VAR cycle versus inlet temperature of compressor

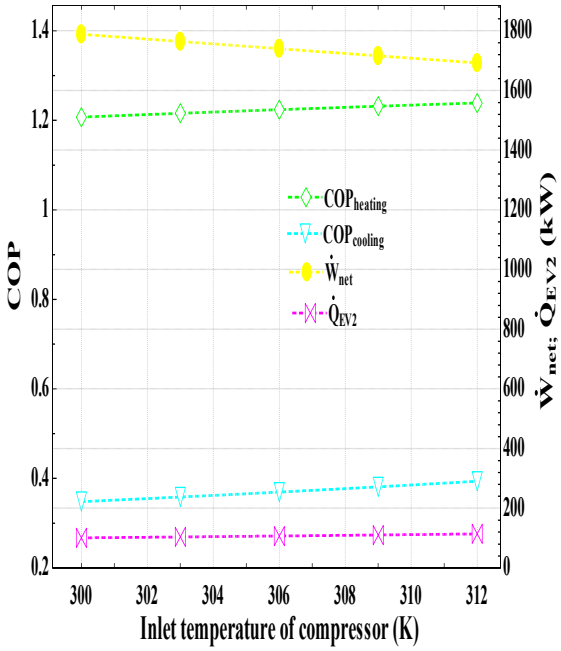

Figure 5.88. Effect of inlet temperature of compressor on the $COP_{cooling}$, $COP_{heating}$, $\dot{W}_{net}$, and $\dot{Q}_{EV2}$ [214]

5.3.6. Effect of variation in generator temperature on the system performance

Now Figure 5.89 illustrates effect of generator temperature over the performance of combined cycle (SCO_2-VAR cycle), and it has been found that exergy efficiency slightly decreases from 80.75% to 79.64% and thermal efficiency also slightly decreases from 44.98% to 44.37% with the increase in generator temperature from 365 K to 401 K [214].

Whereas, Figure 5.90 depicts the influence of generator temperature over the performance of the complete plant (SPTC-SCO_2-VAR cycle), and revealed that the exergy efficiency reduces marginally from 69.07% to 68.08% and thermal efficiency also decreases slightly from 38.48% to 37.93% with the augmentation in generator temperature from 365 K to 401 K. Alternatively, Figure 5.91 displays that the exergy destruction rate of SCO_2-VAR cycle and SPTC-SCO_2-VAR cycle upsurges from 3523 kW to 3725 kW and 6359 kW to 6563 kW, respectively as the generator temperature upsurges from 365 K to 401 K [214].

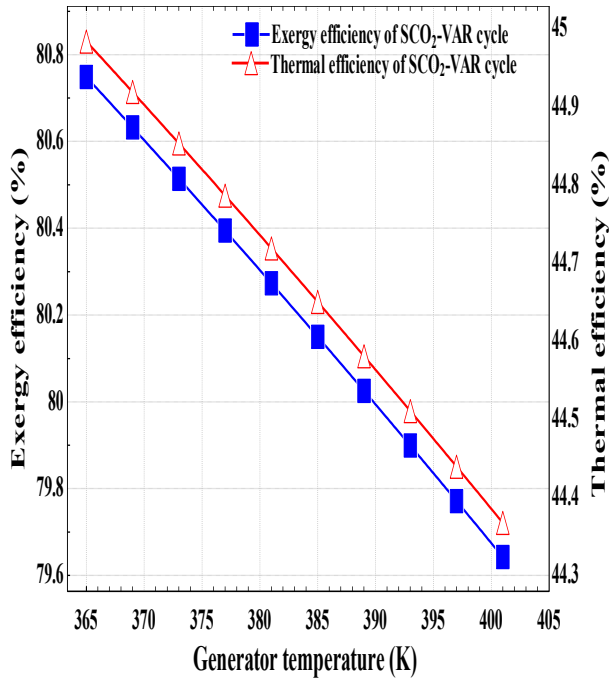

Figure 5.89. Exergy and thermal efficiency of combined cycle without solar collector (SCO_2-VAR cycle) versus generator temperature

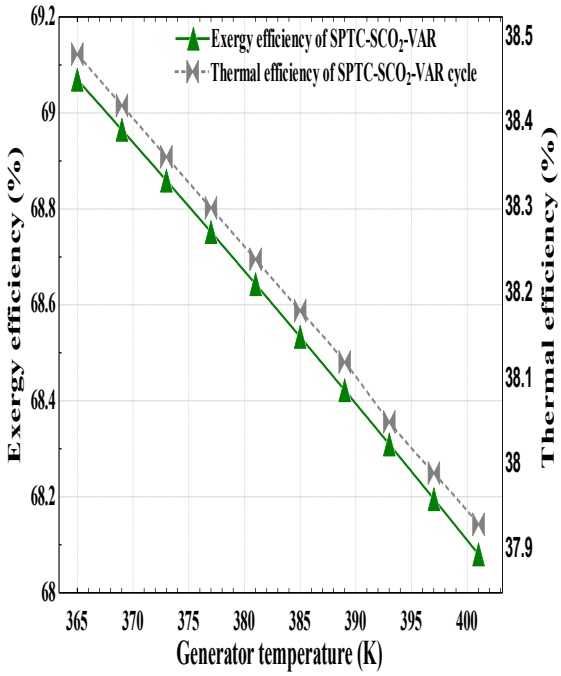

Figure 5.90. Exergy and thermal efficiency of complete plant (SPTC-SCO_2-VAR cycle) versus generator temperature

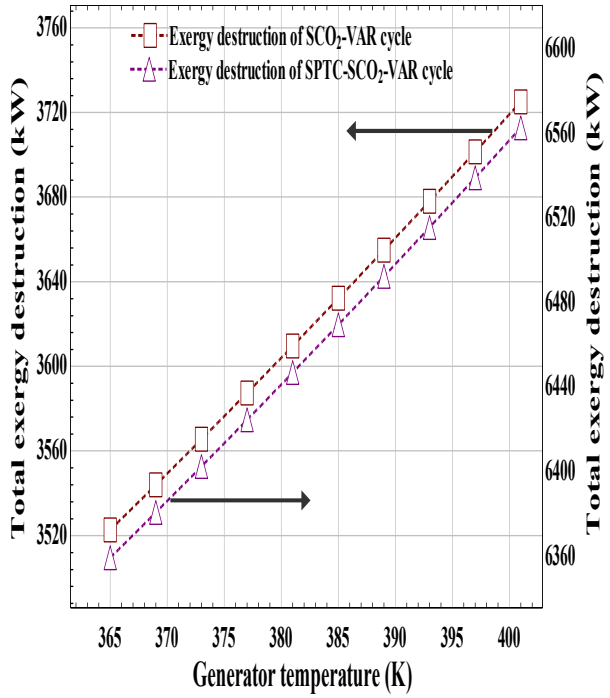

Figure 5.91. Total exergy destruction of SCO_2-VAR cycle and SPTC-SCO_2-VAR cycle versus generator temperature

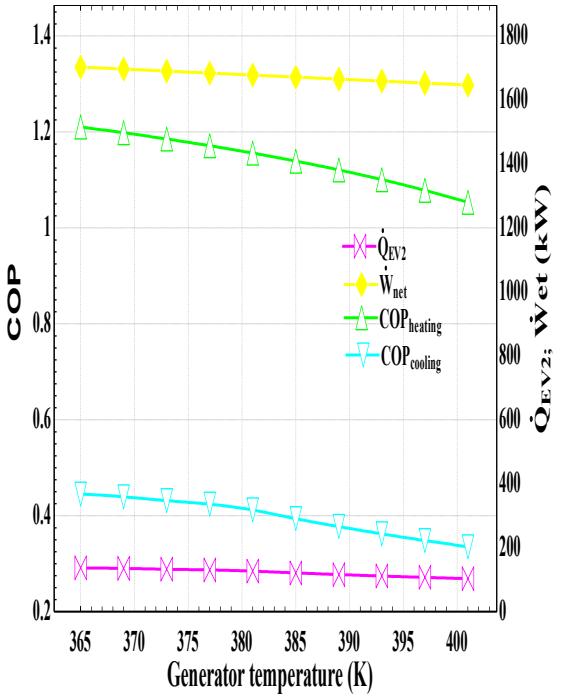

Figure 5.92. Effect of generator temperature on the $COP_{cooling}$, $COP_{heating}$, $\dot{W}_{net}$, and $\dot{Q}_{EV2}$ [214]

Furthermore, Figure 5.92 demonstrates that the $COP_{cooling}$ and $COP_{heating}$ declines from 0.4448 to 0.3351 and 1.21 to 1.053, correspondingly with increase in generator temperature from 365 K to 401 K [214].

The explanation for falling efficiency and COP is that with the increase in generator temperature, the temperature of running refrigerant leaving the generator enhances that can further augment the average temperature of absorber & condenser unit in VAR cycle that results in more heat transfer losses or exergy losses happen at higher generator temperature. Therefore, Figure 5.92 indicates that the $\dot{W}_{net}$ somewhat declines from 1702 kW to 1646 kW and $\dot{Q}_{EV2}$ similarly reduces from 136.5 kW to 102.9 kW with in definite range of generator temperature (i.e. 365 K to 401 K) [214].

5.3.7. Effect of variation in absorber and condenser temperature on the system performance

In this section, Figure 5.93 shows the effect of absorber and condenser temperature over the performance of combined cycle (SCO_2-VAR cycle), and observed that the exergy efficiency decreases from 79.88% to 76.62% and thermal efficiency decreases from 44.5% to 42.69% as the absorber & condenser temperature upsurges from 315 K to 351 K. Whereas, in case of complete plant (SPTC-SCO_2-VAR cycle), the exergy efficiency decreases from 68.29% to 65.44% and thermal efficiency decreases from 38.04% to 36.46% as the absorber and condenser temperature upsurges from 315 K to 351 K as described in Figure 5.94 [214].

Alternatively, Figure 5.95 illustrates that the exergy destruction rate of SCO_2-VAR cycle and SPTC-SCO_2-VAR cycle upsurges from 3682 kW to 4277 kW and 6520 kW to 7106 kW, respectively with the increase in temperature of absorber & condenser from 315 K to 351 K [214].

In addition, Figure 5.96 depicts that the $COP_{cooling}$ and $COP_{heating}$ declines from 0.2522 to 0.1682 and 1.411 to 1.197, correspondingly as the temperature of absorber & condenser upsurges from 315 K to 351 K. The decline in efficiency and COP can be due to increase in pressure of generator correspondingly with the increase in temperature of absorber and condenser, as a result, less ammonia vapour permitted to release from the generator [213].

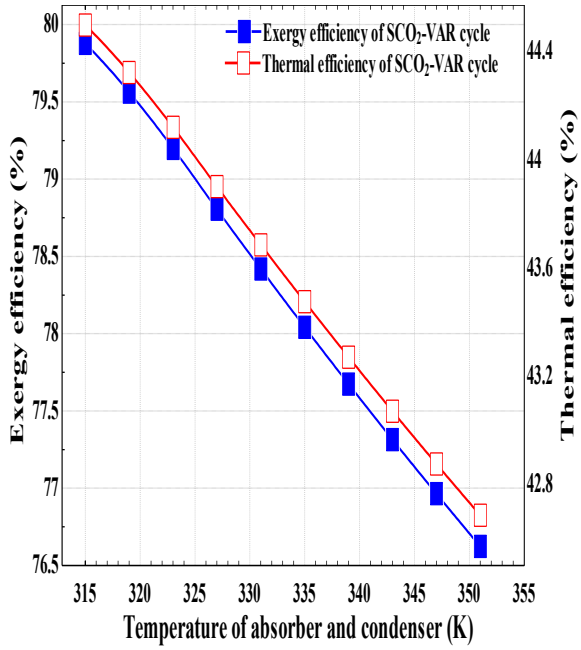

Figure 5.93. Exergy and thermal efficiency of combined cycle without solar collector (SCO_2-VAR cycle) versus temperature of absorber and condenser

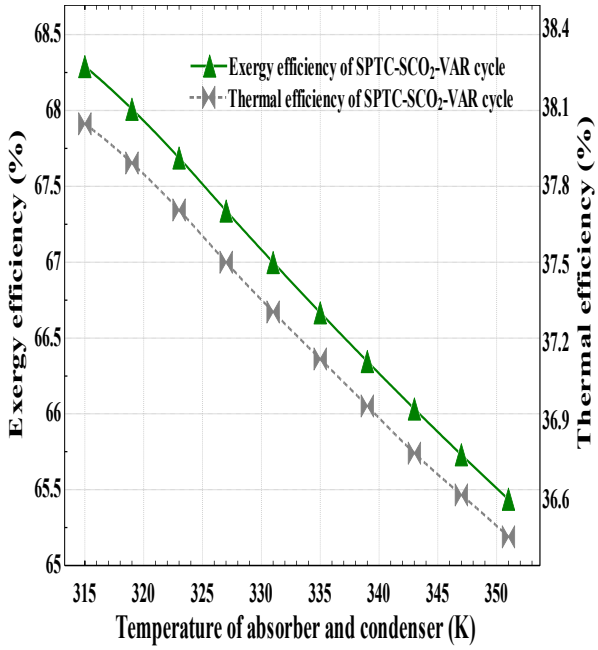

Figure 5.94. Exergy and thermal efficiency of complete plant (SPTC-SCO_2-VAR cycle) versus temperature of absorber and condenser

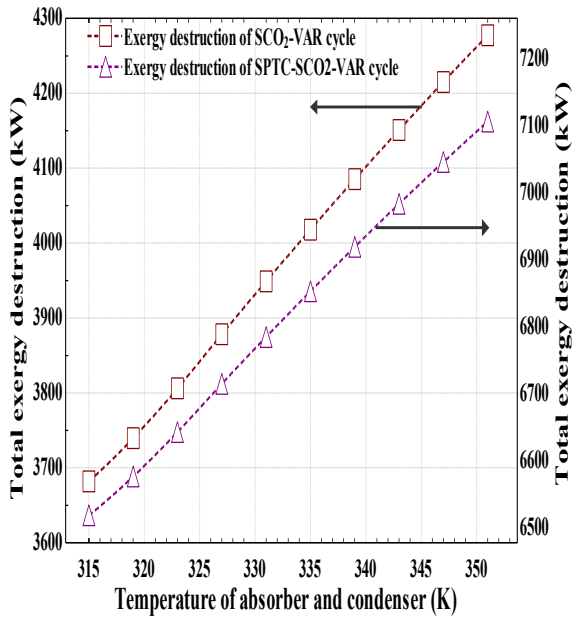

Figure 5.95. Total exergy destruction of SCO_2-VAR cycle and SPTC-SCO_2-VAR cycle versus temperature of absorber and condenser

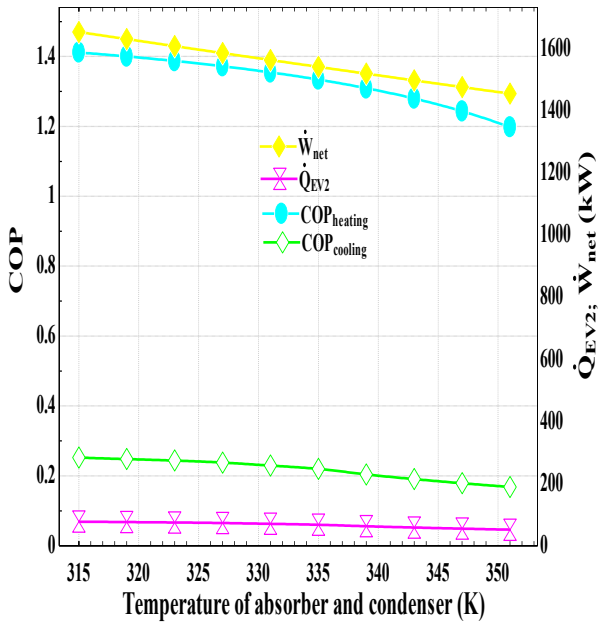

Figure 5.96. Effect of the temperature of absorber and condenser on the $COP_{cooling}$, $COP_{heating}$, $\dot{W}_{net}$, and $\dot{Q}_{EV2}$ [214]

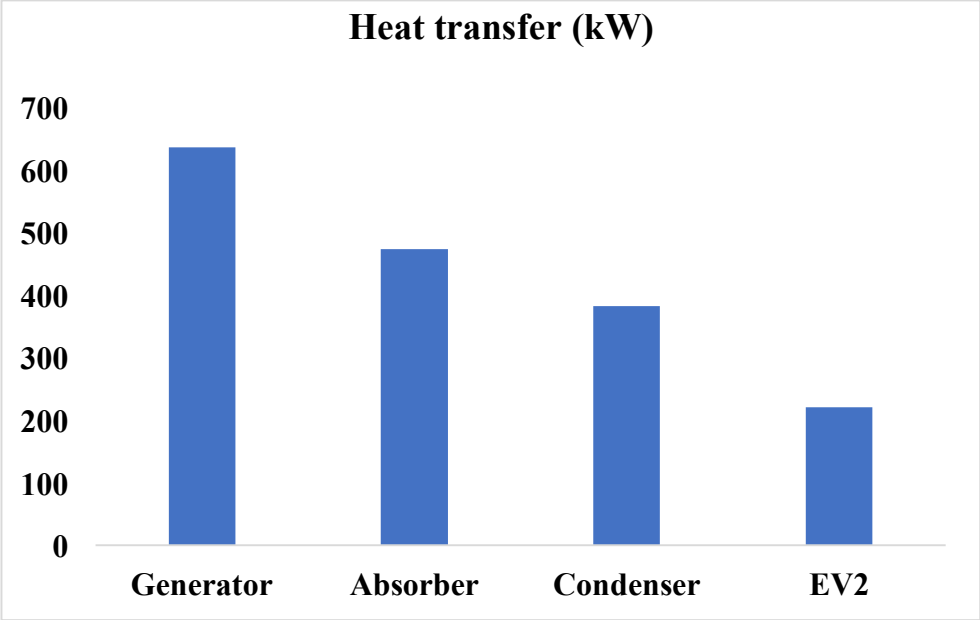

Figure 5.97. Heat transfer in main components of VAR cycle [214]

Accordingly, exergy destruction enhances and performance of system could be lower. In a different way, if the absorber temperature rises, both pump work and heat duty of generator enhances that outcomes in input exergy to generator also enhances in contrast to the exergy needed to generate cooling effect that remains constant. Subsequently, exergy performance reduces. Besides, due to the constant refrigerant mass flow rate, the EV2 load remains uniform that outcomes in COP reduces [234].

Likewise, Figure 5.96 depicts that with the increase in absorber & condenser temperature from 315 K to 351 K, the $\dot{W}_{net}$ of SCO_2-VAR cycle declines from 1654 kW to 1455 kW and $\dot{Q}_{EV2}$ also declines from 77.42 kW to 51.63 kW. Lastly, Figure 5.97 illustrates the heat transfer load in different essential components of VAR cycle [214].

5.3.8. Validation of SCO_2 cycle and VAR cycle

In this portion, the validation of SCO_2 cycle & VAR cycle has been presented. In this direction, the thermal efficiency results of SCO_2 cycle have been compared with the outcomes computed by the Besarati et al. [172] and Wang et al. [235] at the identical fixed baseline conditions as registered in Table 5.12.

Table 5.15. Validation results of SCO_2 topping cycle

Cycle	Literature work	Results of thermal efficiency in literature work	Results of thermal efficiency estimated in present work	Error approximation
SCO_2	Besarati et al. [172]	0.4507	0.4333	-3.8%
SCO_2	Wang et al. [235]	0.3770	0.3619	-4%

Source: Mishra and Singh (2018) [214]

Moreover, the $COP_{cooling}$ and $COP_{heating}$ of VAR cycle also have been compared with the results computed by the Gupta et al. [213] and Anand et al. [236] at the similar fixed baseline conditions as registered in Table 5.13. Conclusively, it has been estimated from the current study outcomes that the existing model is in good arrangement alongside the results found from the literature work.

Table 5.16. Validation results of VAR bottoming cycle

Cycle	Literature work	Results in literature work		Results estimated in present work	
		$COP_{cooling}$	$COP_{heating}$	$COP_{cooling}$	$COP_{heating}$
VAR	Gupta et al. [213]	0.4042	1.404	0.3792	1.344
VAR	Anand et al. [236]	0.381	1.381	0.358	1.327

Source: Mishra and Singh (2018) [214]

5.4. SPTC integrated with supercritical ORC (SORC)

In last objective, the energy and exergy analysis of SORC has been discussed. The SORC system has been directly operated with the help of SPTC heat source. The computer based program through the EES software has been applied to analyse the effect of various operating parameters, for instance solar DNI (G_b), inlet pressure of SORC turbine, and effectiveness of recuperator on the performance of system. In addition, six organic fluids such as cyclohexane, isopentane, propane, R600a, n-Hexane, and n-Pentane have been chosen for the SORC system regarding the available fixed exit temperature of SPTC (i.e. 300℃).

5.4.1. Effect of variation in solar DNI on the performance of SORC system

Figure 5.98 indicates the influence of solar DNI on exergy efficiency of SPTC incorporated SORC (SPTC-SORC) which has been analysed under the fixed baseline conditions such as inlet turbine pressure of 8 MPa which is fixed in order to maintain the supercritical conditions and mass flow rate of 2 kg/s, and it has been found that Propane based SPTC-SORC has a highest exergy efficiency which is increases from 67.89% at 500 W/m^2 to 83.15% at 950 W/m^2. Alternatively, isopentane fluid based SPTC-SORC system has a lowest exergy efficiency, which is increases from 55.19% at 500 W/m^2 to 76.49% at 950 W/m^2. However, the exergy efficiency of fluids such as cyclohexane, R600a, n-Hexane, and n-Pentane lies in between these two above mentioned fluids with a maximum value of 81.25%, 80.06%, 79.67%, and 79.24% at 950 W/m^2, respectively as illustrated in Figure 5.98.

On the other hand, Figure 5.99 displays the influence of solar DNI on the thermal efficiency of the SPTC-SORC system which has been analysed under the same baseline conditions as mentioned above, and it has been concluded that propane based SPTC-SORC system has a highest thermal efficiency, which is increases from 32.58% at 500 W/m^2 to 39.9% at 950 W/m^2. Alternatively, isopentane fluid based SPTC-SORC system has a lowest thermal efficiency, which is increases from 26.48% at 500 W/m^2 to 36.7% at 950 W/m^2. Whereas, the thermal efficiency of fluids such as cyclohexane, R600a, n-Hexane, and n-Pentane lies in between these two above mentioned fluids with a maximum value of

38.98%, 38.41%, 38.23%, and 38.02% at 950 W/m^2, respectively as indicated in Figure 5.99.

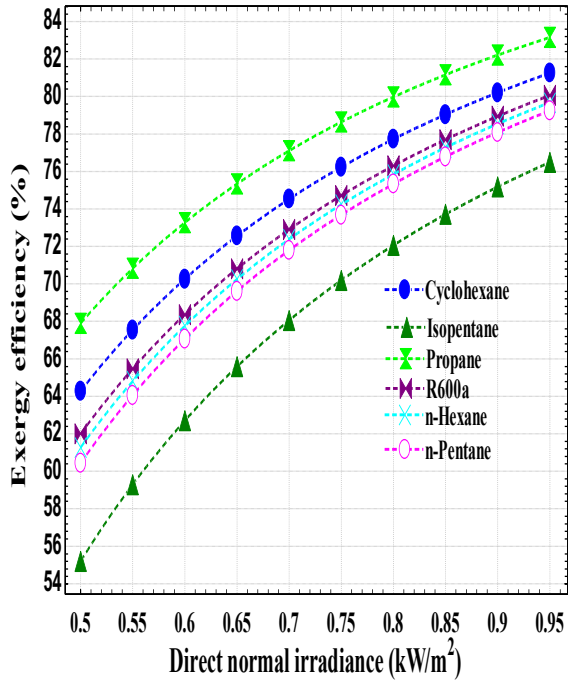

Figure 5.98. Exergy efficiency of SPTC integrated SORC system versus solar DNI

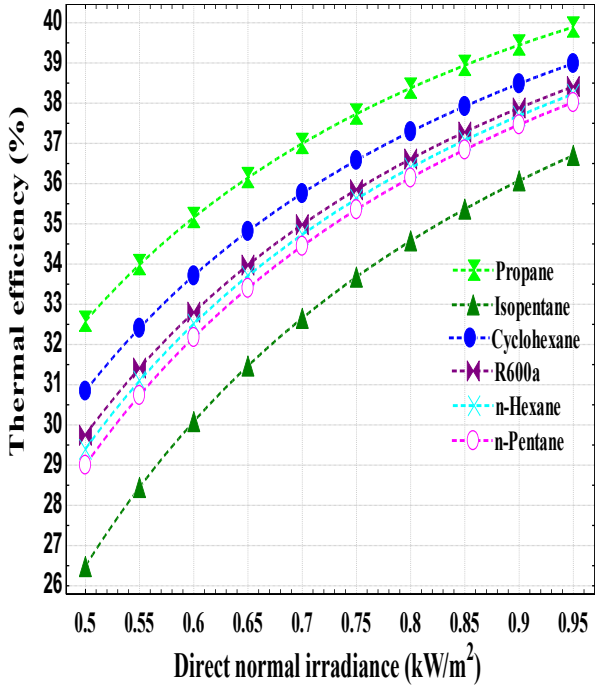

Figure 5.99. Thermal efficiency of SPTC integrated SORC system versus solar DNI

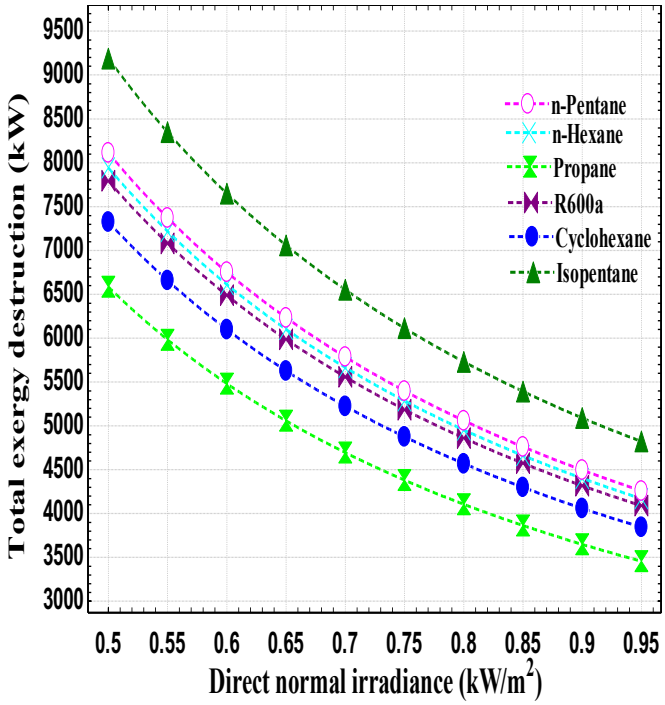

Figure 5.100. Total exergy destruction of SPTC integrated SORC system versus solar DNI

Apart from this, Figure 5.100 demonstrates the effect of solar DNI on the total exergy destruction rate of SPTC-SORC system, and it has been reveal that isopentane fluid

based SPTC-SORC system has a maximum exergy destruction rate, which is decreases from 9189 kW at 500 W/m^2 to 4821 kW at 950 W/m^2. Alternatively, propane fluid based SPTC-SORC system has a minimum exergy destruction rate, which is decreases from 6585 kW at 500 W/m^2 to 3455 kW at 950 W/m^2. However, the exergy destruction rate of fluids such as n-Pentane, n-Hexane, R600a, and cyclohexane lies in between the above-mentioned fluids with a maximum value of 8113 kW, 7943 kW, 7793 kW, and 7325 kW at 500 W/m^2, respectively as illustrated in Figure 5.100. Lastly, in case of propane fluid based SPTC-SORC, it has been concluded that more than 80% of total exergy destruction rate was found to be only in SPTC system. Lastly, thermodynamic parameters (i.e. temperature and pressure) for the selected stations of SPTC-SORC system has been listed in Table 5.106.

Table 5.17. Temperature and pressure for the selected stations of SPTC-SORC [228,229]

Selected stations	Fluid type	P (bar)	T (K)
SPTC inlet (1)	Syltherm 800	100	478.3
SPTC outlet (3)	Syltherm 800	100	573.1
SORC Turbine inlet (5)	Propane	80	538.2
SORC Turbine outlet (6)	Propane	28.57	456.4
Recuperator outlet (7)	Propane	28.57	332.8
Condenser outlet (10)	Propane	28.57	319.6
Pump outlet (11)	Propane	80	324.4
Recuperator outlet (4)	Propane	80	438.7

5.4.2. Effect of variation in turbine inlet pressure on the performance of SORC system

Figure 5.101 demonstrates the effect of inlet pressure of turbine on the exergy efficiency of the SPTC-SORC system, which has been analysed under the fixed baseline conditions such as solar DNI of 850 W/m^2, maximum turbine temperature of 538.2 K, and mass flow rate of 2 kg/s in SORC, and it has been concluded that propane fluid based SPTC-SORC system has a highest exergy efficiency, which is increases from 81.04% at 50 bar to 81.19% at 86 bar. Alternatively, isopentane fluid based SPTC-SORC system has a lowest exergy efficiency, which is increases from 73.06% at 50 bar to 74.34% at 86 bar. While the

exergy efficiency of fluids such as cyclohexane, n-Hexane, R600a, and n-Pentane lies in between these above-mentioned fluids with a maximum value of 80.25%, 79.21%, 78.13%, and 77.36% at 86 bar, respectively as shown in Figure 5.101.

On the other side, Figure 5.102 depicts the effect of inlet pressure of turbine on the thermal efficiency of the SPTC-SORC system, which has been analysed under the same baseline conditions as mentioned above, and it has been observed that propane fluid based SPTC-SORC system has a highest thermal efficiency, which is increases from 38.88% at 50 bar to 38.96% at 86 bar. Conversely, isopentane fluid based SPTC-SORC system has a lowest thermal efficiency, which is increases from 34.98% at 50 bar to 35.68% at 86 bar. Whereas, the thermal efficiency of fluids such as cyclohexane, n-Hexane, R600a, and n-Pentane lies in between these above-mentioned fluids with a maximum value of 38.5%, 38%, 37.49%, and 37.12% at 86 bar, respectively as described in Figure 102.

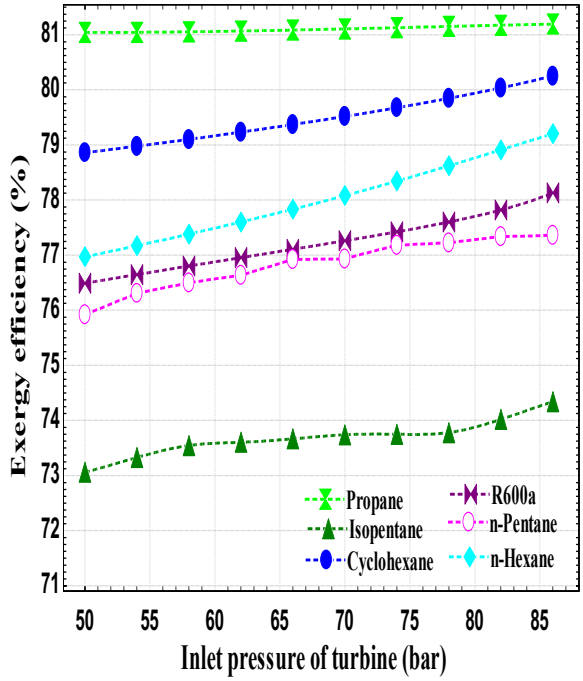

Figure 5.101. Exergy efficiency of SPTC integrated SORC system versus inlet pressure of turbine

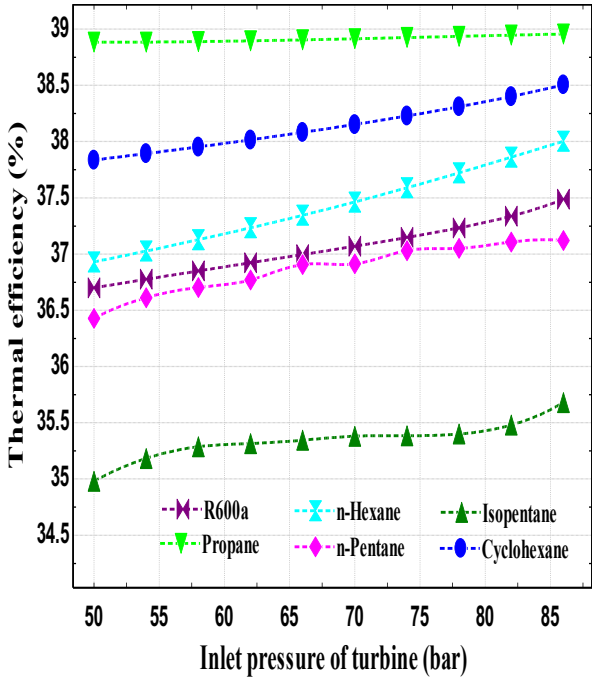

Figure 5.102. Thermal efficiency of SPTC integrated SORC system versus inlet pressure of turbine

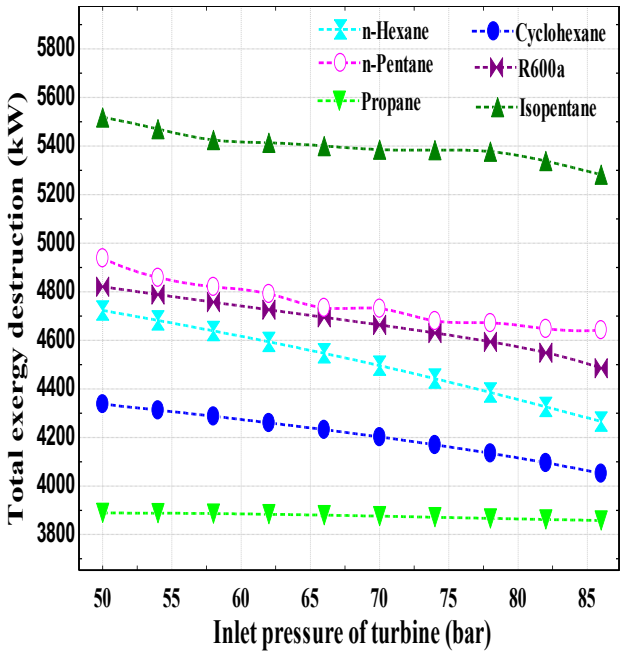

Figure 5.103. Total exergy destruction of SPTC integrated SORC system versus inlet pressure of turbine

Apart from this, Figure 5.103 demonstrates the influence of inlet pressure of turbine on the total exergy destruction rate of SPTC-SORC system, and it has been found that isopentane fluid based SPTC-SORC system has a highest exergy destruction rate, which is decreases from 5518 kW at 50 bar to 5222 kW at 86 bar. Alternatively, propane fluid based SPTC-SORC system has a lowest exergy destruction rate, which is decreases from 3889 kW at 50 bar to 3858 kW at 86 bar. However, the exergy destruction rate of fluids such as n-Pentane, R600a, n-Hexane, and cyclohexane lies in between above mentioned fluids with a maximum value of 4938 kW, 4821 kW, 4723 kW, and 4337 kW at 50 bar, respectively as shown in Figure 5.103.

5.4.3. Effect of variation in recuperator effectiveness on the performance of SORC system

Figure 5.104 depicts that exergy efficiency of SPTC-SORC system upsurges with the upsurge in effectiveness of the recuperator, and it has been found that propane fluid based SPTC-SORC system has a highest value of exergy efficiency, which is increases slightly from 80.89% to 81.89% as the effectiveness increases from 70% to 97%. Alternatively, isopentane fluid based SPTC-SORC system has a lowest value of exergy efficiency, which is increases from 73.41% to 77.66% as the effectiveness increases from

70% to 97%. Whereas, the exergy efficiency of fluids such as cyclohexane, R600a, n-Hexane, and n-Pentane lies in between these two above mentioned fluids with a maximum value of 80.93%, 79.78%, 78.88%, and 78.45% at effectiveness of 97%, respectively as illustrated in Figure 5.104.

Also, Figure 5.105 demonstrates that thermal efficiency also enhances as the effectiveness of recuperator enhances, and it has been concluded that propane fluid based SPTC-SORC system has a maximum value of thermal efficiency, which is increases slightly from 38.81% to 39.29% as the effectiveness increases from 70% to 97%. Conversely, isopentane based SPTC-SORC system has a minimum value of thermal efficiency, which is increases from 35.22% to 37.26% as the effectiveness increases from 70% to 97%. However, the thermal efficiency of fluids such as cyclohexane, R600a, n-Hexane, and n-Pentane lies in between these two above mentioned fluids with a highest value of 38.83%, 38.28%, 37.85%, and 37.64% at effectiveness of 97%, respectively as illustrated in Figure 5.105.

Apart from this, Figure 5.106 indicates that total exergy destruction rate of SPTC-SORC system reduces with the increases in effectiveness of the recuperator and it has been concluded that isopentane fluid based SPTC-SORC has a highest exergy destruction rate, which is decreases from 5452 kW to 4581 kW as the effectiveness increases from 70% to 97%.

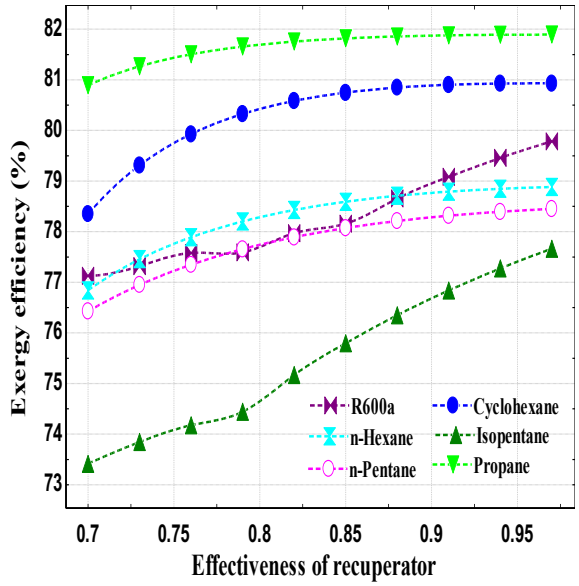

Figure 5.104. Exergy efficiency of SPTC integrated SORC system versus recuperator effectiveness

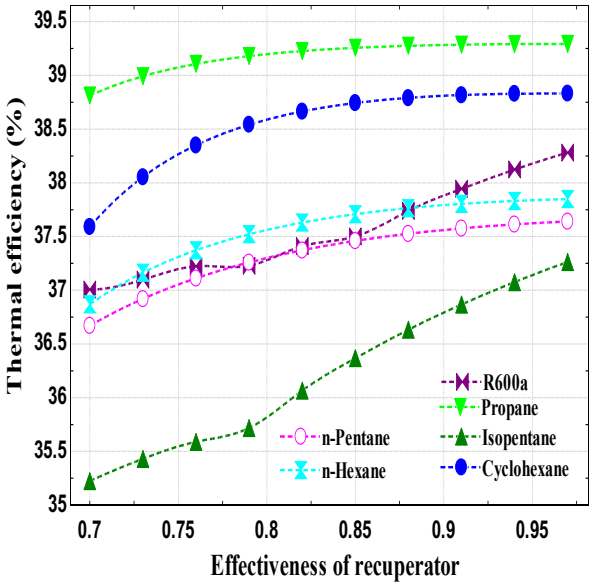

Figure 5.105. Thermal efficiency of SPTC integrated SORC system versus recuperator effectiveness

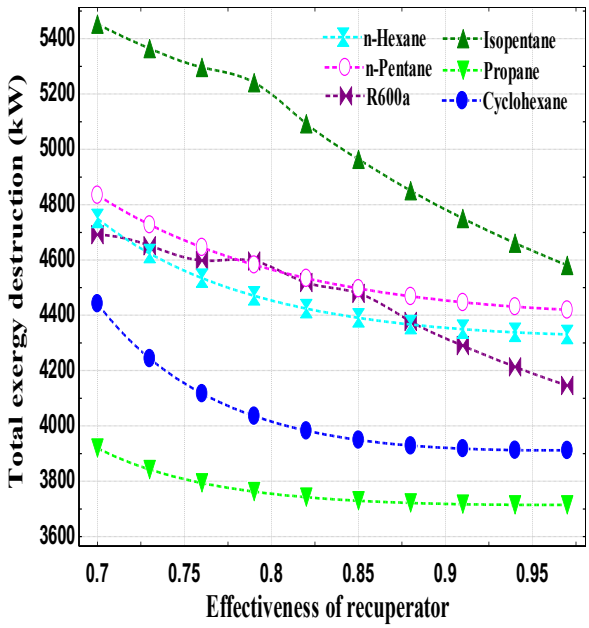

Figure 5.106. Total exergy destruction of SPTC integrated SORC system versus recuperator effectiveness

Alternatively, propane based SPTC-SORC system has a lowest exergy destruction rate, which is decreases from 3920 kW to 3714 kW as the effectiveness increases from 70% to 97%. While, the exergy destruction rate of n-Pentane, n-Hexane, R600a, and cyclohexane lies in between these two above mentioned fluids with a maximum value of 4834 kW, 4750 kW, 4691 kW, and 4442 kW at effectiveness of 70%, respectively as shown in Figure 5.106.

Chapter-6

Conclusions

In this chapter, energy and exergy performance of SPTC driven cycles such as combined SCO_2 cycle and ORC system (SCO_2-ORC system), combined R-SCO_2 cycle and ORC system (R-SCO_2-ORC system), combined SCO_2 cycle and VAR system (SCO_2-VAR cycle), and SORC system have been analysed. Computer based programs have been prepared in EES software to resolve the equations so as to compute the outcomes. Therefore, a short summery of the following results have been concluded and further discussed in the subsections below:

6.1. SPTC integrated with combined SCO_2 cycle and ORC system

In this first objective, the effect of operating parameters such as solar DNI, inlet pressure and temperature of SCO_2 turbine (P_5 & T_5), and inlet temperature of compressor (T_9) over performance of SCO_2-ORC system by choosing five organic fluids for the ORC, for instance R134a, R245fa, R1234yf, R1234ze, and R407c have been assessed.

1. Exergy and thermal efficiency of SCO_2-ORC system upsurges as solar DNI upsurges. Results concluded that the R407c fluid based SCO_2-ORC system has a utmost exergy and thermal efficiency of 78.07% and 43.49%, respectively at DNI of 950 W/m^2. However, R134a fluid has a smallest exergy and thermal efficiency of 75.87% and 42.26%, correspondingly. Besides, the exergy destruction rate continuously follows the opposite trend from the exergy efficiency. Thus, R407c fluid shows a smallest exergy destruction rate of 4093 kW in contrast to 4508 kW in case of R134a fluid at DNI of 950 W/m^2.
2. Exergy and thermal efficiency augments slightly as the 'P_5' augments. Again, R407c fluid based SCO_2-ORC system has a best exergy and thermal efficiency of 75.21% and 41.9%, respectively, while, it has a smallest total exergy destruction rate of 4659 kW at 23 MPa.
3. Exergy and thermal efficiency also rises as the 'T_5' rises. Results found that R407c fluid based SCO_2-ORC system has an uppermost exergy and thermal efficiency of 81.79% and 45.57%, correspondingly, however, it has a smallest total exergy destruction rate of 3524 kW at 850 K.
4. On the other hand, the exergy and thermal efficiency declines as the 'T_9' rises and it has been detected that R407c fluid based SCO_2-ORC system has a maximum exergy and thermal efficiency of 69.75% and 38.86%, respectively at 300 K.

5. Likewise, the prime exergy destruction source is SPTC that means that more than 25% of the solar inlet exergy and nearly 54% of the total exergy destruction rate has been destructed in the SPTC lone. Moreover, other major contributors are SCO_2 turbine and evaporator, i.e. about 9.72% and 8.54%, respectively of the solar inlet exergy has been destructed, and these components accounts almost 38.10% of overall rate of exergy destruction in case of R407c based complete plant.
6. Lastly, it has been remarked that R134a and R245fa fluid has the marginal differences amongst their exergy and thermal performance.

6.2. SPTC integrated with combined R-SCO_2 cycle and ORC system

In this second objective, simple SCO_2 cycle has been replaced by the R-SCO_2 cycle. The effect of operating constraints, for instance 'DNI', 'P_5', 'T_5', 'T_9', mass flow rate of SCO_2 ($\dot{m}_{SCO_2}$), and effectiveness of HTR and LTR (ε_{HTR} & ε_{LTR}) on the performance of R-SCO_2-ORC system by picking eight organic fluids for the ORC, for example R123, R1234ze, R1234yf, toluene, cyclohexane, isopentane, isobutene, and R290 have been inspected.

1. The exergy and thermal efficiency of R-SCO_2-ORC system upsurges with upsurge in 'DNI', 'P_5', 'T_5', '$\dot{m}_{SCO_2}$', and 'ε_{HTR}' & 'ε_{LTR}' in contrast to the 'T_9' as it displays the inverse effect on efficiency.
2. Results found that R123 fluid based R-SCO_2-ORC system has a greatest exergy and thermal efficiency of 86.75% and 48.33% at DNI of 950 W/m^2; 79.04% and 44.03% at P_5 of 23 MPa; 86.59% and 48.24% at T_5 of 920 K; 89.59% and 49.91% at $\dot{m}_{SCO_2}$ of 16 kg/s; 84.64% and 47.15% at T_9 of 327 K; 85.01% and 47.35% at ε_{HTR} of 0.92; 85.1% and 47.41% at ε_{LTR} of 0.92, respectively.
3. Furthermore, R123 fluid displays a maximum net work output of 6231 kJ at T_5 of 920 K and 6090 kJ at T_9 of 327 K. While, R290 fluid has a smallest net work output of 6183 kJ at T_5 of 920 K and 6052 kJ at T_9 of 327 K.
4. Lastly, comparative study found that R123 fluid based combined recompression cycle shows an utmost exergy and thermal efficiency of 85.09% and 47.4%, respectively, which is about 1.74% to 2.4% more than the simple combined configuration.

6.3. SPTC integrated with combined SCO_2 cycle and VAR cycle

In this third objective, the VAR cycle as a bottoming cycle has been directly coupled with topping SCO_2 cycle so as to generate combined power, cooling & heating effect. The influence of various operating constraints like 'LAT', 'DNI', 'T_5', compressor pressure ratio (PR), temperature of generator, and temperature of absorber & condenser on the performance of SCO_2-VAR cycle have been assessed.

1. The greatest exergy efficiency of SPTC for the April 15 and December 15 on the Mumbai was 32.58% at LAT(h) = 1230 and 31.72% at LAT(h) = 1130 & 1230, respectively, but the thermal efficiency was 63.46% and 61.78%, correspondingly.
2. Besides, the exergy and thermal efficiency of SCO_2-VAR cycle was 82.24% and 45.82% at DNI of 950 W/m^2, respectively.
3. For the maximum T_5 of 920 K, the utmost exergy and thermal efficiency, and net work output of SCO_2-VAR cycle were 80.13% and 44.64%, and 1668 kW, respectively. Whereas, at the lower T_5 of 650 K, the uppermost value of $COP_{cooling}$ and $COP_{heating}$ were 0.4675 and 1.435, correspondingly.
4. Likewise, at the highest PR of 2.67, the greatest exergy and thermal efficiency, and net work output of SCO_2-VAR cycle were 81.51% and 45.41%, and 1813 kW, respectively. Also, the highest $COP_{cooling}$ & $COP_{heating}$ were 0.4722 & 1.207, correspondingly.
5. Besides, at the lower generator temperature of 365 K, the utmost exergy and thermal efficiency, and net work output of SCO_2-VAR cycle were 80.75% and 44.98%, and 1702 kW, respectively. Similarly, the highest $COP_{cooling}$ and $COP_{heating}$ were 0.4448 and 1.21, correspondingly.
6. Finally, at the lower absorber and condenser temperature of 315 K, the utmost exergy and thermal efficiency, and net work output of SCO_2-VAR cycle were 79.88% and 44.5%, and 1654 kW, respectively. Also, the utmost $COP_{cooling}$ and $COP_{heating}$ were 0.2522 and 1.411, correspondingly.

6.4. SPTC integrated with SORC system

In this fourth objective, the SORC directly operated by the SPTC field with its fixed outlet temperature of 300℃ (i.e. maximum heat source temperature) which has been assumed to analyse the performance of high temperature heat source based SORC system. The reason behind the selection of SORC system instead of steam Rankine cycle (SRC) because as per literature, SRC is appropriate for the high heat source temperature of greater than 500℃ [193]. Furthermore, the effect of three operating parameters such as DNI, inlet pressure of

SORC turbine (P_5), and effectiveness of recuperator on the performance of SORC by selecting six organic fluids such as cyclohexane, isopentane, propane, R600a, n-Hexane, and n-Pentane have been assessed.

1. At the higher solar DNI of 950 W/m^2, propane based SPTC-SORC system has a highest exergy and thermal efficiency of 83.15% and 39.9%, respectively followed by cyclohexane, R600a, n-Hexane, n-Pentane, and isopentane. Alternatively, propane has a minimum exergy destruction rate of 3455 kW as it follows the inverse trend from exergy efficiency.
2. It has been remarked that more than 80% of total exergy destruction rate was found to be only in SPTC.
3. Furthermore, at the higher P_5 of 86 bar, propane based SPTC-SORC system shows a highest exergy and thermal efficiency of 81.19% and 38.96%, respectively. Alternatively, it has a lowest exergy destruction rate of 3858 kW. Instead, the isopentane has a lowest exergy and thermal efficiency of 74.34% and 35.68%, correspondingly. Whereas, it possesses the highest exergy destruction rate of 5222 kW.
4. Moreover, at the higher effectiveness of 97%, propane based SPTC-SORC system has a highest exergy and thermal efficiency of 81.89% and 39.29%, respectively. Alternatively, it has a lowest exergy destruction rate of 3714 kW. On the other side, isopentane shows a lowest exergy and thermal efficiency of 77.66% and 37.26%, respectively. However, it has a highest exergy destruction rate of 4581 kW.

6.5. Recommendations from the conclusion

1. I found that SPTC field has a highest exergy destruction rate. So, its improvement is necessary for efficient working.

2. Turbine and evaporator also have accountable loss of exergy which is need to be decreased.

3. Apart from SPTC, the LFR and SPT systems could be integrate with these kinds of cycles.

3. Power generation capacity of per unit collection area in case of SPTC integrated SCO_2-ORC system was 1.355 kW/m^2 for R407c fluid.

4. During the analysis, effect of pressure drop has been neglected. In actual, its effect on combined cycle should be analysed in term of performance changes.

5. Combined recompression cycle in contrast to simple cycle illustrates the high efficiency.

6. According to both environmental and performance point of view, R1234ze and R1234yf fluids are the best choice.
7. To avoid any irregularity in solar energy supply, a solar thermal storage facility is required to enhance the working time of combined cycle.

6.6. Scope for future work

In future, a thermal and exergy based economic analysis could be performed. Even a comparative analysis between SPTC, LFR, and SPT driven plants can be conducted on the grounds of performance, economics, and social parameters. Additionally, the mixture of refrigerants can be utilized in ORC to evaluate their performance changes. Furthermore, a multi-objective optimization could be performed on the basis of genetic algorithm. Moreover, working time and performance of plant can be improved with the implication of solar thermal energy storage device especially during non-sunshine hours. Apart from this, we can include the effect of pressure drop in our study and therefore, we can evaluate the most sensitive component in overall plant.

APPENDIX A: Uncertainty analysis

If y is a function of independent variables x_1, x_2, x_3 such as DNI, P_5 and T_5 which can be designated as $y = f(x_1, x_2, x_3)$.

Uncertainty (U) in the dependent variable can be calculated as [229]:

$$U_y=\sqrt{\sum_i(\frac{\partial y}{\partial x_i})^2\, Ux_i^2} \qquad \text{(a.1)}$$

Table A1. Uncertainty in exergy efficiency of R407c based combined cycle

Independent variable±Uncertainty	**Partial derivative**	**% of uncertainty**	**Dependent variable± Uncertainty**
DNI=800±50	∂(Exergy efficiency)/∂(DNI) =29.32	37.52%	Exergy efficiency of combined cycle (SCO_2-ORC) =78.28±2.393
P_5=25MPa±4MPa	∂(Exergy efficiency)/∂(P_5) =4.404*10^{-8}	0.54%	
T_5=625±20	∂(Exergy efficiency)/∂(T_5) =-0.09417	61.94%	

Table A2. Uncertainty in exergy efficiency of solar integrated R407c based combined cycle

Independent variable±Uncertainty	**Partial derivative**	**% of uncertainty**	**Dependent variable± Uncertainty**
DNI=800±50	∂(Exergy efficiency)/∂(DNI) =52.32	33.41%	Exergy efficiency of solar integrated combined cycle (SPTC-SCO_2-ORC) =58.23±4.526
P_5=25MPa±4MPa	∂(Exergy efficiency)/∂(P_5) =3.078*10^{-8}	0.07%	
T_5=625±20	∂(Exergy efficiency)/∂(T_5) =-0.1845	66.51%	

Table A3. Uncertainty in thermal efficiency of R407c based combined cycle

Independent variable±Uncertainty	**Partial derivative**	**% of uncertainty**	**Dependent variable± Uncertainty**
DNI=800±50	∂(Thermal efficiency)/∂(DNI) =16.33	37.52%	Thermal efficiency of combined cycle (SCO_2-ORC) =43.61±1.333
P_5=25MPa±4MPa	∂(Thermal efficiency)/∂(P_5) =2.453*10^{-8}	0.54%	
T_5=625±20	∂(Thermal efficiency)/∂(T_5) =-0.05246	61.94%	

Table A4. Uncertainty in thermal efficiency of solar integrated R407c based combined cycle

Independent variable±Uncertainty	**Partial derivative**	**% of uncertainty**	**Dependent variable± Uncertainty**
DNI=800±50	∂(Thermal efficiency)/∂(DNI) =29.15	33.41%	Thermal efficiency of solar integrated combined cycle (SPTC-SCO_2-ORC) =32.44±2.521
P_5=25MPa±4MPa	∂(Thermal efficiency)/∂(P_5) =$1.715*10^{-8}$	0.07%	
T_5=625±20	∂(Thermal efficiency)/∂(T_5) =-0.1028	66.51%	

Table A5. Uncertainty in the exergy destruction rate of R407c based combined cycle

Independent variable±Uncertainty	Partial derivative	% of uncertainty	Dependent variable± Uncertainty
DNI=800±50	∂(Exergy destruction rate)/∂(DNI) = $-4.729*10^{-10}$	0.00%	Exergy destruction rate of combined cycle (SCO_2-ORC) =3901±306.8
P_5=25MPa±4MPa	∂(Exergy destruction rate)/∂(P_5) = $-5.956*10^{-6}$	0.60%	
T_5=625±20	∂(Exergy destruction rate)/∂(T_5) =15.3	99.40%	

Table A6. Uncertainty in exergy destruction rate of solar integrated R407c based combined cycle

Independent variable±Uncertainty	Partial derivative	% of uncertainty	Dependent variable± Uncertainty
DNI=800±50	∂(Exergy destruction rate)/∂(DNI) = $-4.729*10^{-10}$	0.00%	Exergy destruction rate of solar integrated combined cycle (SCO_2-ORC) =8081±714.6
P_5=25MPa±4MPa	∂(Exergy destruction rate)/∂(P_5) = $-5.956*10^{-6}$	0.11%	
T_5=625±20	∂(Exergy destruction rate)/∂(T_5) =35.71	99.89%	

Publications

Published in international journals:

1. Harwinder Singh and R. S. Mishra, Performance analysis of solar parabolic trough collectors driven combined supercritical CO_2 and organic Rankine cycle, Engineering Science and Technology, an International Journal 21 (2018) 451–464. **(Elsevier)**
2. Harwinder Singh and R. S. Mishra, Detailed parametric analysis of solar driven supercritical CO_2 based combined cycle for power generation, cooling and heating effect by vapor absorption refrigeration as a bottoming cycle, Thermal Science and Engineering Progress 8 (2018) 397–410. **(Elsevier)**
3. Harwinder Singh and R. S. Mishra, Performance Evaluation of the Supercritical Organic Rankine Cycle (SORC) Integrated with Large Scale Solar Parabolic Trough Collector (SPTC) System: An Exergy Energy Analysis, Environment Progress and Sustainable Energy 37 (2018) 891-899. **(John & Wiley Sons)**
4. Harwinder Singh and R. S. Mishra, Energy- and exergy-based performance evaluation of solar powered combined cycle (recompression supercritical carbon dioxide cycle/organic Rankine cycle), Clean Energy 2 (2018) 140–153. **(Oxford University Press)**
5. Harwinder Singh and R. S. Mishra, Performace evaluation by exergy analysis and optimization of organic rankine cycle (ORC) by using low-grade waste heat, International Journal for Research in Applied Science & Engineering Technology (IJRASET) 5 (2017) 154-173.
6. Harwinder Singh and R. S. Mishra, Thermal performance analysis of novel combined cycle through different working fluids-a detailed analysis, Intenational Research Journal of Sustainable Science and Engineering 5 (2017) 1-10.

Published in International conferences

1. Harwinder Singh and R. S. Mishra, Perfortmance evaluations of concentrated solar thermal power technology, International Conference of Advance Research and Innovation (ICARI-2016) ISBN 978-93-5156-328-0, ICARI-ME-16-02-57.
2. Harwinder Singh and R. S. Mishra, Solar thermal integrated organic Rankine cycle technology, International Conference on Innovative Research in Applied Physical, Mathematical/ Statistical, Chemical Sciences and Emerging Energy Technology for Sustainable Development (APMSCSET-2019) e-ISSN 2350-0255.

3. Harwinder Singh and R. S. Mishra, Supercritical carbon dioxide cycle based combined cycle for power generation and waste heat recovery, International Conference of Advance Research and Innovation (ICARI-2019) ISBN 978-93-5156-328-0, ICARI-ME-19-01-79.

References

[1]. Sukhatme, S. P., Nayak, J. K. Solar Energy: Principles of thermal collection and storage, Third Edition, Tata McGraw-Hill Education, New Delhi, 2008, 1-431, ISBN-13: 978-0070260641.

[2]. Abbasi, T., Abbasi, S. A. Renewable Energy Sources: Their impact on global warming and pollution, Second Edition, PHI Learning Private Limited, New Delhi, 2011, 1-320, ISBN-978-81-203-3994-1.

[3]. Goswami, D. Y. Principles of solar engineering, third edition, CRC press, Taylor and Francis Group, Boca Raton, FL, 2015, 1-822.

[4]. IEA (International Energy Agency), World Energy Outlook 2010, International Energy Agency, Paris, France, 2010. < https://www.iea.org/newsroom/news/2010/november/world-energy-outlook-2010.html> accessed on 13/5/2019.

[5]. BP Statistical Review of World Energy and the BP Energy Outlook 2019, London, UK, 2019. <https://www.bp.com/content/dam/bp/business-sites/en/global/corporate/pdfs/energy-economics/statistical-review/bp-stats-review-2019-full-report.pdf> accessed on 25/10/2019.

[6]. IEA (International Energy Agency), World Energy Outlook 2013, International Energy Agency, Paris, France, 2013. < https://www.iea.org/newsroom/news/2013/november/world-energy-outlook-2013.html> accessed on 13/5/2019.

[7]. Caineng, Z., Qun, Z., Guosheng, Z., Bo, X. Energy revolution: From a fossil energy era to a new energy era, Natural Gas Industry B 3 (2016) 1-11.

[8]. Sen, S., Ganguly, S., Das, A., Sen, J., Dey, S. Renewable energy scenario in India: opportunities and challenges, African Earth Sciences 2016 (122) 25-31.

[9]. Pappas, D., Chalvatzis, K. J. Energy and industrial growth in India: the next emissions superpower?, Energy Procedia 105 (2017) 3656 – 3662.

[10]. Power Sector Glance All India, Ministry of Power (Government of India) <https://powermin.nic.in/en/content/power-sector-glance-all-india> accessed on 4/5/2018.

[11]. Nigam, D. The national solar mission: India marching ahead in solar energy. Akshay Urja (June 2016), 2016, 11–15. <https://mnre.gov.in/file-manager/akshay-urja/june-2016/11-15.pdf> accessed on 5/5/2018.

[12]. Singh, R. Energy sufficiency aspirations of India and the role of renewable resources: scenarios for future, Renewable and Sustainable Energy Reviews 81 (2018) 2783-2795.

[13]. The World Bank, Electric power consumption (kWh per capita), ⟨http://data.worldbank.org/indicator/EG.USE.ELEC.KH.PC⟩ accessed on 5/5/2018.

[14]. Mishra, U. C. Environmental impact of coal industry and thermal power plants in India, Journal of Environmental Radioactivity 72 (2004) 35-40.

[15]. Asif, M., Muneer, T. Energy supply, its demand and security issues for developed and emerging economies, Renewable and Sustainable Energy Reviews 11 (2007) 1388–1413.

[16]. Mathews, J. A, Tan, H. Manufacture renewables to build energy security, Nature 513 (2014) 166-168.

[17]. Rastogi, C. Changing geo-politics of oil and the impact on India, Procedia - Social and Behavioral Sciences 133 (2014) 93-105.

[18]. Kar, S. K., Gupta, A. Natural gas markets in India - opportunities and challenges, Springer Nature Singapore Pte. Ltd., First Edition, 2017, 1-385, ISBN-13: 978-9811031168.

[19]. Briscoe, J., Malik, R. P. S. India's Water Economy: bracing for a turbulent future. The World Bank, Oxford University Press, New Delhi, 2006, 1-79.

[20]. Pandit, M. K., Grumbine, R. E. Potential effects of ongoing and proposed hydropower development on terrestrial biological diversity in the Indian Himalaya, Conservation Biology 26 (2012) 1061–1071.

[21]. Grumbine, R. E., Pandit, M. K. Threats from India's Himalaya dams, Science 339 (2013) 36–37.

[22]. International Atomic Energy Agency (IAEA). PRIS - Country Details. ⟨https://www.iaea.org/PRIS/CountryStatistics/CountryDetails.aspx?Current=IN⟩ assessed on 6/5/2018.

[23]. Jewell, J. Ready for nuclear energy?: An assessment of capacities and motivations for launching new national nuclear power programs, Energy Policy 39 (2011) 1041–1055.

[24]. Grover, R. B., Chandra, S. Scenario for growth of electricity in India, Energy Policy 34 (2006) 2834–2847.

[25]. Grover, R. B. Policy initiatives by the government of India to accelerate the growth of installed nuclear power capacity in the coming years, Energy Procedia 7 (2011) 74–78.

[26]. Ramana, M. V., D'Sa, A., Reddy, A. K. N. Nuclear energy economics in India, Energy for Sustainable Development 9 (2005) 35-48.

[27]. Bajaj, S. S. Challenges of atomic energy regulation in Indian context, Energy Procedia 7 (2011) 55–59.

[28]. Joskow, P. L, Parsons J. E. The future of nuclear power after Fukushima, MIT CEEPR 2012, 1-30.

[29]. Panwar, N. L., Kaushik, S. C., Kothari, S. Role of renewable energy sources in environmental protection: A review, Renewable and Sustainable Energy Reviews 15 (2011) 1513–1524.

[30]. Demirbas, A. Recent advances in biomass conversion technologies, Energy Educational Science and Technology 6 (2000) 19–40.

[31]. Demirbas, A. Global renewable energy resources, Energy Sources, Part A: Recovery, Utilization, and Environmental Effects 28 (2006) 779–792.

[32]. Kralova, I., Sjöblom, J. Biofuels-renewable energy sources: a review, Journal of Dispersion Science and Technology 31 (2010) 409–425.

[33]. Dincer, I. Energy and environmental impacts: present and future perspectives, Energy Sources, Part A: Recovery, Utilization, and Environmental Effects 20 (1998) 427–453.

[34]. Dincer, I. Renewable energy and sustainable development: a crucial review, Renewable and Sustainable Energy Reviews 4 (2000) 157–175.

[35]. Zakhidov, R. A. Central Asian countries energy system and role of renewable energy sources, Applied Solar Energy 44 (2008) 218–223.

[36]. Thirugnanasambandam, M., Iniyan, S., Goic, R. A review of solar thermal technologies, Renewable and Sustainable Energy Reviews 14 (2010) 312–322.

[37]. Winston, R., Minano, J. C., Benitez, P. Nonimaging optics, First Edition, Elsevier Academic Press, New York, 2005, 1-217, eBook ISBN 9780080479736.

[38]. Rai, G. D. Solar energy utilization, Khanna Publishers New Delhi, 1-644, 1996, ISBN-13 978-81-7409-184-X.

[39]. Tyagi, A. P. Solar radiant energy over india, India meteorological department, Ministry of earth sciences, New Delhi, 2009.
<https://mnre.gov.in/file-manager/UserFiles/solar_radiant_energy_over_India.pdf> accessed on 13/4/2018

[40]. Biermann, E., Grupp, M., Palmer, R. Solar cooker acceptance in South Africa: results of a comparative field-test, Solar Energy 66 (1999) 401–407.

[41]. Tucker, M. Can solar cooking save the forests?, Ecological Economics 31 (1999) 77–89.

[42] Wentzel, M., Pouris, A. The development impact of solar cookers: a review of solar cooking impact research in South Africa, Energy Policy 35 (2007) 1909–1919.

[43]. Kalogirou, S. Thermal performance, economic and environmental life cycle analysis of thermosiphon solar water heaters, Solar Energy 83 (2009) 39–48.

[44]. Kumar, A., Kandpal, T. C. CO_2 emissions mitigation potential of some renewable energy technologies in India, Energy Sources, Part A: Recovery, Utilization, and Environmental Effects 29 (2007) 1203–1214.

[45]. Sharma, A., Chen, C. R, Lan, N. V. Solar-energy drying systems: a review, Renewable and Sustainable Energy Reviews 13 (2008) 1185–1210.

[46]. Piacentini, R. D., Mujumdar, A. S. Climate change and drying of agricultural products, Drying Technology 27 (2009) 629–635.

[47]. Xiaowu, W., Ben, H. Exergy analysis of domestic-scale solar water heaters, Renewable and Sustainable Energy Reviews 9 (2005) 638–645.

[48]. Demirbas, M. F. Electricity production using solar energy, Energy Sources, Part A: Recovery, Utilization, and Environmental Effects 29 (2007) 563–569.

[49]. Mills, D. Advances in solar thermal electricity technology, Solar Energy 76 (2004) 19–31.

[50]. Sharma, N. K., Tiwari, P. K., Sood, Y. R. Solar energy in India: strategies, policies, perspectives and future potential, Renewable and Sustainable Energy Reviews 16 (2012) 933–941.

[51]. Sharma, A. A comprehensive study of solar power in India and World, Renewable and Sustainable Energy Reviews 15 (2011) 1767–1776.

[52]. Khare, V., Nema, S., Baredar, P. Status of solar wind renewable energy in India, Renewable and Sustainable Energy Reviews 27 (2013) 1–10.

[53]. Ansari, M. F., Kharb, R. K., Luthra, S., Shimmi, S. L., Chatterji, S. Analysis of barriers to implement solar power installations in India using interpretive structural modelling technique, Renewable and Sustainable Energy Reviews 27 (2013) 163–174.

[54]. Ministry of Statistics and Programme Implementation, Government of India (MOSPI), Key indicators of household consumer expenditure in India 2009–2010, NSS 66th Round, New Delhi, 2011.

[55]. Kalogirou, S. A. Solar thermal collectors and applications, Progress in Energy and Combustion Science 30 (2004) 231–295.

[56]. Garg, H. P., Prakash, J. Solar Energy Fundamental and Applications, Tata McGraw Hill, 1st revised edition, 1997, 1-435, ISBN 0-07-463631-6.

[57]. Thomas, A., Guven, H. M. Parabolic trough concentrators---design, construction and evaluation, Energy Conversion and Management 34 (1993) 401-416.

[58]. Francia, G. Pilot plants of solar steam generation systems, Solar Energy 1968 (12) 51–64.

[59]. Feher, E. G. The supercritical thermodynamic power cycle, Energy Conversion 1968 (8) 85-90.

[60]. Angelino, G. Perspectives for the liquid phase compression gas turbine, Journal of Engineering for Power, Transactions of the ASME 89 (1967) 229-236.

[61]. Angelino, G. Carbon dioxide condensation cycles for power production, Journal of Engineering for Power, Transactions of the ASME 90 (1968) 287-295.

[62]. Angelino, G. Real gas effects in carbon dioxide cycles, ASME Paper No. 69-GT-103, ASME, Cleveland, Ohio, USA, 1969.

[63]. Dostal, V., Hejzlar, P., Driscoll, M. J. The supercritical carbon dioxide power cycle: Comparison to other advanced power cycles, Nuclear Technology 154 (2006) 283–301.

[64]. Moisseytsev, A., Sienicki, J. J. Investigation of alternative layouts for the supercritical carbon dioxide Brayton cycle for a sodium-cooled fast reactor, Nuclear Engineering and Design 239 (2009) 1362–1371.

[65]. Turchi, C. S., Ma, Z., Neises, T., Wagner, M. Thermodynamic study of advanced supercritical carbon dioxide power cycles for high performance concentrating solar power systems, Proceedings of the ASME 2012, 6th International Conference on Energy Sustainability ES2012, San Diego, CA, USA, 2012.

[66]. Ahn, Y., Bae, S. J., Kim, M., Cho, S. K., Baik, S., Lee, J. I., Cha, J. E. Review of supercritical CO_2 power cycle technology and current status of research and development, Nuclear Engineering Technology 47 (2015) 647-661.

[67]. Macchi, E., Astolfi, M. Organic Rankine cycle (ORC) Power Systems: Technologies and Applications, Woodhead publishing publications, Elsevier, 2016, 1-698.

[68]. Tchanche, B. F., Lambrinos, G., Frangoudakis, A., Papadakis, G. Low-grade heat conversion into power using organic Rankine cycles – A review of various applications, Renewable and Sustainable Energy Reviews 15 (2011) 3963–3979.

[69]. Wali, E. Optimum working fluids for solar powered Rankine cycle cooling of buildings, Solar Energy 25 (1980) 235–241.

[70]. Roy, J. P., Mishra, M. K., Misra, A. Performance analysis of an Organic Rankine Cycle with superheating under different heat source temperature conditions, Applied Energy 88 (2011) 2995–3004.

[71]. Quoilin, S., Broek, M. V. D., Declaye, S., Dewallef, P., Lemort, V. Techno-economic survey of Organic Rankine Cycle (ORC) systems, Renewable and Sustainable Energy Reviews 22 (2013) 168–186.

[72]. Crespi, F., Gavagnin, G., Sánchez, D., Martínez, G. S. Supercritical carbon dioxide cycles for power generation: A review, Applied Energy 195 (2017) 152–183.

[73]. Bauer, M. L., Vijaykumar, R., Lausten, M., Stekli, J. Pathway to cost competitive concentrated solar power via supercritical CO_2 power cycles, In: The 5th supercritical CO_2 power cycles symposium, 2016, San Antonio, TX.

[74]. Osorio, J. D., Hovsapian, R., Ordonez, J. C. Effect of multi-tank thermal energy storage, recuperator effectiveness, and solar receiver conductance on the performance of a concentrated solar supercritical CO_2-based power plant operating under different seasonal conditions, Energy 115 (2016) 353–368.

[75]. Wright, S., Davidson, C., Scammell, W. Thermo-economic analysis of four sCO_2 waste heat recovery power cycle systems. In: The 5th supercritical CO_2 power cycles symposium, 2016, San Antonio, TX.

[76]. Abram, T., Ion, S. Generation-IV nuclear power: a review of the state of the science, Energy Policy 36 (2008) 4323–4330.

[77]. Yoon, H. J., Ahn, Y., Lee, J. I., Addad, Y. Potential advantages of coupling supercritical CO_2 Brayton cycle to water cooled small and medium size reactor, Nuclear Engineering and Design 245 (2012) 223–232.

[78]. Heo, J. Y., Kim, M. S., Baik, S., Bae, S. J., Lee, J. I. Thermodynamic study of supercritical CO_2 Brayton cycle using an isothermal compressor, Applied Energy 206 (2017) 1118–1130.

[79]. Kim, Y. M., Sohn, J. L., Yoon, E. S. Supercritical CO_2 Rankine cycles for waste heat recovery from gas turbine, Energy 118 (2016) 893-905.

[80]. Khadse, A., Blanchette, L., Kapat, J., Vasu, S., Hossain, J., Donazzolo, A. Optimization of supercritical CO_2 Brayton cycle for simple cycle gas turbines exhaust heat recovery using genetic algorithm, ASME Turbo Expo 2017: Turbomachinery Technical Conference and Exposition, Charlotte, North Carolina, USA, 2017.

[81]. Muto, Y., Kato, Y. Optimal cycle scheme of direct cycle supercritical CO_2 gas turbine for nuclear power generation systems, International Conference on Power Engineering, Hangzhou, China, 2007.

[82]. Cardemil, J. M., da Silva, A. K. Parametrized overview of CO_2 power cycles for different operation conditions and configurations – An absolute and relative performance analysis, Applied Thermal Engineering 100 (2016) 146–154.

[83]. Mecheri, M., Moullec, Y. L. Supercritical CO_2 Brayton cycles for coal-fired power plants, Energy 103 (2016) 758-771.

[84]. Park, S. H., Kim, J. Y., Yoon, M. K., Rhim, D. R., Yeom, C. S. Thermodynamic and economic investigation of coal-fired power plant combined with various supercritical CO_2 Brayton power cycle, Applied Thermal Engineering 130 (2018) 611–623.

[85]. Neises, T., Turchi, C. Supercritical carbon dioxide power cycle design and configuration optimization to minimize levelized cost of energy of molten salt power towers operating at 650°C, Solar Energy 181 (2019) 27–36.

[86]. Li, L., Ge, Y. T. Luo, X., Tassou, S. A. Experimental analysis and comparison between CO_2 transcritical power cycles and R245fa organic Rankine cycles for low-grade heat power generations, Applied Thermal Engineering 136 (2018) 708–717.

[87]. Song, J., Li, X. S., Ren, X. D., Gu, C. W. Performance improvement of a preheating supercritical CO_2 (S-CO_2) cycle based system for engine waste heat recovery, Energy Conversion and Management 161 (2018) 225–233.

[88]. Banik, S., Ray, S., De, S. Thermodynamic modelling of a recompression CO_2 power cycle for low temperature waste heat recovery, Applied Thermal Engineering 107 (2016) 441–452.

[89]. Sarkar, J. Second law analysis of supercritical CO_2 recompression Brayton cycle, Energy 34 (2009) 1172–1178.

[90]. Ma, Y., Liu, M., Yan, J., Liu, J. Thermodynamic study of main compression intercooling effects on Supercritical CO_2 recompression Brayton cycle, Energy 140 (2017) 746-757.

[91]. Kim, S., Cho, Y., Kim, M. S., Kim, M. Characteristics and optimization of supercritical CO_2 recompression power cycle and the influence of pinch point temperature difference of recuperators, Energy 147 (2018) 1216-1226.

[92]. Gkountas, A. A., Stamatelos, A. M., Kalfas, A. I. Recuperators investigation for high temperature supercritical carbon dioxide power generation cycles, Applied Thermal Engineering 125 (2017) 1094–1102.

[93]. Padilla, R. V., Benito, R. G., Stein, W., An exergy analysis of recompression supercritical CO_2 cycles with and without reheating, Energy Procedia 69 (2015) 1181–1191.

[94]. Yari, M. A novel cogeneration cycle based on a recompression supercritical carbon dioxide cycle for waste heat recovery in nuclear power plants, International Journal of Exergy 10 (2012) 346–364.

[95]. Wołowicz, M., Milewski, J., Ziembicki, G. Mathematical modelling and analysis of recompression supercritical CO_2 Brayton cycle in terms of maximum pressure and temperature at turbine inlet, International Conference of Numerical Analysis and Applied Mathematics (ICNAAM 2018), AIP Conference Proceedings 1978, 470080-1-4.

[96]. Atif, M., Al-Sulaiman, F. A. 2018. Energy and exergy analyses of recompression Brayton cycles integrated with a solar power tower through a two-tank thermal storage system, Journal of Energy Engineering 144 (2018) 04018036-1-15.

[97]. Garg, P., Kumar, P., Srinivasan, K. Supercritical carbon dioxide Brayton cycle for concentrated solar power, Journal of Supercritical Fluids 76 (2013) 54–60.

[98]. Garg, P., Srinivasan, K., Duttac, P., Kumar, P. Comparison of CO_2 and steam in transcritical Rankine cycles for concentrated solar power, Energy Procedia 49 (2014) 1138–1146.

[99]. Turchi, C. S., Ma, Z., Neises, T. W., Wagner, M. J. Thermodynamic Study of advanced supercritical carbon dioxide power cycles for concentrating solar power systems, Journal of Solar Energy Engineering 135 (2013), 041007-1-7.

[100]. Chacartegui, R., Sánchez, D., Jiménez-Espadafor, F., Muñoz, A., Sánchez, T. Analysis of intermediate temperature combined cycles with a carbon dioxide topping cycle, Proceedings of ASME Turbo Expo 2008: Power for Land, Sea and Air, 2008, 1-8.

[101]. AlZahrania, A. A., Dincer, I. Energy and exergy analyses of a parabolic trough solar power plant using carbon dioxide power cycle, Energy Conversion and Management 158 (2018) 476–488.

[102]. Osorio, J. D., Hovsapian, R., Ordonez, J. C. Dynamic analysis of concentrated solar supercritical CO_2-based power generation closed-loop cycle, Applied Thermal Engineering 93 (2016) 920–934.

[103]. Niu, X-D., Yamaguchi, H., Iwamoto, Y., Zhang, X-R. Optimal arrangement of the solar collectors of a supercritical CO_2-based solar Rankine cycle system, Applied Thermal Engineering 50 (2013) 505-510.

[104]. Yamaguchi, H., Zhang, X. R., Fujima, K., Enomoto, M., Sawada, N. Solar energy powered Rankine cycle using supercritical CO_2, Applied Thermal Engineering 26 (2006) 2345–2354.

[105]. Iverson, B. D., Conboy, T. M., Pasch, J. J., Kruizenga, A. M. Supercritical CO_2 Brayton cycles for solar-thermal energy, Applied Energy 111 (2013) 957–970.

[106]. Padilla, R. V., Soo Too, Y. C., Benito, R., Stein, W. Exergetic analysis of supercritical CO_2 Brayton cycles integrated with solar central receivers, Applied Energy 148 (2015) 348–365.

[107]. Wang, X., Liu, Q., Bai, Z., Lei, J., Jin, H., Thermodynamic analysis of the cascaded supercritical CO2 cycle integrated with solar and biomass energy, Energy Procedia 105 (2017) 445 – 452.

[108]. Chapman, D. J., Arias, D. A. An assessment of the supercritical carbon dioxide cycle for use in a solar parabolic trough power plant, Proceedings of $SCCO_2$ Power Cycle Symposium 2009 RPI, Troy, NY.

[109]. Luu, M. T., Milani, D., McNaughton, R., Abbas, A. Analysis for flexible operation of supercritical CO_2 Brayton cycle integrated with solar thermal systems, Energy 124 (2017) 752-771.

[110]. Heo, J. Y., Kwon, J., Lee, J. I. A study of supercritical carbon dioxide power cycle for concentrating solar power applications using an isothermal compressor, Journal of Engineering for Gas Turbines and Power 140 (2018) 071702-1-8.

[111]. Enrıquez, L. C., Munoz-Anton, J., Martınez-Val Penalosa, J. M. Thermodynamic optimization of supercritical CO_2 Brayton power cycles coupled to line-focusing solar fields, Journal of Solar Energy Engineering 139 (2017) 061005-1-8.

[112]. Reyes-Belmonte, M. A., Sebastian, A., Romero, M., Gonzalez-Aguilar, J. Optimization of a recompression supercritical carbon dioxide cycle for an innovative central receiver solar power plant, Energy 112 (2016) 17-27.

[113]. Al-Sulaiman, F. A., Atif, M. Performance comparison of different supercritical carbon dioxide Brayton cycles integrated with a solar power tower, Energy 82 (2015) 61-71.

[114]. Neises, T., Turchi, C. A comparison of supercritical carbon dioxide power cycle configurations with an emphasis on CSP applications, Energy Procedia 49 (2014) 1187–1196.

[115]. Singh, R., Miller, S. A., Rowlands, A. S., Jacobs, P. A. Dynamic characteristics of a direct-heated supercritical carbon-dioxide Brayton cycle in a solar thermal power plant, Energy 50 (2013) 194–204.

[116]. Singh, R., Rowlands, A. S., Miller, S. A. Effects of relative volume-ratios on dynamic performance of a direct-heated supercritical carbon-dioxide closed Brayton cycle in a solar-thermal power plant, Energy 55 (2013) 1025–1032.

[117]. Milani, D., Luu, M. T., McNaughton, R., Abbas, A. A comparative study of solar heliostat assisted supercritical CO_2 recompression Brayton cycles: Dynamic modelling and control strategies, Journal of Supercritical Fluids 120 (2017) 113–124.

[118]. Chacartegui, R., Muñoz de Escalona, J. M., Sánchez, D., Monje, B., Sánchez, T. Alternative cycles based on carbon dioxide for central receiver solar power plants, Applied Thermal Engineering 31 (2011) 872-879.

[119]. Cheng, W. L., Huang, W. X., Nian, Y. L. Global parameter optimization and criterion formula of supercritical carbon dioxide Brayton cycle with recompression, Energy Conversion and Management 150 (2017) 669–677.

[120]. Wang, X., Liu, Q., Bai, Z., Lei, J., Jin, H. Thermodynamic investigations of the supercritical CO_2 system with solar energy and biomass, Applied Energy 227 (2018) 108–118.

[121]. Mago, P. J., Chamra, L. M., Somayaji, C. Performance analysis of different working fluids for use in organic Rankine cycles, Proceedings of the Institution of Mechanical Engineers, Part A: Journal of Power and Energy 221 (2007) 255-264.

[122]. Mago, P. J. Exergetic evaluation of an organic Rankine cycle using medium-grade waste heat, Energy Sources, Part A Recovery Utilization and Environmental Effects 34 (2012) 1768–1780.

[123]. Wang, E., Yu, Z., Zhang, H., Yang, F. A regenerative supercritical-subcritical dual-loop organic Rankine cycle system for energy recovery from the waste heat of internal combustion engines, Applied Energy 190 (2017) 574-590.

[124]. Tchanche, B. F., Papadakis, G., Lambrinos, G., Frangoudakis, A. Fluid selection for a low temperature solar organic Rankine cycle, Applied Thermal Engineering 29 (2009) 2468–2476.

[125]. Xia, X. X., Qi, W. Z., Hua, H. Y., Jun, Z. N. A novel comprehensive evaluation methodology of organic Rankine cycle for parameters design and working fluid selection, Applied Thermal Engineering 143 (2018) 283–292.

[126]. Ahmadi, P., Dincer, I., Rosen, M. A. Exergo-environmental analysis of an integrated organic Rankine cycle for trigeneration, Energy Conversion and Management 64 (2012) 447–453.

[127]. Roy, J. P., Mishra, M. K., Misra, A. Parametric optimization and performance analysis of a regenerative organic Rankine cycle using low–grade waste heat for power generation, International Journal of Green Energy 8 (2011) 173–196.

[128]. Baral, S., Kim, K. C. Thermodynamic modeling of the solar organic Rankine cycle with selected organic working fluids for cogeneration, Distributed Generation and Alternative Energy Journal, 29, 2014, 7-28.

[129]. Guo, C., Du, X., Goswami, D. Y., Yang, L. Investigation on working fluids selection for organic rankine cycles with low-temperature heat sources, International Journal of Green Energy 13 (2016) 556–565.

[130]. Fu, B-R., Lee, Y-R., Hsieh, J-C. Experimental investigation of a 250-kW turbine organic Rankine cycle system for low-grade waste heat recovery, International Journal of Green Energy 13 (2016) 1442-1450.

[131]. Li, J., Alvi, J. Z., Pei, G., Ji, J., Li, P., Fu, H. Effect of working fluids on the performance of a novel direct vapor generation solar organic Rankine cycle system, Applied Thermal Engineering 98 (2016) 786–797.

[132]. Nafey, A.S., Sharaf, M.A. Combined solar organic Rankine cycle with reverse osmosis desalination process: energy, exergy, and cost evaluations, Renewable Energy 35 (2010) 2571-2580.

[133]. Delgado-Torres, A. M., García-Rodríguez, L. Preliminary design of seawater and brackish water reverse osmosis desalination systems driven by low-temperature solar organic Rankine cycles (ORC), Energy Conversion and Management 51 (2010) 2913–2920.

[134]. Al-Sulaiman, F. A., Hamdullahpur, F., Dincer, I. Performance assessment of a novel system using parabolic trough solar collectors for combined cooling, heating, and power production, Renewable Energy 48 (2012) 161-172.

[135]. Gao, W., Li, H., Xu, G., Quan, Y. Working fluid selection and preliminary design of a solar organic Rankine cycle system, Environmental Progress & Sustainable Energy 34 (2015), 619-626.

[136]. Tunc, M., Sisbot, S., Camdali, U. Exergy analysis of electricity generation for the geothermal resources using organic rankine cycle: kızıldere-denizli case, Environmental Progress & Sustainable Energy 32 (2012) 830-836.

[137]. Calise, F., d'Accadia, M. D., Macaluso, A., Piacentino, A., Vanoli, L. Exergetic and exergoeconomic analysis of a novel hybrid solar– geothermal polygeneration system producing energy and water, Energy Conversion and Management 115 (2016) 200–220.

[138]. He, Y. L., Mei, D. H., Tao, W. Q., Yang, W. W., Liu, H. L. Simulation of the parabolic trough solar energy generation system with organic Rankine cycle, Applied Energy 97 (2012) 630–641.

[139]. Bryszewska-Mazurek, A., S´wieboda, T., Mazurek, W. Performance analysis of a solar-powered organic Rankine cycle engine, Journal of the Air & Waste Management Association 61 (2011) 3–6.

[140]. Gang, P., Jing, L., Jie, J. Analysis of low temperature solar thermal electric generation using regenerative organic Rankine cycle, Applied Thermal Engineering 30 (2010) 998–1004.

[141]. Yu¨ksel, Y. E. Thermodynamic assessment of modified Organic Rankine Cycle integrated with parabolic trough collector for hydrogen production, International Journal of Hydrogen Energy 43 (2018) 5832–5841.

[142]. Reddy, V. S., Kaushik, S. C., Tyagi, S. K. Exergetic analysis and performance evaluation of parabolic trough concentrating solar thermal power plant (PTCSTPP), Energy 39 (2012) 258-273.

[143]. Bellos, E., Tzivanidis, C., Torosian, K. Energetic, exergetic and financial evaluation of a solar driven trigeneration system, Thermal Science and Engineering Progress 7 (2018) 99–106.

[144]. Bellos, E., Tzivanidis, C. Investigation of a hybrid ORC driven by waste heat and solar energy, Energy Conversion and Management 156 (2018) 427–439.

[145]. Bellos, E., Tzivanidis, C., Antonopoulos, K. A. A detailed working fluid investigation for solar parabolic trough collectors, Applied Thermal Engineering 114 (2017) 374–386.

[146]. Lizarte, R., Palacios-Lorenzo, M. E., Marcos, J. D. Parametric study of a novel organic Rankine cycle combined with a cascade refrigeration cycle (ORC-CRS) using natural refrigerants, Applied Thermal Engineering 127 (2017) 378–389.

[147]. Zhou, C. Hybridisation of solar and geothermal energy in both subcritical and supercritical organic Rankine cycles, Energy Conversion and Management 81 (2014) 72–82.

[148]. Kalra, C., Becquin, G., Jackson, J., Laursen, A.L., Chen, H., Myers, K., Hardy, A., Klockow, H., Zia, J. High-potential power cycles & working fluids for next generation binary supercritical organic Rankine cycle for enhanced geothermal systems, Proceedings, Thirty Seventh Workshop on Geothermal Reservoir Engineering 2012, Stanford University, Stanford, California.

[149]. Chen, H., Goswami, D. Y., Stefanakos, E. K. A review of thermodynamic cycles and working fluids for the conversion of low-grade heat, Renewable and Sustainable Energy Reviews 14 (2010) 3059–3067.

[150]. Pan, L., Wang, H., Shi, W. Performance analysis in near-critical conditions of organic Rankine cycle, Energy 37 (2012) 281-286.

[151]. Xu, G., Song, G., Zhu, X., Gao, W., Li, H., Quan, Y. Performance evaluation of a direct vapor generation supercritical ORC system driven by linear Fresnel reflector solar concentrator, Applied Thermal Engineering 80 (2015) 196–204.

[152]. Mocarski, S., Borsukiewicz-gozdur, A. Selected aspects of operation of supercritical (transcritical) organic Rankine cycle, Archives of thermodynamics 36 (2015) 85-103.

[153]. Yaglı, H., Koç, Y., Koç, A., Gorgülü, A., Tandiroglu, A. Parametric optimization and exergetic analysis comparison of subcritical and supercritical organic Rankine cycle (ORC) for biogas fuelled combined heat and power (CHP) engine exhaust gas waste heat, Energy 111 (2016) 923-932.

[154]. Wang, T., Gao, N., Zhu, T. Investigation on the optimal condensation temperature of supercritical organic Rankine cycle systems considering meteorological parameters, Energy Conversion and Management 174 (2018) 54–64.

[155]. Javanshir, A., Sarunac, N. Thermodynamic analysis of a simple Organic Rankine Cycle, Energy 118 (2017) 85-96.

[156]. Braimakis, K., Preißinger, M., Brüggemann, D., Karellas, S., Panopoulos, K. Low grade waste heat recovery with subcritical and supercritical Organic Rankine Cycle based on natural refrigerants and their binary mixtures, Energy 88 (2015) 80-92.

[157]. Moloney, F., Almatrafi, E., Goswami, D.Y. Working fluid parametric analysis for recuperative supercritical organic Rankine cycles for medium geothermal reservoir temperatures, Energy Procedia 129 (2017) 599-606.

[158]. Khaliq, A., Kumar, R., Dincer, I. Exergy analysis of an industrial waste heat recovery based cogeneration cycle for combined production of power and refrigeration, Journal of Energy Resources Technology 131 (2009) 022402-1-9.

[159]. Wang, X., Dai, Y. Exergoeconomic analysis of utilizing the transcritical CO_2 cycle and the ORC for a recompression supercritical CO_2 cycle waste heat recovery: A comparative study, Applied Energy 170 (2016) 193-207.

[160]. Akbari, A. D., Mahmoudi, S. M. S. Thermoeconomic analysis & optimization of the combined supercritical CO_2 (carbon dioxide) recompression Brayton/organic Rankine cycle, Energy 78 (2014) 501-512.

[161]. Saleh, B. Parametric and working fluid analysis of a combined organic Rankine-vapor compression refrigeration system activated by low-grade thermal energy, Journal of Advanced Research 7 (2016) 651-660.

[162]. Polyzakis, A. L., Koroneos, C., Xydis, G. Optimum gas turbine cycle for combined cycle power plant, Energy Conversion and Management 49 (2008) 551–563.

[163]. Ersayin, E., Ozgener, L. Performance analysis of combined cycle power plants: A case study, Renewable and Sustainable Energy Reviews 43 (2015) 832–842.

[164]. Njoku, I. H., Oko, C.O.C., Ofodu, J. C. Performance evaluation of a combined cycle power plant integrated with organic Rankine cycle and absorption refrigeration system, Cogent Engineering 5 (2018) 1451426-1-30.

[165]. Wu, C., Wang, S. S., Feng, X. J., Li, J. Energy, exergy and exergoeconomic analyses of a combined supercritical CO_2 recompression Brayton/absorption refrigeration cycle, Energy Conversion and Management 148 (2017) 360–377.

[166]. Hou, S., Cao, S., Yu, L., Zhou, Y., Wu, Y., Zhang, F. Y. Performance optimization of combined supercritical CO_2 recompression cycle and regenerative organic Rankine cycle using zeotropic mixture fluid, Energy Conversion and Management 166 (2018) 187–200.

[167]. Song, J., Li, X. S., Ren, X. D., Gu, C. W. Performance analysis and parametric optimization of supercritical carbon dioxide (S-CO_2) cycle with bottoming organic Rankine cycle (ORC), Energy 143 (2018) 406-416.

[168]. Javanshir, A., Sarunac, N., Razzaghpanah, Z. Thermodynamic analysis and optimization of single and combined power cycles for concentrated solar power applications, Energy 157 (2018) 65-75.

[169]. Al-Sulaiman, F. A. Exergy analysis of parabolic trough solar collectors integrated with combined steam and organic Rankine cycles, Energy Conversion and Management 77 (2014) 441–449.

[170]. Gao, W., Li, H., Nie, P., Zhang, Y., Yang, Y., Wang, Y., Yao, M. Parameter and layout optimization of a high temperature solar combined cycle using low temperature thermal storage, Environmental Progress & Sustainable Energy 36 (2017) 1234-1243.

[171]. Sánchez, D., Brenes, B. M., Muñoz de Escalona, J. M., Chacartegui, R. Non-conventional combined cycle for intermediate temperature systems, International Journal of Energy Research 37 (2013) 403–411.

[172]. Besarati, S. M., Goswami, D. Y. Analysis of advanced supercritical carbon dioxide power cycles with a bottoming cycle for concentrating solar power applications, Transactions of ASME, Journal of Solar Energy Engineering 136 (2014) 010904-1-7.

[173]. Wang, X., Yang, Y., Zheng, Y., Dai, Y. Exergy and exergoeconomic analyses of a supercritical CO_2 cycle for a cogeneration application, Energy 119 (2017) 971-982.

[174]. AlZahrani, A. A., Dincer, I. Comparative energy and exergy studies of combined CO_2 Brayton-organic Rankine cycle integrated with solar tower plant, International Journal of Exergy 26 (2018) 21-40.

[175]. Garcıa, J. M., Padilla, R. V., Sanjuan, M. E. Response surface optimization of an ammonia–water combined power/cooling cycle based on exergetic analysis, Journal of Energy Resources Technology 139 (2017) 022001-1-9.

[176]. Kizilkan, O. Exergetic performance assessment of solar driven combined CO_2 power and refrigeration system, International Journal of Exergy 27 (2018) 147-164.

[177]. Bao, J., Zhao, L. A review of working fluid and expander selections for organic Rankine cycle, Renewable and Sustainable Energy Reviews 24 (2013) 325–342.

[178]. Zhu, Q. Innovative power generation systems using supercritical CO_2 cycles, Clean Energy 1 (2017) 68–79.

[179]. Qiu, Y., Li, M-J., He, Y-L., Tao, W-Q. Thermal performance analysis of a parabolic trough solar collector using supercritical CO_2 as heat transfer fluid under nonuniform solar flux, Applied Thermal Engineering 115 (2017) 1255–1265.

[180]. Bellos, E., Korres, D., Tzivanidis, C., Antonopoulos, K. A. Design, simulation and optimization of a compound parabolic collector, Sustainable Energy Technologies and Assessments 16 (2016) 53–63.

[181]. Cheng, Z. D., He, Y. L., Qiu, Y. A detailed non-uniform thermal model of a parabolic trough solar receiver with two halves and two inactive ends, Renewable Energy 74 (2015) 139–147.

[182]. Guo, J., Huai, X. Multi-parameter optimization design of parabolic trough solar receiver, Applied Thermal Engineering 98 (2016) 73–79.

[183]. Seidel, W. Model development and annual simulation of the supercritical carbon dioxide Brayton cycle for concentrating solar power applications, Master's thesis, The University of Wisconsin-Madison, 2010.

[184]. Turchi, C. S. Supercritical CO_2 for application in concentrating solar power systems, Proceedings of $SCCO_2$ Power Cycle Symposium 2009, RPI, Troy, NY, 2009.

[185]. Paty, F. Conception of an ORC module for high temperature recovery, Master of Science Thesis, KTH industrial engineering and management, 2016.

[186]. Oyewunmi, O. A., Ferré-Serres, S., Lecompte, S., van den Broek, M., Paepe, M. D., Markides, C. N. An assessment of subcritical and trans-critical organic Rankine cycles for waste-heat recovery, Energy Procedia 105 (2017) 1870–1876.

[187]. Walraven, D., Laenen, B., D'haeseleer, W. Comparison of thermodynamic cycles for electricity production from low-temperature geothermal heat sources, 2012, WP EN2012-006.

[188]. Lee, H. J., Kim, H., Jang, C. Compatibility of candidate structural materials in high-temperature S-CO_2 environment, in: Supercritical CO_2 Power Symposium, Pittsburgh (PA), 2014.

[189]. Was, G. S., Ampornrat, P., Gupta, G., Teysseyre, S., West, E. A., Allen, T. R., Sridharan, K., Tan, L., Chen, Y., Ren, X., Pister, C. Corrosion and stress corrosion cracking in supercritical water, Journal of Nuclear Materials 371 (2007) 176-201.

[190]. Dincer, I. Cengel, Y. A. Energy, entropy and exergy concepts and their roles in thermal engineering, Entropy 3 (2001) 116–149.

[191]. Karakoc, T. H., Ozerdem, M. B., Sogut, M. Z., Colpan, C. O., Altuntas, O., Açıkkalp, E. Sustainable aviation: energy and environmental issues, First Edition, Springer international publishing Switzerland, 2016, 1-423, ISBN-13: 978-3319341798.

[192]. Blanco, M., Santigosa, L. R. Advances in concentrating solar thermal research and technology, First Edition, Woodhead publishing series in energy (Elsevier), 2016, 1-494, ISBN: 978-0-08 100516-3.

[193]. Zhang, X., Wu, L., Wang, X., Ju, G. Comparative study of waste heat steam SRC, ORC and S-ORC power generation systems in medium-low temperature, Applied Thermal Engineering 106 (2016) 1427–1439.

[194]. Zarza, E., Rojas, M. E., González, L., Caballero, J. M., Rueda, F. INDITEP: the first precommercial DSG solar power plant, Solar Energy 80 (2006) 1270–1276.

[195]. Plataforma Solar de Almería (PSA). Annual report 2002. <http://www.psa.es/en/techrep/2002/atr2002_ing.pdf> accessed on 24.03.2017.

[196]. Valenzuela, L., Zarza, E., Berenguel, M., Camacho, E. F. Control concepts for direct steam generation in parabolic troughs, Solar Energy 78 (2005) 301–311.

[197]. Price, H., Kearney, D. Reducing the cost of energy from parabolic trough solar power plants, in: International Solar Energy Conference 2003, Hawaii, USA, 2003, 591–599.

[198]. Nouman, J. Comparative studies and analyses of working fluids for Organic Rankine Cycles – ORC. KTH School of Industrial Engineering and Management, Master of Science Thesis 2012, Stockholm.

[199]. Singh, H., Mishra, R. S. Performance analysis of solar parabolic trough collectors driven combined supercritical CO_2 and organic Rankine cycle, Engineering Science and Technology, an International Journal 21 (2018) 451–464.

[200]. Goswami, Y. Thermodynamic cycles for CSP, University of South Florida, Tampa, Florida. <http://www.iitj.ac.in/CSP/material/19dec/thermodynamic.pdf> accessed on 28.12.2017.

[201]. Wright, S. A., Radel, R. F., Conboy, T. M., Rochau, G. E. Modeling and experimental results for condensing supercritical CO_2 power cycles, Sandia Report, SAND2010-8840, Sandia National Laboratories, Livermore (CA), January 2011.

[202]. Wright, S. A., Conboy, T. M., Rochau, G. E. Overview of supercritical CO_2 power cycle development at sandia national laboratories, University Turbine Systems Research Workshop, Columbus, Ohio, 2011.
<https://www.netl.doe.gov/publications/proceedings/11/utsr/pdf/wed/Wright%20SCO2%20Power%20Cycle%20Summary%20UTSR%202011%20v2a.pdf> accessed on 19/9/2018.

[203]. Mwesigye, A., Bello-Ochende, T., Meyer, J. P. Minimum entropy generation due to heat transfer and fluid friction in a parabolic trough receiver with nonuniform heat flux at different rim angles and concentration ratios, Energy 73 (2014) 606–617.

[204]. Vivian, J., Manente, G., Lazzaretto, A. A general framework to select working fluid and configuration of ORCs for low-to-medium temperature heat sources, Applied Energy 156 (2015) 727–746.

[205]. Aghahosseini, S., Dincer, I. Exergoenvironmental analysis of renewable/waste heat based organic rankine cycle (ORC) using different working fluids, Proceeding of global conference on global warming, Lisbon, Portugal, 2011.

[206]. Chys, M., van den Broek, M., Vanslambrouck, B., De Paepe, M. Potential of zeotropic mixtures as working fluids in organic Rankine cycles, Energy 44 (2012) 623–632.

[207]. Wang, E., Yu, Z., Zhang, H., Fubin, Y. A regenerative supercriticalsubcritical dual-loop organic Rankine cycle system for energy recovery from the waste heat of internal combustion engines, Applied Energy 190 (2017) 574–590.

[208]. Kuo, C-R., Hsu, S-W., Chang, K-H., Wang, C-C. Analysis of a 50 kW organic Rankine cycle system, Energy 36 (2011) 5877-5885.

[209]. Habibi, H., Zoghi, M., Chitsaz, A., Javaherdeh, K., Ayazpour, M. Thermo-economic analysis and optimization of combined PERC - ORC - LNG power system for diesel engine waste heat recovery, Energy Conversion and Management 173 (2018) 613–625.

[210]. Sarangi, S. K., Barpujari, B., Dawar, R. Emerging technology option for clean power generation - concentrated solar power (CSP), In: Petrotech-2009, New Delhi, India, 2009.

[211]. Singh, H., Mishra, R. S. Energy- and exergy-based performance evaluation of solar powered combined cycle (recompression supercritical carbon dioxide cycle/organic Rankine cycle), Clean Energy 2 (2018) 140–153.

[212]. Dyreby, J., Klein, S., Nellis, G., Reindl, D. Design considerations for supercritical carbon dioxide Brayton cycles with recompression, Journal of Engineering for Gas Turbines Power 136 (2014) 101701-1-9.

[213]. Gupta, A., Anand, Y., Anand, S., Tyagi, S. K. Thermodynamic optimization and chemical exergy quantification for absorption-based refrigeration system, Journal of Thermal Analysis and Calorimetry 122 (2015) 893–905.

[214]. Mishra, R. S., Singh, H. Detailed parametric analysis of solar driven supercritical CO_2 based combined cycle for power generation, cooling and heating effect by vapor absorption refrigeration as a bottoming cycle, Thermal Science and Engineering Progress 8 (2018) 397–410.

[215]. Kalogirou, S. Solar energy engineering: processes and systems, First Edition, Academic Press/Elsevier, California, USA, 2009, 1-755, ISBN-13: 978-0-12-397270-5.

[216]. Duffie, J., Beckman, W. Solar engineering of thermal processes, Fourth Edition, John Wiley & Sons Inc., Hoboken, New Jersey, USA, 2013, 1-928, ISBN 978-0-470-87366-3.

[217]. Chafie Ben, M., Aissa, M. F., Bouadila, S., Balghouthi, M., Farhat, A., Guizani, A. Experimental investigation of parabolic trough collector system under Tunisian climate: design, manufacturing and performance assessment, Applied Thermal Engineering 101 (2016) 273–283.

[218]. Sahoo, U., Kumar, R., Pant, P. C., Chaudhary, R. Resource assessment for hybrid solar-biomass power plant and its thermodynamic evaluation in India, Solar Energy 139 (2016) 47–57.

[219]. LUZ International Limited, Solar electric generating system IX technical description, LUZ International Limited, 1990.

[220]. Petela, R. Exergy analysis of the solar cylindrical-parabolic cooker, Solar Energy 79 (2005) 221–233.

[221]. Boehm, R. Maximum performance of solar heat engines, Applied Energy 23 (1986) 281–296.

[222]. Petela, R. Exergy of undiluted thermal radiation, Solar Energy 74 (2003) 469–488.

[223]. Wu, C., Wang, S. S., Feng, X. J., Li, J. Energy, exergy and exergoeconomic analyses of a combined supercritical CO_2 recompression Brayton/absorption refrigeration cycle, Energy Conversion Management 148 (2017) 360–377.

[224]. Turchi, C. S., Ma, Z., Neises, T., Wagner, M. Thermodynamic study of advanced supercritical carbon dioxide power cycles for high performance concentrating solar power systems, ASME 2012 6th International Conference on Energy Sustainability (ES2012), San Diego, CA, 2012, ASME Paper No. ES2012-91179.

[225]. Dincer, I., Midilli, A., Kucuk, H. Progress in exergy, energy, and the environment, First Edition, Springer international publishing Switzerland, 2014, 1-1086, ISBN 978-3-319-04681-5.

[226]. Gibbs, J. P. Corrosion of various engineering alloys in supercritical carbon dioxide, Ph.D. thesis, Massachusetts Institute of Technology, Cambridge, MA, 2010.

[227]. Parks, C. J. Corrosion of candidate high temperature alloys in supercritical carbon dioxide, Master's thesis, Carleton University, Ottawa, Ontario, Canada, 2013.

[228]. Lemmon, E. W., McLinden, M. O., Huber, M. L. NIST Reference Fluid Thermodynamic and Transport Properties—REFPROP, National Institute of Standards and Technology, Gaithersburg, MD, NIST Standard Reference Database 23.

[229]. Klein, S. A. Engineering Equation Solver (EES), Academic Commercial V7.714. F-Chart Software, www.fChart.com, 2006.

[230]. Dudley, V. E., Koib, G. J., Mahoney, A. R., Mancini, T. R., Matthews, C. W., Sloan, M. Keamey, D. SEGS LS-2 solar collector test results, Report of Sandia National Laboratories, SANDIA94-1884, 1994.

[231]. Forristall, R. Heat Transfer Analysis and Modeling of a Parabolic Trough Solar Receiver Implemented in Engineering Equation Solver. Golden, CO: National Renewable Energy Laboratory (NREL), 2003.

[232]. Clemente, S., Micheli, D., Reini, M., Taccani, R. Bottoming organic Rankine cycle for a small scale gas turbine: a comparison of different solutions, Applied Energy 106 (2013) 355–364.

[233]. Kulhánek, M., Dostál, V. Thermodynamic analysis and comparison of supercritical carbon dioxide cycles. In: Proceedings of Supercritical CO_2 Power Cycle Symposium, Boulder, Colorado, 24–25 May 2011. <https://drive.google.com/file/d/1KcvMoLYNYXxxkbXjJWjSSixKQr4DVhmnHqAFQk-R3mybERAXd3TieAus5QmQ/view> accessed on 2/6/2018.

[234]. Arora, A., Kaushik, S. C. Theoretical analysis of LiBr/H_2O absorption refrigeration systems, International Journal of Energy Research 33 (2009) 1321–1340.

[235]. Wang, X., Wang, J., Zhao, P., Dai, Y. Thermodynamic comparison and optimization of supercritical CO_2 Brayton cycles with a bottoming transcritical CO_2 cycle, Journal of Energy Engineering 142 (2016) 04015028-1–11.

[236]. Anand, S., Gupta, A., Anand, Y., Tyagi, S. K. Use of process steam in vapor absorption refrigeration system for cooling and heating applications: an exergy analysis, Cogent Engineering 3 (2016) 1160639-1–14.

[237]. Singh, H., Mishra, R. S. Performance evaluation of the supercritical organic Rankine cycle (SORC) integrated with large scale solar parabolic trough collector (SPTC) system: an exergy energy analysis, Environment Progress and Sustainable Energy 37 (2018) 891-899.

[238]. Maran, J. P., Sivakumar, V., Thirugnanasambandham, K., Sridhar R. Artificial neural network and response surface methodology modeling in mass transfer parameters predictions during osmotic dehydration of Carica papaya L., Alexandria Engineering Journal 52 (2013) 507–516.

[239]. Maran, J. P., Manikandan, S., Thirugnanasambandham, K., Nivetha, C. V., Dinesh, R. Box–Behnken design based statistical modeling for ultrasound-assisted extraction of corn silk polysaccharide, Carbohydrate Polymers 92 (2013) 604–611.

[240]. Myers, R. H., Montgomery, D. C., Anderson-Cook, C. M. Response surface methodology: process and product optimization using designed experiments, Third Edition, John Wiley and Sons, New York, 2002, 1-705, ISBN 978-0-470-17446-3.

[241]. Madhlopa, A. Principles of solar gas turbines for electricity generation, First Edition, Springer International Publishing AG, Cape Town, 2018, 1-220, ISBN 978-3-319-68388-1.